



**Cláudia Susana Pedreira Correia**

Mestre em Biotecnologia

**Bioprocessing of human Pluripotent Stem  
Cells for cardiac cell therapy and pre-  
clinical research**

Dissertação para obtenção do Grau de Doutor em  
Bioengenharia

Orientador: Paula M. Alves, PhD, ITQB-NOVA

Co-orientador: Margarida Serra, PhD, ITQB-NOVA

 **FACULDADE DE  
CIÊNCIAS E TECNOLOGIA  
UNIVERSIDADE NOVA DE LISBOA**

**Setembro, 2016**

**Bioprocessing of human Pluripotent Stem Cells for cardiac cell therapy and pre-clinical research**

Copyright © Cláudia Susana Pedreira Correia, Faculdade de Ciências e Tecnologia, Universidade Nova de Lisboa.

A Faculdade de Ciências e Tecnologia e a Universidade Nova de Lisboa têm o direito, perpétuo e sem limites geográficos, de arquivar e publicar esta dissertação através de exemplares impressos reproduzidos em papel ou de forma digital, ou por qualquer outro meio conhecido ou que venha a ser inventado, e de a divulgar através de repositórios científicos e de admitir a sua cópia e distribuição com objetivos educacionais ou de investigação, não comerciais, desde que seja dado crédito ao autor e editor.

*Ao Meu melhor Amigo*

*Aos meus Pais, Irmã e Avó*



## Acknowledgements

I would like to express my gratitude to all the people, directly or indirectly, involved in this thesis, which supported and helped me during this journey

To my supervisor, Dr Paula Alves, for the scientific support, knowledge and experience shared with me throughout these years. Thank you for all the professional advices, for the challenges and for all the opportunities provided, including courses, conferences and the visit to MGH/HMS that contributed for my development as a scientist.

To my co-supervisor, Dr Margarida Serra, for all the endless scientific discussions, support, guidance, confidence, motivation and friendship provided during this journey. Thanks for always believing in me and for promoting my independence, pushing me towards my goals and broadening my scientific perspectives.

To Professor Manuel Carrondo, for being an inspiring example of leadership and for transmitting us the excellence, rigor, hard work and pro-activity that are fundamental for success in science.

To Dr. Ibrahim Domian, for such a warm welcome in your laboratory at MGH/HMS, Boston. I'm thankful for your scientific enthusiasm and all the knowledge shared. Thank you also to all Domian' group members, specially, DJ and Abir, for all the help, from bench work, to data analysis, to scientific discussions.

To Dr. Tomo Saric, from University of Cologne, for being part of my CAT and for all the scientific support and guidance provided during our collaborative projects.

To Dr. Pedro Lima, from FCM-UNL, for the help with the electrophysiology analyses, for all the advices and good sense of humour.

To Alexey Koshkin, Patrícia Duarte and Nuno Espinha, I would like to emphasize my very special "thank you". It was a pleasure to teach you and also to learn from you. Seeing you growth, every day, as scientists was a truth reward! Thank you for having shared with me the hurdles and joys of working with such amazing and full of energy cells, for your hard work and commitment, for your loyalty, for always maintaining the enthusiasm and being in the lab with a smile, particularly during those long working marathons, for your true friendship, for always being there when I most needed, for supporting me and believing in me and in my ideas, for all the shared laughs and pleasant conversations in the lab. Thank you very much to each one of you for being who you are.

To Dr Ana Teixeira for the support in cellular metabolic analysis, for being always available (even when far away from the lab), and for the fruitful discussions.

To Dr Madalena Carido, for helping me with the hypothermic storage studies, for all the scientific and personal advices, for one year of very funny and pleasant lunch breaks, for always motivating me, and for being a good friend in and outside the lab.

To the MIT-Portugal program and to all my Professors for a year of intense learning and experiences, which stimulated further my interest in the bioengineering field, to Dr José Silva Lopes for always being available to help in any subject, to my colleagues, in special to Patricia and Tomás, my CandiFriends, it was really a pleasure to work with you, we did an amazing team.

To the hosting institutions, iBET and ITQB-NOVA, for the excellent working conditions. To the financial support provided by Fundação para a Ciência e Tecnologia (SFRH/BD/51573/2011).

To all animal cell technology unit colleagues, in particular to those of the Stem Cell team for the scientific discussions, critical suggestions and good working environment in the lab, to Marcos Sousa for the support with bioprocess operations in the beginning of this journey, to Dr Catarina Brito for helpful discussions, to Dr Carina Silva for always being available to help, to Hugo Soares for all the encouraging words and friendship, and to all the people who contributed to the great environment in the lab and during lunch times.

To Katrina and Chuck for having received me with open arms in Boston, for made me feel welcome in your lovely home, for your endless kindness and friendship. It was a great pleasure to meet you during this journey.

Pessoalmente gostaria de agradecer,

Aos meus amigos da licenciatura (e de hoje), ao Hélio, à Lúcia, à Cristiana, à Joana, ao André e à Ana Cláudia por me fazerem rir e descontraír.

Aos meus amigos de longa data, em especial às minhas amigas do PN, por todos estes anos de amizade.

Ao Hélio, por todo o apoio que me deu durante todos estes anos, por me ter ajudado a crescer e a ter coragem e força para vencer todos os obstáculos.

Ao meu melhor amigo, pelo apoio incondicional, por sempre me dar força, elogiar e acreditar em mim, por toda a confiança, por estar sempre presente tanto nas alegrias como nas tristezas. Obrigada pelas infindáveis gargalhadas, pelo carinho, amizade e paciência. Esta tese não teria sido a mesma sem ti.

A toda a minha família. Aos meus tios, primos e priminhos. Em especial à minha prima Telma por sempre acreditar em mim como cientista e por ter tanto gosto em ouvir e perceber o meu trabalho. Ao Bob pela boa disposição e palavras de incentivo. Aos meus queridos Pais, por serem a base de tudo. Pelo apoio incondicional que me dão e que me ajuda a enfrentar tudo na vida. Obrigado por estarem sempre presentes, por toda a confiança e por toda a imensurável ajuda. À minha irmã por ser o meu exemplo de coragem, perseverança, força e determinação. À minha querida e linda avó, o meu porto de abrigo.

## Abstract

Cardiovascular diseases remain the leading cause of death worldwide. Some of these diseases, e.g. myocardial infarction (MI), are associated with a massive and permanent loss of cardiomyocytes (CMs), a non-proliferative and terminally differentiated cell population in the heart. Available pharmacological and interventional therapies are not suitable to amend the effects of this cell loss, mainly due to the limited regenerative capacity of the myocardium, and heart transplantation is limited by the number of compatible organs donated. Recently, human pluripotent stem cells (hPSCs), have emerged as attractive candidate cell sources to obtain CMs. Due to their inherent capacity to proliferate indefinitely and to differentiate into all mature cells of the human body, hPSCs constitute the unique cell source that can provide, *ex-vivo*, an unlimited number of functional CMs suitable for cell therapy and other applications including disease modeling and cardiotoxicity drug testing. Nonetheless, the complex nets of signaling pathways involved in cardiomyogenesis as well as the line-to-line variability compromise the effectiveness of the existing differentiation protocols to reproducibly produce high-quality CM from multiple hPSC lines. The immature phenotype of the produced hPSC-CMs and the lack of efficient methods for worldwide shipment of these cells also constrain the applicability of these cells in the clinic and industry.

The main aim of this thesis was to devise robust, scalable and integrated approaches for the production and maturation of hPSC-CMs. The strategy consisted in exploring the impact of environmental factors, cell culture configuration, and metabolic substrate availability on bioprocess yields and cell's quality using a set of "-omic" tools, namely transcriptomics, metabolomics and fluxomics, and cell characterization assays.

In **Chapter 1**, the recent advances on the use of hPSC for cardiac cell therapy were reviewed.

In **Chapter 2**, the effect of dissolved oxygen and bioreactor hydrodynamics on CM differentiation was explored. It was demonstrated that combining a hypoxia culture (4% O<sub>2</sub> tension) with wave-induced agitation enables the differentiation of iPSCs towards CMs at faster kinetics and with higher yields.

**Chapter 3** focused on the development and characterization of a robust protocol for directed differentiation of hPSC towards CMs, suitable to generate CMs in both 2D monolayer and 3D aggregate culture formats. The culture of hPSC-cardiac progenitors as 3D aggregates revealed to be an efficient approach to improve CM enrichment and commitment. Although hPSC-CMs generated from both methods revealed to be highly glycolytic, 3D aggregate cultures showed slightly improved metabolic energetics (including increased TCA-cycle activity and ATP production). **Chapter 4** assessed whether alterations in hPSC-CM culture medium composition to mimic *in vivo* substrate availability during cardiac development would induce hPSC-CM maturation *in vitro*. It was demonstrated that shifting hPSC-CMs from glucose-containing to galactose- and fatty acid-containing media promotes their maturation into adult-like CMs with higher oxidative metabolism, transcriptional signatures closer to ventricular CMs, higher myofibril density and alignment, improved calcium handling, enhanced contractility, and more physiological action

potential kinetics, within 10-20 days. The feasibility to cold store hPSC-CMs monolayers and aggregates in a fully-defined clinical compatible formulation was evaluated in **Chapter 5**. It was demonstrated that hPSC-CMs are more resistant to prolonged hypothermic storage–induced cell injury in 3D aggregates than in 2D monolayers, showing high cell recoveries, typical (ultra)structure and functionality after 7 days of storage.

**Chapter 6** consists of a general discussion, where the main scientific and technological outcomes of this thesis are outlined.

Overall, by pursuing an holistic approach that brought together a quantitative molecular and metabolic characterization, this thesis provides novel insights into the interaction of metabolism and CM differentiation/maturation but also establishes robust and scalable methods for production, functional maturation and short-term storage of hPSC-CMs. This will pave the way for the widespread application of hPSC-CMs in clinical and preclinical applications.



## Resumo

As doenças cardiovasculares constituem uma das principais causas de morte a nível mundial e estão normalmente associadas a uma perda massiva e permanente de cardiomiócitos (CMs), uma população celular não proliferativa e completamente diferenciada. As terapias farmacológicas disponíveis actualmente não são adequadas para reparar os efeitos nefastos causados pela destruição destas células e a implementação do transplante cardíaco como tratamento convencional é restringida pelo número limitado de órgãos compatíveis doados. Recentemente, as células estaminais pluripotentes humanas (hPSCs), surgiram como uma fonte celular promissora para a obtenção de CMs. Devido à sua inerente propriedade de proliferação ilimitada e capacidade de se diferenciar em todas as células adultas do corpo humano, as hPSCs constituem a única fonte de células que pode proporcionar, ex-vivo, um número ilimitado de CMs funcionais adequados para terapia celular e outras aplicações, como por exemplo o rastreio de novos medicamentos ou como modelo celular para avaliar o desenvolvimento e progressão de várias doenças. No entanto, a complexidade do processo de desenvolvimento cardíaco aliado à elevada variabilidade entre diferentes linhas de células tem vindo a dificultar o desenvolvimento de um protocolo de diferenciação que reprodutivamente origine CMs com elevada qualidade a partir de linhas diferentes de hPSC. O fenótipo imaturo dos hPSC-CMs produzidos e a falta de métodos eficientes para o transporte adequado destas células a nível mundial também têm restringido a aplicabilidade destas células na clínica/indústria.

Esta tese teve como principal objectivo o desenvolvimento de métodos robustos, escalonáveis e integrados para a produção e maturação de hPSC-CMs. A estratégia consistiu em explorar o impacto de factores ambientais, configuração do sistema de cultura, e disponibilidade de substratos metabólicos nos rendimentos do bioprocessamento e na qualidade das células usando um conjunto diversificado de ferramentas incluindo transcriptómica, metabolómica e fluxómica, e ensaios de caracterização celular.

No **Capítulo 1**, foram descritos os avanços mais recentes no uso de hPSC para terapia celular cardíaca. No **Capítulo 2**, foi explorado o efeito da concentração de oxigénio dissolvido e da hidrodinâmica de biorreactores na diferenciação em CMs. Demonstrou-se que a cultura celular num bioreactor do tipo Wave em condições de hipoxia permite acelerar a cinética de diferenciação de iPSCs em CMs e aumentar os rendimentos de diferenciação cardíaca.

O **Capítulo 3** foca-se no desenvolvimento e caracterização de um protocolo robusto para a diferenciação dirigida de hPSC em CMs, capaz de produzir CMs em monocamadas e em agregados. A cultura de células progenitoras cardíacas derivadas de hPSCs sob a forma de agregados revelou ser uma abordagem eficiente para melhorar a diferenciação em CMs e a pureza final da cultura. Demonstrou-se que apesar de os hPSC-CMs produzidos em ambos os tipos de cultura apresentarem um metabolismo principalmente glicolítico, as culturas de agregados apresentaram um aumento na actividade do ciclo do TCA e produção de ATP.

No **Capítulo 4** avaliou-se o efeito da alteração da composição do meio de cultura de hPSC-CMs, de modo a mimetizar a disponibilidade de substratos durante o desenvolvimento cardíaco, *in vivo*, na maturação de hPSC-CMs *in vitro*. Demonstrou-se que substituir o meio de cultura base rico em glucose por um meio sem glucose suplementado com ácidos gordos e galactose promove a maturação de hPSC-CMs, após 10-20 dias em cultura, originando hPSC-CMs que apresentam: um metabolismo mais oxidativo, um perfil de transcrição de genético mais semelhante a CMs ventriculares, miofibrilas em maior densidade e mais alinhadas, e melhorias na funcionalidade.

A possibilidade de preservar monocamadas e agregados de hPSC-CMs numa formulação compatível com o uso clínico foi avaliada no **Capítulo 5**. Foi demonstrado que hPSC-CMs na forma de agregados são mais resistentes aos danos provocados por um armazenamento hipotérmico prolongado que na forma de monocamadas, mostrando recuperações celulares elevadas após o descongelamento e uma (ultra)estrutura e funcionalidade típica de CMs após 7 dias de armazenamento.

O **Capítulo 6** consiste em uma discussão geral, onde são identificados os principais resultados científicos e tecnológicos desta tese.

Em suma, esta tese contribuiu para o estado da arte no campo das células estaminais, apresentando uma abordagem holística que reuniu uma caracterização molecular e metabólica quantitativa, proporcionando novas perspectivas sobre a interação do metabolismo com a diferenciação e maturação de CMs. Além disso permitiu desenvolver métodos robustos e escalonáveis para a produção, maturação funcional e armazenagem a curto prazo de hPSC-CMs, facilitando a transferência de hPSC-CMs para aplicações clínicas e pré-clínicas.

## Thesis Publications

Serra M., Brito C., **Correia C.**, Alves P.M. (2012). Process engineering of human pluripotent stem cells for clinical applications. Trends Biotechnol. 30, 350-9.

**Correia C.**, Serra M., Espinha N., Sousa M., Brito C., Burkert K., Zheng Y., Hescheler J., Carrondo M.J., Sarić T., Alves P.M. (2014). Combining Hypoxia and Bioreactor Hydrodynamics Boosts Induced Pluripotent Stem Cell Differentiation Towards Cardiomyocytes. Stem Cell Rev. 10, 786-801.

**Correia C.**, Koshkin A., Carido M., Espinha N., Šarić T., Lima P.A., Serra M., Alves P.M. (2016). Effective Hypothermic Storage of Human Pluripotent Stem Cell-Derived Cardiomyocytes Compatible With Global Distribution of Cells for Clinical Applications and Toxicology Testing. Stem Cells Transl. Med. 5, 658-69.

**Correia C.**, Koshkin A., Duarte P., Hu D., Teixeira A.P., Domian I.J., Serra M., Alves P.M. (2016). Metabolic substrate availability controls the maturation of human induced pluripotent stem cells derived cardiomyocytes. (*submitted*)

**Correia C.**, Koshkin A., Duarte P., Hu D., Carido M., Sebastião M., Alves P., Domian I., Teixeira A.P., Serra M., Alves P.M. (2016). 3D aggregates of human pluripotent stem cells derived cardiac progenitors: Impact of culture strategy in transcriptional and metabolic signatures of cardiomyocytes (*submitted*)

## Book Chapter

Serra M., **Correia C.**, Brito C., Alves, P.M. (2014). Bioprocessing of Human Pluripotent Stem Cells for Cell Therapy Applications. Stem Cells and Cell Therapy, Cell Engineering 8, SpringerScience, 71-95.

## Additional Publications

**Correia C.**, Espinha N., Brito C., Serra M., Alves P.M. (2013). Bioengenharia de células estaminais pluripotentes humanas para aplicação clínica. Boletim Biotecnologia 4, 31-33 (in Portuguese).

Babo P, Santo V.E., Duarte A.R.C., **Correia C.**, Costa M.H.G, Mano J.F., Reis R.L., Gomes M.E. (2014). Platelet lysate membranes as new autologous templates for tissue engineering applications. Inflammation and Regeneration, 34, 033–044.

Silva M.M., Rodrigues A.F., **Correia C.**, Sousa M.F., Brito C., Coroadinha A.S., Serra M., Alves P.M. (2015). Robust Expansion of Human Pluripotent Stem Cells: Integration of Bioprocess Design With Transcriptomic and Metabolomic Characterization. Stem Cells Transl Med. 4, 731-42.

Santo V.E., Babo P., Amador M., **Correia C.**, Cunha B., Coutinho D.F., Neves N.M., Mano J.F., Reis R.L., Gomes M.E. (2016). Engineering Enriched Microenvironments with Gradients of Platelet Lysate in Hydrogel Fibers. Biomacromolecules, 17,1985-97

Cunha B., Silva J.S., **Correia C.**, Koshkin A., Carrondo M.J.T., Serra M., Peixoto C., Alves P.M. (2016). Finding the design space of a filtration-based operation for the concentration of human pluripotent stem cells using design of experiments approach. (*submitted*)

**Correia C.**, Koshkin A., Duarte P., Teixeira A.P., Serra M., Alves P.M. (2016). Exploring the effect of 3D aggregate culture on the metabolic substrate plasticity of human pluripotent stem cells derived cardiomyocytes. (*in preparation*)

## Table of Contents

Chapter 1 - Introduction.....	1
Chapter 2 - Combining Hypoxia and Bioreactor Hydrodynamic Boosts Induced Pluripotent Stem Cell Differentiation Towards Cardiomyocytes .....	39
Chapter 3 - 3D aggregates of human pluripotent stem cells derived cardiac progenitors: impact of culture strategy in transcriptional and metabolic signatures of cardiomyocytes .....	71
Chapter 4 - Metabolic substrate availability controls the maturation of human induced pluripotent stem cells derived cardiomyocytes .....	107
Chapter 5 - Effective hypothermic storage of human pluripotent stem cell derived cardiomyocytes compatible with global distribution of cells for clinical applications and toxicology testing .....	147
Chapter 6 - Discussion .....	179

## List of Figures

<b>Figure 1.1.</b> hPSC technology for cardiac cell therapy: Major benefits, limitations and possible solutions.....	6
<b>Figure 1.2.</b> Schematic representation of signaling pathways and factors involved in cardiomyocyte differentiation in embryology.....	7
<b>Figure 1.3.</b> Examples of different suspension culture systems used for large-scale stem cell production.....	12
<b>Figure 1.4.</b> Main approaches used to improve hPSC-CM maturation and parameters typically evaluated to assess maturation status of hPSC-CMs.....	18
<b>Figure 1.5.</b> Schematic representation of the myofibril organization and ultrastructural features of sarcomeres.....	20
<b>Figure 1.6.</b> Metabolic pathways that are regulated to support stem cell growth <i>in vitro</i> .....	21
<b>Figure 1.7.</b> Overview of the various pathways of energy substrate metabolism that contribute to the production of ATP.....	22
<b>Figure 1.8.</b> Methodologies routinely used for characterization of hPSC-CMs.....	25
<b>Figure 1.9.</b> Schematic representation of the major aims of this thesis.....	29
<b>Figure 2.1.</b> Experimental scheme for differentiation and purification of iPSC-CMs in stirred tank and WAVE bioreactors.....	49
<b>Figure 2.2.</b> Effect of dissolved oxygen on CM differentiation of iPSCs in stirred tank bioreactors.....	51
<b>Figure 2.3.</b> Impact of the agitation profile on CM differentiation of iPSCs in stirred tank bioreactors.....	53
<b>Figure 2.4.</b> Differentiation of iPSC into CMs in WAVE and stirred tank bioreactors.....	55
<b>Figure 2.5.</b> Scanning-electron and confocal microscopy of iPSC-derived cell aggregates and cardiospheres.....	57
<b>Figure 2.6.</b> Structural properties of CMs generated in stirred tank and WAVE optimized bioprocesses.....	58
<b>Figure 2.7.</b> Functional characterization of CMs produced in stirred tank and WAVE bioreactors..	59
<b>Figure A-2.1.</b> Viability analysis of cell aggregates from day 2 cultures.....	64
<b>Figure A-2.2.</b> Elongation and roundness of aggregates from day 9 cultures .....	64
<b>Figure A-2.3.</b> Structural analysis of cells dissociated from day 9 aggregates cultured in Stirred tank and WAVE bioreactors.....	65
<b>Figure A-2.4.</b> Cumulative LDH release in stirred tank and WAVE bioreactor.....	65
<b>Figure 3.1.</b> Direct differentiation of hPSCs towards cardiomyocytes in 2D monolayer cultures.....	81
<b>Figure 3.2.</b> Metabolic profiling of hiPSC during CM differentiation in 2D monolayers.....	83

<b>Figure 3.3.</b> Effect of 3D aggregate culture of cardiac progenitors on CM enrichment and commitment.....	85
<b>Figure 3.4.</b> Impact of 3D aggregate culture of cardiac progenitors on hPSC-CM functionality.....	86
<b>Figure 3.5.</b> Comparison of the transcriptional profile of hiPSC-CMs obtained in both 2D monolayer and 3D aggregate cultures.....	88
<b>Figure 3.6.</b> Metabolic flux map of the central carbon metabolism of both hiPSC-CM-2D and hiPSC-CM-3D at day 15.....	91
<b>Figure 3.7.</b> Comparison of central carbon metabolism and metabolic transcriptional profile in both 2D monolayers and 3D aggregates of hiPSC-CM.....	92
<b>Figure A-3.1.</b> Comparison of CM purity obtained after directed differentiation of 2D monolayers of hiPSC and hESCs.....	96
<b>Figure A-3.2.</b> Experimental and simulated intracellular <sup>13</sup> C-labelling dynamics in hiPSC-CM-2D using [1,2- <sup>13</sup> C]GLC.....	97
<b>Figure A-3.3.</b> Experimental and simulated intracellular <sup>13</sup> C-labelling dynamics in hiPSC-CM-3D using [1,2- <sup>13</sup> C]GLC.....	97
<b>Figure A-3.4.</b> Metabolic profiling of hiPSC-CMs in both 2D monolayers and 3D aggregates.....	99
<b>Figure 4.1.</b> Effect of culture medium composition on central carbon metabolism of hiPSC-CM.....	116
<b>Figure 4.2.</b> In the absence of a sugar source, fatty acid rich medium induces lipotoxicity in hiPSC-CM.....	118
<b>Figure 4.3.</b> Effect of culture media composition on the fluxome and metabolic transcriptome of hiPSC-CM.....	119
<b>Figure 4.4.</b> Effect of culture medium composition on hiPSC-CM transcriptional profiling.....	122
<b>Figure 4.5.</b> Structural and ultrastructural analyses of hiPSC-CM after culture in different media.....	125
<b>Figure 4.6.</b> Impact of metabolic manipulation on hiPSC-CM functionality.....	127
<b>Figure 4.7.</b> Summary of major findings in this study.....	129
<b>Figure A-4.1.</b> Experimental and simulated intracellular <sup>13</sup> C-labelling dynamics in GLCM condition using [1,2- <sup>13</sup> C]GLC and [U- <sup>13</sup> C]GLN.....	132
<b>Figure A-4.2.</b> Experimental and simulated intracellular <sup>13</sup> C-labelling dynamics in GFAM condition using [U- <sup>13</sup> C]GAL, [U- <sup>13</sup> C]PA, [U- <sup>13</sup> C]OA and [U- <sup>13</sup> C]Gln.....	133
<b>Figure A-4.3.</b> Experimental and simulated intracellular <sup>13</sup> C-labelling dynamics in FAM condition using [U- <sup>13</sup> C]PA, [U- <sup>13</sup> C]OA and [U- <sup>13</sup> C]Gln.....	134
<b>Figure A-4.4.</b> Density Plots generated with fold change in expression of genes from representative metabolic categories.....	135
<b>Figure A-4.5.</b> Schematic representation of the expression levels of OXPHOS related genes provided by IPA for GLCM and GFAM cultures at day 20.....	136

<b>Figure A-4.6.</b> Impact of culture media composition on metabolic activity and proliferative capacity.....	137
<b>Figure A-4.7.</b> Impact of culture media composition and culture time on the expression of genes related with extracellular matrix composition in hiPSC-CMs cultivated in different culture media.....	137
<b>Figure A-4.8.</b> hiPSC-CM culture in GLCM showed up-regulation of fibroblastic markers.....	138
<b>Figure A-4.9.</b> Impact of metabolic manipulation in hiPSC-CM functionality.....	138
<b>Figure A-4.10.</b> Impact of metabolic manipulation in beating rate and paced capacity.....	139
<b>Figure 5.1.</b> Hypothermic storage of hiPSC-CM as 2D monolayers.....	160
<b>Figure 5.2.</b> Hypothermic storage of hiPSC-CM as 3D aggregates.....	162
<b>Figure 5.3.</b> Characterization of hiPSC-CMs stored as 2D monolayers in hypothermic conditions for up to 7 days.....	164
<b>Figure 5.4.</b> Characterization of hiPSC-CMs stored as 3D aggregates in hypothermic conditions for up to 7 days.....	165
<b>Figure 5.5.</b> Ultrastructural characterization of hiPSC-CMs after hypothermic preservation.....	166
<b>Figure 5.6.</b> Functional characterization of hiPSC-CMs subjected to hypothermic storage for 7 days.....	168
<b>Figure A-5.1.</b> Hypothermic storage of murine iPSC-CMs.....	172
<b>Figure A-5.2.</b> Hypothermic preservation of hESC-CM as 2D monolayers.....	173
<b>Figure A-5.3.</b> Immunofluorescence labelling of miPSC-CMs after hypothermic storage as 2D monolayers.....	173
<b>Figure A-5.4.</b> Functional characterization of miPSC-CMs subjected to hypothermic storage for 7 days.....	174
<b>Figure 6.1.</b> Major bottlenecks, aims and achievements of each chapter of this thesis.....	182
<b>Figure 6.2.</b> Microenvironmental features which were studied in this thesis.....	183



## List of Tables

<b>Table 1.1.</b> Methods for guided differentiation of hPSC towards CMs, <i>in vitro</i> .....	9
<b>Table 1.2.</b> Advantages and disadvantages of 2D monolayer and 3D aggregate culture systems for stem cell bioprocessing.....	11
<b>Table 1.3.</b> Large scale culture systems used for CM differentiation from murine PSCs.....	14
<b>Table 1.4.</b> Large scale culture systems used for CM differentiation from human PSCs.....	14
<b>Table 1.5.</b> Phenotypic differences between adult-CMs and hPSC-CMs in terms of structure, sarcoplasmic reticulum (SR), gene expression, metabolism and electrophysiology.....	17
<b>Table 2.1.</b> Quantitative characterization of CM differentiation of iPSC in stirred tank and WAVE bioreactors.....	54
<b>Table A-2.1.</b> Primers for RT-PCR and quantitative RT-PCR .....	66
<b>Table A-2.2.</b> Mean aggregate size throughout time of iPSC-CMs produced in both stirred tank and WAVE bioreactor systems.....	66
<b>Table A-2.3.</b> Action potential properties of iPSC-CMs produced in both stirred tank and WAVE bioreactor systems.....	66
<b>Table A-3.1.</b> Metabolic network reactions and simulated fluxes determined by nonstationary <sup>13</sup> C-MFA.....	98
<b>Table A-4.1.</b> Metabolic network reactions and simulated fluxes determined by nonstationary <sup>13</sup> C-MFA.....	140
<b>Table A-4.2.</b> Comparison of contractility kinetics and contractile force generated by cells cultivated in LACM&GFAM at d10 and d20.....	142
<b>Table 5.1.</b> Evaluation of hiPSC-CM recovery after 3 (S3), 5 (S5) and 7 (S7) days of storage at 4°C in HTS preservation solution.....	161
<b>Table 6.1.</b> Comparison of structural, functional and metabolic features of hPSC-CMs cultured in GFAM and other approaches reported in the literature with human adult CMs.....	191



## List of Abbreviations

<b>AcCoA</b>	Acetyl-CoA
<b>AKG</b>	alpha-ketoglutarate
<b>ALA</b>	alanine
<b>ARG</b>	arginine
<b>ASP</b>	aspartate
<b>ATP</b>	adenosine triphosphate
<b>BMP</b>	bone morphogenic protein
<b>Bry T T</b>	brachyury transcription factor
<b>BSA</b>	bovine serum albumin
<b>CIT</b>	citrate
<b>CMS</b>	cardiomyocytes
<b>CO<sub>2</sub></b>	carbon dioxide
<b>CPC</b>	cardiac progenitor cells
<b>cTnI</b>	cardiac muscle troponin I
<b>cTnT</b>	cardiac muscle troponin T
<b>cTnC</b>	cardiac muscle troponin C
<b>CVD</b>	cardiovascular diseases
<b>CYS</b>	cysteine
<b>DKK1</b>	dickkopf homolog 1
<b>DMEM</b>	Dulbecco Modified Eagle Medium
<b>DMSO</b>	dimethyl sulfoxide
<b>ECM</b>	extracellular matrix
<b>EDTA</b>	ethylenediaminetetraacetic acid
<b>eGFP</b>	enhanced green fluorescent protein
<b>EMU</b>	elementary metabolic unit
<b>END-2</b>	esisceral endoderm-like cell line
<b>F6P</b>	fructose-6-phosphate
<b>FA</b>	fatty acids
<b>FBS</b>	fetal bovine serum
<b>FGF</b>	fibroblast growth factors
<b>FSG</b>	fish skin gelatin
<b>FUM</b>	fumarate
<b>G6P</b>	glucose-6-phosphate
<b>GAL</b>	galactose
<b>GAP</b>	glyceraldehyde 3-phosphate
<b>GAPDH</b>	glyceraldehyde-3-Phosphate Dehydrogenase
<b>GATA4</b>	transcription factor GATA-4
<b>GC-MS</b>	gas chromatography–mass spectrometry
<b>GFP</b>	green fluorescent protein
<b>GLC</b>	glucose
<b>GLN</b>	glutamine
<b>GLU</b>	glutamate

**GLUT** glucose transporter  
**GPI** glucose-6-phosphate isomerase  
**GSK3-β** glycogen synthase kinase-3 beta  
**hCMs** human cardiomyocytes  
**HCN4** hyperpolarization activated cyclic nucleotide-gated potassium channel 4  
**hESCs** human embryonic stem cells  
**hESC-CMs** human embryonic stem cell derived cardiomyocytes  
**hiPSC** human induced pluripotent stem cells  
**hiPSC-CMs** human induced pluripotent stem cell derived cardiomyocytes  
**HIS** histidine  
**HPLC** high performance liquid chromatography  
**hPSC** human pluripotent stem cells  
**hPSC-CMs** human pluripotent stem cell derived cardiomyocytes  
**ICM** inner cell mass  
**IgG** immunoglobulin G  
**IgM** immunoglobulin M  
**ILE** isoleucine  
**IPA** ingenuity pathway analysis  
**ISL-1** insulin gene enhancer protein ISL-1  
**IWR** inhibitors of Wnt response  
**KDR** kinase insert domain receptor  
**LAC** lactate  
**LDH** lactate dehydrogenase  
**LEU** leucine  
**Lin28** Lin-28 homolog A  
**LYS** lysine  
**MAL** malate  
**MDH** malate dehydrogenase  
**MEF** mouse embryonic fibroblast  
**MET** methionine  
**MFA** metabolic flux analysis  
**MI** myocardial infarction  
**MID** mass isotopomer distributions  
**MSCs** mesenchymal stem cells  
**MYH6** gene encoding myosin heavy chain, α isoform protein  
**MYH7** myosin, heavy chain 7  
**MYL2** myosin light chain 2 (myosin regulatory light chain 2, ventricular/cardiac muscle isoform)  
**MYL7** myosin regulatory light chain 2 (myosin regulatory light chain 2, atrial isoform (MLC2a))  
**NCX** sodium-calcium exchanger  
**NKX-2.5** NK2 homeobox 5  
**NMR** nuclear magnetic resonance  
**OA** oleic acid  
**OAA** oxaloacetate  
**Oct4** transcription factor octamer 4

**OXPHOS** oxidative phosphorylation  
**P5P** pentose-5-phosphate  
**PA** palmitic acid  
**PBS** phosphate-buffered saline  
**PC** pyruvate carboxylase  
**PDGFR $\alpha$**  platelet-derived growth factor receptor  $\alpha$   
**PDH** pyruvate dehydrogenase  
**PFA** paraformaldehyde  
**PHE** phenylalanine  
**PK** pyruvate kinase  
**PPP** pentose phosphate pathway  
**PRO** proline  
**PYR** pyruvate  
**qMet** specific metabolic rate  
**R5P** ribose-5-phosphate  
**ROS** reactive oxygen species  
**RT-qPCR** real time-quantitative polymerase chain reaction  
**RYR** ryanodine receptor  
**SER** serine  
**SERCA** sarco/endoplasmic reticulum calcium atpase  
**SIRP $\alpha/\beta$**  signal-regulatory protein alpha/beta  
**SR** sarcoplasmic reticulum  
**SSEA-1** stage-specific embryonic antigen-1  
**SSEA-4** stage-specific embryonic antigen-4  
**sTnI** slow skeletal muscle isoform of troponin I  
**SUC** succinate  
**TALDO** transaldolase  
**TCA** Citric acid cycle  
**TGF- $\beta$**  transcription growth factor  $\beta$   
**THR** threonine  
**TNNT2** cardiac muscle troponin T  
**TRA-1-60** the human embryonal carcinoma marker antigen  
**TYR** tyrosine  
**VAL** valine  
**VCAM1** vascular cell adhesion molecule 1  
**VEGF** vascular endothelial growth factor  
**WB** washing buffer  
**WNT** Wingless-related integration site





# Introduction

This chapter was adapted from:

Serra M., Brito C., Correia C., Alves P.M. (2012). Process engineering of human pluripotent stem cells for clinical application. *Trends Biotechnol.* 30, 350–358.

Serra M., Correia C., Brito C., Alves, P.M. (2014). Bioprocessing of Human Pluripotent Stem Cells for Cell Therapy Applications. *Stem Cells and Cell Therapy, Cell Engineering* 8, SpringerScience. 71-95.

**Contents**

<b>1. Introduction.....</b>	<b>3</b>
1.1. Stem cell-based therapies for cardiac repair.....	3
1.2. Human pluripotent stem cells (hPSCs): Characteristics and Applications.....	4
1.3. Differentiation of hPSC towards cardiomyocytes .....	6
1.4. Improving scalability of cardiomyocyte differentiation protocols .....	10
1.5. Improving recapitulation of the native cardiac microenvironment <i>in vitro</i> - Biophysical signals .....	14
1.6. Enrichment of hPSC-CMs .....	15
1.7. Maturation of hPSC-CMs .....	15
1.8. Characterization of hPSC-CMs .....	23
1.9. Hypothermic storage of hPSC-CMs .....	26
<b>2. Scope of the thesis.....</b>	<b>27</b>
<b>3. References .....</b>	<b>30</b>



## 1. Introduction

### 1.1. Stem cell-based therapies for cardiac repair

Despite the recent advances in medicine, cardiovascular diseases remain the leading cause of death worldwide (Moran et al., 2014; WHO, 2016). Several of these diseases, e.g. myocardial infarction, are associated with a massive and permanent loss of CMs (CMs), a non-proliferative and terminally differentiated cell population (Chien and Olson, 2002; Saraste et al., 1999). The current pharmacological and interventional therapies are not suitable to amend the effects of this cell loss, mainly due to the limited regenerative capacity of the myocardium (Beltrami et al., 2003; Saraste et al., 1999). Bergmann et al. estimated that the renewal rate in human CMs gradually decreases from 1% per year at age of 25 to 0.45% annually at the age of 75 (Bergmann et al., 2009). Even though a subpopulation of cardiac stem cells reside in the adult human heart, their minor contribution towards CM renewal (estimated to be 0.03% to 0.008%) (van Berlo et al., 2015) is insufficient to assure a meaningful functional recovery after a myocardial infarction that can damage approximately 1 billion CMs (Saraste et al., 1999). Additionally, the proliferation and migration of fibroblasts to the injury site forms scar tissue with impaired contractile function that ultimately leads to the progression of cardiac damage (Deb and Ubil, 2014). The only current treatment to address CM loss and fully restore cardiac function is heart transplantation, however this procedure is limited by the number of compatible organs donated and the requirement of lifelong immunosuppression (WHO, 2014). Therefore, the development of novel regenerative therapies as well as the generation of more reliable human cardiac disease models for cardiac drug discovery and toxicology testing represents a major public health priority.

Stem cell technology is a great promise in regenerative medicine, due to stem cells' ability to proliferate indefinitely, while maintaining an unspecialized state, and to differentiate into multiple cell lineages (Evans and Kaufman, 1981; Thomson et al., 1998). In fact, numerous groups have reported the use of different stem cells types, derived from different sources, to improve cardiac function after injury (Chong et al., 2014; Menasché et al., 2008). The promising results in pre-clinical studies using animal models rapidly led to clinical trials, initially using bone marrow-derived mononuclear cells, mesenchymal stromal cell populations and, more recently, progenitor cells from the adult heart itself (Le et al., 2016). Though the efficacy of these in the clinical trials has been inconsistent. Various studies suggested that most of the beneficial effects of these cells are mediated through paracrine actions (secretion of exosomes, anti-apoptotic, immunomodulatory or proangiogenic factors), and modulation of extracellular matrix (ECM), rather than providing a true cardiomyogenic ability (reviewed in (Gnecchi et al., 2008; Le et al., 2016)). An ideal cell type for regeneration of the failing heart, besides ensuring safety and be expandable should integrate and synchronize with the rest of host myocardium (Carvajal-Vergara and Prósper, 2016). Thus, human pluripotent stem cells (hPSCs), including human embryonic stem cells (hESC) and human induced pluripotent stem cells (hiPSC), have emerged as more attractive candidates for cardiac regeneration due to their theoretically ability to produce unlimited numbers of multiple cardiac cell

types (including CMs) that can directly replace the damage cells and contribute to remuscularization of the infarcted tissue. The capability of hPSC-derived cardiomyocytes (hPSC-CMs) and cardiac progenitors (hPSC-CPCs) to engraft in the infarcted heart and contribute to cardiac function improvement has been demonstrated in many pre-clinical studies in both small and large animal models of myocardial infarction (Chong and Murry, 2014; Chong et al., 2014; Funakoshi et al., 2016; Laflamme et al., 2007; Shiba et al., 2012, 2016). A clinical trial ESCORT (ClinicalTrials.gov identifier: NCT02057900; phase I) that relies on the transplantation of cardiac progenitors derived from hESC, embedded in a fibrin scaffold for the treatment of severe heart failure is currently ongoing (Menasche et al., 2015).

## **1.2. Human pluripotent stem cells (hPSCs): Characteristics and Applications**

Murine embryonic stem cells (ESCs) were first isolated in 1981 (Evans and Kaufman, 1981) and their human counterparts in 1998 (Thomson et al., 1998) from the inner cell mass of blastocysts, pre-implanted embryos at day 5 of embryonic development. Despite their enormous potential for cell-based therapies, ESCs are inevitably associated with ethical issues, are technically difficult to derive and induce immune rejection after transplantation (Nussbaum et al., 2007).

In 2006 a major breakthrough occurred in the stem cell field. The reversion of somatic cells to a pluripotent state, by overexpression of 4 transcription factors (Oct4, Sox2, Klf4 and c-Myc), was reported for the first time in mice (Takahashi and Yamanaka, 2006). This finding had such impact in the scientific community that the reprogramming of human induced pluripotent stem cells (hiPSC) derived from human dermal fibroblast was described shortly after the initial discovery in mice (Takahashi et al., 2007). These iPSCs exhibited characteristics very similar to ESCs.

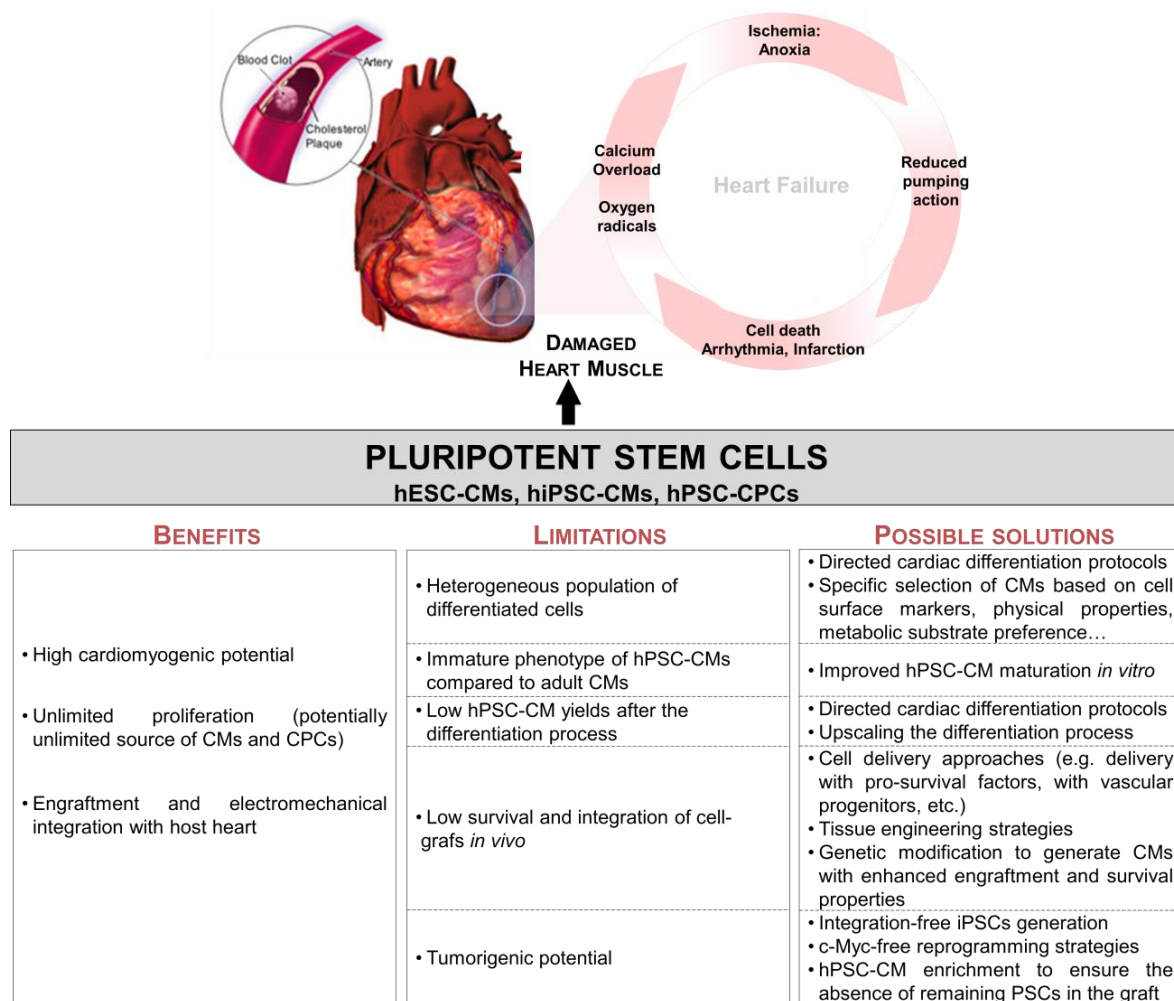
However, it was demonstrated that occasional reactivation of one of the reprogramming factors, c-Myc, could result in tumour formation (Okita et al., 2007). Therefore, in a later study reported by Thomson and co-workers, c-Myc and Klf4, well known proto-oncogenes, were replaced by Nanog and Lin28 (Yu et al., 2007).

The first reprogramming protocols relied on the use of integrating vectors to deliver desired transgenes into the genome of somatic cells. These integrating vectors were mainly retroviral or lentiviral (Takahashi et al., 2007; Thorrez and Sampaolesi, 2011). Even though reprogramming was possible, random transgene insertion could interrupt existing genes causing tumor formation (after transplantation) and disturb the maintenance of the undifferentiated cell state. This approach presents other drawbacks such as low stability, difficult cellular targeting and possible insertion of mutagenesis. To overcome these limitations and establish safer iPSC lines, methods that allow the expression of pluripotency genes without integrating the genome of the host are currently being explored. Some examples include the use of: i) non-integrating virus (e.g. adenoviruses, baculoviruses, Sendai virus), ii) episomal vectors or excisable transposon systems (e.g. PiggyBac or Cre/loxP systems), which integrate the cells but can be removed by transposase, without leaving genetic material behind, iii) exogenous plasmids, protein factors, small molecules and microRNAs (Brouwer et al., 2016; Thorrez and Sampaolesi, 2011; Zhou and Zeng, 2013).

Since the ability to generate iPSC in culture from adult human skin fibroblasts has been established, pluripotency has been induced in a variety of somatic cells including cardiac fibroblasts (Linares et al., 2016), keratinocytes (Aasen et al., 2008), T-lymphocytes (Brown et al., 2010), cord blood (Giorgetti et al., 2009), placenta (Ge et al., 2012), neural stem cells (Kim et al., 2009), adipose tissue (Zapata-Linares et al., 2016) and renal epithelial cells present in urine samples (Zhou et al., 2012). In the last few years, iPSC technology has boosted the field of regenerative medicine, offering numerous advantages over adult stem cells and ESCs. iPSCs can circumvent the need for embryo use, being ethically less controversial. Also, differentiated cells derived from iPSCs have been shown to present limited immunogenicity and could therefore be used in autologous personalized (Araki et al., 2013) (patient specific) or allogeneic off-the-shelf therapies (universal donor-derived cells).

hPSCs inherent capability of unlimited self-renewal coupled with efficient directed differentiation protocols allow for the large-scale production of specific human cell types, which can be used not only in regenerative medicine (Hartman et al., 2016) but also in developmental biology (Ueno et al., 2007), human disease modeling (Drawnel et al., 2014), and drug screening (Drawnel et al., 2014). Even though animal models have been essential in biomedical research, intrinsic differences with human physiology limit the reliable use of these models. For instance, mouse CMs display shorter action potentials compared with human ones because of differential expression of ion channels (Nerbonne, 2004). As such, hPSCs and their differentiated progeny hold great potential as a human cellular model (Drawnel et al., 2014). Up to now more than 70 hiPSC models of human diseases have been published (Ko and Gelb, 2014). In particular, hPSC-CMs have been used as *in vitro* models of several monogenic diseases, such as channelopathies and cardiomyopathies (Hartman et al., 2016). These models will contribute to improve our understanding of disease mechanisms, and potentially lead to new therapeutic strategies. The ability to evaluate the direct effects and toxicity of new drugs on the patients' own cells will ultimately enable the prediction of individual patient's responses to target treatments, fostering the transition to personalized medicine. Importantly, since many new drugs have unexpected cardiac toxicity resulting in sudden cardiac death (Pacher and Kecskemeti, 2004), hPSC-CMs can provide a high-quality platform for drug toxicity screening unanticipated possible side-effects of these new drugs in earlier stage of the drug development process.

Although hPSCs have proved promising in all these applications, there are still challenges to overcome in order to transfer hPSCs to cardiac cell therapy and pre-clinical applications including improved methods to consistently generate pure differentiated hPSC-CM populations with more mature structural and functional properties, and avoid or minimize graft cell death, immune rejection of graft cells, arrhythmogenesis, and the risk of tumorigenesis (Hartman et al., 2016). Figure 1.1 summarizes the main benefits and challenges of using hPSCs for heart regeneration and repair and indicates some of the solutions being pursued to address these issues.

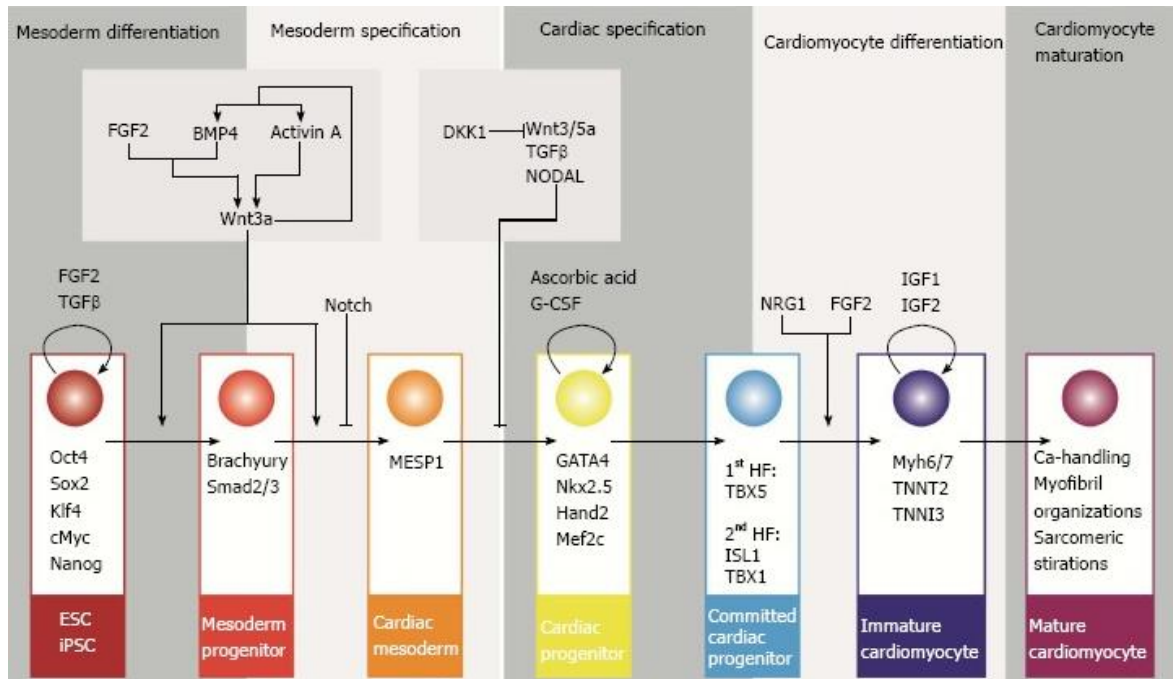


**Figure 1.1. hPSC technology for cardiac cell therapy: Major benefits, limitations and possible solutions** (adapted from (Le et al., 2016; Zwi-Dantsis and Gepstein, 2012))

### 1.3. Differentiation of hPSC towards cardiomyocytes

Differentiation of hPSCs to CMs was first reported in 2001 and since then distinct approaches have been thoroughly explored, namely differentiation with cells cultivated as embryoid bodies (EBs, three-dimensional aggregates of pluripotent stem cells) (Kehat et al., 2001), co-culture with inducer END-2 cells (Mummery et al., 2003) and guided differentiation strategies (induced by growth factors and/or small molecules) in two dimensional (2D) monolayers (Lian et al., 2013). Significant improvements in cardiac differentiation efficiency have been achieved through tightly timed, leveled and combined application of cardiogenic growth factors or small molecules that manipulate key signaling pathways (BMP, FGF, TGF/Activin/Nodal and WNT) involved in specific stages of *in vivo* cardiac development, including mesoderm formation, cardiac mesoderm specification and cardiac lineage specification (Figure 1.2) (Kadari et al., 2015; Kattman et al., 2011; Lian et al., 2012; Paige et al., 2010; Sumi et al., 2008). The use of small molecules in guided differentiation protocols is currently preferred to growth factors and recombinant protein based methods (Mummery et al., 2012). Small molecules can diffuse more efficiently throughout multiple

cell layers within EBs to modulate signaling, thus yielding more consistent results. There are also less expensive than growth factors, offering greater flexibility and scale-up prospects to directed differentiation protocols (Wang et al., 2011). Table 1.1 lists the multiple and different combinations of growth factors and small molecules that have been used to induce directed differentiation of hPSCs towards CMs, *in vitro*.



**Figure 1.2. Schematic representation of signaling pathways and factors involved in cardiomyocyte differentiation in embryology.** Factors that influence the progression through the five steps in cardiomyocyte differentiation and maturation: mesoderm differentiation, mesoderm specification, cardiac specification, cardiomyocyte differentiation and cardiomyocyte maturation. Transcription factors characteristic of each cell population during CM differentiation are presented in the respective boxes. Adapted from (Kamps and Krenning, 2016).

Differentiation of hPSCs into CMs from a confluent monolayer was first reported for hESCs (cell line H7) in 2007 (Laflamme et al., 2007). hESCs were cultured in chemically defined RPMI-B27 medium supplemented with Activin-A for 24 hours, and then 4 days in medium supplemented with BMP4. Spontaneous beating cells were observed on the 12<sup>th</sup> day of differentiation, and the final cell population contained 30% of MHC positive cells. By the time of development, this technique was the most efficient one, outperforming EB-based techniques. In 2010, it was found that the mechanism of the Activin/BMP4 differentiation is dependent upon endogenous Wnt/ $\beta$ -catenin signaling. Particularly, Wnt/ $\beta$ -catenin signaling has a biphasic role in cardiogenesis: Wnt activation is required for mesoderm formation and subsequent Wnt inhibition is necessary for cardiac specification (Ueno et al., 2007). Wnt pathway inhibits glycogen synthase kinase 3 beta (Gsk3- $\beta$ ) leading to accumulation of  $\beta$ -catenin that is translocated to the nucleus, where it binds to transcription factors that regulate Wnt-responsive genes (Ueno et al., 2007). Hence, CHIR99021, a small molecule that inhibits Gsk3- $\beta$ , has been widely used in directed differentiation protocols to activate Wnt signaling, whereas subsequent inhibition has been explored with a wide range of Wnt

antagonist such as IWP4, IWP2, IWR1, Wnt-C59 or XAV939 (Burrige et al., 2014; Kadari et al., 2015; Lian et al., 2012). Temporal modulation of Wnt signaling has shown great progress towards the generation of hPSC-CMs with high purity from both hESC and hiPSC lines (Lian et al., 2012, 2013). Consequently, nowadays most protocols rely on the regulation of the Wnt pathway (Table 1.1). Lian and colleagues also demonstrated the importance of understanding the role of media components used for differentiation. They showed that insulin, which is a component of the B27 medium supplement, suppresses cell differentiation during the first five days. After insulin was removed from the medium, the consistency of the CM yields increased dramatically (83–95% of cTnT positive cells, Table 1.1) (Lian et al., 2013). However, the B27 medium supplement, normally used for CM differentiation still contains some media components with unknown effects on differentiation efficiency and phenotype of the generated hPSC-CMs. In an attempt to improve differentiation efficiency across different PSC lines a recent study focused on the development of a chemically defined medium (Burrige et al., 2014). This study demonstrated that using a chemically defined medium consisting of just three components (the basal medium RPMI 1640, l-ascorbic acid 2-phosphate and rice-derived recombinant human albumin), along with small molecule-based induction of differentiation, is possible to obtain consistently high CM purities (80-95% of cTnT positive cells in 11 hiPSC lines, Table 1.1).

Other small molecules with potential to enhance cardiomyogenesis have been studied (Lewandowski et al., 2016). For example, ascorbic acid, has been shown to enhance differentiation of iPSCs into CMs (Cao et al., 2012). More specifically, the addition of ascorbic acid at early stages of culture showed to improve by 7.3-fold and 30.2-fold the yields of mouse and human PSC-CMs, respectively. Ascorbic acid promotes CM differentiation by increasing collagen synthesis, enhancing proliferation of cardiac progenitor cells and upregulating late stage markers of cardiomyogenesis (Cao et al., 2012; Takahashi et al., 2003). Although efficiencies of > 80% positive cells for CM markers are now regularly reported for hPSC differentiation towards CMs (Table 1.1), several evidences suggest that cardiac differentiation efficiencies are still highly variable between batch-to-batch, different hPSC lines and different laboratories. Thus, there is still space to improve reproducibility, robustness and standardization of the protocols to ensure greater consistency between cell lines and laboratories. Also, cardiac differentiation protocols still generate a mixed population of CM subtypes, including ventricular-, atrial- and pacemaker-like cells (Table 1.1) and cultures containing a single subtype are preferred for some applications. For example the transplantation of highly purified ventricular-like CMs might prove less likely to promote arrhythmias than the transplantation of cell preparations including significant quantities of nodal or other non-ventricular CMs (Hartman et al., 2016). Retinoic acid (RA) and Wnt signaling appear to play a critical role in determining atrial versus ventricular cardiomyocyte fate in differentiating hPSCs (Karakikes et al., 2014; Zhang et al., 2011), however more studies need to be performed to validate their utility in CM sub-lineage specification. The cellular heterogeneity with respect to lineage commitment state and/or degree of maturation among the final differentiation population is also an issue (Atmanli and Domian, 2016).

**Table 1.1. Methods for guided differentiation of hPSC towards CMs, *in vitro*.** Abbreviations: AA, activin A; V, ventricular; A, atrial; N, nodal (or pacemaker); Wo/I, without insulin; RPMI-B27 Wo/albumin, RPMI-B27 without albumin

Cell lines	Differentiation Procedure	CM purity (%)	CM subtype	Reference
hESC: 1 line		30 (MHC)	V,A	Lafame et al, 2007
hESC: 1 line hiPSC: 4 lines		30-70 (cTnT)	V,A	Uosaki et al, 2012
hESC: 3 lines		60.6 (MHC)	V,A	Hudson et al, 2011
hESC: 2 lines hiPSC: 4 lines		80 (cTnT)	V,A,N	Zhang et al, 2012
hESC: 3 lines hiPSC: 3 lines		83-95 (cTnT)	V,A	Lian et al, 2012
hESC: 2 lines hiPSC: 11 lines		80-95 (cTnT)	V,A	Burridge et al, 2014
Multiple hESC and hiPSC lines		88-98 (cTnT)	V	Lian et al, 2015
hESC: 2 lines hiPSC: 2 lines		5-85 (cTnT)	N,A	Kim et al, 2015
hESC: 1 line		80 (cTnT)	V,A	Tan et al, 2015
hESC: 2 lines hiPSC: 10 lines		80-95 (cTnT)	V,A,N	Lin et al, 2016

#### 1.4. Improving scalability of cardiomyocyte differentiation protocols

The average human heart contains approximately 4 billion CMs (Murry et al., 2006), and the typical infarct involves the loss of approximately one-quarter of these cells. Thus, cell-based therapies may require  $10^8$  to  $10^9$  hPSC-CMs per patient to regenerate the amount of working myocardial lost in myocardial infarction. Recently, Chong and colleagues demonstrated the feasibility of CM production and transplantation at this scale in a preclinical study using a primate model (Chong et al., 2014). While a monolayer-based CM differentiation protocol has sufficed for this early preclinical work, the labour intensive nature of this method (approximately one-dozen 150 cm<sup>2</sup> flasks of human ESC-derived cardiomyocytes were harvested to obtain the cell dose needed for each primate (Hartman et al., 2016)) reveals that this method is not suitable for the large-scale and clinical-grade production that would be required for transplantation in humans. Also, large numbers of cells are needed for drug screening pipelines and *in vitro* toxicology tests (Mummery et al., 2012). Thus, there is a need to translate small-scale culture protocols developed at research laboratories into validated bioprocesses that can guarantee reproducibility, scalability, standardization, robustness and safety. One attractive strategy for manufacturing hPSC-CMs consists in engineering stem cell niches by identifying key factors inducing CM differentiation of hPSC and creating culture approaches that allow 3D cell organization in a bioreactor-based system where key environmental conditions can be manipulated and finely controlled (Serra et al., 2012, 2014).

##### 1.4.1. Cell culture strategies: 3D aggregate vs 2D monolayers

In the last years, several 2D cell monolayer protocols were described for the differentiation of PSCs into functional CMs. However, 2D culture systems do not resemble the *in vivo* microenvironment and can be misleading regarding phenomena related with cell-cell or cell-ECM interaction, tissue architecture and biochemical signals (Serra et al., 2012). These culture systems also present an inherent uncontrollability, low scalability and low differentiation yields, that make them unattractive for clinical and industrial applications (Serra et al., 2012, 2014).


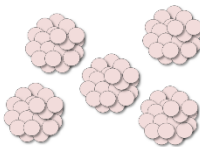
By providing a cellular context closer to what occurs in a native microenvironment, 3D culture strategies can significantly improve cell viability, functionality and proliferation/differentiation potential, offering a higher degree of efficiency, robustness, and predictability to the resulting hPSC manufacturing process (Lund et al., 2009; Serra et al., 2014) (Table 1.2.).

Formation of cell aggregates is one of the most common 3D cell culture strategies used in stem cell bioprocessing. When cultured as aggregates, cells re-establish mutual contacts allowing them to express a tissue-like structure, enhancing cell differentiation and functionality (Lund et al., 2009; Pal et al., 2013). Cell aggregates offer easy handling, scalable and reproducible opportunities to process development. The main limitation of this approach is the need to control aggregate size, avoiding diffusion gradients inside the aggregate that lead to necrotic centers and/or spontaneous differentiation (Serra et al., 2012). Cell harvesting is also an issue as dissociation of aggregates can compromise cell viability (Table 1.2.).



Several methods have been used to induce and/or accelerate cell aggregation including seeding single hPSCs or clumps in static low attachment dishes or in multi-well dishes to prompt cell agglomeration by gravity or through the use of external forces, such as centrifugation, ultrasound, magnetic or electrical forces (Günter et al., 2016; Matthys et al., 2016; Pettinato et al., 2015). Nonetheless, these methods present several limitations including the generation of aggregates with variable size, the difficulty to scale-up and the use of a harsh production environment using external forces (Günter et al., 2016). Recently, STEMCELL Technologies introduced the AggreWell™ plates, the first commercially available plates for the generation of standardized EBs from hPSCs. These plates allow the generation of large quantities of uniform-sized EB. EB size can be adjusted by altering the number of cells added to each well. However, commercially available single use microwell based consumables are still very costly and therefore large-scale experiments may be hardly affordable for most researchers. Some groups have reported the in-house production of microwell plates using soft lithography procedures (Dahlmann et al., 2013).

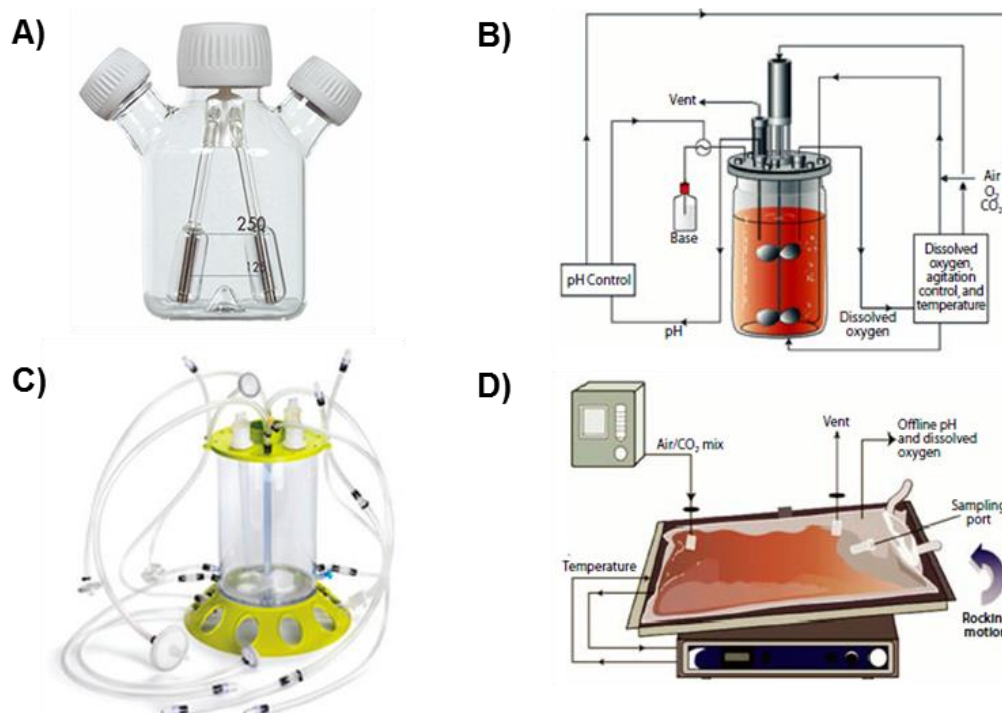
**Table 1.2. Advantages and disadvantages of 2D monolayer and 3D aggregate culture systems for stem cell bioprocessing**

CULTURE SYSTEM	ADVANTAGES	DISADVANTAGES
2D Monolayer culture 	<ul style="list-style-type: none"> <li>▪ Easy visualization/monitoring</li> <li>▪ Affordable</li> <li>▪ Suitable for small-scale studies</li> </ul>	<ul style="list-style-type: none"> <li>▪ Low reproducibility</li> <li>▪ Low scalability</li> <li>▪ Difficult to control culture parameters and diffusion gradients</li> <li>▪ Low cell production yields</li> <li>▪ Limited resemblance to <i>in vivo</i> tissues</li> </ul>
3D Aggregate culture 	<ul style="list-style-type: none"> <li>▪ Easy handling</li> <li>▪ Scalable</li> <li>▪ High reproducibility</li> <li>▪ 3D cell-cell contact is preserved</li> <li>▪ Can mimic stem cells' native microenvironment</li> <li>▪ High differentiation efficiency</li> <li>▪ High cell production yields</li> </ul>	<ul style="list-style-type: none"> <li>▪ Difficult to control culture outcome</li> <li>▪ Control of aggregate size</li> <li>▪ Single cell harvesting (difficult to dissociate aggregates without compromising cell viability)</li> <li>▪ Cell damage due to physical forces</li> </ul>

#### 1.4.2. The use of bioreactors for hPSCs culture

One of the most used strategies for scaling-up the production of PSC derivatives consists in the use of suspension culture systems that have become the standard for industrial-grade production of other cell types. Spinner flasks (Figure 1.3A) have been widely used for PSCs expansion and/or differentiation into CMs (Chen and Couture, 2015; Chen et al., 2012; He et al., 2012; Niebruegge et al., 2009; Serra et al., 2011; Zwi-Dantsis et al., 2011). However this culture system lacks culture control over parameters like temperature, pH or gas exchanges (e.g. oxygen). The use of fully controlled bioreactors overcomes this issue allowing accurately controlling and monitoring culture environment (e.g. pH, temperature, pO<sub>2</sub>, gas composition). Also, these systems offer enormous engineering prospects, as they are scalable, reproducible, versatile and fully automated. Different bioreactor types have been used for PSC culture such as microfluidic culture

systems, rotatory culture systems, stirred tank bioreactors, WAVE bioreactor, bioreactors using Vertical-Wheel™ technology (PBS-VW) (reviewed in (Placzek et al., 2009; Serra et al., 2012, 2014)). Stirred tank bioreactors (Figure 1.3B-C) have been widely used for PSC culture and cardiac differentiation (Table 1.3 and 1.4). Impeller-controlled stirring characteristic of these bioreactors ensures homogeneous mixing and distribution of cells, nutrients and gases. The impeller design, stirring rate and the cell inoculation density can be adjusted to control initial cell aggregation and improve aggregate culture (Olmer et al., 2012). One of the main limitations of stirred tank bioreactors is the hydrodynamic shear stress caused by stirring (reviewed in (Fridley et al., 2012)) which could detrimentally affect aggregate culture and cell differentiation.



**Figure 1.3. Examples of different suspension culture systems used for large-scale stem cell production. A)** Spinner flask. **B)** Stirred tank bioreactor (Fries et al., 2005). Single-use disposable bioreactors: **C)** Single-use stirred tank bioreactor (Mobius CellReady, Millipore) ([www.millipore.com](http://www.millipore.com)). **D)** Wave bioreactor (WAVE Bioreactor, GE Healthcare) (Fries et al., 2005).

During the last decade, single-use disposable bioreactors have been developed and applied in pre-clinical, clinical, and production-scale biotechnological facilities (Löffelholz et al., 2014). In contrast to reusable bioreactors made from glass or stainless steel, single-use bioreactors are made of FDA (Food and Drug Administration) approved plastics. Single-use bioreactors offer several advantages such as reduced costs in construction of production facilities, reduced risk of cross-contamination, less cleaning validation needed and rapid changeover of processes (Eibl et al., 2010; Löffelholz et al., 2014; Shukla and Gottschalk, 2013). However, these bioreactors also present limitations including lack of instrumentation for single-use sensors, possible secretion of leachables and extractables from the plastic cover (Löffelholz et al., 2014).

Today, there are different disposable bioreactor types commercially available (Eibl et al., 2010; Löffelholz et al., 2014; Shukla and Gottschalk, 2013). Some examples include spinner vessels, such as the SuperSpinner D 1000 (Sartorius); stirred tank disposables: Mobius CellReady (Millipore; Figure 1.3C), Univessel SU (Sartorius), CelliGen BLU (Eppendorf); and Vertical-Wheel™ bioreactors (PBS-VW) (PBS Biotech). Another example is the wave induced bioreactor (WAVE Bioreactor from GE Healthcare and BIOSTAT CultiBag from Sartorius-Stedim). This bioreactor (Figure 1.3D) has a rocking platform capable of inducing a wave motion in the culture media without an impeller or other invasive mixer. This rocking system promotes rapid medium homogeneity and provides the optimal oxygen transfer in the inflated bag (Shukla and Gottschalk, 2013; Singh, 1999). A study has shown that this bioreactor presents lower shear stress when compared to the stirred tank bioreactor (Oncül et al., 2009). In addition, this bioreactor has a simple design, appealing to either biological engineers or medical professionals. Recently, it was reported that the lower shear experienced during hESC expansion on Cytodex 1 microcarriers in a rocker (wave type) platform resulted in higher CM yields than when cultured in spinner cultures (Ting et al., 2014).

Optimization of PSC bioprocessing should result in large cell yields through process intensification, specialization and integration, rather than just scale-up technologies (Serra et al., 2012). The majority of culture approaches described up to now are based on substantial pre-expansion of hPSC (at the pluripotent state), before induction of cardiac differentiation, since cells become progressively post-mitotic along differentiation. The establishment of platforms capable of integrating expansion, differentiation, purification and harvesting would result in the scale-up of the production of differentiated cells to clinical relevant numbers (Serra et al., 2012). Also, significant benefits would derive from implementing sophisticated sensing/monitoring tools and devices (such as probes based on near infrared (NIR), Raman or fluorescence spectroscopy) within the manufacturing platform to assess real-time cell culture status, including cell viability, phenotype and functionality (Pais et al., 2014). Integration of online monitoring of metabolites such as glucose and lactate will also be of great value, further supporting the traceability, efficacy, safety and quality of the bioprocess.

Several bioprocesses combining PSC expansion and CM differentiation have been reported in recent years (Kempf et al., 2016). For example, Kempf and colleagues recently published a protocol for integrated hPSC expansion and CM differentiation in 100 mL stirred tank bioreactors (Kempf et al., 2014). After 4 days of expansion directed differentiation was induced by applying chemical Wnt pathway modulators and approximately 40 million CMs were generated in one bioreactor run. Table 1.3 and 1.4 summarize the main results of recent studies reporting integrated expansion and cardiac differentiation of murine and human PSC (respectively) in stirred culture systems. However, as shown in Table 1.4, the efficiency of differentiation of human PSCs in suspension systems has been variable.

**Table 1.3. Large scale culture systems used for CM differentiation of murine PSCs.** (embryoid body (EB)-based differentiation method).

System	Culture volume (mL)	Initial PSC number	CM production	CM/PSC ratio	Reference
Spinner flask	250	$5 \times 10^7$	$5.86 \times 10^7$	1.17	(He et al., 2012)
DASGIP Cellferm-Pro (DASGIP Tech.)	250	$1 \times 10^6$	$3.77 \times 10^6$	3.77	(Bauwens et al., 2005)
Biostat MD (Sartorius)	2000	$2 \times 10^8$	$1.28 \times 10^9$	6.4	(Schroeder et al., 2005)
Biostat MD (Sartorius)	2000	$2 \times 10^8$	$4.6 \times 10^9$	23	(Niebruegge et al., 2008)

**Table 1.4. Large scale culture systems for CM differentiation of human PSCs.** (GF – Growth Factors; SM – Small molecules; n.d. – not determined).

System	Culture volume (mL)	Cardiogenic GF/SM	CM production <sub>6</sub> ( $\times 10^6$ cells)	CM purity	Reference
Spinner flask	125	Spontaneous	n.d.	49% (contracting EBs/day 16)	(Niebruegge et al., 2009)
Spinner flask	125	BMP4, bFGF, Activin A, DKK1, VEGF	n.d.	27% (cTnT/day 19)	(Chen et al., 2012)
Spinner flask	125, 500, 1000	CHIR, IWP-4	168–1344	92–96% (cTnT/day 18)	(Chen et al., 2015)
Spinner flask	125	BMP4, Activin A, IWR-1, ascorbic acid	10–100	25% (actinin/day 18) 99% (actinin/day 25, metabolic selection)	(Natsuko et al., 2014)
Stirred tank bioreactor	100	CHIR, IWP2	22.1–76.5	26–90% (actinin, MHC, cTnT/day 10)	(Kempf et al., 2014) (Kempf et al., 2015)
Spinner flask	100	CHIR, IWP2, SB431542, purmorphamine	n.d.	>90% (cTnT/day 15)	(Hananeh et al., 2015)

### 1.5. Improving recapitulation of the native cardiac microenvironment *in vitro* - Biophysical signals

The cardiac microenvironment represents a niche that harbours biochemical and biophysical cues required for normal cardiac function. *In vivo*, the myriad of biophysical *stimuli* that cardiac tissue is exposed to controls normal development, physiology as well as pathophysiology (Atmanli and Domian, 2016). Biophysical cues are sensed by CMs through mechanosensors that convert the physical stimulus into a biochemical signal that mediates cell structure, survival, migration proliferation and differentiation. These sensors typically comprise membrane-associated protein complexes that interact with the ECM and link it to the cytoskeletal scaffold. Numerous efforts have been made to simulate the biophysical properties of the heart *in vitro* by manipulating ECM composition, growth substrate stiffness and elasticity, and applying mechanical stress (Atmanli and Domian, 2016). Mechanical preload has been mostly recapitulated *in vitro* by applying cyclic strain

and stretch, fluid shear stress and hydrostatic compression to CMs (Geuss and Suggs, 2013; Gwak et al., 2006; Happe and Engler, 2016; Schmelter et al., 2006; Stoppel et al., 2016). Under mechanical load hPSC-CMs have improved cellular alignment and enhanced levels of gene expression, calcium handling, and contractile force (Happe and Engler, 2016; Stoppel et al., 2016). Nevertheless, the low high-throughput design and scalability of the devices (typically custom built), that apply mechanical strains makes them unsuitable to generate large numbers of cells on a therapeutically relevant scale. More sophisticated engineering techniques capable of providing mechanical stimuli to cells should be investigated. For example, perfusion and mixing in scalable bioreactor culture systems can be manipulated to apply mechanical stress to cells. However, further studies on the impact of these physical forces on cell functionality will be needed.

### **1.6. Enrichment of hPSC-CMs**

The persistence of undifferentiated hPSC after the differentiation process is a great safety concern for clinical applications, as the tumorigenic potential of hPSC may lead to the formation of malignant tumors when transplanted into the host (Fujikawa et al., 2005). Thus, throughout the years several strategies have been explored to remove these cell contaminants and improve the purity of hPSC-CMs. For instance, the use of percoll gradients (Xu et al., 2002), Flow Activated Cell Sorting for specific surface markers (Skelton et al., 2014) and for cells incubated with mitochondrial dyes (Hattori et al., 2010) or molecular beacons (Wile et al., 2014) have already been reported. Recently, synthetic miRNA switches were used to efficiently purify hPSC-CMs. However, these approaches are neither economically nor practically viable for large scale production of hPSC-CMs. Switches encoding the apoptosis inducer Bim improved enrichment of CMs without cell sorting (Miki et al., 2015). It remains to be validated whether this strategy can be applied for lineage purification in large-scale and the efficiency achieved. Nguyen and colleagues demonstrated that the combined technique of forced aggregation and 3D suspension culture is capable of robustly and rapidly enriching CMs from heterogeneous differentiation cultures (Nguyen et al., 2014).

One elegant, cheaper and more scalable approach is to culture hPSC-CM in medium containing lactate (Lac) instead of glucose (Glc) (Tohyama et al., 2013). Since in hPSC and fibroblasts, Glc is the major source of energy, only CMs, which can use both metabolites, survive when cultured in this medium (Tohyama et al., 2013). From an engineering perspective this method is perfectly compatible with large-scale bioreactor approaches for cell production (Natsuko et al., 2014).

### **1.7. Maturation of hPSC-CMs**

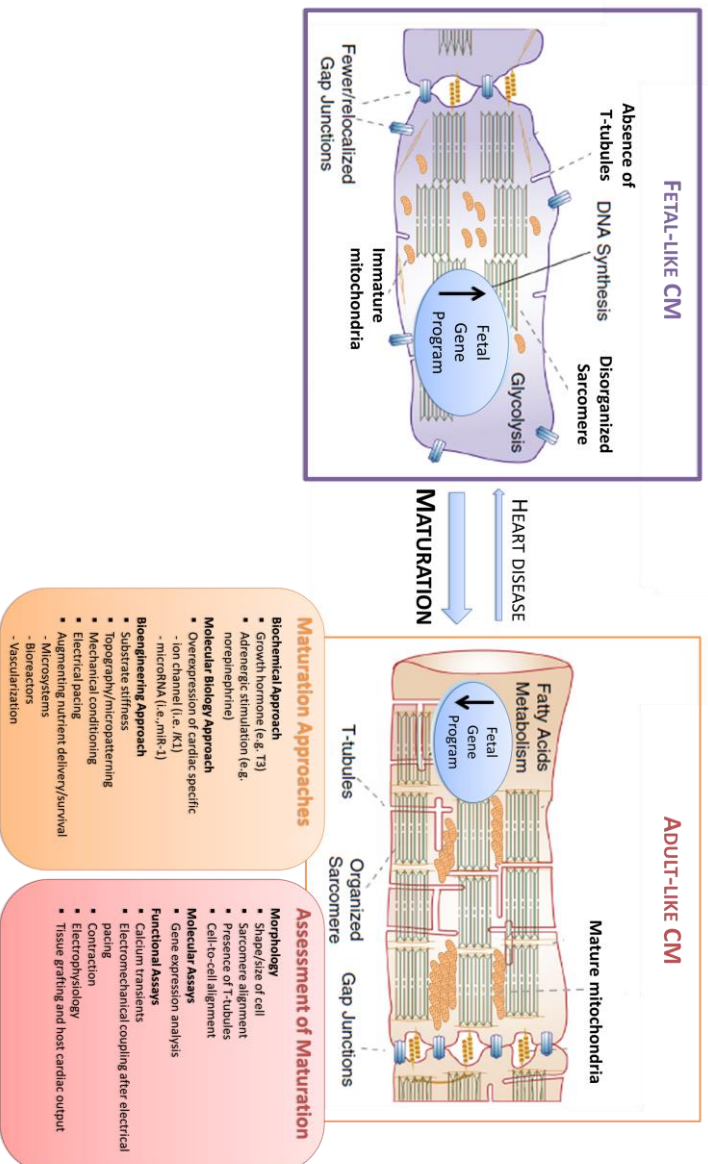
Notwithstanding the progress made in improving differentiation protocols, the generated hPSC-CMs obtained remain with a immature phenotype, consistent with mid-gestation of human foetal heart development (Veerman et al., 2015), in terms of structure/morphology (Snir et al., 2003), gene expression (Synnergren et al., 2012), metabolism (Lopaschuk and Jaswal, 2010), contractile function and electrophysiology (Brito-Martins et al., 2008). hPSC-CMs are smaller in size have irregular shapes (round/oval rather than rod-like shapes), show disorganized sarcomeres,

metabolic dependence on glycolysis, reduced contraction force, and small action potentials (APs) compared with adult working CMs (Veerman et al., 2015).

Table 1.5 provides a summary of the main differences between hPSC-CMs and adult CMs. hPSC-CMs immaturity is currently a critical obstacle hampering the potential of these cells for clinical applications, modeling late-onset diseases, and accurate drug testing (White et al., 2016). In the context of tissue repair, their immature properties such as spontaneous activity and slow conduction may cause lethal arrhythmias after transplantation in the heart (Chong et al., 2014). Thus, a wide range of strategies (biochemical, molecular biology and bioengineering approaches) to improve maturation of hPSC-CM *in vitro* have been explored so far (Figure 1.4) (Tzatzalos et al., 2016; Veerman et al., 2015; Yang et al., 2014a). These include the overexpression of microRNAs that regulate cardiac development (Kuppusamy et al., 2015); addition of chemical supplements to the culture medium, like the growth hormone T3 (Yang et al., 2014b); culture of hPSC-CMs in organic or synthetic scaffolds coupled with cyclic stretching (Mihic et al., 2014) and/or electrical cues (Heidi Au et al., 2009); co-culture of hPSC-CMs with non-CM (e.g. fibroblasts or endothelial cells; (Kim et al., 2010); growth as 3-D tissues (Zhang et al., 2013), which have been reported to improve the maturation status as assessed by the cell morphology, molecular assays (e.g. expression of cardiac markers) and functional assays. However up to now, there is no current consensus as to what constitutes a mature adult CM or which approaches for maturation assessment can be used to accurately and specifically track the maturity of hPSC-CMs, which hampers the comparison of the results obtained between different maturation approaches. Also various structural or physiological markers – e.g.  $\text{Ca}^{2+}$  handling, cell morphology/striation pattern, and beating – undergo developmental reversion under conditions of pathological hypertrophy or disease (Feric and Radisic, 2016), which may mislead the results. In sum, despite the recent advances in the field, a mature phenotype fully recapitulating adult CMs has yet to be achieved.

**Table 1.5. Phenotypic differences between adult-CMs and hPSC-CMs in terms of structure, sarcoplasmic reticulum (SR), gene expression, metabolism and electrophysiology.** (Denning et al., 2015)

	Adult-CM	hPSC-CM
<b>Structure</b>	Rod-shaped Longitudinally aligned ~30% cells bi- or poly-nuclear Highly organised 5–9.5:1 Z-discs, I-, H-, A- and M-bands 2.2 $\mu\text{m}$ Well developed e.g. CSQ, PLN, RYR2, SERCA/ATP2A2 Yes	Round or polygonal Chaotically organised Very limited bi-nucleation Disorganised 2–3:1 Mainly Z-discs and I-bands 1.6 $\mu\text{m}$ Mixed response: caffeine, Thapsigargin & ryanodine Expression lower than adult No
<b>SR</b>	Sarcomere length Sarcoplasmic reticulum SR proteins T-Tubules	
<b>Expr.</b>	Gene expression MYH7 ( $\beta$ -MHC) > MYH6 ( $\alpha$ MHC) TNNI3 (cTnl) > TNNI1 (foetal ssTnl) MYL2 (MLC2v) > MYL7 (MLC2a) Titin isoform N2B predominates ADRA1A ( $\alpha$ -adrenoceptor) expressed	MYH6 ( $\alpha$ MHC) > MYH7 ( $\beta$ MHC) TNNI1 (foetal ssTnl) > TNNI3 (cTnl) MYL2:MYL7 ratio not determined Titin isoform N2BA predominates ADRA1A ( $\alpha$ -adrenoceptor) not expressed Glucose and lactate but can use fatty acids
<b>Energy &amp; force</b>	Metabolism Energy production Mitochondria Beating Force Capacitance Resting mem potential Upstroke velocity Conduction velocity Location of gap junctions	Mainly oxidative phosphorylation Near nuclei; numbers increase during differentiation Many cells spontaneous 0.08–4 $\text{mN}/\text{mm}^2$ (3D constructs) ~200 nN (single cells) 20–50 pF –20 to –60 mV 10–50 V/s 10–20 $\text{cm}/\text{s}$ Circumference of cells
<b>Conduct<sup>a</sup></b>		



**Figure 1.4. Main approaches used to improve hPSC-CM maturation and parameters typically evaluated to assess maturation status of hPSC-CMs.** Many strategies have been reported for the maturation of hPSC-CMs including: biochemical approaches (addition of growth hormones or adrenergic agonists to induce changes in CM function), molecular biology approaches (cardiac specific ion channels and microRNA are overexpressed to elicit changes in the electrophysiology and calcium handling of CMs), bioengineering approaches (improve sarcomeric organization and contractile function by incorporating controlled substrate stiffness, topography, electrical/mechanical conditioning, and integrated systems that improve nutrient delivery). Assessment of CM maturation status ranges from examining morphology (i.e., cell shape/size, sarcomeres, T-tubules, and alignment), to molecular assays (sarcomeric and ion channel expression), and functional assays (i.e., calcium transients, electromechanical coupling, contraction, electrophysiology, and tissue grafting). Adapted from (Tzatzalos et al., 2016).

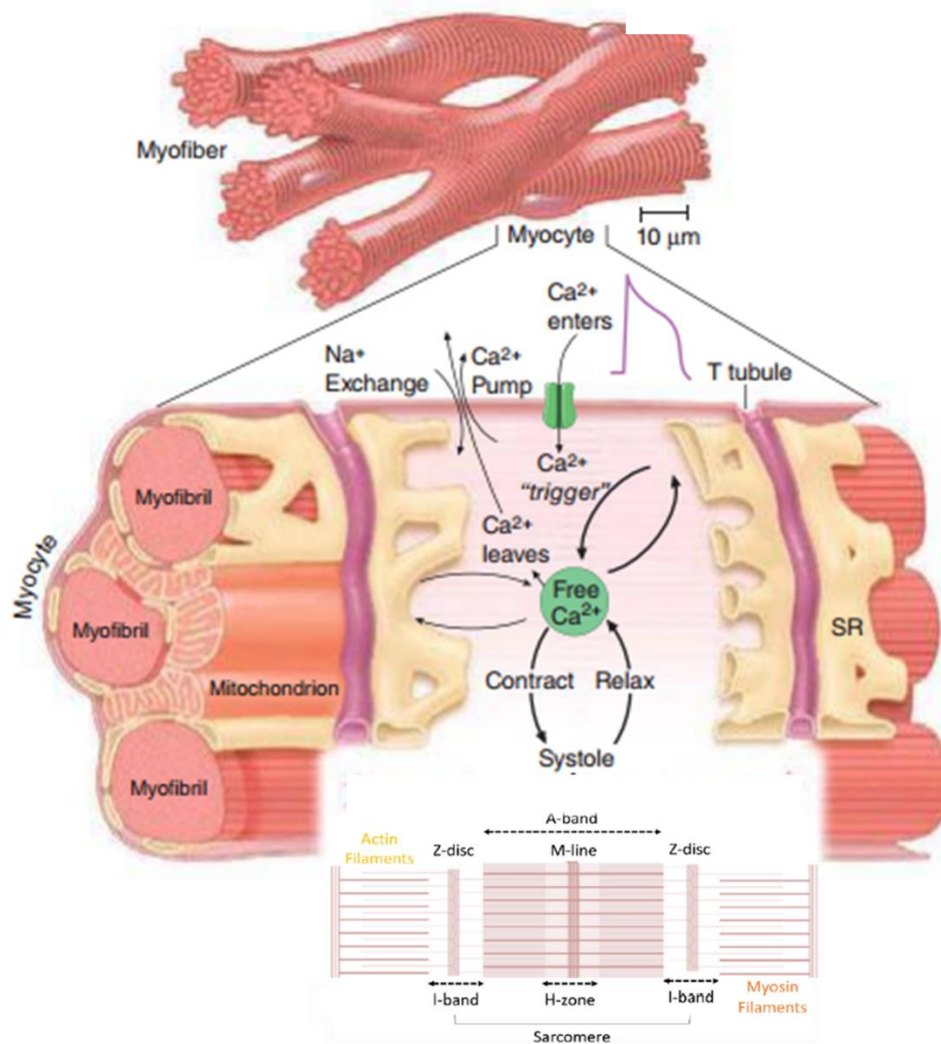


### 1.7.1. Cardiomyocyte structure and contraction

Adult CMs have an elongated rod-like shape and present a highly organized internal structure composed of numerous parallel myofibrils, which consist of longitudinal repetitions of sarcomeres, the functional units of muscle (Gerdes et al., 1992). CM shape and sarcomere alignment have functional implications in excitation-contraction coupling and in the generation of contractile force (Chung et al., 2007). During pathogenic hypertrophy CMs adopt a rounder shape and display disorganized sarcomeres (Dorn 2nd et al., 2005), as such pathogenic growth has been reported to accompany several forms of heart disease (Engelhardt et al., 1999). In contrast, in physiological hypertrophy, which occurs during normal heart development, the addition of new sarcomeric units is in longitudinal series or parallel to pre-existing ones thus maintaining sarcomere alignment and CM shape (Dorn 2nd et al., 2005).

The sarcomere is composed of a complex assembly of both thick and thin filaments, the former consists of myosin while the latter includes actin, troponin and tropomyosin. Each sarcomere is delimited at either end by a Z-disc, which is included in the I-band, composed by thin filaments that extend in both directions (Figure 1.5). The A-band comprises the portion of the sarcomere where thick and thin filaments overlay, while the H-zone in the center of the A-band contains only thick filaments. In the middle of the H-zone is the M-line that corresponds to the center of the sarcomere (Huxley, 2002).

During an action potential of adult CMs, membrane depolarization activates voltage gated calcium ( $\text{Ca}^{2+}$ ) channels allowing the entry of  $\text{Ca}^{2+}$  into the cell. This triggers the release of  $\text{Ca}^{2+}$  from the sarcoplasmic reticulum in a positive feedback process, the  $\text{Ca}^{2+}$ -induced- $\text{Ca}^{2+}$  release (Altamirano and Bers, 2007). The binding of  $\text{Ca}^{2+}$  to troponin induces a conformational change and displaces tropomyosin, thereby exposing the binding sites of actin to which energized myosin heads will attach forming cross-bridges (Lehman et al., 1994). Consequent release of ADP and  $\text{P}_i$  (inorganic phosphate) bend the myosin heads, which switch to a low energy state, pulling the actin filaments toward the center of the sarcomere (M-line). Binding of ATP to the myosin heads lead to cross-bridge detachment, and ATP hydrolysis restores myosin to the energized state and raised conformation. Since thin filaments are anchored to the Z-discs, this process leads to sarcomere shortening, thus resulting in cell contraction (Huxley, 2002). During relaxation,  $\text{Ca}^{2+}$  is pumped back into the sarcoplasmic reticulum and to a lesser degree extruded from the cell, so as to return the cell to resting  $\text{Ca}^{2+}$  levels. As  $\text{Ca}^{2+}$  detaches from troponin, this protein returns to the initial conformation simultaneously moving tropomyosin to cover the actin binding sites. This blocks myosin from forming cross-bridges, therefore a new cycle of contraction is only possible after a new *stimuli* (Altamirano and Bers, 2007).



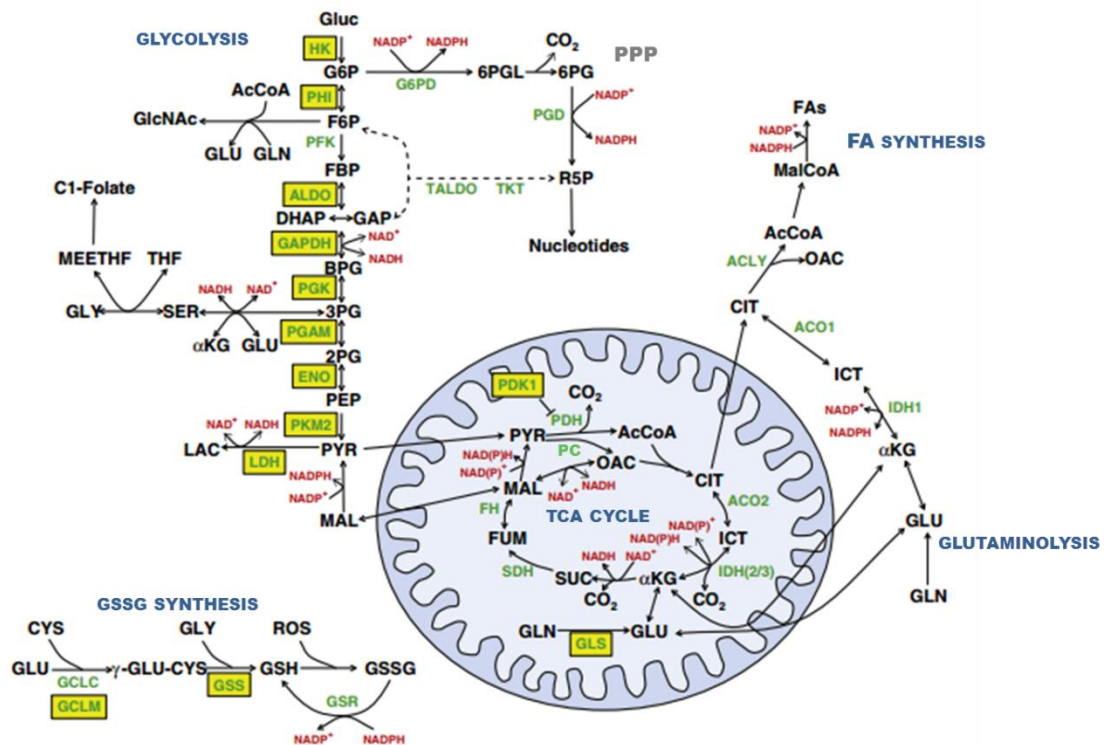
**Figure 1.5. Schematic representation of myofibril organization and ultrastructural features of sarcomeres.** The critical role played by changes in  $[Ca^{2+}]$  in the cytosol of CMs is also highlighted.  $Ca^{2+}$  ions are schematically shown as entering through the calcium channel that opens in response to the wave of depolarization that travels along the sarcolemma. These  $Ca^{2+}$  ions “trigger” the release of more calcium from the sarcoplasmic reticulum (SR) and thereby initiate a contraction-relaxation cycle. Adapted from (Feric and Radisic, 2016; Opie, 2004).

### 1.7.2. Metabolic dynamics during heart development

hESCs and hiPSCs, rely mainly on glycolysis (Facucho-Oliveira and St John, 2009), to produce energy (ATP's). PSCs have unlimited self-renewal capacity and thus to maintain high level of proliferation, these cells should balance energetic and biosynthetic needs (Zhang et al., 2012). Glycolytic flux is therefore elevated in PSCs to provide ATP and intermediate metabolites through the pentose phosphate pathway (PPP) for the synthesis of nucleotide and reducing equivalents in the form of nicotinamide adenine dinucleotide phosphate (NADPH).

NADPH is particularly important to regulate the abundance of oxidative species (ROS) by maintaining glutathione (GSH) in the reduced state. The TCA cycle in PSCs provides intermediate metabolites such as citrate and  $\alpha$ -ketoglutarate that are siphoned for lipid and amino acid biosynthesis (Figure 1.6) (Zhang et al., 2012). The incessant contractile function of the human

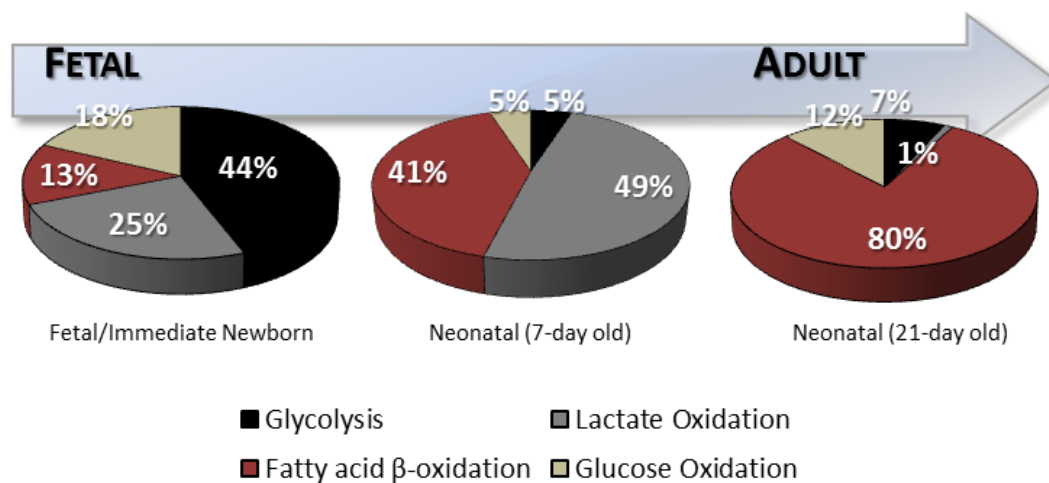
heart, along with CMs minimal ability to store high-energy phosphates, results in a high metabolic demand requiring a continuous high production rate of ATP to sustain proper cell function (Lopaschuk and Jaswal, 2010; Schönfeld et al., 1996). However, the metabolic profile of the fetal heart is not compliant with this demand, since at this point of development CMs are highly dependent on glycolysis, and to a lesser extent lactate oxidation, to produce ATP (Lopaschuk and Jaswal, 2010). Hence, during heart development, a metabolic shift occurs from primarily glycolytic to an oxidative metabolism (Ellen Kreipke et al., 2016; Gaspar et al., 2014; Kolwicz et al., 2013).



**Figure 1.6. Metabolic pathways that are regulated to support stem cell growth *in vitro*.** Glucose taken up by cells is phosphorylated and metabolized in glycolysis, the hexosamine biosynthesis pathway, or the pentose phosphate pathway (PPP). Glucose-derived pyruvate is either diverted to lactate or oxidized in the TCA cycle to support energy generation in mitochondria or biosynthesis in the cytosol. Anaplerotic pathways including glutaminolysis and pyruvate carboxylase are often necessary to maintain flux through the TCA cycle. Reduced glutathione (GSH) is synthesized from glutamate, cysteine, and glycine and protects cells from oxidative damage by reacting with ROS. Enzymes which are differentially regulated in stem cell populations are highlighted in yellow. Adapted from (Vacanti and Metallo, 2013).

The fetal heart resides in a low oxygen environment where levels of circulating fatty acids are low (less than 0.1 mM (Lopaschuk and Jaswal, 2010)), therefore fetal CMs rely mainly on glycolysis for ATP generation, with fatty acid  $\beta$ -oxidation contributing for only a small fraction (less than 15%) of the total myocardial ATP production (Figure 1.7). The glycolytic phenotype of the fetal heart may in part be due to transcriptional changes mediated by HIF-1 $\alpha$ . This transcription factor increases the activities of glycolytic enzymes and the regulation of the glycolytic pathway itself. Furthermore, the fetal heart predominantly expresses LDH-A, which effectively converts pyruvate to lactate, contributing to maintaining the high glycolytic levels. Despite the high reliance on glycolysis and low fatty acid oxidation rates, fetal hearts have the ability to readily extract and

oxidize lactate, which is present at high levels in the fetal heart. As such, lactate oxidation accounts for the majority of myocardial oxygen consumption in the fetal heart. In the neonatal heart, though, the metabolic profile of CMs undergoes a substantial shift. After birth, there is an increased workload placed on the heart, as well as a period of significant cellular growth characterized by hypertrophy (ie, increased cell size/growth) and binucleation. As such, the metabolic demands placed on the CMs greatly increase, exceeding the cells' ability to keep pace via glucose and lactate oxidation alone. Furthermore, after birth blood levels of lactate drastically decrease (from 5–7 mM to approximately 0.5 mM (Lopaschuk and Jaswal, 2010)). As such, the contribution of lactate oxidation to ATP production in neonatal period also markedly decreases. Nonetheless, the circulating levels of free fatty acids increase immediately after birth to levels that are normally seen in adults (0.2–0.4 mM (Lopaschuk and Jaswal, 2010)). Concomitantly there is also an increase in the contribution of fatty acid  $\beta$ -oxidation to overall cardiac energetics. This, combined with transcriptional regulation of proteins involved in fatty acid oxidation (e.g. through PGC-1 $\alpha$ /PPAR $\alpha$  (Lopaschuk and Jaswal, 2010)), mediates a switch in the metabolic profile of CMs from being glycolysis-dependent as immature CMs to predominately relying on oxidative metabolism as mature CMs (Lopaschuk et al., 2010). Nevertheless, CMs retain metabolic plasticity to use other substrates (glucose, lactate, amino acids, ketone), depending on their availability (Kolwicz et al., 2013; Lopaschuk and Jaswal, 2010).



**Figure 1.7. Overview of the various pathways of energy substrate metabolism that contribute to the production of ATP for the purposes of maintaining contractile function and the requirements of basal metabolism in CMs.** Percent contributions of glycolysis and oxidative metabolism including glucose oxidation, lactate oxidation, and fatty acid oxidation to cardiac ATP production during the immediate newborn/fetal period and the neonatal period (from 7 to 21 days) in the isolated working rabbit heart. Adapted from (Lopaschuk and Jaswal, 2010).

*In vitro*, hPSC-CMs rely mainly on glycolysis when cultured in glucose media even if glucose is present at low concentrations and in combination with other substrates, such as fatty acids (Rana et al., 2012; Tohyama et al., 2013). In the absence of glucose, hPSC-CMs were able to metabolize other substrates, such as lactate and galactose to support cell function (Rana et al., 2012; Tohyama et al., 2013). Notably, galactose alone or in combination with fatty acids was able to

induce the metabolic switch in hiPSC-CMs, as well as an increase in mitochondrial reserve and maximum respiratory capacity (Rana et al., 2012). Even so, a link between the metabolic shift and maturation of hPSC-CM *in vitro* has not been established yet.

### 1.8. Characterization of hPSC-CMs

Phenotypic characterization of the generated hPSC-CMs is essential to evaluate the outcome of the differentiation protocols. For cell therapies, characterization of the cells to be used in transplantation is important to minimize the risk of host rejection, tumor formation or arrhythmias (Dierickx et al., 2012). In the last few years, extensive characterization of PSC-CMs have been carried out to evaluate and confirm their cardiac phenotype through gene and protein expression, morphology, (ultra)structural, electrophysiology, calcium and contractility analysis (Figure 1.8A) (Mummery et al., 2012; Vidarsson et al., 2010).

Flow cytometry (Figure 1.8B) provides a quantitative method to evaluate the purity of the differentiated and enriched population, by measuring the number of cells expressing cardiac-specific proteins (Dierickx et al., 2012). Reverse transcription-polymerase chain reaction (RT-PCR, Figure 1.8C) can be used to assess changes in gene expression throughout the differentiation process. Recently, due to their robustness and unlimited data generated, proteomics and transcriptomics analysis are also becoming a routine approach for proteome and transcriptional profiling in some laboratories, replacing the more traditional techniques.

Immunofluorescence microscopy (Figure 1.8D) using antibodies for specific cardiac proteins is routinely used for structural characterization of CMs (Mummery et al., 2012).

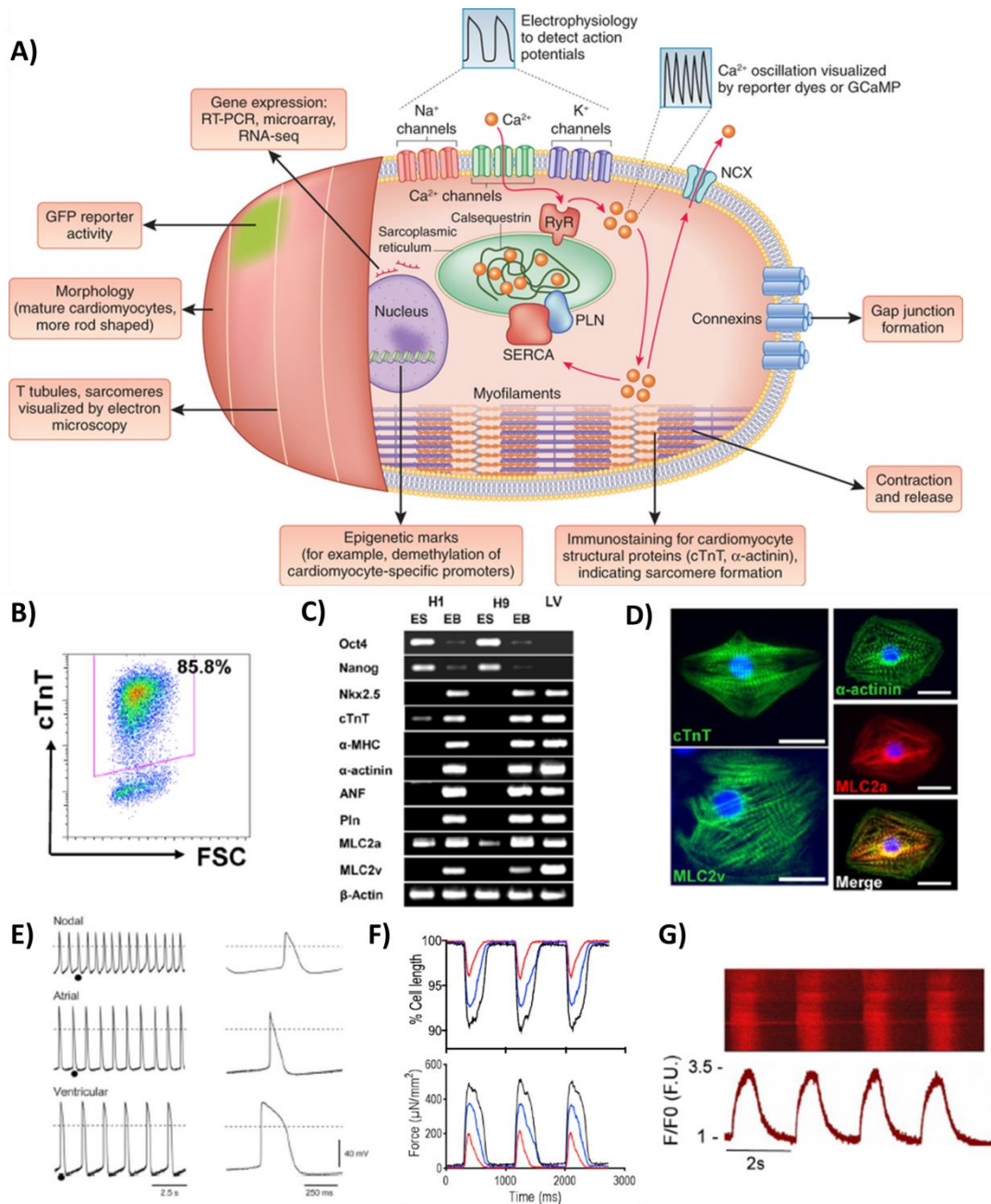
CMs are also characterized based on their functional properties (Figure 1.8E-G). The hallmarks of CM function are the generation of an action potential, the influx of calcium ions, and the consequent cellular contraction and force generation. For a comprehensive assessment of CM function, all of these processes have to be simultaneously evaluated (Rajala et al., 2011; Vidarsson et al., 2010). Electrophysiological analyses (including patch clamp techniques) are often used to measure action potentials (APs, Figure 1.8E) and evaluate the response to adrenergic/cholinergic stimulation as well as to chemicals that can act on various types of ion channels. Calcium indicator assays (e.g. Fluo-4, Rhod-3) are routinely used to assess calcium transients (Figures 1.8G). Since intracellular  $\text{Ca}^{2+}$  concentration ranges from hundreds of nanomolar to millimolar, calcium imaging using a  $\text{Ca}^{2+}$  sensitive fluorescence dye and confocal microscopy revealed a convenient and reliable way to assess calcium transients. Small molecule voltage sensor probes (VSPs) like the ANEPPS dyes are also being used to study APs in CMs (Denning et al., 2015). These lipophilic fluorescent molecules bind to the cell membrane and alter their emission properties in response to changes in a transmembrane voltage potential as the membrane depolarizes, allowing action potential detection with high spatial and temporal resolution (Herron, 2016). Therefore VSPs show some advantages over the high complex, low-throughput, labour-intensive conventional patch clamp electrophysiology. The major limitations of the fluorescent dyes are their inherent phototoxicity, which can cause temporal degradation of sample and signal quality over time,

thereby limiting recording times (Liao et al., 2015). Also VSPs provide surrogates of membrane potentials and tend to overestimate action potential duration (Liao et al., 2015).

Excitation–contraction coupling leads to force generation, which is the ultimate goal of the working myocardium (Figure 1.8F) (Denning et al., 2015; van Meer et al., 2016). CM force generation has been assessed previously by a number of different methods, including fluorescent microsphere-based traction force microscopy, atomic force microscopy, and micropost deformation measurements (Liu et al., 2012; McCain et al., 2014; Rodriguez et al., 2014). However, these techniques are highly specialized, require advanced instrumentation, and each method measures and reports force in a different way, which hampers cross-comparison of the values produced in different studies.

Recently, Kijlstra and colleagues reported a novel method that is based on transmitted light microscopy to calculate the kinetics of contraction through an algorithm evaluating frame-to-frame similarities. This technique compares well with other measurement techniques, and can be applied simultaneously with other single-cell physiological assays for the quantification of calcium cycling and action potentials (Kijlstra et al., 2015).

The metabolites involved in biochemical reactions can be identified and quantified using omic technologies (Smith et al., 2006; Sreekumar et al., 2009). Analysis of the metabolome, the complete set of small-molecule chemicals, can provide useful information on the metabolic flux distributions occurring in the cell, which by turn are a function of gene expression, protein modifications and interactions at different levels (Nielsen, 2003; Nöh and Wiechert, 2011). Comparing with regulatory networks composed of protein-DNA and protein-protein interactions, where there are still many unknown components, metabolic networks consisting of all metabolic reactions occurring in cellular metabolism can be described and predicted using mathematical models (Price et al., 2003). However, accurate estimation of metabolic fluxes can only be achieved using a combination of computational, intra-metabolomic (intracellular metabolites) and extra-metabolomic (extracellular metabolites, that is, present in the cell culture medium) techniques, including isotopic tracing studies (using substrate molecules in which one or more of the atoms is replaced by a different isotope) (Kelleher, 2004; Oldiges et al., 2007). Isotopic tracers have been used since the inception of metabolism investigation in the 20<sup>th</sup> century. These were firstly radioactive species (e.g. <sup>14</sup>C, <sup>3</sup>H) administered to cells in small quantities followed by the measurement of radioactivity in end products and other metabolites (Gibbs et al., 1954; Kelleher, 2001). The use of parallel radioisotope experiments allowed the determination of structures, precursors and activities of pathways such as PPP, TCA cycle, anaplerosis, gluconeogenesis and fatty acid metabolism. More recently, advances in stable isotope (e.g. <sup>13</sup>C, <sup>2</sup>H, <sup>15</sup>N) measurement through nuclear magnetic resonance (NMR) and mass spectrometry (MS) have replaced the use of radioactive isotopes in metabolic studies, owing to easier experimental implementation and greater information generated (Bier, 1987). Stable isotope experiments, when combined with metabolic flux analysis (MFA), allow the greatest quantitative resolution of metabolic flux distributions in cultured cells.



**Figure 1.8. Methodologies routinely used for characterization of hPSC-CMs.** **A)** Schematic representation of the phenotypic features of CMs typically assayed to determine the quality of the generated hPSC-CMs. These specific features range from expression of a panel of genes or the activation of a reporter transgene (such as  $\alpha$ -MHC-GFP) to more complex functional characteristics, such as the ability to fire action potentials and show calcium oscillation. Other characteristics include the presence of cardiomyocyte-specific epigenetic marks, the ability of CMs to generate force, form gap junctions and electrically couple with host CMs after transplantation. **B)** Flow cytometry is a quantitative method to evaluate relative yield and purity of CMs. **C)** Reverse transcription-polymerase chain reaction is used as a first assessment for changes in gene expression typical of cardiogenesis. **D)** Immunofluorescence microscopy with antibodies specific for myofilament proteins determines whether cells exhibit organized sarcomeres typical of CMs. **E)** Functional assessment of CMs can be provided by cellular electrophysiology measurements to determine whether cardiac action potentials of different CM subtypes are present; **F)** Assessment of contractile kinetics quantifies the contraction force generated by CMs; **G)** Detection of Ca<sup>2+</sup> transients typical of CMs providing another assessment of functional integrity of differentiating CMs. Adapted from (Addis and Epstein, 2013; Mummy et al., 2012).

In fact MFA is currently the preferred technique to obtain quantitative data about *in vivo* metabolism (Woo Suk and Antoniewicz, 2013). Initially, MFA studies relied on metabolite balances within an assumed network stoichiometry, where external rate measurements provided constraints to determine intracellular fluxes. However this approach could not distinguish fluxes of parallel pathways (e.g. glycolysis vs. PPP), reversible reactions, and cyclic pathways. A shortcoming overcome by combining MFA with measurement of the metabolic conversion of stable isotopic tracers, like  $^{13}\text{C}$ , by mass spectrometry or nuclear magnetic resonance (Goudar et al., 2010). Thus, providing additional independent constraints for flux estimation, greatly improving quantitative resolution of metabolic flux distributions, at the expense of increased experimental and computational complexity. The elementary metabolic unit (EMU) method is considered the most advanced and efficient computational approach for simulating isotopic labeling distributions (Antoniewicz et al., 2007).

In summary, nonstationary  $^{13}\text{C}$ -MFA relies on computational simulation to estimate a set of feasible intracellular metabolic fluxes that minimize the variance-weighted sum of squared residuals between the predicted and measured transient  $^{13}\text{C}$ -labeling data and extracellular rate measurements (Woo Suk and Antoniewicz, 2013). Despite the increasing role of nonstationary  $^{13}\text{C}$ -MFA in metabolism studies of a wide range of biological systems (Carinhas et al., 2016; Hofmann et al., 2008; Woo Suk and Antoniewicz, 2013), a metabolic network model of hiPSC-CMs has yet to be explored.

### **1.9. Hypothermic storage of hPSC-CMs**

The therapeutic use of hPSC-CMs is also dependent on developing efficient and scalable methods for storage of CMs. Several companies and academic institutes have aimed at establishing good manufacturing practices (GMP) compatible, efficient and customized protocols for storage of hPSC-CMs (reviewed in (Abbasalizadeh and Baharvand, 2013)). For successful cell therapies, banking and recovery of stored cells must be accomplished without compromising cell viability or function (Abbasalizadeh and Baharvand, 2013). Preserving cells also allows the generation of master and working cell banks so that consistent and quality-controlled off-the-shelf cells are available for *in vitro* toxicology studies or drug screening purposes (Hunt, 2011). Nonetheless, cryopreservation of CMs is considered a critical step, since it can exert tremendous influence on CM viability and irreversible effects on CM quality. Cryopreservation-induced events, such as ice crystallization or osmotic shock induced-necrosis, activated apoptosis, disruption of cell-cell and cell-ECM adhesions, affect survival and fate of stored cells during cryopreservation (Preininger and Singh, 2016). Thus, developing of improved cryopreservation and storage processes that have minimal adverse effects on hPSC-CMs is crucial for successful banking and shipping (Coopman, 2011).

Cold storage preservation (or hypothermic storage) may constitute an alternative approach for transport and delivery of cells during short time periods (Coopman, 2011). Hypothermic storage consists in the use of non-frozen temperatures to store biologics. The temperatures used often range between 4 and 10°C. Hypothermic storage currently serves as the most effective strategy for



organ preservation, therefore several efforts have been made towards improving the hypothermic storage protocols including the development of efficient commercial and clinical grade hypothermic solutions. Specifically, commercially available hypothermic solutions (e.g. Prime-XV™ Hypothermic Preservation Solution, Irvine Science, and HypoThermosol®-FRS, BioLife Solutions Inc.) were carefully formulated to maintain the ionic and osmotic balances, inhibit acidosis, and prevent cell swelling at low temperatures. These features facilitate preservation of cell homeostasis, which is not achievable when using standard culture medium as a preservation formulation. The development of efficient hypothermic storage strategies for hPSC-CMs will enable cell products to be manufactured off-site in certified companies and then shipped to clinical, biopharmaceutical companies or to research institutes worldwide.

## 2. Scope of the thesis

This thesis aims at developing novel approaches for robust generation of relevant numbers of hPSC-CMs with high purity and enhanced maturity to fulfill the needs of clinical and pre-clinical applications. The strategy consisted in modulating key environmental factors (such as oxygen tension and bioreactor hydrodynamics), cell culture configuration (3D cell aggregates vs. 2D monolayers), and metabolic substrate availability to improve reproducibility, scalability and efficiency of hPSC differentiation towards CMs *in vitro*. The impact of these parameters on cell production yields and on cell's quality was assessed using a set of “-omics” tools (including transcriptomics, metabolomics and fluxomics) and a vast range of cell characterization assays. The design of efficient clinically compatible methods for short-term storage of the generated hPSC-CMs was also addressed to facilitate global distribution of these cells.

The major aims of each chapter of this thesis are summarized in Figure 1.9.

Briefly, **Chapter 2** focused on the development of robust, scalable and integrated platforms for iPSC-derived CM production and enrichment using bioreactor systems with automated process control, including online measurement and adjustment of the culture parameters. The effect of dissolved oxygen and mechanical forces, on CM differentiation, using different hydrodynamic environments through the use of distinct bioreactor systems (Stirred tank and WAVE bioreactors), was evaluated. A spontaneous differentiation protocol was used to identify the impact of each process variable tested.

**Chapter 3** aimed to establish a reproducible protocol for directed differentiation of hPSCs towards CMs, suitable to generate CMs in both 2D monolayer and 3D aggregate culture formats. Specifically, 3D aggregation was promoted after addition of growth factors and small molecules, when the culture was enriched in hPSC-derived cardiac progenitors. An integrated experimental and computational systems biology approach was pursued to compare the differentiated populations obtained in both culture configurations in terms of CM purity, transcriptome, metabolome, fluxome and functionality. The modest expression of maturation features and the predominant fetal-like glycolytic metabolism observed in both culture conformations by the end of the directed differentiation process, motivated to investigate whether alterations in culture medium

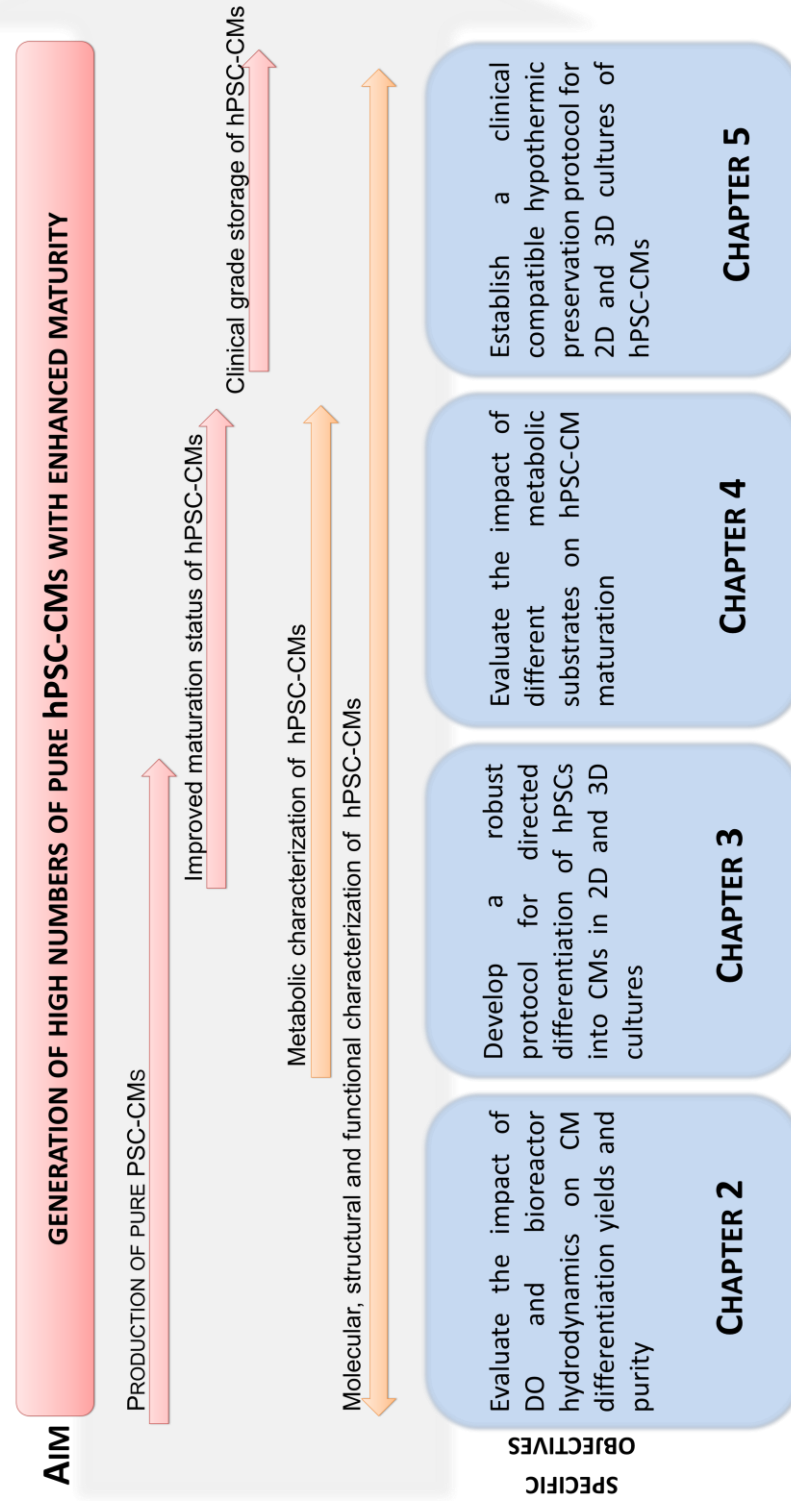
composition to mimic substrate availability during *in vivo* cardiac development would promote *in vitro* hPSC-CM maturation. Therefore, in **Chapter 4** several culture media compositions were tested based on the fact that during cardiac development CMs undergo postnatal metabolic changes, from a glycolytic to an oxidative metabolism, relying first on Lac and then on FA as major sources of energy (Lopaschuk and Jaswal, 2010). Transcriptomic, metabolomic and fluxomic analyses were carry out and the data obtained were combined with structural, morphological and functional analyses to provide a comprehensive molecular basis and a quantitative dissection of hiPSC-CM phenotypes. Noteworthy, this systems-level approach enabled the identification of the feeding strategy that most efficiently improved metabolic, structural and functional maturation of hiPSC-CM in 20 days.

In **Chapter 5** efficient strategies for short-term storage of the produced hPSC-CMs without affecting their viability, phenotype and function were developed. The feasibility to cold store 2D monolayers and 3D aggregates of functional hPSC-CMs using a fully-defined clinical compatible formulation was investigated and the time frame for hPSC-CM hypothermic storage without detrimentally affecting cell viability and metabolic activity recovery was determined. The efficiency of the method was also confirmed by assessing cell phenotype, including structure, ultrastructure, gene and protein expression, and functionality after storage.

It is important to highlight that several analytical tools were implemented (or adapted) in the laboratory to evaluate the efficiency of the approaches developed and assess the quality of the generated CMs in terms of morphology/structure (immunofluorescent microscopy), gene and protein expression (quantitative RT-PCR, flow cytometry), metabolism ( $^{13}\text{C}$ -MFA, GC-MS-based metabolite profiling, Seahorse Extracellular Flux Analysers) and functionality (using  $\text{Ca}^{2+}$  dyes). Other methodologies were established and performed in collaboration with other institutions; Instituto Gulbenkian de Ciência (IGC) (TEM analysis); Medical Faculty, University of Cologne and Faculdade de Ciências Médicas, Universidade Nova de Lisboa (FCM-UNL) (Electrophysiology analysis); and Massachusetts General Hospital, Harvard Medical School (MGH-HMS) (contractility analysis).

In **Chapter 6**, the results described in **Chapters 2-5**, were discussed and contextualized with the available literature and state-of-the-art of the fields addressed throughout the thesis.

**Figure 1.9 – Schematic representation of the major aims of this thesis.** Arrows highlight the bioprocess workflow (red) and the qualitative and quantitative assessment of cell quality (orange).



### 3. References

- Aasen, T., Raya, A., Barrero, M.J., Garreta, E., Consiglio, A., Gonzalez, F., Vassena, R., Acute, J.B., Pekarik, V., Tiscornia, G., et al. (2008). Efficient and rapid generation of induced pluripotent stem cells from human keratinocytes. *Nat. Biotechnol.* *26*, 1276–1284.
- Abbasalizadeh, S., and Baharvand, H. (2013). Technological progress and challenges towards cGMP manufacturing of human pluripotent stem cells based therapeutic products for allogeneic and autologous cell therapies. *Biotechnol. Adv.* *31*, 1600–1623.
- Addis, R.C., and Epstein, J. a (2013). Induced regeneration--the progress and promise of direct reprogramming for heart repair. *Nat. Med.* *19*, 829–836.
- Altamirano, J., and Bers, D.M. (2007). Voltage dependence of cardiac excitation-contraction coupling: Unitary Ca<sup>2+</sup> current amplitude and open channel probability. *Circ. Res.* *101*, 590–597.
- Antoniewicz, M.R., Kelleher, J.K., and Stephanopoulos, G. (2007). Elementary metabolite units (EMU): A novel framework for modeling isotopic distributions. *Metab. Eng.* *9*, 68–86.
- Araki, R., Uda, M., Hoki, Y., Sunayama, M., Nakamura, M., Ando, S., Sugiura, M., Ideno, H., Shimada, A., Nifuji, A., et al. (2013). Negligible immunogenicity of terminally differentiated cells derived from induced pluripotent or embryonic stem cells. *Nature* *494*, 100–104.
- Atmanli, A., and Domian, I.J. (2016). Recreating the Cardiac Microenvironment in Pluripotent Stem Cell Models of Human Physiology and Disease. *Trends Cell Biol.* 1–13.
- Bauwens, C., Yin, T., Dang, S., Peerani, R., and Zandstra, P.W. (2005). Development of a perfusion fed bioreactor for embryonic stem cell-derived cardiomyocyte generation: oxygen-mediated enhancement of cardiomyocyte output. *Biotechnol. Bioeng.* *90*, 452–461.
- Beltrami, A.P., Barlucchi, L., Torella, D., Baker, M., Limana, F., Chimenti, S., Kasahara, H., Rota, M., Musso, E., Urbanek, K., et al. (2003). Adult cardiac stem cells are multipotent and support myocardial regeneration. *Cell* *114*, 763–776.
- Bergmann, O., Bhardwaj, R.D., Bernard, S., Zdunek, S., Barnabé-Heider, F., Walsh, S., Zupicich, J., Alkass, K., Buchholz, B.A., Druid, H., et al. (2009). Evidence for cardiomyocyte renewal in humans. *Science* *324*, 98–102.
- van Berlo, J.H., Kanisicak, O., Maillet, M., Vagnozzi, R.J., Karch, J., Lin, S.-C.J., Middleton, R.C., Marbán, E., and Molkentin, J.D. (2015). C-Kit<sup>+</sup> Cells Minimally Contribute Cardiomyocytes To the Heart. *Nature* *509*, 337–341.
- Brito-Martins, M., Harding, S.E., and Ali, N.N. (2008). Beta(1)- and Beta(2)-Adrenoceptor Responses in Cardiomyocytes Derived from Human Embryonic Stem Cells: Comparison with Failing and Non-Failing Adult Human Heart . *Br. J. Pharmacol.* *153*, 751–759.
- Brouwer, M., Zhou, H., and Nadif Kasri, N. (2016). Choices for Induction of Pluripotency: Recent Developments in Human Induced Pluripotent Stem Cell Reprogramming Strategies. *Stem Cell Rev* *12*, 54–72.
- Brown, M.E., Rondon, E., Rajesh, D., Mack, A., Lewis, R., Feng, X., Zitur, L.J., Learish, R.D., and Nuwaysir, E.F. (2010). Derivation of induced pluripotent stem cells from human peripheral blood T lymphocytes. *PLoS One* *5*, e11373.
- Burridge, P.W., Matsa, E., Shukla, P., Lin, Z.C., Churko, J.M., Ebert, A.D., Lan, F., Diecke, S., Huber, B., Mordwinkin, N.M., et al. (2014). Chemically defined generation of human cardiomyocytes. *Nat. Methods* *11*, 855–860.
- Cao, N., Liu, Z., Chen, Z., Wang, J., Chen, T., Zhao, X., Ma, Y., Qin, L., Kang, J., Wei, B., et al. (2012). Ascorbic acid enhances the cardiac differentiation of induced pluripotent stem cells through promoting the proliferation of cardiac progenitor cells. *Cell Res.* *22*, 219–236.
- Carinhas, N., Pais, D.A.M., Koshkin, A., Fernandes, P., Coroadinha, A.S., Carrondo, M.J.T., Alves, P.M., and Teixeira, A.P. (2016). Metabolic flux profiling of MDCK cells during growth and canine adenovirus vector production. *Sci. Rep.* *6*, 1–11.
- Carvajal-Vergara, X., and Prósper, F. (2016). Are we closer to cardiac regeneration? *Stem Cell Investig.* *3*, 59–59.

- Chen, V.C., and Couture, L.A. (2015). The Suspension Culture of Undifferentiated Human Pluripotent Stem Cells Using Spinner Flasks. *Methods Mol. Biol.* 13–21.
- Chen, V.C., Couture, S.M., Ye, J., Lin, Z., Hua, G., Huang, H.I.P., Wu, J., Hsu, D., Carpenter, M.K., and Couture, L.A. (2012). Scalable GMP compliant suspension culture system for human ES cells. *Stem Cell Res.* 8, 388–402.
- Chen, V.C., Ye, J., Shukla, P., Hua, G., Chen, D., Lin, Z., Liu, J. chang, Chai, J., Gold, J., Wu, J., et al. (2015). Development of a scalable suspension culture for cardiac differentiation from human pluripotent stem cells. *Stem Cell Res.* 15, 365–375.
- Chien, K.R., and Olson, E.N. (2002). Converging pathways and principles in heart development and disease. In *Cell*, pp. 153–162.
- Chong, J.J.H., and Murry, C.E. (2014). Cardiac regeneration using pluripotent stem cells-Progression to large animal models. *Stem Cell Res.* 13, 654–665.
- Chong, J.J.H., Yang, X., Don, C.W., Minami, E., Liu, Y.-W., Weyers, J.J., Mahoney, W.M., Van Biber, B., Cook, S.M., Palpant, N.J., et al. (2014). Human embryonic-stem-cell-derived cardiomyocytes regenerate non-human primate hearts. *Nature* 510, 273–277.
- Chung, C.Y., Bien, H., and Entcheva, E. (2007). The role of cardiac tissue alignment in modulating electrical function. *J. Cardiovasc. Electrophysiol.* 18, 1323–1329.
- Coopman, K. (2011). Large-scale compatible methods for the preservation of human embryonic stem cells: Current perspectives. *Biotechnol. Prog.* 27, 1511–1521.
- Dahlmann, J., Kensah, G., Kempf, H., Skvorc, D., Gawol, A., Elliott, D.A., Dräger, G., Zweigerdt, R., Martin, U., and Gruh, I. (2013). The use of agarose microwells for scalable embryoid body formation and cardiac differentiation of human and murine pluripotent stem cells. *Biomaterials* 34, 2463–2471.
- Deb, A., and Ubil, E. (2014). Cardiac fibroblast in development and wound healing. *J. Mol. Cell. Cardiol.* 70, 47–55.
- Denning, C., Borgdorff, V., Crutchley, J., Firth, K.S.A., George, V., Kalra, S., Kondrashov, A., Hoang, M.D., Mosqueira, D., Patel, A., et al. (2015). Cardiomyocytes from human pluripotent stem cells: From laboratory curiosity to industrial biomedical platform. *Biochim. Biophys. Acta - Mol. Cell Res.* 1863, 1728–1748.
- Dierickx, P., Doevendans, P.A., Geijsen, N., and van Laake, L.W. (2012). Embryonic template-based generation and purification of pluripotent stem cell-derived cardiomyocytes for heart repair. *J. Cardiovasc. Transl. Res.* 5, 566–580.
- Dorn 2nd, G.W., Force, T., and Li, G.W.D. (2005). Protein kinase cascades in the regulation of cardiac hypertrophy. *J Clin Invest* 115, 527–537.
- Drawnel, F.M., Boccardo, S., Prummer, M., Delobel, F., Graff, A., Weber, M., Gérard, R., Badi, L., Kam-Thong, T., Bu, L., et al. (2014). Disease modeling and phenotypic drug screening for diabetic cardiomyopathy using human induced pluripotent stem cells. *Cell Rep.* 9, 810–820.
- Eibl, R., Kaiser, S., Lombriser, R., and Eibl, D. (2010). Disposable bioreactors: The current state-of-the-art and recommended applications in biotechnology. *Appl. Microbiol. Biotechnol.* 86, 41–49.
- Ellen Kreipke, R., Wang, Y., Miklas, J.W., Mathieu, J., and Ruohola-Baker, H. (2016). Metabolic remodeling in early development and cardiomyocyte maturation. *Semin. Cell Dev. Biol.* 52, 84–92.
- Engelhardt, S., Hein, L., Wiesmann, F., and Lohse, M.J. (1999). Progressive hypertrophy and heart failure in beta1-adrenergic receptor transgenic mice. *Proc. Natl. Acad. Sci. U. S. A.* 96, 7059–7064.
- Evans, M.J., and Kaufman, M.H. (1981). Establishment in culture of pluripotential cells from mouse embryos. *Nature* 292, 154–156.
- Feric, N.T., and Radisic, M. (2016). Maturing human pluripotent stem cell-derived cardiomyocytes in human engineered cardiac tissues. *Adv. Drug Deliv. Rev.* 96, 110–134.
- Fridley, K.M., Kinney, M. a, and McDevitt, T.C. (2012). Hydrodynamic modulation of pluripotent stem cells. *Stem Cell Res. Ther.* 3, 45.
- Fujikawa, T., Oh, S.-H.H., Pi, L., Hatch, H.M., Shupe, T., and Petersen, B.E. (2005). Teratoma

formation leads to failure of treatment for type I diabetes using embryonic stem cell-derived insulin-producing cells. *Am. J. Pathol.* 166, 1781–1791.

Funakoshi, S., Miki, K., Takaki, T., Okubo, C., Hatani, T., Chonabayashi, K., Nishikawa, M., Takei, I., Oishi, A., Narita, M., et al. (2016). Enhanced engraftment, proliferation, and therapeutic potential in heart using optimized human iPSC-derived cardiomyocytes. *Sci. Rep.* 6, 19111.

Gaspar, J.A., Doss, M.X., Hengstler, J.G., Cadenas, C., Hescheler, J.J., and Sachinidis, A. (2014). Unique metabolic features of stem cells, cardiomyocytes, and their progenitors. *Circ. Res.* 114, 1346–1360.

Ge, X., Wang, I.-N.E., Toma, I., Sebastiano, V., Liu, J., Butte, M.J., Reijo Pera, R.A., and Yang, P.C. (2012). Human amniotic mesenchymal stem cell-derived induced pluripotent stem cells may generate a universal source of cardiac cells. *Stem Cells Dev.* 21, 2798–2808.

Gerdes, a M., Kellerman, S.E., Moore, J. a, Muffly, K.E., Clark, L.C., Reaves, P.Y., Malec, K.B., McKeown, P.P., and Schocken, D.D. (1992). Structural remodeling of cardiac myocytes in patients with ischemic cardiomyopathy. *Circulation* 86, 426–430.

Geuss, L.R., and Suggs, L.J. (2013). Making cardiomyocytes: how mechanical stimulation can influence differentiation of pluripotent stem cells. *Biotechnol. Prog.* 29, 1089–1096.

Gibbs, M., and Horecker, B.L. (1954). The mechanism of pentose phosphate conversion to hexose monophosphate. II. With pea leaf and pea root preparations. *J. Biol. Chem.* 208, 813–820.

Giorgetti, A., Montserrat, N., Aasen, T., Haase, A., Olmer, R., Schwanke, K., Wunderlich, S., Merkert, S., Hess, C., Zweigerdt, R., et al. (2009). Generation of induced pluripotent stem cells from human cord blood using OCT4 and SOX2. *Cell Stem Cell* 5, 353–357.

Gnecchi, M., Zhang, Z., Ni, A., and Dzau, V.J. (2008). Paracrine mechanisms in adult stem cell signaling and therapy. *Circ. Res.* 103, 1204–1219.

Goudar, C., Biener, R., Boisart, C., Heidemann, R., Piret, J., de Graaf, A., and Konstantinov, K. (2010). Metabolic flux analysis of CHO cells in perfusion culture by metabolite balancing and 2D [<sup>13</sup>C, <sup>1</sup>H] COSY NMR spectroscopy. *Metab. Eng.* 12, 138–149.

Günter, J., Wolint, P., Bopp, A., Steiger, J., Cambria, E., Hoerstrup, S.P., and Emmert, M.Y. (2016). Microtissues in Cardiovascular Medicine: Regenerative Potential Based on a 3D Microenvironment. *Stem Cells Int.* 2016.

Gwak, S., Bhang, S.H., Kim, I., Kim, S., Cho, S.-W., Jeon, O., Yoo, K.J., Putnam, A.J., Kim, B.-S., Ho, S., et al. (2006). The effect of cyclic strain on embryonic stem cell-derived cardiomyocytes. *Biomaterials* 27, 4409–4418.

Hananeh, F., Hassan, A., Saeed, A., Rezaei, L.M., Sahar, K., Shiva, H., Sharifi, Z.A., Alexis, B., M., B.G., Sara, P., et al. (2015). A Universal and Robust Integrated Platform for the Scalable Production of Human Cardiomyocytes From Pluripotent Stem Cells. *Stem Cells Transl. Med.* 4, 1–13.

Happe, C.L., and Engler, A.J. (2016). Mechanical Forces Reshape Differentiation Cues That Guide Cardiomyogenesis. *Circ. Res.* 118, 296–310.

Hartman, M.E., Dai, D.F., and Laflamme, M.A. (2016). Human pluripotent stem cells: Prospects and challenges as a source of cardiomyocytes for in vitro modeling and cell-based cardiac repair. *Adv. Drug Deliv. Rev.* 96, 3–17.

Hattori, F., Chen, H., Yamashita, H., Tohyama, S., Satoh, Y., Yuasa, S., Li, W., Yamakawa, H., Tanaka, T., Onitsuka, T., et al. (2010). Nongenetic method for purifying stem cell-derived cardiomyocytes. *Nat. Methods* 7, 61–66.

He, W., Ye, L., Li, S., Liu, H., Wang, Q., Fu, X., Han, W., and Chen, Z. (2012). Stirred Suspension Culture Improves Embryoid Body Formation and Cardiogenic Differentiation of Genetically Modified Embryonic Stem Cells. *Biol. Pharm. Bull.* 35, 308–316.

Heidi Au, H.T., Cui, B., Chu, Z.E., Veres, T., and Radisic, M. (2009). Cell culture chips for simultaneous application of topographical and electrical cues enhance phenotype of cardiomyocytes. *Lab Chip* 9, 564–575.

Herron, T.J. (2016). Calcium and voltage mapping in hiPSC-CM monolayers. *Cell Calcium* 59, 84–

90.

Hofmann, U., Maier, K., Reuss, M., and Mauch, K. (2008). Identification of metabolic fluxes in hepatic cells from transient <sup>13</sup>C-labeling experiments: Part II. Flux estimation. *Biotechnol. Bioeng.* *100*, 355–370.

Hunt, C.J. (2011). Cryopreservation of Human Stem Cells for Clinical Application: A Review. *Transfus. Med. Hemotherapy Off. Organ Der Dtsch. Gesellschaft Fur Transfusionsmedizin Und Immunhamatologie* *38*, 107–123.

Huxley, H.E. (2002). The mechanism of muscular contraction. *Science* *164*:1356-1366, 1969. *Clin. Orthop. Relat. Res.* *164*, S6–S17.

Kadari, A., Mekala, S., Wagner, N., Malan, D., Köth, J., Doll, K., Stappert, L., Eckert, D., Peitz, M., Matthes, J., et al. (2015). Robust generation of cardiomyocytes from human iPS cells requires precise modulation of BMP and WNT signaling. *Stem Cell Rev. Reports* *11*, 560–569.

Kamps, J.A., and Krenning, G. (2016). Micromanaging cardiac regeneration: Targeted delivery of microRNAs for cardiac repair and regeneration. *World J. Cardiol.* *8*, 163–179.

Karakikes, I., Senyei, G.D., Hansen, J., Kong, C.-W., Azeloglu, E.U., Stillitano, F., Lieu, D.K., Wang, J., Ren, L., Hulot, J.-S., et al. (2014). Small molecule-mediated directed differentiation of human embryonic stem cells toward ventricular cardiomyocytes. *Stem Cells Transl. Med.* *3*, 18–31.

Kattman, S.J., Witty, A.D., Gagliardi, M., Dubois, N.C., Niapour, M., Hotta, A., Ellis, J., and Keller, G. (2011). Stage-specific optimization of activin/nodal and BMP signaling promotes cardiac differentiation of mouse and human pluripotent stem cell lines. *Cell Stem Cell* *8*, 228–240.

Kehat, I., Kenyagin-Karsenti, D., Snir, M., Segev, H., Amit, M., Gepstein, A., Livne, E., Binah, O., Itskovitz-Eldor, J., and Gepstein, L. (2001). Human embryonic stem cells can differentiate into myocytes with structural and functional properties of cardiomyocytes. *J Clin Invest* *108*, 407–414.

Kelleher, J.K. (2001). Flux Estimation Using Isotopic Tracers: Common Ground for Metabolic Physiology and Metabolic Engineering. *Metab. Eng.* *3*, 100–110.

Kelleher, J.K. (2004). Probing metabolic pathways with isotopic tracers: insights from mammalian metabolic physiology. *Metab. Eng.* *6*, 1–5.

Kempf, H., Olmer, R., Kropp, C., Rückert, M., Jara-Avaca, M., Robles-Diaz, D., Franke, A., Elliott, D.A., Wojciechowski, D., Fischer, M., et al. (2014). Controlling expansion and cardiomyogenic differentiation of human pluripotent stem cells in scalable suspension culture. *Stem Cell Reports* *3*, 1132–1146.

Kempf, H., Kropp, C., Olmer, R., Martin, U., and Zweigerdt, R. (2015). Cardiac differentiation of human pluripotent stem cells in scalable suspension culture. *Nat. Protoc.* *10*, 1345–1361.

Kempf, H., Andree, B., and Zweigerdt, R. (2016). Large-scale production of human pluripotent stem cell derived cardiomyocytes. *Adv. Drug Deliv. Rev.* *96*, 18–30.

Kijlstra, J.D., Hu, D., Mittal, N., Kausel, E., Van Der Meer, P., Garakani, A., and Domian, I.J. (2015). Integrated Analysis of Contractile Kinetics, Force Generation, and Electrical Activity in Single Human Stem Cell-Derived Cardiomyocytes. *Stem Cell Reports* *5*, 1226–1238.

Kim, C., Majdi, M., Xia, P., Wei, K.A., Talantova, M., Spiering, S., Nelson, B., Mercola, M., Chen, H.V., and Al, K.I.M.E.T. (2010). Non-cardiomyocytes influence the electrophysiological maturation of human embryonic stem cell-derived cardiomyocytes during differentiation. *Stem Cells Dev.* *19*, 783–795.

Kim, J., Greber, B., Araúzo-Bravo, M., Meyer, J., Park, K., Zaehres, H., and Schöler, H. (2009). Direct reprogramming of human neural stem cells by OCT4. *Nature* *461*, 643–649.

Ko, H.C., and Gelb, B.D. (2014). Concise Review: Drug Discovery in the Age of the Induced Pluripotent Stem Cell. *Stem Cells* *32*, 500–509.

Kolwicz, S.C., Purohit, S., and Tian, R. (2013). Cardiac metabolism and its interactions with contraction, growth, and survival of cardiomyocytes. *Circ. Res.* *113*, 603–616.

Kuppusamy, K.T., Jones, D.C., Sperber, H., Madan, A., Fischer, K. a., Rodriguez, M.L., Pabon, L., Zhu, W.-Z., Tulloch, N.L., Yang, X., et al. (2015). Let-7 family of microRNA is required for maturation and adult-like metabolism in stem cell-derived cardiomyocytes. *Proc. Natl. Acad. Sci.*

201424042.

Laflamme, M.A., Chen, K.Y., Naumova, A. V, Muskheli, V., Fugate, J.A., Dupras, S.K., Reinecke, H., Xu, C., Hassanipour, M., Police, S., et al. (2007). Cardiomyocytes derived from human embryonic stem cells in pro-survival factors enhance function of infarcted rat hearts. *Nat. Biotechnol.* *25*, 1015–1024.

Le, T.Y.L., Thavapalachandran, S., Kizana, E., and Chong, J.J. (2016). New Developments in Cardiac Regeneration. *Hear. Lung Circ.* 1–7.

Lehman, W., Craig, R., and Vibert, P. (1994). Ca(2+)-induced tropomyosin movement in *Limulus* thin filaments revealed by three-dimensional reconstruction. *Nature* *368*, 65–67.

Lewandowski, J., Kolanowski, T.J., and Kurpisz, M. (2016). Techniques for the induction of human pluripotent stem cell differentiation towards cardiomyocytes. *J. Tissue Eng. Regen. Med.* *4*, 1–17.

Lian, X., Hsiao, C., Wilson, G., Zhu, K., Hazeltine, L.B., Azarin, S.M., Raval, K.K., Zhang, J., Kamp, T.J., and Palecek, S.P. (2012). Robust cardiomyocyte differentiation from human pluripotent stem cells via temporal modulation of canonical Wnt signaling. *PNAS* 1–10.

Lian, X., Zhang, J., Azarin, S.M., Zhu, K., Hazeltine, L.B., Bao, X., Hsiao, C., Kamp, T.J., and Palecek, S.P. (2013). Directed cardiomyocyte differentiation from human pluripotent stem cells by modulating Wnt/ $\beta$ -catenin signaling under fully defined conditions. *Nat. Protoc.* *8*, 162–175.

Liao, M.L.C., De Boer, T.P., Mutoh, H., Raad, N., Richter, C., Wagner, E., Downie, B.R., Unsöld, B., Arooj, I., Streckfuss-Bömeke, K., et al. (2015). Sensing Cardiac Electrical Activity with a Cardiac Myocyte-Targeted Optogenetic Voltage Indicator. *Circ. Res.* *117*, 401–412.

Linares, J., Arellano-Viera, E., Iglesias-García, O., Ferreira, C., Iglesias, E., Abizanda, G., Prósper, F., and Carvajal-Vergara, X. (2016). Generation of iPSC from cardiac and tail-tip fibroblasts derived from a second heart field reporter mouse. *Stem Cell Res.* *16*, 617–621.

Liu, J., Sun, N., Bruce, M.A., Wu, J.C., and Butte, M.J. (2012). Atomic force mechanobiology of pluripotent stem cell-derived cardiomyocytes. *PLoS One* *7*.

Löffelholz, C., Kaiser, S.C., Kraume, M., Eibl, R., and Eibl, D. (2014). Dynamic Single-Use Bioreactors Used in Modern Liter- and m3- Scale Biotechnological Processes: Engineering Characteristics and Scaling Up. *Adv Biochem Eng Biotechnol.* *138*, 1–44.

Lopaschuk, G.D., and Jaswal, J.S. (2010). Energy metabolic phenotype of the cardiomyocyte during development, differentiation, and postnatal maturation. *J. Cardiovasc. Pharmacol.* *56*, 130–140.

Lopaschuk, G.D., Ussher, J.R., Folmes, C.D.L., Jaswal, J.S., and STANLEY, W.C. (2010). Myocardial Fatty Acid Metabolism in Health and Disease. *Physiol. Rev.* *90*, 207–258.

Lund, A.W., Yener, B., Stegemann, J.P., and Plopper, G.E. (2009). The Natural and Engineered 3D Microenvironment as a Regulatory Cue During Stem Cell Fate Determination. *Tissue Eng. Part B* *15*, 371–380.

Matthys, O.B., Hookway, T.A., and McDevitt, T.C. (2016). Design Principles for Engineering of Tissues from Human Pluripotent Stem Cells. *Curr. Stem Cell Reports* *2*, 43–51.

McCain, M.L., Yuan, H., Pasqualini, F.S., Campbell, P.H., and Parker, K.K. (2014). Matrix elasticity regulates the optimal cardiac myocyte shape for contractility. *Am. J. Physiol. Heart Circ. Physiol.* *306*, H1525-39.

van Meer, B.J., Tertoolen, L.G.J., and Mummery, C.L. (2016). Measuring physiological responses of human pluripotent stem cell derived cardiomyocytes to drugs and disease. *Stem Cells* 2008–2015.

Menasche, P., Vanneau, V., Hagege, A., Bel, A., Cholley, B., Cacciapuoti, I., Parouchev, A., Benhamouda, N., Tachdjian, G., Tosca, L., et al. (2015). Human embryonic stem cell-derived cardiac progenitors for severe heart failure treatment: First clinical case report. *Eur. Heart J.* *36*, 2011–2017.

Menasché, P., Alfieri, O., Janssens, S., McKenna, W., Reichenspurner, H., Trinquart, L., Vilquin, J.T., Marolleau, J.P., Seymour, B., Larghero, J., et al. (2008). The myoblast autologous grafting in ischemic cardiomyopathy (MAGIC) trial: First randomized placebo-controlled study of myoblast



transplantation. *Circulation* 117, 1189–1200.

Mihic, A., Li, J., Miyagi, Y., Gagliardi, M., Li, S.-H., Zu, J., Weisel, R.D., Keller, G., and Li, R.-K. (2014). The effect of cyclic stretch on maturation and 3D tissue formation of human embryonic stem cell-derived cardiomyocytes. *Biomaterials* 35, 2798–2808.

Miki, K., Endo, K., Takahashi, S., Funakoshi, S., Takei, I., Katayama, S., Toyoda, T., Kotaka, M., Takaki, T., Umeda, M., et al. (2015). Efficient Detection and Purification of Cell Populations Using Synthetic MicroRNA Switches. *Cell Stem Cell* 16, 699–711.

Moran, A.E., Forouzanfar, M.H., Roth, G.A., Mensah, G.A., Ezzati, M., Murray, C.J.L., and Naghavi, M. (2014). Temporal trends in ischemic heart disease mortality in 21 world regions, 1980 to 2010: The global burden of disease 2010 study. *Circulation* 129, 1483–1492.

Mummery, C., Ward-van Oostwaard, D., Doevendans, P., Spijker, R., van den Brink, S., Hassink, R., van der Heyden, M., Opthof, T., Pera, M., de la Riviere, A.B., et al. (2003). Differentiation of human embryonic stem cells to cardiomyocytes: role of coculture with visceral endoderm-like cells. *Circulation* 107, 2733–2740.

Mummery, C.L., Zhang, J., Ng, E.S., Elliott, D. a, Elefanty, A.G., and Kamp, T.J. (2012). Differentiation of human embryonic stem cells and induced pluripotent stem cells to cardiomyocytes: a methods overview. *Circ. Res.* 111, 344–358.

Murry, C.E., Reinecke, H., and Pabon, L.M. (2006). Regeneration Gaps. Observations on Stem Cells and Cardiac Repair. *J. Am. Coll. Cardiol.* 47, 1777–1785.

Natsuko, H., Shugo, T., Kazuaki, N., Hideaki, K., Tomoyuki, S., Fumiyouki, H., Tomohisa, S., Yoshikazu, K., Akinori, H., Marina, O., et al. (2014). A Massive Suspension Culture System With Metabolic Purification for Human Pluripotent Stem Cell-Derived Cardiomyocytes. *Stem Cells Transl. Med.* 3, 1–11.

Nerbonne, J.M. (2004). Studying cardiac arrhythmias in the mouse - A reasonable model for probing mechanisms? *Trends Cardiovasc. Med.* 14, 83–93.

Nguyen, D.C., Hookway, T.A., Wu, Q., Jha, R., Preininger, M.K., Chen, X., Easley, C.A., Spearman, P., Deshpande, S.R., Maher, K., et al. (2014). Microscale generation of cardiospheres promotes robust enrichment of cardiomyocytes derived from human pluripotent stem cells. *Stem Cell Reports* 3, 260–268.

Niebruegge, S., Nehring, A., Ba, H., Schroeder, M., Zweigerdt, R., and Lehmann, J. (2008). Cardiomyocyte Production in Mass Suspension Culture: Embryonic Stem Cells as a Source for Great Amounts of Functional Cardiomyocytes. *Tissue Eng. Part A* 14, 1591–1601.

Niebruegge, S., Bauwens, C.L., Peerani, R., Thavandiran, N., Masse, S., Sevaptisidis, E., Nanthakumar, K., Woodhouse, K., Husain, M., Kumacheva, E., et al. (2009). Generation of human embryonic stem cell-derived mesoderm and cardiac cells using size-specified aggregates in an oxygen-controlled bioreactor. *Biotechnol. Bioeng.* 102, 493–507.

Nielsen, J. (2003). It Is All about Metabolic Fluxes. *J. Bacteriol.* 185, 7031–7035.

Nöh, K., and Wiechert, W. (2011). The benefits of being transient: isotope-based metabolic flux analysis at the short time scale. *Appl. Microbiol. Biotechnol.* 91, 1247–1265.

Okita, K., Ichisaka, T., and Yamanaka, S. (2007). Generation of germline-competent induced pluripotent stem cells. *Nature* 448, 313–318.

Oldiges, M., Lütz, S., Pflug, S., Schroer, K., Stein, N., and Wiendahl, C. (2007). Metabolomics: current state and evolving methodologies and tools. *Appl. Microbiol. Biotechnol.* 76, 495–511.

Olmer, R., Lange, A., Selzer, S., Kasper, C., Haverich, A., Martin, U., and Zweigerdt, R. (2012). Suspension culture of human pluripotent stem cells in controlled, stirred bioreactors. *Tissue Eng. Part C Methods* 18, 772–784.

Opie, L.H. (2004). *Heart Physiology: From Cell to Circulation*, 4th ed. (Philadelphia,; Lippincott Williams & Wilkins).

Pacher, P., and Kecskemeti, V. (2004). Cardiovascular Side Effects of New Antidepressants and Antipsychotics: New Drugs, old Concerns? *Curr Pharm Des* 10, 2463–2475.

Paige, S.L., Osugi, T., Afanasiev, O.K., Pabon, L., Reinecke, H., and Murry, C.E. (2010).

Endogenous Wnt/beta-catenin signaling is required for cardiac differentiation in human embryonic stem cells. *PLoS One* 5, e11134.

Pais, D.A.M., Carrondo, M.J.T., Alves, P.M., and Teixeira, A.P. (2014). Towards real-time monitoring of therapeutic protein quality in mammalian cell processes. *Curr. Opin. Biotechnol.* 30, 161–167.

Pal, R., Mamidi, M.K., Das, A.K., and Bhonde, R. (2013). Comparative analysis of cardiomyocyte differentiation from human embryonic stem cells under 3-D and 2-D culture conditions. *J. Biosci. Bioeng.* 115, 200–206.

Pettinato, G., Wen, X., and Zhang, N. (2015). Engineering Strategies for the Formation of Embryoid Bodies from Human Pluripotent Stem Cells. *Stem Cells Dev.* 24, 1595–1609.

Placzek, M.R., Chung, I.-M., Macedo, H.M., Ismail, S., Mortera Blanco, T., Lim, M., Cha, J.M., Fauzi, I., Kang, Y., Yeo, D.C.L., et al. (2009). Stem cell bioprocessing: fundamentals and principles. *J. R. Soc. Interface* 6, 209–232.

Preininger, M.K., and Singh, M. (2016). Cryopreservation of Human Pluripotent Stem Cell-Derived Cardiomyocytes: Strategies, Challenges, and Future Directions. In *Biobanking and Cryopreservation of Stem Cells*, pp. 123–135.

Price, N.D., Papin, J.A., Schilling, C.H., and Palsson, B.O. (2003). Genome-scale microbial in silico models: the constraints-based approach. *Trends Biotechnol.* 21, 162–169.

Rajala, K., Pekkanen-Mattila, M., and Aalto-Setälä, K. (2011). Cardiac differentiation of pluripotent stem cells. *Stem Cells Int.* 2011, 383709.

Rana, P., Anson, B., Engle, S., and Will, Y. (2012). Characterization of Human Induced Pluripotent Stem Cell Derived Cardiomyocytes: Bioenergetics and Utilization in Safety Screening. *Toxicol. Sci.* 130, 117–131.

Rodriguez, M.L., Graham, B.T., Pabon, L.M., Han, S.J., Murry, C.E., and Sniadecki, N.J. (2014). Measuring the contractile forces of human induced pluripotent stem cell-derived cardiomyocytes with arrays of microposts. *J. Biomech. Eng.* 136, 51005.

Saraste, A., Pulkki, K., Kallajoki, M., Heikkilä, P., Laine, P., Mattila, S., Nieminen, M.S., Parvinen, M., and Voipio-Pulkki, L.M. (1999). Cardiomyocyte apoptosis and progression of heart failure to transplantation. *Eur. J. Clin. Invest.* 29, 380–386.

Schmelter, M., Ateghang, B., Helmig, S., Wartenberg, M., and Sauer, H. (2006). Embryonic stem cells utilize reactive oxygen species as transducers of mechanical strain-induced cardiovascular differentiation. *FASEB J.* 20, E294–E306.

Schönfeld, P., Schild, L., and Bohnsack, R. (1996). Expression of the ADP/ATP carrier and expansion of the mitochondrial (ATP + ADP) pool contribute to postnatal maturation of the rat heart. *Eur. J. Biochem.* 241, 895–900.

Schroeder, M., Niebruegge, S., Werner, A., Willbold, E., Burg, M., Ruediger, M., Field, L.J., Lehmann, J., and Zweigerdt, R. (2005). Differentiation and lineage selection of mouse embryonic stem cells in a stirred bench scale bioreactor with automated process control. *Biotechnol. Bioeng.* 92, 920–933.

Serra, M., Correia, C., Malpique, R., Brito, C., Jensen, J., Bjorquist, P., Carrondo, M.J.T., and Alves, P.M. (2011). Microencapsulation Technology: A Powerful Tool for Integrating Expansion and Cryopreservation of Human Embryonic Stem Cells. *PLoS One* 6, 1–13.

Serra, M., Brito, C., Correia, C., and Alves, P.M. (2012). Process engineering of human pluripotent stem cells for clinical application. *Trends Biotechnol.* 30, 1–10.

Serra, M., Correia, C., Brito, C., and Alves, P.M. (2014). Bioprocessing of Human Pluripotent Stem Cells for Cell Therapy Applications. In *Stem Cells and Cell Therapy.*, pp. 71–95.

Shiba, Y., Fernandes, S., Zhu, W.-Z., Filice, D., Muskheli, V., Kim, J., Palpant, N.J., Gantz, J., Moyes, K.W., Reinecke, H., et al. (2012). Human ES-cell-derived cardiomyocytes electrically couple and suppress arrhythmias in injured hearts. *Nature* 489, 322–325.

Shiba, Y., Gomibuchi, T., Seto, T., Wada, Y., Ichimura, H., Tanaka, Y., Ogasawara, T., Okada, K., Shiba, N., Sakamoto, K., et al. (2016). Allogeneic transplantation of iPS cell-derived

cardiomyocytes regenerates primate hearts. *Nature* 538, 388–391.

Shukla, A.A., and Gottschalk, U. (2013). Single-use disposable technologies for biopharmaceutical manufacturing. *Trends Biotechnol.* 31, 147–154.

Skelton, R.J.P., Costa, M., Anderson, D.J., Bruveris, F., Finnin, B.W., Koutsis, K., Arasaratnam, D., White, A.J., Rafii, A., Ng, E.S., et al. (2014). SIRPA, VCAM1 and CD34 identify discrete lineages during early human cardiovascular development. *Stem Cell Res.* 13, 172–179.

Smith, C. a, Want, E.J., O'Maille, G., Abagyan, R., and Siuzdak, G. (2006). XCMS: processing mass spectrometry data for metabolite profiling using nonlinear peak alignment, matching, and identification. *Anal. Chem.* 78, 779–787.

Snir, M., Kehat, I., Gepstein, A., Coleman, R., Itskovitz-Eldor, J., Livne, E., and Gepstein, L. (2003). Assessment of the ultrastructural and proliferative properties of human embryonic stem cell-derived cardiomyocytes. *Am. J. Physiol. Heart Circ. Physiol.* 285, H2355–H2363.

Sreekumar, A., Poisson, L.M., Rajendiran, T.M., Khan, A.P., Cao, Q., Yu, J., Laxman, B., Mehra, R., Lonigro, R.J., Li, Y., et al. (2009). Metabolomic profiles delineate potential role for sarcosine in prostate cancer progression. *Nature* 457, 910–914.

Stoppel, W.L., Kaplan, D.L., and Black, L.D. (2016). Electrical and mechanical stimulation of cardiac cells and tissue constructs. *Adv. Drug Deliv. Rev.* 96, 135–155.

Sumi, T., Tsuneyoshi, N., Nakatsuji, N., and Suemori, H. (2008). Defining early lineage specification of human embryonic stem cells by the orchestrated balance of canonical Wnt/beta-catenin, Activin/Nodal and BMP signaling. *Development* 135, 2969–2979.

Synnergren, J., Améen, C., Jansson, A., and Sartipy, P. (2012). Global transcriptional profiling reveals similarities and differences between human stem cell-derived cardiomyocyte clusters and heart tissue. *Physiol. Genomics* 44, 245–258.

Takahashi, K., and Yamanaka, S. (2006). Induction of pluripotent stem cells from mouse embryonic and adult fibroblast cultures by defined factors. *Cell* 126, 663–676.

Takahashi, K., Tanabe, K., Ohnuki, M., Narita, M., Ichisaka, T., and Tomoda, K. (2007). Induction of Pluripotent Stem Cells from Adult Human Fibroblasts by Defined Factors. *Cell* 131, 1–12.

Takahashi, T., Lord, B., Schulze, P.C., Fryer, R.M., Sarang, S.S., Gullans, S.R., and Lee, R.T. (2003). Ascorbic acid enhances differentiation of embryonic stem cells into cardiac myocytes. *Circulation* 107, 1912–1916.

Thomson, J.A., Itskovitz-Eldor, J., Shapiro, S.S., Waknitz, M.A., Swiergiel, J.J., Marshall, V.S., and Jones, J.M. (1998). Embryonic stem cell lines derived from human blastocysts. *Science* (80-. ). 282, 1145–1147.

Thorrez, L., and Sampaolesi, M. (2011). The future of induced pluripotent stem cells for cardiac therapy and drug development. *Curr. Pharm. Des.* 17, 3258–3270.

Ting, S., Chen, A., Reuveny, S., and Oh, S. (2014). An intermittent rocking platform for integrated expansion and differentiation of human pluripotent stem cells to cardiomyocytes in suspended microcarrier cultures. *Stem Cell Res.* 13, 202–213.

Tohyama, S., Hattori, F., Sano, M., Hishiki, T., Nagahata, Y., Matsuura, T., Hashimoto, H., Suzuki, T., Yamashita, H., Satoh, Y., et al. (2013). Distinct metabolic flow enables large-scale purification of mouse and human pluripotent stem cell-derived cardiomyocytes. *Cell Stem Cell* 12, 127–137.

Tzatzalos, E., Abilez, O.J., Shukla, P., and Wu, J.C. (2016). Engineered heart tissues and induced pluripotent stem cells: Macro- and microstructures for disease modeling, drug screening, and translational studies. *Adv. Drug Deliv. Rev.* 96, 234–244.

Ueno, S., Weidinger, G., Osugi, T., Kohn, A.D., Golob, J.L., Pabon, L., Reinecke, H., Moon, R.T., and Murry, C.E. (2007). Biphasic role for Wnt/beta-catenin signaling in cardiac specification in zebrafish and embryonic stem cells. *Proc. Natl. Acad. Sci. U. S. A.* 104, 9685–9690.

Vacanti, N.M., and Metallo, C.M. (2013). Exploring metabolic pathways that contribute to the stem cell phenotype. *Biochim. Biophys. Acta - Gen. Subj.* 1830, 2361–2369.

Veerman, C.C., Kosmidis, G., Mummery, C.L., Casini, S., Verkerk, A.O., and Bellin, M. (2015). Immaturity of human stem-cell-derived cardiomyocytes in culture: fatal flaw or soluble problem?

Stem Cells Dev. 24, 1035–1052.

Vidarsson, H., Hyllner, J., and Sartipy, P. (2010). Differentiation of human embryonic stem cells to cardiomyocytes for in vitro and in vivo applications. *Stem Cell Rev.* 6, 108–120.

Wang, H., Hao, J., and Hong, C.C. (2011). Cardiac Induction of Embryonic Stem Cells by a Small Molecule Inhibitor of Wnt/ $\beta$ -Catenin Signaling. *ACS Chem. Biol* 6, 192–197.

White, M.C., Pang, L., and Yang, X. (2016). MicroRNA-mediated maturation of human pluripotent stem cell-derived cardiomyocytes: Towards a better model for cardiotoxicity? *Food Chem. Toxicol.*

WHO (2014). Global status report on noncommunicable diseases 2014. World Health 176.

WHO (2016). World health statistics - monitoring health for the SDGs. World Heal. Organ.

Wile, B.M., Ban, K., Yoon, Y.-S., and Bao, G. (2014). Molecular beacon-enabled purification of living cells by targeting cell type-specific mRNAs. *Nat. Protoc.* 9, 2411–2424.

Woo Suk, A., and Antoniewicz, M.R. (2013). Parallel labeling experiments with [1,2-<sup>13</sup>C]glucose and [U-<sup>13</sup>C]glutamine provide new insights into CHO cell metabolism. *Metab. Eng.* 15, 34–47.

Xu, C., Police, S., Rao, N., and Carpenter, M. (2002). Characterization and Enrichment of Cardiomyocytes Derived From Human Embryonic Stem Cells. *Circ. Res.* 91, 501–508.

Yang, X., Pabon, L., and Murry, C.E. (2014a). Engineering adolescence: Maturation of human pluripotent stem cell-derived cardiomyocytes. *Circ. Res.* 114, 511–523.

Yang, X., Rodriguez, M., Pabon, L., Fischer, K. a., Reinecke, H., Regnier, M., Sniadecki, N.J., Ruohola-Baker, H., and Murry, C.E. (2014b). Tri-iodo-L-thyronine promotes the maturation of human cardiomyocytes-derived from induced pluripotent stem cells. *J. Mol. Cell. Cardiol.* 72, 296–304.

Yu, J., Vodyanik, M.A., Smuga-Otto, K., Antosiewicz-Bourget, J., Frane, J.L., Tian, S., Nie, J., Jonsdottir, G.A., Ruotti, V., Stewart, R., et al. (2007). Induced Pluripotent Stem Cell Lines Derived from Human Somatic Cells. *Science* (80-. ). 318, 1917–1920.

Zapata-Linares, N., Rodriguez, S., Mazo, M., Abizanda, G., Andreu, E.J., Barajas, M., Prosper, F., and Rodriguez-Madoz, J.R. (2016). Generation and characterization of human iPSC line generated from mesenchymal stem cells derived from adipose tissue. *Stem Cell Res.* 16, 20–23.

Zhang, D., Shadrin, I.Y., Lam, J., Xian, H.Q., Snodgrass, H.R., and Bursac, N. (2013). Tissue-engineered cardiac patch for advanced functional maturation of human ESC-derived cardiomyocytes. *Biomaterials* 34, 5813–5820.

Zhang, Q., Jiang, J., Han, P., Yuan, Q., Zhang, J., Zhang, X., Xu, Y., Cao, H., Meng, Q., Chen, L., et al. (2011). Direct differentiation of atrial and ventricular myocytes from human embryonic stem cells by alternating retinoid signals. *Cell Res.* 21, 579–587.

Zhou, Y., and Zeng, F. (2013). Integration-free methods for generating induced pluripotent stem cells. *Genomics. Proteomics Bioinformatics* 11, 284–287.

Zhou, T., Benda, C., Dunzinger, S., Huang, Y., Ho, J.C., Yang, J., Wang, Y., Zhang, Y., Zhuang, Q., Li, Y., et al. (2012). Generation of human induced pluripotent stem cells from urine samples. *Nat Protoc* 7, 2080–2089.

Zwi-Dantsis, L., and Gepstein, L. (2012). Induced pluripotent stem cells for cardiac repair. *Cell. Mol. Life Sci.* 69, 3285–3299.

Zwi-Dantsis, L., Mizrahi, I., Arbel, G., Gepstein, A., and Gepstein, L. (2011). Scalable production of cardiomyocytes derived from c-Myc free induced pluripotent stem cells. *Tissue Eng. Part A* 17, 1027–1037.

# 2

## **Combining Hypoxia and Bioreactor Hydrodynamics Boosts Induced Pluripotent Stem Cell Differentiation Towards Cardiomyocytes**

This chapter was adapted from:

Correia C., Serra M., Espinha N., Sousa M., Brito C., Burkert K., Zheng Y., Hescheler J., Carrondo M.J.T., Sarić T., Alves P.M. (2014). Combining Hypoxia and Bioreactor Hydrodynamics Boosts Induced Pluripotent Stem Cell Differentiation Towards Cardiomyocytes. *Stem Cell Rev* 22, 10:786–801.

**Contents**

<b>1. Introduction</b> .....	<b>42</b>
<b>2. Methods</b> .....	<b>44</b>
2.1. iPSC culture on feeder layers .....	44
2.2. iPSC differentiation in stirred tank bioreactors .....	44
2.3. iPSC differentiation in WAVE bioreactors .....	45
2.4. Dissociation of cardiospheres .....	45
2.5. Evaluation of cell concentration and viability .....	45
2.6. Monitorization of CM differentiation .....	46
2.7. Evaluation of cell growth and differentiation towards CMs .....	47
2.8. Characterization of iPSC-CMs .....	47
2.9. Statistical analysis.....	48
<b>3. Results</b> .....	<b>50</b>
3.1. Effect of dissolved oxygen on CM differentiation of iPSCs in stirred tank bioreactors .....	50
3.2. Impact of agitation profile on CM differentiation of iPSC in stirred tank bioreactors .....	51
3.3. CM differentiation of iPSCs in WAVE bioreactors .....	54
3.4. Structural properties and action potential (AP) parameters of CMs generated in stirred tank and WAVE optimized bioprocesses.....	58
<b>4. Discussion</b> .....	<b>60</b>
<b>5. Appendix</b> .....	<b>64</b>
<b>6. Acknowledgments</b> .....	<b>67</b>
<b>7. References</b> .....	<b>67</b>

## Abstract

Induced pluripotent stem cells derived cardiomyocytes (iPSC-CMs) hold great promise for patient-specific disease modeling, drug screening and cell therapy. However, existing protocols for CM differentiation of iPSCs besides being highly dependent on the application of expensive growth factors show low reproducibility and scalability. The aim of this work was to develop a robust and scalable strategy for mass production of iPSC-CMs by designing a bioreactor protocol that ensures a hypoxic and mechanical environment.

Murine iPSCs were cultivated as aggregates in either stirred tank or WAVE bioreactors. The effect of dissolved oxygen and mechanical forces, promoted by different hydrodynamic environments, on CM differentiation was evaluated. Combining a hypoxia culture (4% O<sub>2</sub> tension) with an intermittent agitation profile in stirred tank bioreactors resulted in an improvement of about 1000-fold in CM yields when compared to normoxic (20% O<sub>2</sub> tension) and continuously agitated cultures. Additionally, we showed for the first time that wave-induced agitation enables the differentiation of iPSCs towards CMs at faster kinetics and with higher yields (60 CMs/input iPSC). In an 11-day differentiation protocol, clinically relevant numbers of CMs (2.3 x10<sup>9</sup> CMs/1L) were produced, and CMs exhibited typical cardiac sarcomeric structures, calcium transients, electrophysiological profiles and drug responsiveness.

This work describes significant advances towards scalable cardiomyocyte differentiation of murine iPSC, paving the way for implementation of this strategy for mass production of their human counterparts and their use for cardiac repair and cardiovascular research.

## 1. Introduction

The inability of mature cardiomyocytes (CMs) to proliferate leads to a permanent loss of functional cells after injury (Kawaguchi and Nakanishi, 2013). Previous studies in animal models of myocardial infarction have demonstrated that the function of a damaged heart may be improved by transplantation of sufficient numbers of functional CMs (Laflamme and Murry, 2011). Over the last years, pluripotent stem cells (PSCs), including embryonic stem cells (ESCs) and induced pluripotent stem cells (iPSCs), have emerged as an attractive candidate stem cell source for obtaining CMs (Braam et al., 2009; Rajala et al., 2011). The inherent capacity to grow indefinitely and to differentiate into all mature cells of the human body make PSCs the only cell source that can provide *ex-vivo* an unlimited number of functional and potentially autologous CMs for transplantation. The clinical translation of human ESC-derivatives has been greatly hampered by the risk of immune rejection due to their allogenicity and by ethical concerns (Zwi-Dantsis and Gepstein, 2012). iPSCs can circumvent these drawbacks, allowing for ethically “acceptable” and safe patient-specific therapies (Oh et al., 2012; Yoshida and Yamanaka, 2011). Moreover, iPSCs constitute a promising tool to establish disease-specific models of human inherited cardiac disorders and platforms for drug discovery and toxicity testing (Grskovic et al., 2011; Oh et al., 2012).

In the last years, several methodologies have been described for the differentiation of murine (Kuzmenkin et al., 2009; Mauritz et al., 2008; Narazaki et al., 2008; Zwi-Dantsis et al., 2011) and human (Burrige et al., 2011; Lian et al., 2013; Lundy et al., 2013; Minami et al., 2012; Tohyama et al., 2013; Zhang et al., 2012) iPSCs into functional CMs based on the knowledge acquired in previous studies with ESCs. Still, several challenges remain that currently preclude their widespread application. Those protocols typically involve a complex stage-specific application of exogenous growth factors which are costly, degrade rapidly, do not readily diffuse into complex 3D aggregates and exhibit lot-to-lot variation in their bioactivity (Mummery et al., 2012). Moreover, despite recent improvements in cardiac differentiation protocols (Lian et al., 2013; Minami et al., 2012; Tohyama et al., 2013; Zhang et al., 2012) these are still associated with low reproducibility and scalability (Zwi-Dantsis and Gepstein, 2012), being unsuitable to provide the large numbers of CMs needed to exert functional benefit after a heart attack (about  $1-2 \times 10^9$  CMs per patient) (Murry et al., 2006). Therefore, robust and scalable bioprocesses for CM production less dependent on the use of inductive factors are required for a faster transition of iPSCs to the clinical and industrial fields.

One of the most powerful strategies for scaling-up the production of iPSC derivatives consists in cultivating the cells as 3D cell aggregates called embryoid bodies in bioreactor systems that continuously assure monitoring and control of the environmental conditions (pH,  $pO_2$  and agitation profile) (Serra et al., 2010, 2012). A close control of the physical environment was shown to be essential for guiding cell fate decisions through expansion and differentiation routes. Low oxygen tensions (2–5%  $O_2$ ) have been shown to enhance the proliferation of PSCs (Forsyth et al., 2006;



Gibbons et al., 2006; Serra et al., 2010) and their differentiation to CMs (Bauwens et al., 2005; Horton and Auguste, 2012; Niebruegge et al., 2009). Indeed, it is well known that cells in the early developing embryo are exposed to low-oxygen levels. In hamsters and rabbits, for example, intrauterine oxygen concentrations decrease during blastulation and implantation to 5.3% O<sub>2</sub> and 3.5% O<sub>2</sub>, respectively (Fischer and Bavister, 1993). Thus, lowering the oxygen concentration from normoxic atmospheric levels (20% O<sub>2</sub>) to more physiological levels (2–5% O<sub>2</sub> or atmospheric hypoxia) might be beneficial in PSC cultures due to the importance of this environmental condition during embryonic development.

Mechanical cues from the environment are also translated into biological signals that mediate cell structure, survival, migration, proliferation, and differentiation (Li et al., 2011; Nava et al., 2012). Several studies have provided evidence that applied mechanical forces including cyclic strain and stretch, fluid shear stress and hydrostatic compression modulate differentiation of cells that reside in mechanically dynamic environments, such as CMs (Geuss and Suggs, 2013; Gwak et al., 2006; Schmelter et al., 2006), vascular smooth muscle cells (Shimizu et al., 2008), endothelial cells (Matsumoto et al., 2007) and chondrocytes (Elder et al., 2001). In particular, CMs are continuously subjected to cyclic mechanical strain promoted by the rhythmic heart beating (Keung et al., 2010). CM-enriched tissue constructs are often subjected to cyclic tensions to increase their force of contraction, facilitate organization of cellular structures and consequently improve their cardiac function *in vivo* (Zimmermann et al., 2002). Thus, the hypothesis that mechanical loading promotes cardiomyogenesis of PSCs has started to be explored (Gwak et al., 2006; Shimko and Claycomb, 2008; Teramura et al., 2012). It was recently reported that ESCs cultured on elastic polymer [poly(lactide-co-caprolactone), PLCL] scaffolds and subjected to 1% cyclic uniaxial stretch, in a custom-made strain device, demonstrated commitment towards CM lineage as noted by an increased cardiac gene expression compared to unstrained controls (Gwak et al., 2006). Nevertheless, the low high-throughput design and scalability of these devices, custom built to apply mechanical strains, makes them unsuitable to generate large numbers of cells on a therapeutically relevant scale.

In the present work we focused on the development of robust, scalable and integrated platforms for iPSC-CM production and purification using bioreactor systems with automated process control, including online measurement and adjustment of the culture parameters. Our strategy consisted on modulating key environmental parameters for efficient and reliable differentiation of iPSC towards the CM lineage, reducing the need of using inductive factors. We explored the impact of dissolved oxygen (DO) and mechanical forces on CM differentiation of iPSCs by using two distinct bioreactor systems, namely stirred tank and WAVE bioreactors. We applied mechanical forces to cells by manipulating the hydrodynamic environment, more specifically the type and profile of agitation. We describe for the first time a protocol for efficient mass production of functional CMs derived from murine iPSCs that combines a hypoxic environment with an intermittent stirring or a wave-induced agitation profile.

## 2. Methods

### 2.1. iPSC culture on feeder layers

A murine transgenic  $\alpha$ PIG-iPS cell line, in which the puromycin-N-acetyl transferase and the enhanced green fluorescent protein (eGFP) genes are under the control of the cardiospecific alpha-myosin heavy chain ( $\alpha$ -MHC) promoter (Halbach et al., 2013), was used in this study to facilitate bioprocess development. The fluorescence marker and the antibiotic resistance genes specifically expressed in CMs allow easy monitoring of the cardiac differentiation process and selection of a highly pure CM population upon addition of puromycin into the media, respectively. iPSCs were cultivated on a monolayer of mitotically inactivated murine embryonic fibroblasts (MEFs) in Dulbecco's modified Eagle medium (DMEM) supplemented with 15% (v/v) fetal bovine serum (FBS), 1% (v/v) non-essential amino acids (NEAA), 2 mM L-glutamine, 50  $\mu$ M  $\beta$ -mercaptoethanol, 500  $\mu$ g/mL neomycin sulfate (all from Invitrogen, UK), and 1000 U/mL leukemia inhibitory factor (LIF) (ESGRO, Merck Millipore, Germany), at 37°C in a humidified atmosphere of 5% CO<sub>2</sub>. Cells were passaged every two days as previously reported (Halbach et al., 2013).

### 2.2. iPSC differentiation in stirred tank bioreactors

To promote cell aggregation 0.7x10<sup>5</sup> cell/mL were inoculated into plastic Erlenmeyer flasks (Corning, USA) containing 100 mL of differentiation medium (Iscove's modified Dulbecco's medium (IMDM) with GlutaMAX, supplemented with 20% (v/v) FBS, 1x NEAA, 1% (v/v) Pen/Strep, 50  $\mu$ M  $\beta$ -mercaptoethanol (all from Invitrogen, UK) and 100  $\mu$ M ascorbic acid (Wako, Germany), and incubated at 37°C in a 5% CO<sub>2</sub> humidified atmosphere on an orbital shaker at 80-90 rpm. After two days aggregates were transferred into stirred tank bioreactors (DasGip cellferm-pro bioreactor system, Germany) and cultured at a concentration of 150 aggregates/mL in 200 mL of differentiation medium. Medium was partially changed at days 9 (50% v/v), 12 (70% v/v) and 14 (50% v/v) by selection medium (differentiation media without ascorbic acid supplemented with puromycin at a final concentration of 8  $\mu$ g/mL (InvivoGen, USA)) to eliminate non-CMs and promote CM selection. Antibiotic treatment resulted in the generation of pure aggregates of CMs (designated hereafter as cardiospheres). The experimental set up is illustrated in Figure 2.1 (Page 49). All cultures were performed in computer-controlled stirred tank bioreactors equipped with a trapezoid shaped paddle impeller with arms and operated under defined conditions (CO<sub>2</sub>: 5%; temperature: 37°C; DO: 20% O<sub>2</sub> tension (atmospheric normoxia) or 4% O<sub>2</sub> tension (atmospheric hypoxia); surface aeration rate: 0.1 vvm (gas volume flow per unit of liquid volume per minute); agitation rate: 90 rpm for complete continuous stirred-tank reactor (CSTR) behavior; agitation profile: continuous or intermittent (ON: 30 sec, OFF: 0 sec) with or without direction change; cyclic mechanical frequency (defined by the number of stirring interruptions per unit of time): 0.033Hz). Data acquisition and process control were performed using DasGip Control Software 4.0. Three independent bioreactor runs were performed for every experimental setting.

### 2.3. iPSC differentiation in WAVE bioreactors

Cell aggregation was promoted in Cellbag™ – WAVE bioreactors (GE Healthcare, Sweden) for 2 days (Figure 2.1). Briefly,  $0.7 \times 10^5$  cell/mL were inoculated as single cells into WAVE bioreactors containing 500 mL of differentiation medium. At day 2, aggregate concentration was adjusted to 150 aggregates/mL by increasing the working volume to 1 L. At day 9 of differentiation, CM purification was initiated by exchanging half of the culture media with selection medium. Aggregates were cultivated for additional 2 days in these conditions. The experimental set up is shown in Figure 2.1. All cultures were performed in computer-controlled WAVE bioreactor systems under defined conditions (CO<sub>2</sub>: 5%; temperature: 37°C; DO: 4% O<sub>2</sub> tension; surface aeration rate: 0.1 vvm; rocking angle: 4; rocking rate (adjusted throughout culture time according to the aggregate size): 10 rocks/minute (day0-day1), 12 rocks/minute (day1-day2), 25 rocks/minute (day2-day7), 26 rocks/minute (day7-day11); cyclic mechanical frequency from day 2 to day 11 (defined by the change in wave motion per unit of time): 0.82 to 0.86 Hz). Data acquisition and process control were performed using UNICORN\* DAQ 1.0 software. Three independent bioreactor runs were performed for every experimental setting.

### 2.4. Dissociation of cardiospheres

At the end of the differentiation process, cardiospheres were harvested from the bioreactor, dissociated to single cells by incubation with 0.25% (w/v) Trypsin-EDTA (Invitrogen, UK) for 5-7 minutes at 37°C and transferred to CELLstart™ (Invitrogen, UK) coated 6- or 24-well plates for further characterization.

### 2.5. Evaluation of cell concentration and viability

#### 2.5.1. Cell membrane integrity assay

The qualitative assessment of the cell membrane integrity during culture was done using the enzyme substrate fluorescein diacetate (FDA; Sigma-Aldrich, Germany) and the DNA intercalating dye propidium iodide (PI; Sigma-Aldrich, Germany) as previously described (Serra et al., 2011).

#### 2.5.2. Trypan blue exclusion assay

Cell aggregates were dissociated to single cells by a 5-7 minutes incubation with 0.25% (w/v) Trypsin-EDTA (Invitrogen, UK) at 37°C. Cell concentration and viability was assessed by the trypan blue exclusion method using a 0.1% (v/v) solution prepared in PBS and counting cells in a Fuchs-Rosenthal haemocytometer (Brand, Wertheim, Germany).

#### 2.5.3. Lactate dehydrogenase activity

The extent of cell lysis during iPSC differentiation was assessed by measuring the activity of the intracellular enzyme lactate dehydrogenase (LDH) in the culture supernatant. LDH activity was determined by following spectrophotometrically (at 340 nm) the rate of oxidation of NADH to NAD<sup>+</sup> coupled with the reduction of pyruvate to lactate. The specific rate of LDH release (qLDH, U.day<sup>-1</sup>.cell<sup>-1</sup>) was calculated for every time interval using the following equation:  $qLDH = \Delta LDH / (\Delta t \cdot \Delta X_v)$ , where  $\Delta LDH$  (U) is the change in LDH activity over the time period  $\Delta t$  (day) and  $\Delta X_v$  (cell) is the

average of total cells during the same time period. The cumulative value ( $qLDH_{cum}$ ) was estimated by  $qLDH_{cum\ t+1} = qLDH_{cum\ t} + qLDH_{t+1}$ .

#### **2.5.4. Evaluation of aggregate concentration**

The number of total aggregates and beating/eGFP-positive aggregates was determined in 4-6 wells of a 24-well plate containing 250-400  $\mu$ L aliquots of bioreactor culture samples by using an inverted-microscope (DMI6000, Leica, Germany).

#### **2.5.5. Evaluation of aggregate size, elongation and roundness**

The aggregate size was determined using an inverted-microscope (DMI6000, Leica, Germany) by measuring two perpendicular diameters of each aggregate, from a minimum of 30 aggregates. These measures were used to calculate the average diameter of each aggregate. The elongation and roundness of aggregates was analyzed using measurement analysis tool of ImageJ software. Elongation (or aspect ratio) is defined by the ratio between the major and the minor axis. Roundness is the measure of how closely the shape of an object approaches that of a circle and is defined by the following:  $4 \times \frac{Area}{\pi \times (Major\ axis)^2}$ . Both, elongation and roundness parameters were analyzed from a minimum of 30 aggregates per condition.

### **2.6. Monitorization of CM differentiation**

#### **2.6.1. Flow cytometry**

After dissociation of aggregates or cardiospheres with 0.25% (w/v) Trypsin-EDTA as described above, cells were re-suspended in washing buffer (PBS with 5% (v/v) FBS) and the percentage of live (as assessed with PI dye), eGFP-positive cells were analyzed in a CyFlow® space (Partec GmbH, Germany) instrument, registering 10000 events/sample. The results throughout this analysis constituted a measurement of the percentage of CMs in culture at each time point, reflecting the purity level of the culture.

#### **2.6.2. Semiquantitative and quantitative RT-PCR**

Aggregates or cardiospheres were washed with PBS and centrifuged at 300xg for 5 min. The pellet containing  $10^6$  cells was snap-frozen by immersion in liquid nitrogen. Total RNA was extracted using the High Pure RNA Isolation Kit (Roche, Germany) and reverse transcription was performed with High Fidelity cDNA Synthesis Kit (Roche, Germany) using 200ng of RNA, following manufacturer's instructions.

Gene expression profiles of various markers during cardiac differentiation were analyzed by semiquantitative reverse transcriptase polymerase chain reaction (RT-PCR) using the DreamTaq Green PCR Master Mix (Thermo Scientific, USA). Analyses were performed in 20  $\mu$ L reactions containing 0.5  $\mu$ M of each primer and 1  $\mu$ L of undiluted cDNA template. PCR products (10  $\mu$ L) were electrophoretically separated on 1.5 % agarose (Invitrogen, UK) gel and ethidium bromide-stained bands were detected with a CCD camera using Intas UV-System and Intas GDS application (Intas, Germany). The primer sequences used in RT-PCR are listed in Table A-2.1 (Page 66).

Quantitative RT-PCR was performed in triplicate, for each sample and each gene, using SYBR Advantage qPCR Premix (Clontech, USA) in 10  $\mu$ l reactions with 1:25 diluted cDNA template and 0.2  $\mu$ M of each primer. The reactions were performed in 384-well plates using AB 7900HT Fast Real Time PCR System (Applied Biosystems, Germany). Cycle threshold (Ct's) and melting curves were determined by SDS 2.1 Software. All data was analyzed using the  $2^{-\Delta\Delta Ct}$  method for relative gene expression analysis. Changes in gene expression were normalized to GAPDH gene expression as internal control.

## **2.7. Evaluation of cell growth and differentiation towards CMs**

### **2.7.1. Cell expansion fold**

The cell expansion fold was evaluated based on the ratio  $X_{d9}/X_{d0}$ , where  $X_{d9}$  is the total cell number at day 9 (before purification) and  $X_{d0}$ , the total initial cell number. In Stirred tank bioreactors  $X_{d0}$  represents the initial cell number corresponding to the 30000 aggregates inoculated per bioreactor at day 2.

### **2.7.2. Final CM yield**

The final number of CMs was determined by flow cytometry of eGFP-positive cells at the end of the differentiation process. The CM yield was calculated by the number of eGFP-positive cells divided by the total initial number of iPSCs.

### **2.7.3. CMs produced per liter of culture medium throughput**

The number of CMs produced per liter of culture medium throughput was determined by the number of eGFP-positive cells at the end of the process divided by the total volume of culture medium used throughout the differentiation process, considering all medium exchanges.

## **2.8. Characterization of iPSC-CMs**

### **2.8.1. Immunocytochemistry**

At the end of the differentiation process, aggregates were dissociated and plated on CellStart-coated 6-well plates. Adherent cells were fixed with 4% (w/v) buffered paraformaldehyde (pH 7.5) for 15 minutes at 37°C and permeabilized with 0.5 M ammonium chloride (Sigma-Aldrich), 0.25% Triton X-100 in PBS for 10 min at room temperature (RT). After blocking with 5% (v/v) FBS in PBS for 1 h at room temperature, cells were incubated with primary antibody overnight at 4°C in 0.8% (w/v) bovine serum albumin (BSA) in PBS. The primary antibodies used were anti-sarcomeric- $\alpha$ -actinin (1:800; clone EA-53, Sigma-Aldrich, Germany), anti-titin (E-2; 1:100 dilution; Santa Cruz Biotechnology, USA), anti-troponin I (1:100 dilution; Merck Millipore, Germany), and anti-atrial natriuretic peptide (ANP; 1:200 dilution; Merck Millipore, Germany). After two washing steps with PBS, samples were incubated for 60 min at RT with the secondary antibody anti-mouse-IgG1 AlexaFluor 594 (1:200 dilution in 0.8% (w/v) BSA in PBS; Invitrogen, UK). Nuclei were stained using Hoechst 33432 (1:5000 dilution in PBS; Sigma-Aldrich, Germany). Images were acquired using an inverted fluorescence microscope (DMI6000, Leica, Germany). For immunostaining of whole mounted aggregates, the permeabilization step was performed with 0.2% (w/v) fish skin gelatine and 0.1% (w/v) TX-100 in PBS for 2 h at RT. In this case, the anti-collagen type I (1:200

dilution, Abcam, UK) and the anti-Ki-67 (1:200 dilution, Merck Millipore, Germany) antibodies were used. Aggregates were visualized using spinning disk confocal microscope (Andor Revolution XD, Nikon Eclipse Ti-E, confocal scanner: Yokogawa CSU-x1).

### **2.8.2. Scanning electron microscopy**

For scanning electron microscopy analysis, aggregates were washed twice in Sorensen's Buffer (0.1M NaH<sub>2</sub>PO<sub>4</sub>, 0.1M Na<sub>2</sub>HPO<sub>4</sub>, pH 7.4), fixed with 4% (w/v) formaldehyde and 2.5% (w/v) glutaraldehyde solution for 1 hour at RT, followed by overnight incubation at 4°C. Samples were then washed with Sorensen's Buffer again. After dehydration all samples were dried, coated in a sputter-coater with a layer of gold and observed under a scanning electron microscope (FEG-SEM: JEOL 7001F/Oxford INCA Energy 250/HKL).

### **2.8.3. Detection of Ca<sup>2+</sup> Transients**

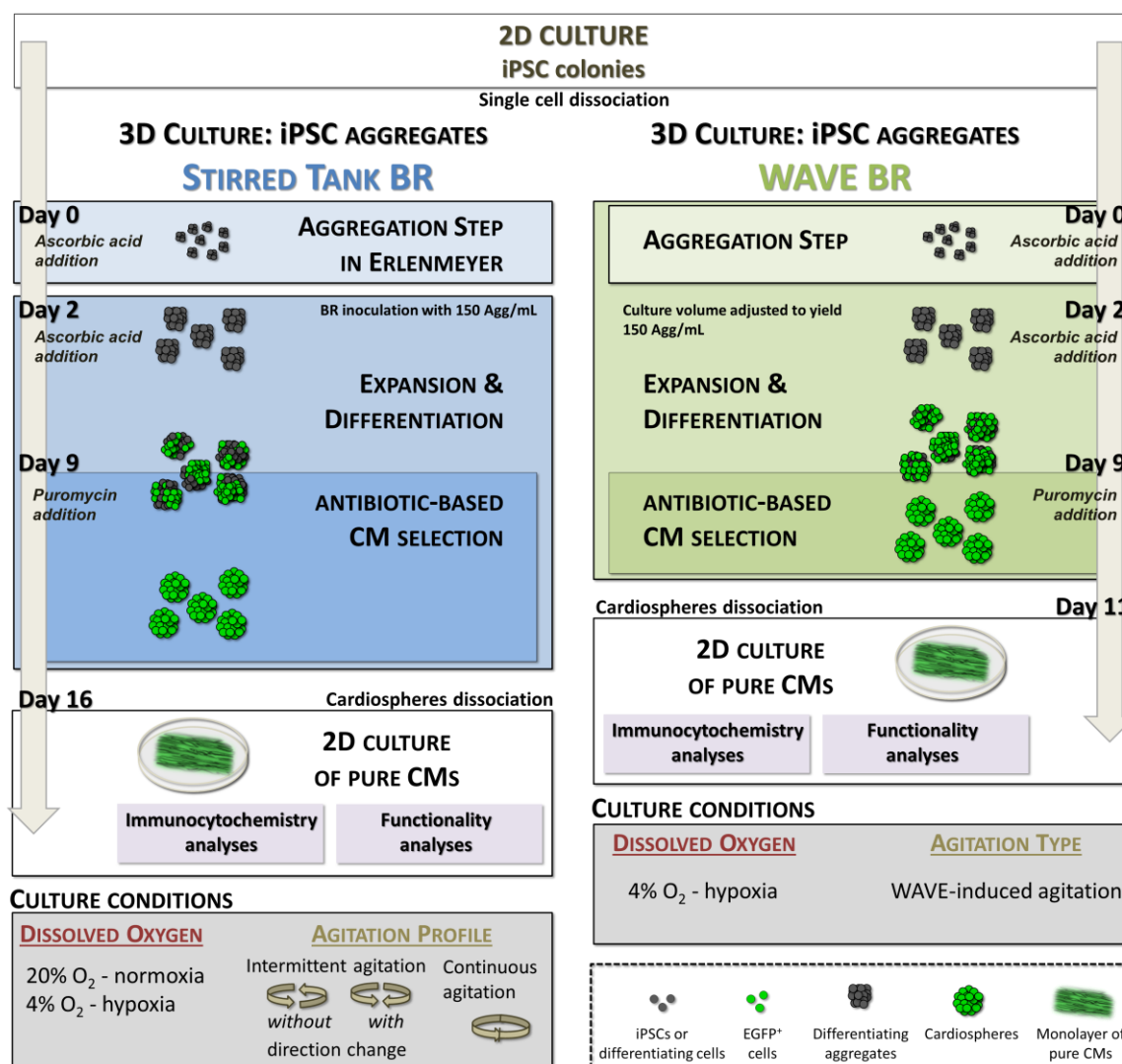
Ca<sup>2+</sup> imaging was performed according to the standard protocol provided in Rhod-3 - Calcium Imaging kit (Invitrogen). Briefly, cardiospheres were plated onto eight-well culture slides coated with CellStart. After one week in culture to promote cell adherence to the plate, the beating CMs were loaded with the cell permeant calcium indicator dye Rhod-3 for 1h at 37°C, washed twice in PBS, and incubated for 1h with a water-soluble reagent to reduce baseline signal and washed again in PBS. Cells were imaged live using a spinning disk confocal microscope (Andor Revolution XD). Fluorescence was measured by manually defining each region of interest and quantified in relation to baseline fluorescence (F/F<sub>0</sub>) using Micro-Manager 1.4 and ImageJ softwares.

### **2.8.4. Electrophysiological characterization**

Purified cardiac clusters were washed twice with PBS and dissociated using 0.05% Trypsin/EDTA 2 days before measurement. Single CMs were plated on glass cover slips coated with 0.1% gelatin. The patch clamp-experiments were performed as described previously (Kuzmenkin et al., 2009). Briefly, the cover slips were placed into a recording chamber (37°C) and cells were continuously perfused with extracellular solution. Cell membrane capacitance was determined online using Pulse software (Heka Elektronik, Germany). Action potential (AP) recordings of spontaneously beating CMs were performed utilizing the whole-cell current-clamp technique with an EPC-9 amplifier (HEKA Elektronik) and operated through the Pulse acquisition software. Response to hormonal regulation was analyzed by administering 1 μM isoproterenol (Iso, Sigma-Aldrich, USA) or 1 μM carbachol (Cch, Sigma-Aldrich, USA).

## **2.9. Statistical analysis**

For each culture system evaluated, at least three independent experiments were performed. The results were presented as the mean±SD. For the electrophysiological characterization data are shown as mean±SEM. Statistical significance was assessed by one-way analysis of variance (ANOVA). Values of p<0.05 were considered statistically significant.



**Figure 2.1. Experimental scheme for differentiation and purification of iPSC-CMs in stirred tank and WAVE bioreactors.** In stirred tank bioreactors, an aggregation step was first performed in an Erlenmeyer for 48 hours. After this time, aggregates were transferred to bioreactors to yield 150 aggregates/mL and cultured in the presence of ascorbic acid for additional 7 days. At day 9, puromycin was added to the medium to eliminate non-CMs. After 7 days of antibiotic-based CM selection, pure CM aggregates (cardiospheres) were harvested, dissociated and CMs were cultured in 2D plates for characterization studies (immunofluorescence microscopy and electrophysiological studies). In WAVE bioreactor cultures, cells were inoculated as single cells directly into the WAVE bioreactor and at day 2 the culture volume was adjusted to obtain 150 aggregates/mL. Aggregates were cultured in the presence of ascorbic acid for additional 7 days. At day 9, CM lineage selection was initiated and lasted 3 days. At day 11, aggregates were harvested, dissociated and plated in 2D plates for further characterization. Culture conditions evaluated in each bioreactor system are depicted in the bottom of the schematic workflow.

### 3. Results

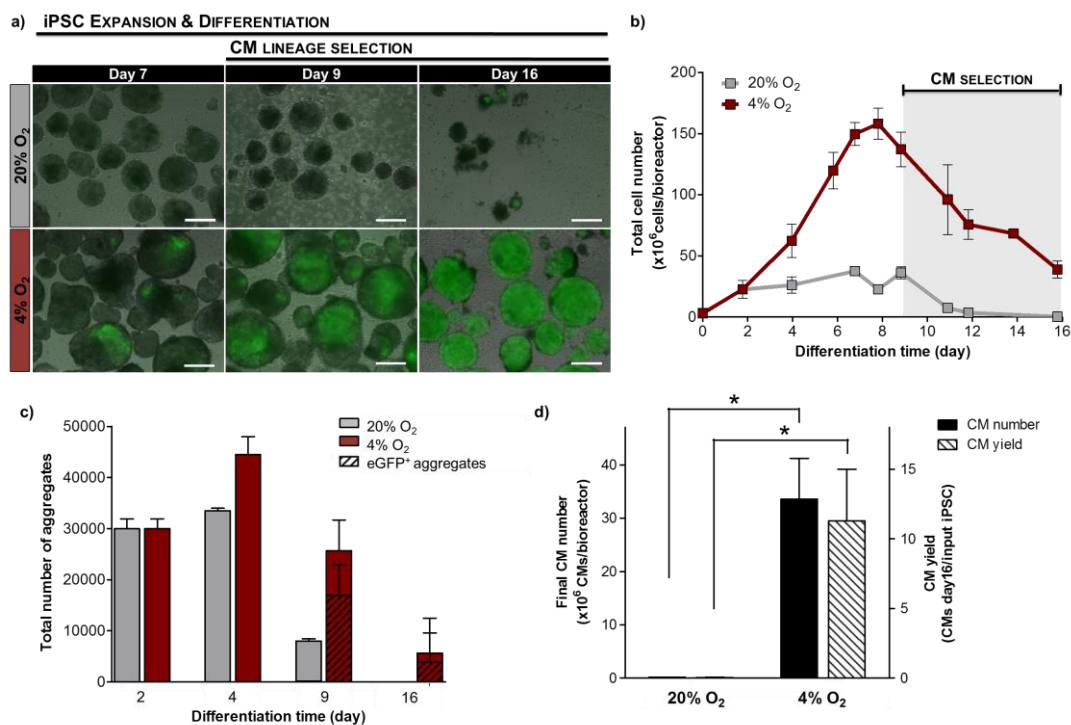
#### 3.1. Effect of dissolved oxygen on CM differentiation of iPSCs in stirred tank bioreactors

In order to establish a robust and scalable platform for production of functional iPSC-CMs, we first investigated the effect of DO on cardiac iPSC differentiation in stirred tank bioreactor systems. For that purpose, we compared the effect of normoxic atmospheric oxygen levels (20% O<sub>2</sub> tension) with physiological oxygen levels (2–5% O<sub>2</sub> tension or atmospheric hypoxia). Within this range of physiological oxygen levels, we selected a value of 4% O<sub>2</sub> since previously reported studies showed that this oxygen concentration improves cardiomyocyte differentiation in ESC aggregate cultures (Bauwens et al., 2005; Niebruegge et al., 2009).

Aggregation of single cell suspension was promoted in Erlenmeyers and orbital agitation for 48 hours under normoxia conditions; these conditions resulted in the formation of small aggregates with a mean size of 155±56 μm that readily metabolized the vital dye fluorescein diacetate but not the dead cell marker propidium iodide (Figure A-2.1, Page 64). These aggregates were transferred to fully controlled stirred tank bioreactors and cultured under either normoxic (DO=20% O<sub>2</sub>) or hypoxic (DO=4% O<sub>2</sub>) conditions for additional 14 days (Figure 2.1).

The results showed that a DO of 4% O<sub>2</sub> maximizes cell proliferation and CM differentiation (Figure 2.2). In these culture conditions, the size of aggregates, the total number of cells and aggregates were higher throughout the culture (Figure 2.2A-C) resulting in a significantly higher expansion fold on day 9 of differentiation when compared to normoxic conditions (44.9±2.7 versus 12.2±1.4 cells/initial iPSC, p=0.001, Table 2.1). Moreover, first eGFP-positive cells and contracting areas in aggregates cultured under hypoxia were observed already on day 7 of differentiation, contrasting with cell aggregates cultured at 20% O<sub>2</sub> where eGFP-positive cells and beating areas were rarely observed throughout culture time (Figure 2.2A). The higher overall cell expansion in hypoxic cultures corresponded to a significant improvement in CM yield as determined on day 16 of differentiation, after 7 days of puromycin selection (11.3±3.7 vs. 0.05±0.02 CMs/input iPSC, p=0.045, Figure 2.2D), and to an approximately 210-fold enhancement in CM numbers compared to normoxia (33.6±7.6 x10<sup>6</sup> CMs vs. 0.15±0.06 x10<sup>6</sup> CMs per bioreactor run, p=0.01, Figure 2.2D). Since a low DO environment proved to be a key parameter in enhancing CM differentiation of iPSCs, we selected this culture condition to be used in further experiments.





**Figure 2.2. Effect of dissolved oxygen on CM differentiation of iPSCs in stirred tank bioreactors.** Aggregates were inoculated at day 2 in stirred tank bioreactors at DO of 20% O<sub>2</sub> (atmospheric normoxia) or 4% O<sub>2</sub> (atmospheric hypoxia). **A).** Merged phase contrast and fluorescence images showing cell aggregates composed by eGFP-positive cells (green) at days 7, 9 and 16 of culture. Scale bars: 200  $\mu$ m. **B).** Profile of total cell number during culture time. **C).** Total number of aggregates at days 2, 4, 9 and 16. The number of eGFP-positive aggregates is indicated by striped bars. **D).** Total number of CMs produced per bioreactor run (black bars) and CM yield (number of CMs at day 16/input iPSC, striped bars) obtained in both normoxic and hypoxic culture conditions. Error bars (B-D) represent SD of 3 individual bioreactor experiments. Significantly different,  $P < 0.05$  (\*) and  $P < 0.01$  (\*\*).

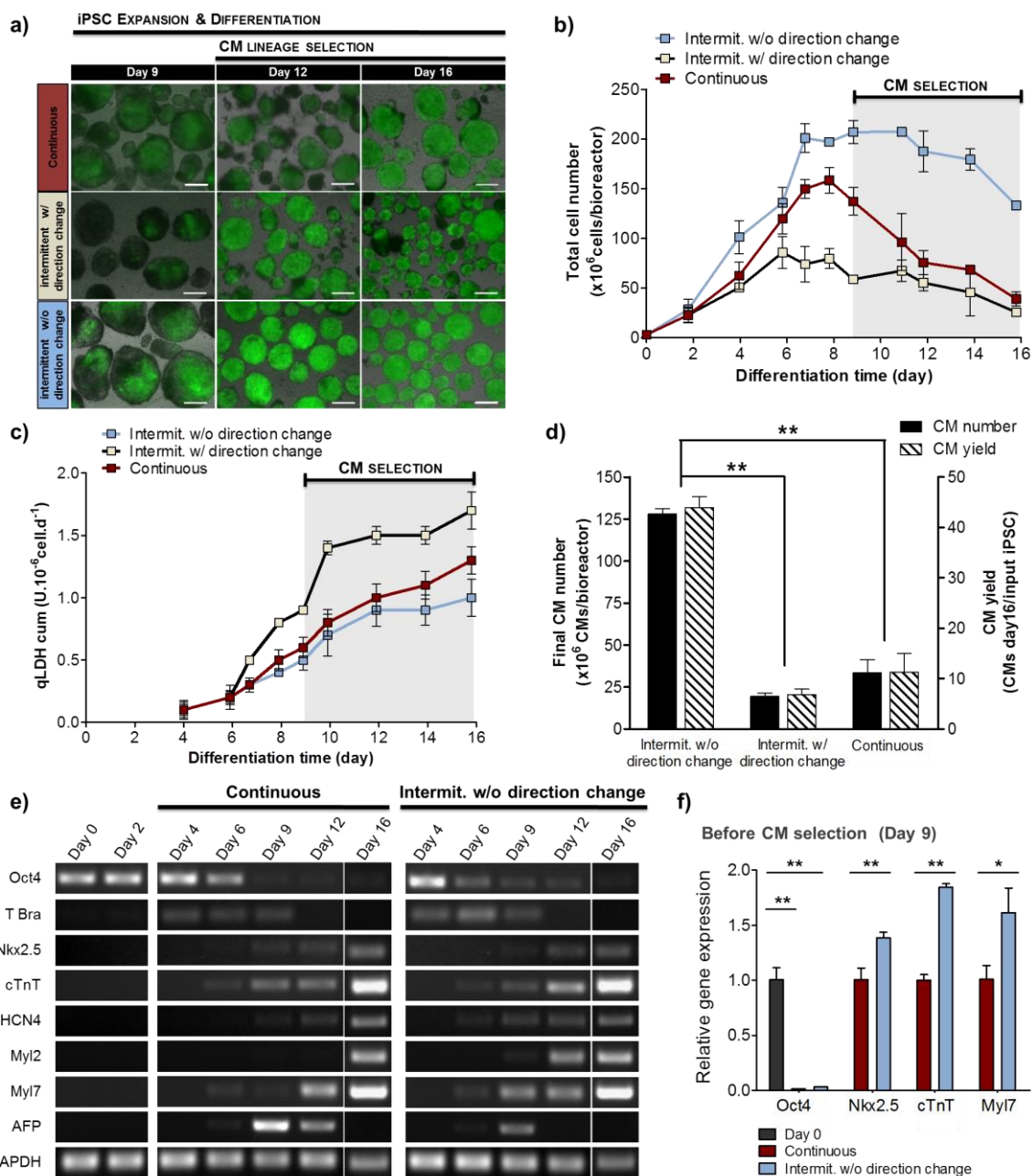
### 3.2. Impact of agitation profile on CM differentiation of iPSC in stirred tank bioreactors

The effect of different agitation profiles on CM differentiation was assessed using stirred tank bioreactors operating under hypoxic conditions. A continuous agitation was compared with an intermittent agitation with and without change in the agitation direction. Based on previous reports that mechanical stimulation enhances contractile function and up-regulates cardiac gene expression (Shimizu et al., 2008; Shimko and Claycomb, 2008), we hypothesized that the hydrodynamic environment imposed by an intermittent agitation composed of repeated and brief stops could provide cyclic mechanical forces to the cells and consequently potentiate iPSC differentiation towards contractile CMs.

Our results show that an intermittent agitation profile without direction change led to a faster cell growth, higher cell number and enhanced CM differentiation when compared to the other agitation profiles evaluated (Figure 2.3, Table 2.1). At day 9, an increase of  $73.4 \pm 7.6$  fold in cell number was obtained in this culture condition (Table 2.1), reflecting more pronounced cell proliferation as compared to other two tested conditions. At this culture time point the percentage of eGFP-positive cells, as determined by flow cytometry analysis of dissociated aggregates, was significantly higher in this culture condition ( $43.9 \pm 6.6\%$ ) than in continuous ( $23.3 \pm 5.0\%$ ,  $p = 0.01$ ) or in intermittent agitation profile with direction change ( $16.5 \pm 3.7\%$ ,  $p = 0.01$ ) cultures (Table 2.1),

suggesting enhanced cardiac differentiation efficiency. In accordance, lower cell death during antibiotic treatment, as indicated by a lower accumulation of intracellular LDH in culture supernatant, was observed (Figure 2.3C), indicating that a higher percentage of puromycin resistant iPSC-CMs and a lower amount of contaminating cells were present in culture. At the end of the process higher CM number ( $128.1 \pm 3.3 \times 10^6$  CMs/bioreactor), yield ( $44.0 \pm 2.1$  CMs/input iPSC) and purity ( $97.4 \pm 0.4\%$ ) were obtained in cultures operated under intermittent agitation without direction change (Figure 2.3D, Table 2.1); in comparison to continuous agitation and intermittent agitation with direction change profiles, this culture condition enabled a significant improvement of 4- and 6.5-fold in CM production, respectively ( $p=0.0001$ , Table 2.1).

RT-PCR analyses of RNA isolated from intermittent agitation profile without direction change and continuous agitation cultures reflect the impact of cyclic mechanical forces promoted by the different hydrodynamic environments on cell phenotype (Figure 2.3E-F). A typical cardiac lineage gene expression pattern was observed in both culture conditions. The expression of the pluripotency marker Oct4 progressively decreased over the course of differentiation reaching very low levels by day 9 (Figure 2.3E-F) and being undetectable at day 16 purified CMs (Figure 2.3E). Additionally, the expression of the early mesoderm marker T brachyury was up-regulated from day 4 to day 6 and down-regulated thereafter. These results allow us to assume that the marked proliferation observed up to day 7 (Figure 2.3B) in these cultures might have resulted from the prevalence of highly proliferative undifferentiated and mesodermal cells up to this timepoint. Afterwards, a progressive increase in the expression of cardiac-progenitor and cardiac-specific gene markers (Nkx2.5, cTnT, HCN4, Myl2 and Myl7) was observed. The higher band intensities at day 9 of differentiation (before initiation of CM selection) indicated that the majority of the cardiac-specific markers were greater expressed in cells cultured under intermittent agitation conditions. RT-qPCR analyses further confirmed that the expression of the cardiac genes Nkx2.5, cTnT and Myl7 in cells at this time point was, respectively, 1.4- ( $p<0.01$ ), 1.8- ( $p<0.01$ ) and 1.6-fold ( $p<0.05$ ) higher in cultures with intermittent agitation than in those with continuous agitation profile (Figure 2.3F). In order to further assess the purity of puromycin-selected CM preparations, we monitored the expression of the endodermal marker  $\alpha$ -fetoprotein (AFP) in cells from both cultures. AFP transcripts were detected on days 6-12 in cell aggregates from both conditions but their expression was higher in cultures with continuous agitation profile. On day 12, the expression of AFP was still observed in these cultures but not in cultures operated under intermittent agitation profile without direction change, thus suggesting that this agitation profile may provide a favorable hydrodynamic environment for cardiac but not endodermal lineage differentiation. Nonetheless, in both culture conditions the expression of AFP was not detectable at the end of the selection process (day 16), confirming the final purity of antibiotic selected CMs (Figure 2.3E). Altogether, these results indicate that the mechanical stimulus provided to the cells by the agitation profile inherent to stirred-tank bioreactors can be modulated to enhance cardiomyogenesis.



**Figure 2.3. Impact of the agitation profile on CM differentiation of iPSCs in stirred tank bioreactors.** Aggregates were inoculated at day 2 in stirred tank bioreactors operating in continuous and intermittent stirring with or without change of direction. **A).** Phase contrast and fluorescence images showing cell aggregates with eGFP-positive cells (green) at days 9, 12 and 16 of culture. Scale bars: 200  $\mu\text{m}$ . **B-C).** Profile of total cell number (B) and cumulative values of specific rates of LDH release (C) in each bioreactor culture condition during time. **D).** Total number of CMs produced in each bioreactor run (black bars) and CM yields (striped bars). **E).** Semiquantitative RT-PCR analyses demonstrating the expression of pluripotency (Oct4), endoderm (AFP), early mesoderm (T-Brachyury) and CM-specific (Nkx2.5, cTnT, HCN4, Myl2, Myl7) genes in differentiating cells cultured in bioreactors operating in continuous agitation (left panel) and intermittent agitation without change of direction (right panel) profiles at different time points. **F).** Quantitative RT-PCR analysis showing the relative expression of Oct4, Nkx2.5, cTnT and Myl7 at day 9. Values were normalized to the continuous agitation culture condition, except Oct4 expression that was normalized to RNA from undifferentiated cells (day 0, black bar). Data are shown as mean  $\pm$  SD of 3 individual bioreactor experiments. Significantly different,  $P < 0.05$  (\*) and  $P < 0.01$  (\*\*).

**Table 2.1. Quantitative characterization of CM differentiation of iPSC in stirred tank and WAVE bioreactors.**

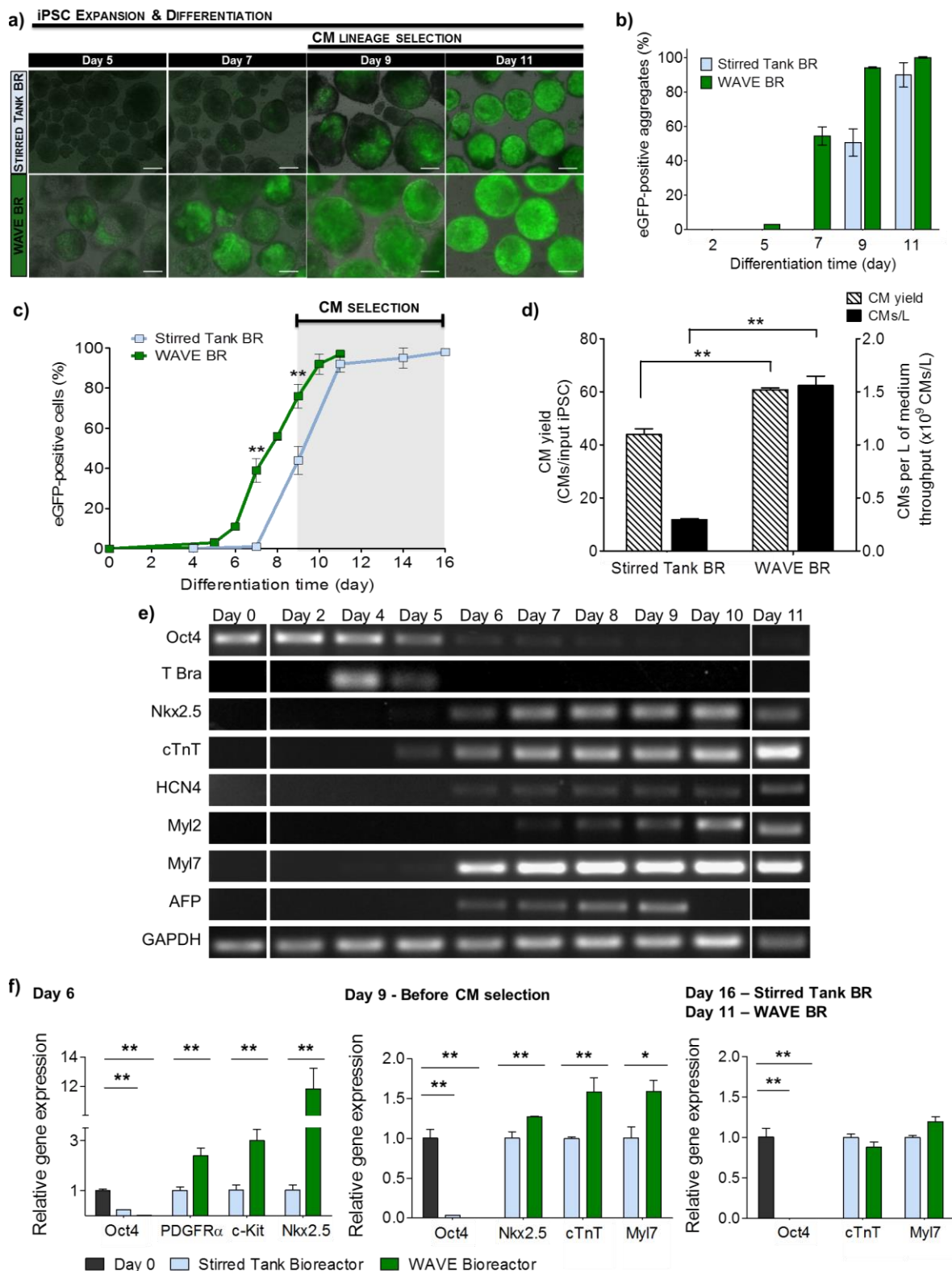
Culture system	Stirred tank bioreactor			WAVE bioreactor
	Continuous	Intermittent with direction change	Intermittent without direction change	Wave-induced
Working volume (mL)	200	200	200	1000
Cyclic strain frequency (Hz)	0	0.033	0.033	0.82 to 0.86
Expansion fold (cells on day 9/input iPSC)	44.9±2.7	23.7±1.7	73.4±7.6	65.7±7.2
CM purity before purification (day 9, %eGFP-positive cells)	23.3±5.0	16.5±3.7	43.9±6.6	76.0±5.8
CM purity after selection (day 16/11, %eGFP-positive cells)	85.7±4.1	77.0±3.0	97.4±0.4	97.6±1.0
Final CM number ( $\times 10^6$ CMs)	33.6±7.6	19.5±1.7	128.1±3.3	2279.8±69.2
Final CM yield (number of CMs/input iPSC)	11.3±3.7	6.8±1.1	44.0±2.1	60.8±0.7
Final CM number <i>per</i> liter of culture medium throughput ( $\times 10^6$ CMs/L)	78.1±11.8	45.4±4.0	295.9±8.8	1561.1±87.3

### 3.3. CM differentiation of iPSCs in WAVE bioreactors

In order to further explore the beneficial impact of mechanical forces induced by bioreactor hydrodynamics on CM differentiation, we evaluated the capacity of iPSCs to differentiate towards CMs in WAVE bioreactors.

Cell aggregation was initiated by inoculating single iPSCs into WAVE bioreactors. After 2 days of cultivation under hypoxic conditions aggregates presented a size of  $167\pm 43$   $\mu\text{m}$ , similar to those obtained in Erlenmeyer flasks (Figure A-2.1, Page 64).

The comparison of CM differentiation efficiency in WAVE and optimized stirred tank bioreactors (operated under 4% O<sub>2</sub> tension and intermittent agitation without direction change) revealed that WAVE bioreactor cultures favored CM lineage commitment, enabling a reduction in the differentiation time and increased CM yields (Figure 2.4). In these cultures, eGFP-positive cells and contracting areas in aggregates were observed from day 5 onwards, increasing rapidly in number and size (Figure 2.4A-C, Movie A-2.1). By day 7,  $54.3\pm 5.2\%$  of the aggregates exhibited a considerable area of eGFP-positive and spontaneously beating cells (Figure 2.4A-B). In accordance with this result, flow cytometry analyses indicated that  $38.6\pm 6.0\%$  of cells in aggregates were eGFP-positive, compared to less than 5% detected in stirred tank bioreactors at this time point (Figure 2.4C). Importantly, on day 9 of culture, i.e. before CM selection, the percentage of eGFP-positive cells among all cells dissociated from aggregates was almost 2-fold higher in WAVE bioreactors ( $76.0\pm 5.8\%$ ) compared to stirred tank cultures ( $43.9\pm 6.6$ , Figure 2.4C, Table 2.1). Consequently, only 2 days of antibiotic treatment were sufficient to obtain a 97.6 % pure CM population in WAVE bioreactors (Figure 2.4C, Table 2.1). In contrast, at day 11 of differentiation, aggregates in stirred tank bioreactors were not yet completely pure and additional 5 days of antibiotic treatment were required to generate a 97.4 % pure CM population (Figure 2.4A, C). In terms of CM productivities, in optimized stirred tank cultures approximately 0.430-L medium throughput (total volume of medium used during the process) resulted in the generation of  $0.1\times 10^9$  CMs, which correspond to a coefficient of  $0.2\times 10^9$  CMs/L. On the other hand, in WAVE bioreactor  $2.3\times 10^9$  CMs were produced in 1.5-L medium throughput (1L until day 9, 0.5L medium exchange at day 9) obtaining  $1.5\times 10^9$  CMs/L (Table 2.1).



**Figure 2.4. Differentiation of iPSC into CMs in WAVE and stirred tank bioreactors.** WAVE cultures were compared with optimized stirred tank bioreactor cultures (operated under 4% O<sub>2</sub> and intermittent agitation without direction change) in terms of CM differentiation efficiency. **A).** Phase contrast and fluorescence images showing cell aggregates composed by eGFP-positive cells (green) at days 5, 7, 9 and 11. Scale bars: 200  $\mu$ m. **B-C).** Percentage of eGFP-positive aggregates during culture time. C. Percentage of eGFP-positive cells during culture time as determined by flow cytometry. **D).** CM yields (stripped bars) and number of CMs generated per liter of culture medium throughput (CMs/L, black bars). **E).** Semiquantitative RT-PCR analyses

showing expression of pluripotency (Oct4), endoderm (AFP), mesoderm (T-Bra) and CM-specific (Nkx2.5, cTnT, HCN4, Myl2, Myl7) genes during the time course of differentiation process in WAVE bioreactors. **F**). Quantitative RT-PCR analysis of cells cultured in optimized stirred tank and WAVE bioreactors, at day 6, before (day 9) and after CM selection (day 16 and 11 for stirred tank and WAVE bioreactor cultures, respectively). Expression was normalized to RNA from stirred tank bioreactor cultures operating with intermittent agitation, except for Oct4 expression that was normalized to RNA of undifferentiated cells (day 0, black bars). Data are given as mean  $\pm$  SD of 3 individual bioreactors experiments. Significantly different,  $P < 0.05$  (\*) and  $P < 0.01$  (\*\*).

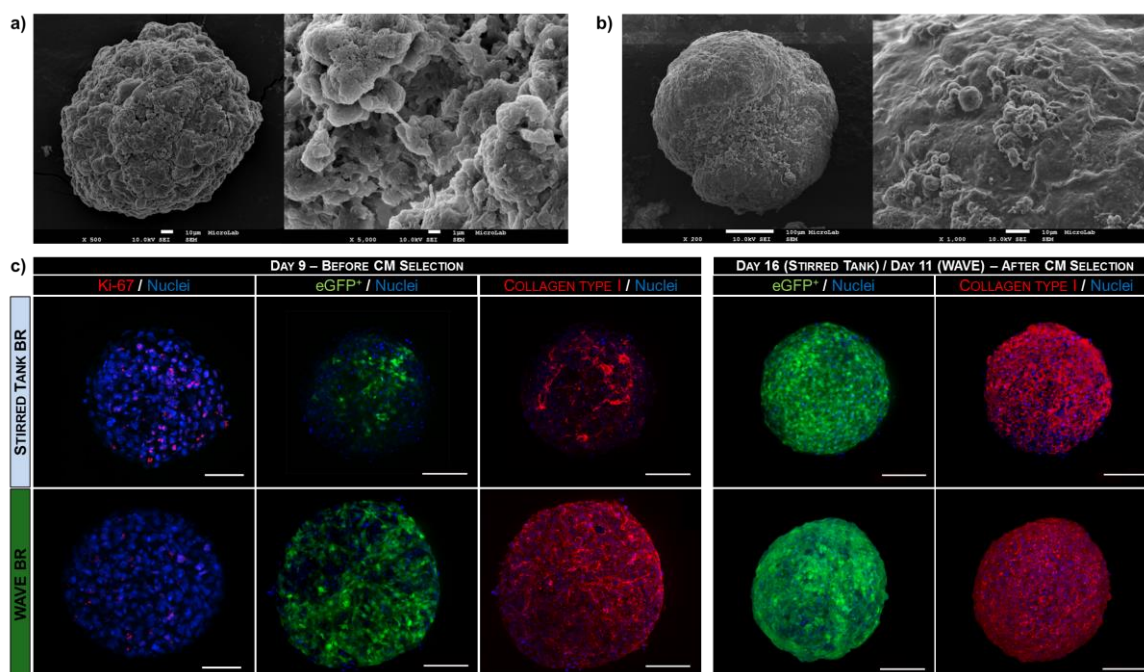
---

Overall, iPSC differentiation in WAVE bioreactors resulted in an improvement of about 40% in CM yield ( $60.8 \pm 0.7$  CMs/input iPSC) and in a 5 times higher CM production per liter of culture medium throughput (CMs/L) in comparison to optimized stirred tank cultures (Figure 2.4D, Table 2.1).

RT-PCR analysis showed that early mesoderm, cardiac progenitor and cardiac-specific genes were expressed earlier and to a higher extent in aggregates from WAVE cultures than in stirred cultures (Figure 2.4E compare to Figure 2.3E). The expression of the pluripotency gene Oct4 decreased more rapidly in aggregates cultured in WAVE bioreactors reaching very low levels on day 6 of differentiation and undetectable levels from day 8–9 onwards (Figure 2.4E–F). In contrast, the Oct4 transcripts were still expressed at this stage of differentiation in stirred cultures and were not detectable only in purified CMs (Figure 2.3E and Figure 2.4F). Additionally, in WAVE cultures the peak in the early mesodermal gene expression (assayed by the expression of T-Brachyury) occurred earlier (day 4, Figure 2.4E) than in stirred tank cultures (day 6, Figure 2.3E). By day 6, the cardiac mesodermal (PDGFR $\alpha$ ) and cardiac progenitor (cKit and Nkx2.5) genes were significantly higher expressed in WAVE than in stirred tank bioreactor cultures. The expression of cardiac specific markers was also detected earlier in WAVE cultures and increased gradually in later stages of differentiation (Figure 2.4E). Importantly, the greater band intensities of cardiac transcripts Nkx2.5, cTnT and Myl7 observed in WAVE cultures before antibiotic selection (day 9) indicate that these cultures contained a substantially higher proportion of CMs than stirred bioreactor cultures (Figure 2.3E, 2.4E). RT-qPCR analyses confirmed that by day 9 of differentiation the expression of these three cardiac markers was significantly higher (1.3, 1.6 and 1.6-fold, respectively) in WAVE cultures than in stirred tank bioreactors (Figure 2.4F). At the end of antibiotic selection, the expression of cTnT and Myl7 were very similar in both bioprocesses (Figure 2.4F) confirming the similar degree of CM purity in both groups (Table 2.1).

Phase-contrast and scanning-electron microscopy (SEM) analysis of aggregates on day 9 of differentiation (i.e. before cell lineage selection) revealed that aggregates from WAVE and stirred tank bioreactor cultures differed in size and morphology (Figure 2.5A-B, Table A-2.1, Figure A-2.2). The mean size of aggregates cultured in WAVE bioreactors was higher ( $440.04 \pm 107.89$   $\mu$ m) and they were less spherical and more elongated than aggregates from stirred tank bioreactors ( $384.41 \pm 124.80$   $\mu$ m) (Figure A-2.2, Page 64 and Table A-2.2, Page 66). This higher size and reduced “sphericity” observed in the aggregates cultured in the WAVE bioreactor might be justified by the different hydrodynamic environment promoted by this type of bioreactor. Additionally, aggregates from WAVE bioreactors showed a smooth outer surface (Figure 2.5B), whereas

aggregates from stirred tank cultures exhibited a looser texture and a rough surface in which cell-cell contacts could be discerned at a higher magnification (Figure 2.5A). Previous studies demonstrated that during cardiac differentiation of ESCs, the extracellular matrix (ECM) mainly composed by collagen type I is deposited on the surface of differentiating aggregates originating a smoother aggregate surface topography (Horton and Auguste, 2012; Taha et al., 2012). Thus, our findings may suggest that prior to CM selection the aggregates cultured in WAVE bioreactors present a higher deposition of extracellular matrix (ECM) than stirred tank aggregates. To further confirm these observations, we stained the whole-mount day 9 aggregates with collagen type I antibody to determine the amount and distribution of this ECM component by confocal microscopy. This analysis clearly revealed that aggregates from WAVE bioreactors contain considerably higher levels of collagen type I than aggregates from stirred tank bioreactors (Figure 2.5C, left panel) and that, based on the fraction of eGFP-positive cells in whole aggregates, the WAVE aggregates presented higher CM purity than the aggregates derived in stirred tank bioreactors, before induction of CM selection. Moreover, at this timepoint a lower percentage of proliferative cells (Ki-67 positive cells) was observed in aggregate derived from WAVE bioreactors when comparing with aggregates from stirred tank bioreactor cultures (approximately 20% vs. 58% of the cells, respectively, Figure 2.5C).



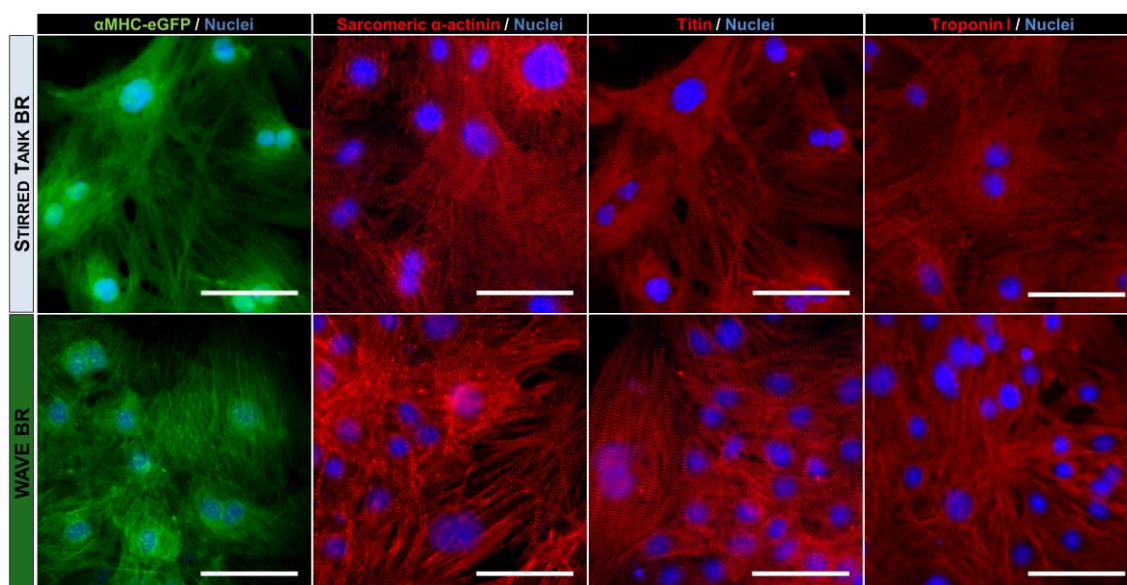
**Figure 2.5. Scanning-electron and confocal microscopy of iPSC-derived cell aggregates and cardiospheres. A-B).** SEM micrograph of differentiating cell aggregates collected from stirred tank (A) and WAVE (B) bioreactors at day 9 of differentiation. Higher magnification images evidence the differences in aggregate surface topography. **C).** Immunofluorescence and confocal microscopy images of the whole-mount day 9 aggregates (left panel) and cardiospheres collected at the end of selection process (right panel). The frequency and distribution of eGFP-positive (green), Ki-67 (red) and collagen type I-positive cells (red) is shown. Nuclei were labeled with DAPI (blue). Scale bars: 100  $\mu$ m.

Taken together, our data show that iPSCs differentiate into CMs in WAVE bioreactors with faster kinetics and higher efficiency than in stirred tank bioreactors. At the end of the differentiation process and the puromycin selection procedure (day 16 for stirred tank and day 11 for WAVE bioreactor), collagen type I staining was similar in intensity and distribution in aggregates from both types of cultures (Figure 2.5C, right panel).

### 3.4. Structural properties and action potential (AP) parameters of CMs generated in stirred tank and WAVE optimized bioprocesses

Before CM selection, some aggregates were dissociated into single cells and seeded in static culture plates for structural analyses. Immunofluorescence staining for sarcomeric  $\alpha$ -actinin, as well as the distribution of  $\alpha$ -MHC protein (GFP staining), indicate that cells from WAVE cultures were more elongated and showed more organized sarcomeric structures, by day 9, when compared to cells from stirred tank cultures (Figure A-2.3, Page 65). These results are in agreement with the findings of other studies showing that cyclic tensions promote elongation of the cell membrane, orientation of actin filaments and a higher structural organization (Geuss and Suggs, 2013; Shimko and Claycomb, 2008).

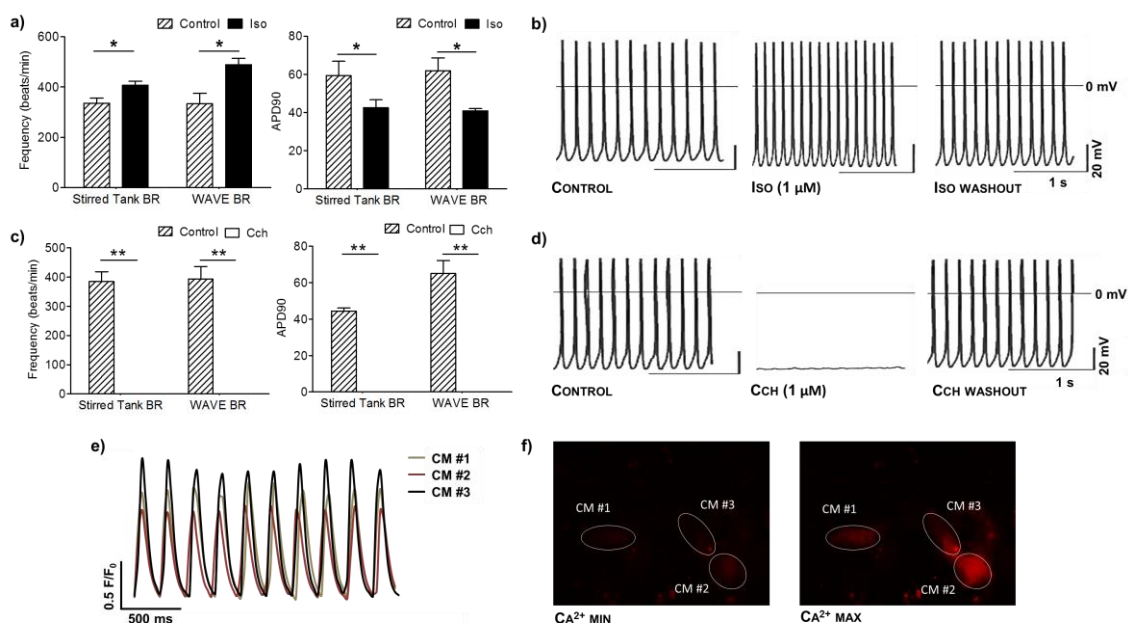
After the differentiation and selection process, beating cardiospheres (Movie A-2.2) were also dissociated into single cells and seeded in 2D plates for structural and functional characterization. Monolayers of pure CMs were obtained and cells maintained their spontaneous beating activity, which became synchronized over culture time (Movie A-2.3). Immunocytochemical analysis of cardiac-specific proteins  $\alpha$ -MHC, sarcomeric  $\alpha$ -actinin, titin and troponin I revealed that iPSC derived-CMs produced in both bioreactor systems stained positive for these cardiac structural proteins (Figure 2.6), presenting an organized striation pattern typical of CMs.



**Figure 2.6. Structural properties of CMs generated in stirred tank and WAVE optimized bioprocesses.** Cardiospheres were dissociated into single cells, plated on 2D plates and after being cultured for up to 2 weeks, stained for CM markers. Immunocytochemical analysis of eGFP-positive CMs (green) using sarcomeric  $\alpha$ -actinin, titin and troponin I (red) antibodies. Nuclei are counterstained with DAPI (blue). Scale bars: 50  $\mu$ m.



In order to assess the electrophysiological properties of CMs generated in both bioreactor systems, AP recordings in single CMs were performed. The great majority of puromycin selected CMs derived from both bioprocesses displayed an atrial-like AP morphology (stirred tank: 100%, WAVE: 92%). These findings are also in agreement with the enhanced expression of atrial transcripts (Myl7) and reduced expression of the transcripts specific for the pacemaker (HCN4) and ventricular-like phenotypes (Myl2) detected in the final differentiated population by RT-PCR (Figure 2.3E and 2.4E). The AP characteristics of purified CMs generated in WAVE and stirred cultures were very similar showing comparable maximum diastolic potential (MDP), beating frequency, AP upstroke velocity ( $V_{max}$ ), velocity of diastolic depolarization ( $V_{dd}$ ) and AP duration (APD) (Table A-2.3, Page 66). Additionally, the CMs generated in WAVE and stirred tank bioreactor cultures exhibited AP parameters similar to the ones described in literature for atrial-like late stage development fetal CMs (day 16-19 of differentiation), such as MDP ( $-63.3 \pm 1.3$  mV), frequency ( $234 \pm 19$  beats/min),  $V_{max}$  ( $27.9 \pm 0.7$  V/s) and  $V_{dd}$  ( $0.115 \pm 0.017$  V/s) (Kuzmenkin et al., 2009). Besides exhibiting largely indistinguishable AP properties, CMs produced in both bioprocesses also responded similarly to adrenergic and muscarinic agonists, isoproterenol and carbachol, respectively. When isoproterenol was administered to CMs a significant increase of AP frequency and a shortening of APD at 90% of repolarization (APD90) was observed (Figure 2.7A).



**Figure 2.7. Functional characterization of CMs produced in stirred tank and WAVE bioreactors. A-D).** Pharmacological response of CMs. Effect of 1  $\mu$ M Isoproterenol (Iso, **A-B**) and 1  $\mu$ M Carbachol (CCh, **C-D**) on beating frequency and on action potential (AP) duration at 90% repolarization (APD90) in iPSC-CMs. (**B,D**) Representative recordings of APs from WAVE bioreactor-derived CMs. APs were recorded before the application of the drug (Control) in the presence of the drug (Iso / CCh), and after washout of the drug (washout). **E-F).** Calcium transients of CMs produced in WAVE bioreactor. **E)** Graphical representation of calcium level cycling, during CMs contraction, determined by confocal imaging of the cell permeant calcium indicator dye Rhod-3, for three different cells. **F)** Pseudo-color images show minimal ( $Ca^{2+}$  min, left image) and maximal ( $Ca^{2+}$  max, right image) Rhod-3 fluorescence intensity in the three analyzed cells. Significantly different,  $P < 0.05$  (\*) and  $P < 0.01$  (\*\*).

Moreover, positive chronotropic effects of isoproterenol were reversible upon washout (Figure 2.7B). In contrast, the administration of carbachol, a synthetic acetylcholine analog, evoked a significant reduction in the beating rate in CMs from stirred tank and WAVE bioreactors, which was also reversible upon washout (Figure 2.7C-D).

In order to further evaluate the functional integrity of CMs produced in WAVE bioreactors we performed real-time intracellular calcium imaging with the calcium indicator dye Rhod-3. This analysis revealed that distinct iPSC-CMs from a beating monolayer present synchronized oscillatory patterns of intracellular calcium concentrations (Figure 2.7E-F). Movie A-2.4 shows a representative live imaging recording of whole-cell calcium transients for contracting CMs produced in WAVE bioreactors.

Overall, these results show that CMs produced using the protocol developed in this work exhibit intact molecular, structural and functional properties.

#### **4. Discussion**

In this study we developed a new method for mass production of murine iPSC-CMs using environmentally controlled bioreactors. The expansion and CM differentiation of human and murine pluripotent stem cells in stirred tank bioreactors have been reported by our group (Serra et al., 2010) and others (Bauwens et al., 2005; Niebruegge et al., 2008, 2009). Aiming to further improve CM yields, we designed a bioreactor protocol that combine low oxygen concentrations with a cyclic mechanical rich environment by manipulating bioreactor hydrodynamics, more specifically the agitation type and profile. In this study, we showed for the first time that a DO of 4% O<sub>2</sub> tension, along with the use of either an intermittent stirring or a wave-induced agitation, favors iPSC differentiation towards the CM lineage. Using an intermittent agitation in stirred tank bioreactors, we were able to improve by 1000-fold CM yields (up to 44 CMs/input iPSC) when compared to normoxic continuously agitated cultures. Moreover, we demonstrated that the wave-induced agitation in combination with 4% O<sub>2</sub> tension from the beginning of iPSC differentiation increases the kinetics of cardiac differentiation, enabling a reduction of bioprocess duration by 5 days, and further improves the CM yields (60 CMs/input iPSC). To our knowledge, this is the first study reporting the use of the WAVE bioreactor for PSC culture. This type of bioreactor presents a simple design, appealing to either biological engineers or medical professionals and offers a low shear environment suitable for growth of sensitive cells such as stem cells (Houtzager et al., 2010).

Oxygen tensions and mechanical cues have been shown to mediate PSCs proliferation and differentiation. In our study, we showed that hypoxic exposure (4% O<sub>2</sub> tension) improves CM differentiation efficiencies by enhancing both cell proliferation and cardiomyogenesis when compared to normoxia conditions. This data is in accordance with previous studies (Niebruegge et al., 2009), reporting that low DO concentrations enhanced the proliferation of ESCs and the expression of mesodermal, early and late cardiac-specific genes (Niebruegge et al., 2009). It is also established that CMs actively respond to mechanical cues from the environment in a frequency-dependent manner and that those cues can modulate electric remodeling, alterations in

gene expression, autocrine and paracrine effects, and consequently cardiac tissue organization and development (Shimko and Claycomb, 2008). Cardiac cells experience mechanical strains with every heartbeat, i.e., at a pulsatile frequency close to 1 Hz (Gupta and Grande-allen, 2006). Aiming to mimic the physiological environment, previous studies have applied mechanical stimulation at frequencies of 1 Hz on commercial or custom built devices to engineered cardiac tissues (Gwak et al., 2006). In our protocol, cells were subjected to distinct mechanical forces by manipulating the hydrodynamic environment in scalable readily available bioreactor systems. In stirred tank bioreactors, using an intermittent stirring, mechanical forces at frequencies close to 0.033 Hz were generated, whereas with a wave-induced agitation higher frequencies were reached (0.82-0.86 Hz). Thus, the differences in the temporal gene expression pattern and cardiac differentiation efficiency observed in stirred and WAVE cultures may be related to the frequency of mechanical loading applied in both systems. In accordance with literature, the effect of mechanical forces on cardiomyogenic differentiation is highly dependent on the experimental setup. Several variables including force magnitude, frequency, direction, duration of application, and at what stage of differentiation the force is applied, have been shown to affect cell fate decisions (Shimko and Claycomb, 2008; Teramura et al., 2012; Wan et al., 2011). In fact, these aspects were noted to also be critical for the success of the protocol herein described. Our results suggest that an intermittent agitation profile with change of stirring direction is not suitable for iPSC differentiation into CMs (low CM numbers and purities were achieved at the end of the differentiation process). Also, higher cell lysis was observed during all culture time, suggesting that this agitation profile may have induced high shear rate for cells, compromising cell viability, proliferation capacity and differentiation efficiency. Herein we considered that the major mechanical stimulus induced to the cells is the hydrodynamic environment provided by an intermittent and wave-induced agitation. However, it should be noted that fluid shear stress per se might also influence cell behavior. The effect of shear stress on cell pluripotency and cardiomyogenesis has already been described. For example, mESCs exposed to laminar shear stress (4 days at 5 dyn/cm<sup>2</sup>) expressed higher levels of mesodermal markers (Wolfe et al., 2012). On the other hand, fluid shear forces promoted by distinct types of impellers, such as single glass-ball stirring pendulum (1.52 dyn/cm<sup>2</sup>, 75 rpm) (Wang et al., 2013), pitched-blade impellers (2–5.2 dyn/cm<sup>2</sup>, 50–100 rpm) (Cormier et al., 2006) and paddled impellers (4.5–7.8 dyn/cm<sup>2</sup>, 80–120 rpm) (Kehoe et al., 2010) have shown to maintain or increase the expression of pluripotency markers in PSC cultured in bioreactor systems. In WAVE bioreactors the mean values of shear stress (0.05 Pa (0.5 dyn/cm<sup>2</sup>) in both 2 L and 20 L working volumes (Kalmbach et al., 2011)) were considerably lower than the ones indicated above for stirred bioreactors. In accordance, we observed a 6-times lower fold increase in the cumulative LDH in WAVE bioreactor cultures, from day 2 to day 9, when compared to stirred tank bioreactor cultures (Figure A-2.4, Page 65). These results reflect the reduced impact that fluid shear stress has on cell viability in WAVE bioreactor cultures. Future experiments using Computational Fluid Dynamics tools should be performed aiming at a deeper characterization of the hydrodynamic environment and quantification of the type and magnitude of the stresses generated in each bioreactor strategy.

It should be pointed out that mechanical forces, besides promoting elongation of the cell membrane and orientation of actin filaments (Geuss and Suggs, 2013; Shimko and Claycomb, 2008), regulate ECM synthesis, more specifically, result in enhanced synthesis of collagen, the most abundant protein in cardiac tissue (Gupta and Grande-allen, 2006). In this study, we showed that by day 9 of differentiation, cultures that have experienced higher mechanical loading (WAVE cultures) are composed by cells with more organized sarcomeric structures, and by aggregates with smoother surface topography due to a higher deposition of collagen type I.

Aside from different hydrodynamic environments, cells were cultured at 4 % O<sub>2</sub> tension during different periods of time in these systems (in WAVE bioreactor from day 0 to day 11 and in stirred tank bioreactor from day 2 to day 16). Therefore, exposing cells to reduced oxygen concentrations from the beginning of differentiation could also have contributed to the beneficial effect on CM differentiation observed in WAVE cultures.

The establishment of pure CM preparations is imperative for future clinical application of these cells. Our finding that a hypoxic environment along with a wave-induced agitation enables the production of CMs at purity of 76% in nine days without growth factor- directed differentiation and without antibiotic selection represents a major advance towards development of robust and clinically applicable bioprocesses. To facilitate the optimization of the described method, we have used a transgenic murine iPSC line, in which the cardiac-restricted  $\alpha$ -MHC promoter drives the expression of a puromycin resistance gene and eGFP. Therefore, antibiotic treatment, after day 9, resulted in the generation of an essentially pure CM population. In WAVE bioreactors, only two days were sufficient to achieve 97% CM purity by puromycin selection whereas in stirred tank cultures 7 days of selection were needed to reach the same purity. CMs generated at faster kinetics may have higher therapeutic potential in their *in vivo* applications. Namely, Boheler and coworkers showed that ESC-derived CMs isolated at day 11 of differentiation, in contrast to cells obtained at day 16-18 of differentiation, were more resistant to hypoxia *in vitro* and survived longer following injection into healthy hearts of athymic nude mice (Boheler et al., 2011). These data suggest that early-stage CMs may have greater potential to engraft and improve the myocardial contractile function following infarction. Therefore, it is appealing to hypothesize that day 11 CMs obtained in WAVE bioreactors may exhibit higher survival and engraftment potential after intramyocardial transplantation than day 16 CMs generated in stirred tank bioreactors. In order to increase the safety of the final CM preparation, non-genetic cell-lineage purification protocols should be considered. Procedures involving density-gradient centrifugation (Xu et al., 2002), the use a mitochondrial dye (Hattori et al., 2010) or antibodies targeting cardiac-specific surface markers (Dubois et al., 2011; Hoof et al., 2010; Uosaki et al., 2011) have been established for CM enrichment and can be combined with the developed bioprocess. However, these methods are either labor intensive or expensive which limit their scalability. Non-genetic CM lineage purification strategies based on distinct metabolic requirements of CMs and non-CM cell types have been described. For example, it has been shown that CMs survive in serum-free medium (Moon et al., 2013; Passier et al., 2005) or in glucose-depleted culture medium containing lactate (Tohyama et al., 2013), while other cell types do not. In addition, selective elimination of remaining

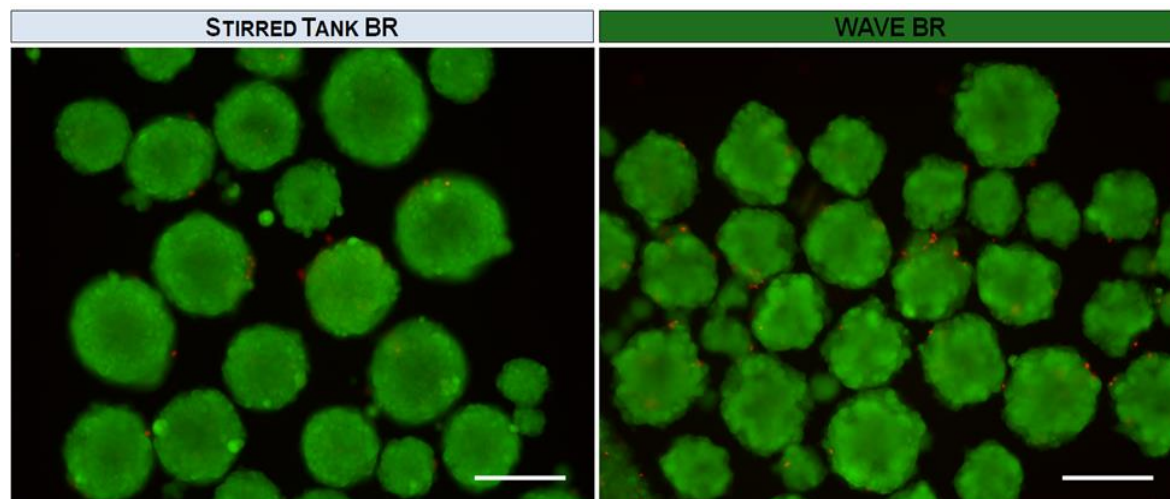
contaminating pluripotent cells could be achieved by treatment of final CM preparations with small molecules that do not compromise CM viability and functionality but are toxic to pluripotent stem cells (Ben-David et al., 2013). From a large-scale production perspective this type of approaches are more appealing and could be easily incorporated in our bioreactor protocol aiming at establishing a clinically scalable and cost-effective integrated bioprocess for CM differentiation and purification.

Another major requirement for the biomanufacturing of stem cell derivatives is to ensure that the final product fulfills the desired quality requisites for biomedical applications including phenotype, potency and functionality (Serra et al., 2012). Here, we showed that CMs obtained in both bioreactor systems presented typical cardiac morphology, electrophysiology, hormonal response to  $\beta$ -adrenergic and muscarinic receptor stimulation and rhythmic intracellular calcium transients. The most predominant CM subtype observed in both bioprocesses was the atrial-like phenotype, which was largely influenced by the type of cardiac specific promoter that was driving the expression of antibiotic resistance gene in our genetically engineered cells. The  $\alpha$ -MHC promoter is active mostly in atrial regions during embryonic and early fetal development (Franco et al., 1998), therefore it seems that the selection strategy used in this work is favoring the production of immature fetal-like cells that present action potentials resembling those found in atrial cells and that have not yet assumed more recognizable cardiac chamber subtypes. Future efforts should be directed towards improving the electrophysiological maturity of the produced CMs and enhancing cardiac subtype specification, for example by extending the time in culture after the selection process.

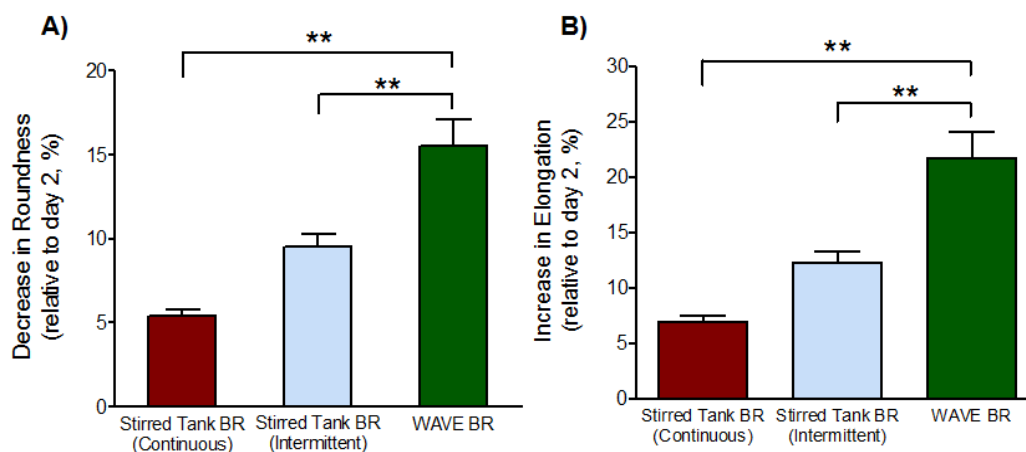
In conclusion, this study describes a robust and scalable protocol for differentiation of murine iPSC into CMs in controlled hypoxic and mechanical environment. In this work we have focused on murine iPSC as a model system for bioprocess development, and on a simple non-directed differentiation protocol to clearly identify the impact of each culture condition tested on CM differentiation. Although human and mouse PSC lines utilize overlapping developmental pathways, much optimization is required when translating protocols between species. We are aware that further optimization to our protocol will be required when translating to human PSCs. For example the use of chemically defined and serum-free media supplemented with cytokines will be of major importance. Nevertheless, it is our conviction that the bioreactor protocol herein described (i.e. the controlled hypoxic and specific hydrodynamic environment promoted by an intermittent stirring or a wave induced agitation) will be able to further improve the protocols already reported for human PSC differentiation towards CMs by enhancing culture homogeneity, process reproducibility, CM yields and productivities. It is widely known that the use of chemically defined media and growth-factor supplements considerably increases the cost of the differentiation process. Thus, the development of cost-effective bioprocesses is also highly dependent on increasing the number of CMs generated per liter of culture medium throughput (CMs/L). Here, by controlling key environmental conditions in cardiac development, we were able to produce up to  $1.6 \times 10^9$  CMs/L in a single WAVE 11-days bioreactor run. To our knowledge this is the highest value that has been reported to date (Niebruegge et al., 2008). Hopefully, our achievements will also contribute for the

development of affordable bioprocesses for mass production of human PSC-derived CMs, by reducing the need/amount of expensive cytokine inductive cocktails and/or the cardiac differentiation protocol duration.

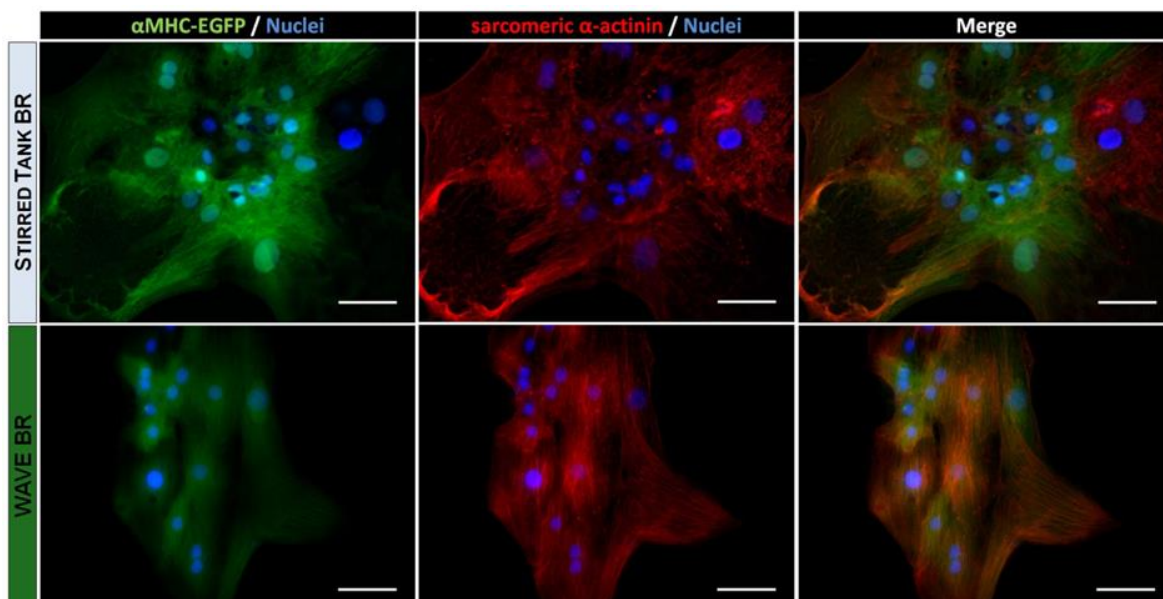
## 5. Appendix



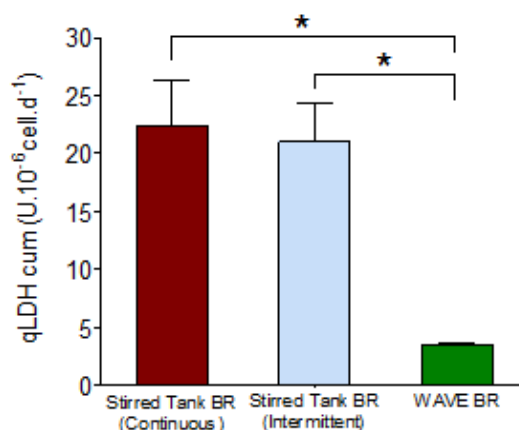
**Figure A-2.1. Viability analysis of cell aggregates from day 2 cultures.** Aggregates from both stirred tank and WAVE bioreactors were stained with fluorescein diacetate to detect live cells (green) and propidium iodide to identify dead cells (red). Scale bars: 200  $\mu$ m



**Figure A-2.2. Elongation and roundness of aggregates from day 9 cultures.** Aggregates from day 9 cultures, in both stirred tank (operated under continuous and intermittent agitation without direction change) and WAVE bioreactors, were analyzed based on their elongation (A) and roundness (B). Values were normalized to day 2 cultures. Significantly different,  $P < 0.05$  (\*) and  $P < 0.01$  (\*\*).



**Figure A-2.3. Structural analysis of cells dissociated from day 9 aggregates cultured in Stirred tank and WAVE bioreactors.** Day 9 aggregates were dissociated into single cells, plated on 2D plates and stained with the sarcomeric  $\alpha$ -actinin (red) antibody. Fluorescence images of  $\alpha$ MHC-eGFP-positive cells (green) are also shown. Nuclei are counterstained with DAPI (blue). Scale bars: 50  $\mu$ m.



**Figure A-2.4. Cumulative LDH release in stirred tank and WAVE bioreactors.** Fold increase in the cumulative LDH release, from day 2 to day 9, in both stirred tank (operated under continuous and intermittent agitation without direction change) and WAVE bioreactors. Significantly different,  $P < 0.05$  (\*).

**Table A-2.1. Primers for RT-PCR and quantitative RT-PCR**

Genes	Sequences (5'-3')	Size (bp)	NCBI ID
<i>GAPDH</i>	F: ACCTTGCCCACAGCCTTG R: GGCTCATGACCACAGTCCAT	142	NM_001289726.1 NM_008084.3
<i>TNNT2</i>	F: GGTGCCACCCAAGATCCCCG R: AATACGCTGCTGCTCGGCC	199	NM_001130174.1
<i>NKX2.5</i>	F: CAGCCAAAGACCCTCGGGCG R: TGCGCCTGCGAGAAGAGCAC	142	NM_008700.2
<i>HCN4</i>	F: TGCTGTGCATTGGGTATGGA R: TTTCCGGCAGTTAAAGTTGATG	337	NM_001081192.1
<i>MLC-2V</i>	F: TGCCAAGAAGCGGATAGA R: CAGTGACCCTTTGCCCTC	328	NM_010861.3
<i>MLC-2A</i>	F: AGTAGGAAGGCTGGGACCCG R: CTCGGGGTCCGTCCCATTGA	306	NM_022879.2
<i>T-BRACHYURY</i>	F: CTGCGCTTCAAGGAGCTAAC R: CCAGGCCTGACACATTTACC	91	NM_009309.2
<i>KIT</i>	F: ATTATGAACGCCAGGAGACG R: GAATCCCTCTGCCACACACT	497	NM_001122733.1 NM_021099.3
<i>PDGFRA</i>	F: CGTCAAAGGGAGGACGTTCA R: GACGAAGCCTTTCTCGTGGA	370	NM_011058.2 NM_001083316.1
<i>AFP</i>	F: CCCACTTCCAGCACTGCCTGC R: GGCTGCAGCAGCCTGAGAGT	374	NM_007423.4
<i>OCT4</i>	F: CATGTGTAAGCTGCGGCC R: GCCCTTCTGGCGCCGTTAC	268	NM_001252452.1

**Table A-2.2. Mean aggregate size throughout time of iPSC-CMs produced in both stirred tank and WAVE bioreactor systems.**

Time (day)	Stirred Tank BR (Continuous)	Stirred Tank BR (Intermittent)	WAVE BR
2	142.65±69.85	155.34±55.57	169.37±45.90
4	147.25±68.90	181.04±66.94	301.79±63.08
7	307.38±116.39	277.84±131.39	371.23±74.79
9	357.64±113.30	384.41±124.80	440.04±107.89

**Table A-2.3. Action potential properties of iPSC-CMs produced in both stirred tank and WAVE bioreactor systems.**

Culture system	N	MDP (mV)	Frequency (beats/min)	$V_{max}$ (dE/dt) (V/s)	$V_{dd}$ (V/s)	APD90 (ms)	APD50 (ms)	APD90/APD50
Stirred tank bioreactor*	22	-59.8±1.0	321.9±23.3	26.5±1.8	0.1±0.0	84.4±16.4	18.1±1.1	5.3±1.3
WAVE bioreactor*	25	-58.0±1.2	296.4±25.1	21.0±2.4	0.1±0.0	84.0±7.3	23.0±1.9	4.1±0.5

\* Data are presented as means ± SEM.

*Abbreviations:* N, total number of cells analyzed; MDP, average maximum diastolic potential for action potentials during the time period examined;  $V_{max}$ , the maximum rate of rise of the action potential upstroke;  $V_{dd}$ , velocity of diastolic depolarization; APD90, action potential duration at 90% of repolarization; APD50, action potential duration at 50% of repolarization.



**Movie A-2.1**

[https://www.ncbi.nlm.nih.gov/pmc/articles/PMC4225049/bin/12015\\_2014\\_9533\\_MOESM1\\_ESM.mpg](https://www.ncbi.nlm.nih.gov/pmc/articles/PMC4225049/bin/12015_2014_9533_MOESM1_ESM.mpg)

**Movie A-2.2**

[https://www.ncbi.nlm.nih.gov/pmc/articles/PMC4225049/bin/12015\\_2014\\_9533\\_MOESM2\\_ESM.mpg](https://www.ncbi.nlm.nih.gov/pmc/articles/PMC4225049/bin/12015_2014_9533_MOESM2_ESM.mpg)

**Movie A-2.3**

[https://www.ncbi.nlm.nih.gov/pmc/articles/PMC4225049/bin/12015\\_2014\\_9533\\_MOESM3\\_ESM.mpg](https://www.ncbi.nlm.nih.gov/pmc/articles/PMC4225049/bin/12015_2014_9533_MOESM3_ESM.mpg)

**Movie A-2.4**

[https://www.ncbi.nlm.nih.gov/pmc/articles/PMC4225049/bin/2015\\_2014\\_9533\\_MOESM4\\_ESM.avi](https://www.ncbi.nlm.nih.gov/pmc/articles/PMC4225049/bin/2015_2014_9533_MOESM4_ESM.avi)

## 6. Acknowledgments

We thank João Clemente for valuable support on biorreactor controlling units; Cornelia Böttinger, Rebecca Dieterich and Nadin Lange for technical assistance; GE Healthcare for technical advice in WAVE Bioreactor™ system. This study was supported by the European Commission FP7, CARE-MI (HEALTH-2009\_242038) project, German Ministry for Education and Research (BMBF, Grant No. 01GN0947), Köln Fortune Program and Dean's Investment Fund to T.Š. Cláudia Correia acknowledges the FCT for her PhD grant (SFRH / BD / 51573 / 2011).

## 7. References

- Bauwens, C., Yin, T., Dang, S., Peerani, R., and Zandstra, P.W. (2005). Development of a perfusion fed bioreactor for embryonic stem cell-derived cardiomyocyte generation: oxygen-mediated enhancement of cardiomyocyte output. *Biotechnol. Bioeng.* 90, 452–461.
- Ben-David, U., Gan, Q.-F., Golan-Lev, T., Arora, P., Yanuka, O., Oren, Y.S., Leikin-Frenkel, A., Graf, M., Garippa, R., Boehringer, M., et al. (2013). Selective elimination of human pluripotent stem cells by an oleate synthesis inhibitor discovered in a high-throughput screen. *Cell Stem Cell* 12, 167–179.
- Boheler, K.R., Joodi, R.N., Qiao, H., Juhasz, O., Urick, A.L., Chuppa, S.L., Gundry, R.L., Wersto, R.P., and Zhou, R. (2011). Embryonic stem cell-derived cardiomyocyte heterogeneity and the isolation of immature and committed cells for cardiac remodeling and regeneration. *Stem Cells Int.* 2011, 214203.
- Braam, S.R., Passier, R., and Mummery, C.L. (2009). Cardiomyocytes from human pluripotent stem cells in regenerative medicine and drug discovery. *Trends Pharmacol. Sci.* 30, 536–545.
- Burridge, P.W., Thompson, S., Millrod, M.A., Weinberg, S., Yuan, X., Peters, A., Mahairaki, V., Koliatsos, V.E., Tung, L., and Zambidis, E.T. (2011). A Universal System for Highly Efficient Cardiac Differentiation of Human Induced Pluripotent Stem Cells That Eliminates Interline Variability. *PLoS One* 6, 16.
- Cormier, J.T., zur Nieden, N.I., Rancourt, D.E., and Kallos, M.S. (2006). Expansion of undifferentiated murine embryonic stem cells as aggregates in suspension culture bioreactors. *Tissue Eng.* 12, 3233–3245.
- Dubois, N.C., Craft, A.M., Sharma, P., Elliott, D.A., Stanley, E.G., Elefanty, A.G., Gramolini, A., and Keller, G. (2011). SIRPA is a specific cell-surface marker for isolating cardiomyocytes derived from human pluripotent stem cells. *Nat. Biotechnol.* 29, 1011–1018.
- Elder, S.H., Goldstein, S.A., Kimura, J.H., Soslowsky, L.J., and Spengler, D.M. (2001). Chondrocyte differentiation is modulated by frequency and duration of cyclic compressive loading.

Ann. Biomed. Eng. 29, 476–482.

Fischer, B., and Bavister, B.D. (1993). Oxygen tension in the oviduct and uterus of rhesus monkeys, hamsters and rabbits. *J. Reprod. Fertil.* 99, 673–679.

Forsyth, N.R., Musio, A., Vezzoni, P., Simpson, a H.R.W., Noble, B.S., and McWhir, J. (2006). Physiologic oxygen enhances human embryonic stem cell clonal recovery and reduces chromosomal abnormalities. *Cloning Stem Cells* 8, 16–23.

Franco, D., Lamers, W.H., and Moorman, a F. (1998). Patterns of expression in the developing myocardium: towards a morphologically integrated transcriptional model. *Cardiovasc. Res.* 38, 25–53.

Geuss, L.R., and Suggs, L.J. (2013). Making cardiomyocytes: how mechanical stimulation can influence differentiation of pluripotent stem cells. *Biotechnol. Prog.* 29, 1089–1096.

Gibbons, J., Hewitt, E., and Gardner, D.K. (2006). Effects of oxygen tension on the establishment and lactate dehydrogenase activity of murine embryonic stem cells. *Cloning Stem Cells* 8, 117–122.

Grskovic, M., Javaherian, A., Strulovici, B., and Daley, G.Q. (2011). Induced pluripotent stem cells—opportunities for disease modelling and drug discovery. *Nat. Rev. Drug Discov.* 10, 915–929.

Gupta, V., and Grande-allen, K.J. (2006). Effects of static and cyclic loading in regulating extracellular matrix synthesis by cardiovascular cells. *Cardiovasc. Res.* 72, 375–383.

Gwak, S., Bhang, S.H., Kim, I., Kim, S., Cho, S.-W., Jeon, O., Yoo, K.J., Putnam, A.J., Kim, B.-S., Ho, S., et al. (2006). The effect of cyclic strain on embryonic stem cell-derived cardiomyocytes. *Biomaterials* 27, 4409–4418.

Halbach, M., Peinkofer, G., Baumgartner, S., Maass, M., Wiedey, M., Neef, K., Krausgrill, B., Ladage, D., Fatima, A., Saric, T., et al. (2013). Electrophysiological integration and action potential properties of transplanted cardiomyocytes derived from induced pluripotent stem cells. *Cardiovasc. Res.* 100, 432–440.

Hattori, F., Chen, H., Yamashita, H., Tohyama, S., Satoh, Y.-S., Yuasa, S., Li, W., Yamakawa, H., Tanaka, T., Onitsuka, T., et al. (2010). Nongenetic method for purifying stem cell-derived cardiomyocytes. *Nat. Methods* 7, 61–66.

Hoof, D. Van, Dormeyer, W., Braam, S.R., Passier, R., Monshouwer-kloots, J., Oostwaard, D.W., Heck, A.J.R., Krijgsveld, J., and Mummery, C.L. (2010). Identification of Cell Surface Proteins for Antibody-Based Selection of Human Embryonic Stem Cell-Derived Cardiomyocytes. *J. Proteome Res.* 9, 1610–1618.

Horton, R.E., and Auguste, D.T. (2012). Synergistic effects of hypoxia and extracellular matrix cues in cardiomyogenesis. *Biomaterials* 33, 6313–6319.

Houtzager, E., Linden, R. Van Der, Roo, G. De, Huurman, S., Priem, P., and Sijmons, P.C. (2010). Linear Scale-Up of Cell Cultures. *Bioprocess Int.* 8, 56–62.

Kalmbach, A., Bordás, R., Oncül, A. a, Thévenin, D., Genzel, Y., and Reichl, U. (2011). Experimental characterization of flow conditions in 2- and 20-L bioreactors with wave-induced motion. *Biotechnol. Prog.* 27, 402–409.

Kawaguchi, N., and Nakanishi, T. (2013). Cardiomyocyte Regeneration. *Cells* 2, 67–82.

Kehoe, D.E., Jing, D., Lock, L.T., and Tzanakakis, E.S. (2010). Scalable stirred-suspension bioreactor culture of human pluripotent stem cells. *Tissue Eng. Part A* 16, 405–421.

Keung, A.J., Healy, K.E., Kumar, S., and Schaffer, D. V (2010). Biophysics and dynamics of natural and engineered stem cell microenvironments. *Wiley Interdiscip. Rev. Syst. Biol. Med.* 2, 49–64.

Kuzmenkin, A., Liang, H., Xu, G., Pfannkuche, K., Eichhorn, H., Fatima, A., Luo, H., Saric, T., Wernig, M., Jaenisch, R., et al. (2009). Functional characterization of cardiomyocytes derived from murine induced pluripotent stem cells in vitro. *FASEB J.* 23, 4168–4180.

Laflamme, M.A., and Murry, C.E. (2011). Heart regeneration. *Nature* 473, 326–335.

Li, D., Zhou, J., Chowdhury, F., Cheng, J., Wang, N., and Wang, F. (2011). Role of mechanical factors in fate decisions of stem cells. *Regen Med* 6, 229–240.

- Lian, X., Zhang, J., Azarin, S.M., Zhu, K., Hazeltine, L.B., Bao, X., Hsiao, C., Kamp, T.J., and Palecek, S.P. (2013). Directed cardiomyocyte differentiation from human pluripotent stem cells by modulating Wnt/ $\beta$ -catenin signaling under fully defined conditions. *Nat. Protoc.* 8, 162–175.
- Lundy, S.D., Zhu, W.-Z., Regnier, M., and Laflamme, M. (2013). Structural and Functional Maturation of Cardiomyocytes Derived From Human Pluripotent Stem Cells. *Stem Cells Dev.* 22, 1991–2002.
- Matsumoto, T., Yung, Y.C., Fischbach, C., Kong, H.J., Nakaoka, R., and Mooney, D.J. (2007). Mechanical strain regulates endothelial cell patterning in vitro. *Tissue Eng.* 13, 207–217.
- Mauritz, C., Schwanke, K., Reppel, M., Neef, S., Maier, L.S., Nguemo, F., Menke, S., Haustein, M., Hescheler, J., Hasenfuss, G., et al. (2008). Generation of functional murine cardiac myocytes from induced pluripotent stem cells. *Circulation* 118, 507–517.
- Minami, I., Yamada, K., Otsuji, T.G., Yamamoto, T., Shen, Y., Otsuka, S., Kadota, S., Morone, N., Barve, M., Asai, Y., et al. (2012). A small molecule that promotes cardiac differentiation of human pluripotent stem cells under defined, cytokine- and xeno-free conditions. *Cell Rep.* 2, 1448–1460.
- Moon, S.-H., Kang, S.-W., Park, S.-J., Bae, D., Kim, S.J., Lee, H.-A., Kim, K.S., Hong, K.-S., Kim, J.S., Do, J.T., et al. (2013). The use of aggregates of purified cardiomyocytes derived from human ESCs for functional engraftment after myocardial infarction. *Biomaterials* 34, 4013–4026.
- Mummery, C.L., Zhang, J., Ng, E.S., Elliott, D. a, Elefanty, A.G., and Kamp, T.J. (2012). Differentiation of human embryonic stem cells and induced pluripotent stem cells to cardiomyocytes: a methods overview. *Circ. Res.* 111, 344–358.
- Murry, C.E., Reinecke, H., and Pabon, L.M. (2006). Regeneration gaps: observations on stem cells and cardiac repair. *J. Am. Coll. Cardiol.* 47, 1777–1785.
- Narazaki, G., Uosaki, H., Teranishi, M., Okita, K., Kim, B., Matsuoka, S., Yamanaka, S., and Yamashita, J.K. (2008). Directed and systematic differentiation of cardiovascular cells from mouse induced pluripotent stem cells. *Circulation* 118, 498–506.
- Nava, M.M., Raimondi, M.T., and Pietrabissa, R. (2012). Controlling Self-Renewal and Differentiation of Stem Cells via Mechanical Cues. *J. Biomed. Biotechnol.* 2012, 797410.
- Niebruegge, S., Nehring, A., Ba, H., Schroeder, M., Zweigerdt, R., and Lehmann, J. (2008). Cardiomyocyte Production in Mass Suspension Culture: Embryonic Stem Cells as a Source for Great Amounts of Functional Cardiomyocytes. *Tissue Eng. Part A* 14, 1591–1601.
- Niebruegge, S., Bauwens, C.L., Peerani, R., Thavandiran, N., Masse, S., Sevaptisidis, E., Nanthakumar, K., Woodhouse, K., Husain, M., Kumacheva, E., et al. (2009). Generation of human embryonic stem cell-derived mesoderm and cardiac cells using size-specified aggregates in an oxygen-controlled bioreactor. *Biotechnol. Bioeng.* 102, 493–507.
- Oh, Y., Wei, H., Ma, D., Sun, X., and Liew, R. (2012). Clinical applications of patient-specific induced pluripotent stem cells in cardiovascular medicine. *Heart* 98, 443–449.
- Passier, R., Oostwaard, D.W., Snapper, J., Kloots, J., Hassink, R.J., Kuijk, E., Roelen, B., de la Riviere, A.B., and Mummery, C. (2005). Increased cardiomyocyte differentiation from human embryonic stem cells in serum-free cultures. *Stem Cells* 23, 772–780.
- Rajala, K., Pekkanen-Mattila, M., and Aalto-Setälä, K. (2011). Cardiac differentiation of pluripotent stem cells. *Stem Cells Int.* 2011, 383709.
- Schmelter, M., Ateghang, B., Helmig, S., Wartenberg, M., and Sauer, H. (2006). Embryonic stem cells utilize reactive oxygen species as transducers of mechanical strain-induced cardiovascular differentiation. *FASEB J.* 20, E294–E306.
- Serra, M., Brito, C., Sousa, M.F.Q., Jensen, J., Tostões, R., Clemente, J., Strehl, R., Hyllner, J., Carrondo, M.J.T., and Alves, P.M. (2010). Improving expansion of pluripotent human embryonic stem cells in perfused bioreactors through oxygen control. *J. Biotechnol.* 148, 208–215.
- Serra, M., Correia, C., Malpique, R., Brito, C., Jensen, J., Bjorquist, P., Carrondo, M.J.T., and Alves, P.M. (2011). Microencapsulation Technology: A Powerful Tool for Integrating Expansion and Cryopreservation of Human Embryonic Stem Cells. *PLoS One* 6, 1–13.
- Serra, M., Brito, C., Correia, C., and Alves, P.M. (2012). Process engineering of human pluripotent

stem cells for clinical application. *Trends Biotechnol.* 30, 1–10.

Shimizu, N., Yamamoto, K., Obi, S., Kumagaya, S., Shimano, Y., Naruse, K., Yamashita, J.K., Igarashi, T., Ando, J., and Masumura, T. (2008). Cyclic strain induces mouse embryonic stem cell differentiation into vascular smooth muscle cells by activating PDGF receptor beta. *J. Appl. Physiol.* 104, 766–772.

Shimko, V.F., and Claycomb, W.C. (2008). Effect of mechanical loading on three-dimensional cultures of embryonic stem cell-derived cardiomyocytes. *Tissue Eng. Part A* 14, 49–58.

Taha, M.F., Valojerdi, M.R., Hatami, L., and Javeri, A. (2012). Electron microscopic study of mouse embryonic stem cell-derived cardiomyocytes. *Cytotechnology* 64, 197–202.

Teramura, T., Takehara, T., Onodera, Y., Nakagawa, K., Hamanishi, C., and Fukuda, K. (2012). Mechanical stimulation of cyclic tensile strain induces reduction of pluripotent related gene expressions via activation of Rho/ROCK and subsequent decreasing of AKT phosphorylation in human induced pluripotent stem cells. *Biochem. Biophys. Res. Commun.* 417, 836–841.

Tohyama, S., Hattori, F., Sano, M., Hishiki, T., Nagahata, Y., Matsuura, T., Hashimoto, H., Suzuki, T., Yamashita, H., Satoh, Y., et al. (2013). Distinct metabolic flow enables large-scale purification of mouse and human pluripotent stem cell-derived cardiomyocytes. *Cell Stem Cell* 12, 127–137.

Uosaki, H., Fukushima, H., Takeuchi, A., Matsuoka, S., Nakatsuji, N., Yamanaka, S., and Yamashita, J.K. (2011). Efficient and Scalable Purification of Cardiomyocytes from Human Embryonic and Induced Pluripotent Stem Cells by VCAM1 Surface Expression. *PLoS One* 6, 1–9.

Wan, C., Chung, S., and Kamm, R.D. (2011). Differentiation of embryonic stem cells into cardiomyocytes in a compliant microfluidic system. *Ann. Biomed. Eng.* 39, 1840–1847.

Wang, Y., Chou, B.-K., Dowey, S., He, C., Gerecht, S., and Cheng, L. (2013). Scalable expansion of human induced pluripotent stem cells in the defined xeno-free E8 medium under adherent and suspension culture conditions. *Stem Cell Res.* 11, 1103–1116.

Wolfe, R.P., Leleux, J., Nerem, R.M., and Ahsan, T. (2012). Effects of shear stress on germ lineage specification of embryonic stem cells. *Integr. Biol.* 4, 1263.

Xu, C., Police, S., Rao, N., and Carpenter, M. (2002). Characterization and Enrichment of Cardiomyocytes Derived From Human Embryonic Stem Cells. *Circ. Res.* 91, 501–508.

Yoshida, Y., and Yamanaka, S. (2011). iPS cells: a source of cardiac regeneration. *J. Mol. Cell. Cardiol.* 50, 327–332.

Zhang, J., Klos, M., Wilson, G.F., Herman, A.M., Lian, X., Raval, K.K., Barron, M.R., Hou, L., Soerens, A.G., Yu, J., et al. (2012). Extracellular Matrix Promotes Highly Efficient Cardiac Differentiation of Human Pluripotent Stem Cells: The Matrix Sandwich Method. *Circ. Res.* 111, 1125–1136.

Zimmermann, W.-H., Didié, M., Wasmeier, G.H., Nixdorff, U., Hess, A., Melnychenko, I., Boy, O., Neuhuber, W.L., Weyand, M., and Eschenhagen, T. (2002). Cardiac grafting of engineered heart tissue in syngenic rats. *Circulation* 106, 1151–1157.

Zwi-Dantsis, L., and Gepstein, L. (2012). Induced pluripotent stem cells for cardiac repair. *Cell. Mol. Life Sci.* 69, 3285–3299.

Zwi-Dantsis, L., Mizrahi, I., Arbel, G., Gepstein, A., and Gepstein, L. (2011). Scalable production of cardiomyocytes derived from c-Myc free induced pluripotent stem cells. *Tissue Eng. Part A* 17, 1027–1037.

# 3

## **3D aggregates of human pluripotent stem cells derived cardiac progenitors: impact of culture strategy in transcriptional and metabolic signatures of cardiomyocytes**

This chapter was adapted from:

Correia, C., Koshkin, A., Duarte P., Dongjian H., Carido, M., Sebastião, M., Alves, P., Domian, I., Teixeira, A.M., Serra, M., and Alves, P.M. (2016). 3D aggregates of human pluripotent stem cells derived cardiac progenitors: impact of culture strategy in transcriptional and metabolic signatures of cardiomyocytes. *Submitted*

**Contents**

<b>1. Introduction.....</b>	<b>74</b>
<b>2. Methods.....</b>	<b>75</b>
2.1. hiPSC and hESC culture.....	75
2.2 Directed differentiation of hPSC toward cardiomyocytes .....	76
2.3. Cell concentration and viability .....	76
2.4. Cell/Aggregate structure and ultrastructure .....	76
2.5. Cell characterization: Protein Expression .....	77
2.6. Cell characterization: Gene Expression.....	77
2.6.2. Microarray analysis .....	78
2.7. Metabolic Analysis .....	79
2.8. Analysis of cell functionality .....	79
2.9. Statistical analysis.....	80
<b>3. Results.....</b>	<b>80</b>
3.1. Directed differentiation protocol induced the robust generation of pure 2D monolayers of CMs from multiple hPSC lines.....	80
3.2. Metabolic characterization during hPSC differentiation towards cardiomyocytes .....	82
3.3. Impact of 3D aggregate culture of cardiac progenitors on cardiomyocyte enrichment and commitment.....	83
3.4. Impact of 3D aggregate culture n hiPSC-CM functionality .....	85
3.5. Impact of 3D culture on hiPSC-CMs transcriptome profile .....	87
3.6. Impact of 3D culture approach on the metabolism of hiPSC-CMs .....	89
<b>4. Discussion.....</b>	<b>92</b>
<b>5. Appendix.....</b>	<b>96</b>
<b>6. References.....</b>	<b>100</b>

## **Abstract**

Three dimensional (3D) cultures of human pluripotent stem cell derived cardiomyocytes (hPSC-CMs) are more predictable models of *in vivo* responses to be used for drug discovery and hold great promise in regenerative medicine applications. However, the transition of CM differentiation protocols from 2D to 3D cultures is not straightforward and often results in lower CM purity and reduced reproducibility. In this work, we relied on the aggregation of hPSC-derived cardiac progenitors to establish a differentiation protocol capable of generating highly pure CM aggregate cultures. In parallel to improved CM enrichment and commitment, we observed significant alterations in the extracellular matrix and metabolic transcriptomes, and a slight increase of TCA-cycle activity, amino acid metabolism and ATP production through glucose oxidation in 3D cultures when compared with 2D monolayer cultures. Although hPSC-CMs generated from both methods are still highly glycolytic, 3D aggregate cultures showed slightly improved metabolic energetics.

Overall, this study provides novel knowledge on the impact of 3D culture on CM differentiation, gene expression and metabolism which will contribute to improve the control over CM differentiation and to enable the identification/characterization of the differentiated population based on its metabolic signature.

## 1. Introduction

Human pluripotent stem cells (hPSCs) offer unique prospects for regenerative medicine, drug discovery, toxicity testing, disease modeling, and developmental biology studies due to their ability to proliferate indefinitely and differentiate into any cell type of the human body (Egashira et al., 2011). Importantly, their capacity to produce cell types that are challenging to obtain from tissues, difficult to maintain in culture, and that present limited proliferative capacity, such as cardiomyocytes (CMs), brought great hope to the cell therapy field. In fact, hPSC derived cardiomyocytes (hPSC-CMs) became promising candidates for cardiac cell therapy and pre-clinical research (Hartman et al., 2016; Youssef et al., 2016). Within this context, an enormous effort has been made towards the development of protocols to direct the differentiation of hPSC towards the cardiac lineage. Most of them rely on the supplementation of culture medium with growth factors and/or small molecules that specifically induce mesoderm differentiation and cardiac lineage specification (Burridge et al., 2013). Laflamme and colleagues were the first to report a directed differentiation protocol in a 2D monolayer culture format, based on BMP4 and Activin A stimulation in RPMI/B27 medium (Laflamme et al., 2007). Nowadays most protocols rely on the temporal modulation of Wnt signaling, which has a biphasic role in cardiogenesis; Wnt activation is required for mesoderm formation (Lian et al., 2013; Ueno et al., 2007) and subsequent Wnt inhibition is necessary for cardiac specification (Ueno et al., 2007). The small molecule CHIR99021, has been widely used as a Wnt signaling activator, whereas subsequent inhibition has been explored with a wide range of Wnt antagonists such as IWP4, IWP2, IWR1, Wnt-C59 or XAV939 (Burridge et al., 2014; Kadari et al., 2015; Lanier et al., 2012; Lian et al., 2012, 2013). These protocols originated CMs with a previously unmet purity of >80% (Lian et al., 2012, 2013).

Suspension culture platforms have also been explored to support large-scale differentiation of hPSC towards CMs. Most of these studies have used embryoid bodies (EBs) as an initial step to induce cardiac differentiation (Bose and Shenoy P, 2016; He, 2003; Huber et al., 2007; Kehat et al., 2001; Liu et al., 2016; Yang et al., 2008; Zhang et al., 2009). More recently, directed differentiation protocols established in 2D monolayer cultures have been adapted to 3D cultures (aggregate and microcarrier based cultures), however final CM purities are typically lower than those obtained in 2D monolayer cultures (reviewed in (Kempf et al., 2016)). Protocol reproducibility is also an issue, particularly due to the difficulty in controlling aggregate size, which has been shown to affect differentiation potential (Niebruegge et al., 2009; Bauwens et al., 2008). These aspects still hinder the practical application of 3D culture methods for large scale production of differentiated cells.

Despite all the progress that has been made in the establishment of CM differentiation protocols, there is still the need to: i) improve the reproducibility of differentiation protocols from batch-to-batch, and between different cell lines and different laboratories, ii) increase the final CM purity, avoiding the presence of undifferentiated hPSC and non-cardiac committed cells in the final differentiation population, and iii) reduce the heterogeneity of the final population of cardiac cells that often contain not only different subtypes of CMs but also cardiac fibroblasts, endothelial cells



and smooth muscle cells. During the last years several strategies have been explored to improve the purity of hPSC-CMs including: percoll gradients (Xu et al., 2002), Flow Activated Cell Sorting for specific surface markers (Skelton et al., 2014) and for cells incubated with mitochondrial dyes (Hattori et al., 2010) or molecular beacons (Wile et al., 2014), or using synthetic modified mRNAs, which target tissue-specific miRNAs (miRNA switches) (Miki et al., 2015). However, these approaches are expensive and present reduced scalability. One elegant and efficient approach consists in culturing hPSC-CMs in medium containing lactate instead of glucose (Tohyama et al., 2013), taking advantage of the different metabolic properties between different cell types: since hPSCs and fibroblasts rely highly on glucose, only CMs, which can use both metabolites, survive when cultured in this medium (Tohyama et al., 2013). In fact, energy metabolism has been shown to be one of the major regulated processes during development. Van Dartel and colleagues used transcriptome analysis to identify metabolic changes during the differentiation of ESC into CMs (van Dartel et al., 2014). Although this study has shown the regulation of common genes involved in energy metabolism during hPSC differentiation, it did not provide direct insights into the type of physiological alterations in energy metabolism that occur during hPSC differentiation. A detailed description of the type of metabolic and fluxomic changes that take place during hPSC differentiation towards CMs is currently lacking and might be useful to facilitate the identification and characterization of the differentiated population by their metabolic signature.

In this work, we first established a robust protocol for directed differentiation of hPSCs towards CMs, suitable to generate CMs in both 2D monolayer and 3D aggregate culture formats, and then we compared both differentiated populations in terms of CM purity, transcriptome, metabolome, fluxome and functionality. More specifically, using an integrated experimental and computational systems biology approach we assessed the impact of a 3D aggregate culture of hPSC-derived cardiac progenitors on: i) CM enrichment and commitment and ii) transcriptional and metabolic signatures of hPSC-CMs.

## **2. Methods**

### **2.1. hiPSC and hESC culture**

Four hPSC lines were used in this study, including two hESC lines (Me1 and H3 reporter lines NKX2-5(eGFP/w) (Elliott et al., 2011), kindly provided by Dr. David Elliott from Murdoch Childrens Research Institute) and two hiPSC lines (DF19-9-11T.H (WiCell) and M4C4, kindly provided by Dr. Tomo Saric from University of Koln). All hPSC lines were propagated on Matrigel® (Corning) coated plates until reaching 80% confluency. hESCs were maintained in DMEM/F12 supplemented with 20% (v/v) KnockOut serum replacement, 1% (v/v) MEM non-essential amino acid, 1% (v/v) L-glutamine, 1% (v/v) Pen/Strep and 50mM  $\beta$ -mercaptoethanol (all from ThermoFisher Scientific) while hiPSCs were cultured in mTESR1 medium (STEMCELL Technologies). The four hPSC lines were kept in a humidified atmosphere of 5% CO<sub>2</sub>.

## **2.2. Directed differentiation of hPSC toward cardiomyocytes**

Differentiation of hPSC into CMs was initiated when cell confluence reached 80-90%. Briefly expansion medium was replaced by RPMI Medium (ThermoFisher Scientific) supplemented with B27 without insulin (RPMI/B27, ThermoFisher Scientific), 12  $\mu$ M CHIR99021 (Biogen Cientifica SL), 80 ng/mL Activin A (Tebu-bio) and 50  $\mu$ g/mL Ascorbic acid (Sigma-Aldrich). After 24 hr, the medium was completely replaced by RPMI/B27 supplemented with 5  $\mu$ M IWR-1 (Sigma-Aldrich) and 50  $\mu$ g/mL ascorbic acid (Sigma-Aldrich). At day 3, i.e. 72 hr after day 0, medium was exchanged for RPMI/B27 supplemented with 5  $\mu$ M IWR-1. At day 6 (when beating zones were observed), cells were dissociated by incubation with TrypLE Select (ThermoFisher Scientific) for 5 min and replated either in 2D static tissue culture plates or in AgreeWell plates as described below.

### **2.2.1. 2D monolayer culture**

Cells harvested at day 6 were inoculated at 200 000 cells per  $\text{cm}^2$  on Matrigel® (Corning) coated plates in RPMI Medium supplemented with B27 (with insulin). Medium was exchanged 24 hr later, and then every two days, until day 15. hPSC-CMs obtained at day 15 were designated by hPSC-CM-2D.

### **2.2.2. 3D Aggregate culture**

Cells harvested at day 6 were inoculated in AggreWell™400Ex (Stem cell technologies) at 1500 cells/microwell (as previously described for aggregation of hPSC-CMs (Nguyen et al., 2014)), centrifuged at 100 g, during 3 min and cultured in RPMI Medium supplemented with B27 (with insulin). After 24 hr, medium was exchanged and aggregates were transferred to orbital suspension cultures (at an agitation rate of 90 rpm), and maintained for additional 8 days (total culture time: 15 days). Medium was replaced every two days. hPSC-CMs obtained at day 15 were designated by hPSC-CM-3D.

## **2.3. Cell concentration and viability**

### **2.3.1. Cell concentration**

Cell concentration was determined by cell counting in a Fuchs-Rosenthal haemocytometer (Brand, Wertheim, Germany) using the trypan blue exclusion method (0.1% (v/v) solution in PBS).

### **2.3.2. Fluorescein diacetate-propidium iodide staining**

The qualitative assessment of cell plasma membrane integrity was performed using the enzyme substrate fluorescein diacetate (FDA, Sigma-Aldrich), and the DNA-binding dye propidium iodide (PI, Sigma-Aldrich). Briefly, cells were incubated with 20  $\mu$ g/mL FDA and 10  $\mu$ g/mL PI in Dulbecco's Phosphate Buffered Saline (DPBS, ThermoFisher Scientific) for 2-3 min and visualized by fluorescence microscopy (DMI 6000, Leica Microsystems GmbH).

## **2.4. Cell/Aggregate structure and ultrastructure**

### **2.4.1. Immunocytochemistry**

hPSC-CMs were washed with DPBS and fixed in 4% (w/v) Paraformaldehyde (PFA) in DPBS solution for 15 min. After being permeabilized and blocked with 5% (v/v) FBS, 1% (w/v) BSA, 0.3% (v/v) Triton X-100 in DPBS for 1 hr, at room temperature (20-25°C), cells were incubated with

primary antibodies diluted in 1% (w/v) BSA, 0.1% (w/v) TX-100 in DPBS overnight at 4°C. The following primary antibodies were used:  $\alpha$ -sarcomeric actinin (1:200, Sigma-Aldrich), titin (1:100, Santa Cruz Biotechnology) and troponin T (1:100, Millipore). Afterwards, cells were washed in DPBS and incubated with secondary antibody, Alexa Fluor 594 goat anti-mouse IgG (1:500, ThermoFisher Scientific), in the dark for 1 hr at room temperature. Cell nuclei were counterstained with Hoechst 33342 nucleic acid dye (1:1000, Thermo Fisher Scientific). Representative images were taken using an inverted fluorescence microscope (DMI 6000, Leica).

#### **2.4.2. Transmission electron microscopy (TEM)**

Monolayers of hPSC-CMs were fixed in 2% (v/v) glutaraldehyde in 0.1 M HEPES buffer (pH 7.4) for 20 min, washed in DPBS and stored in 1% (v/v) glutaraldehyde in DPBS until analyses. TEM analyses were performed as previously described (Correia et al., 2016).

#### **2.4.3. Evaluation of aggregate size**

The aggregate size was determined using an inverted-microscope (DMI 6000, Leica) by measuring two perpendicular diameters of each aggregate using imageJ software. These measurements were used to calculate the average diameter of each aggregate.

### **2.5. Cell characterization: Protein Expression**

#### **2.5.1. Flow cytometry**

2D monolayers and 3D aggregates were dissociated to single cells after incubation with TrypLE™ Select for 5 min and then resuspended in washing buffer (WB) solution (5% (v/v) FBS in DPBS), centrifuged at 300 g during 5 min and washed again. Cells were incubated with the primary/conjugated antibody for 1 hr at 4°C. Afterwards, cells were washed two times in WB solution. Whenever required, cells were incubated with secondary antibodies for 30 min at 4°C. For determination of intracellular markers, cells were washed two times in BD Perm/Wash (PW) solution (BD Biosciences, diluted 1:10 in H<sub>2</sub>O MiliQ), and fixed for 20 min in BD CitoFix/Citoperm (BD Biosciences) solution at 4°C. After a washing step with PW solution, cells were kept in 1% (v/v) BSA solution at room temperature 30 min (for blocking non-specific interactions), washed in PW solution and then incubated with primary antibody at 4°C, during 1 hr. When required, cells were washed twice in PW, and incubated with respective secondary antibodies during 30 min in the dark. Cells were washed twice with WB (for extracellular markers) and with PW (for intracellular markers) before being analyzed in a CyFlow® space (Partec GmbH) instrument, registering 10,000 events per sample. The antibodies used were: Oct4 (Santa Cruz Biotechnology, 6:100), Bry T (R&D Systems, 1:10), KDR/VEGFR $\alpha$  (BioLegend, 5:100), VCAM-1 (CD106-PE, BD Biosciences, 2:10), SIRP $\alpha$ / $\beta$  (CD172a/b-PE, BioLegend, 5:100), cTNT (Thermo Fisher Scientific, 1:100) and isotype controls IgG1, $\kappa$ -PE (BD Biosciences).

### **2.6. Cell characterization: Gene Expression**

#### **2.6.1. Quantitative Real Time PCR**

Total RNA was extracted using the High Pure RNA Isolation Kit (Roche), and reverse transcription was performed with High Fidelity cDNA Synthesis Kit (Roche), following

manufacturer's instructions. Relative quantification of gene expression was performed using LightCycler 480 Probes Master (Roche) in 20  $\mu$ L reactions with 50 ng cDNA template and 20x concentrated TaqMan probes. The reactions were performed in 96-well plates using a LightCycler 480 Real-Time PCR System (Roche). Cycle threshold (Ct's) were determined by LightCycler 480 Software. All data was analyzed using the  $2^{-\Delta\Delta Ct}$  method for relative gene expression analysis. Changes in gene expression were normalized to GAPDH and RPLP0 gene expression as internal controls. The TaqMan probes used were: POU5F1 Hs00999632\_g1, GATA4 Hs00171403\_m1, NKX2.5 Hs00231763\_m1, TNNT2 Hs00165960\_m1, VCAM1 Hs01003372\_m1, MYH7 Hs01110632\_m1, MYL2 Hs00166405\_m1, MYL7 Hs99999905\_m1, HCN4 Hs00221909\_m1, CACNA1C Hs00175760\_m1, ACTC1 Hs00167681\_m1, MYH6 Hs00606316\_m1, GAPDH Hs01101425\_m1 and RPLP0 Hs99999902\_m1.

### **2.6.2. Microarray analysis**

The quality of RNA obtained from hiPSC-CM-2D and hiPSC-CM-3D at day 15, was assessed by the quotient of the 28S to 18S ribosomal RNA electropherogram peak using an Agilent 2100 bioanalyzer and the RNA Nano Chip (Agilent). After this, Illumina HumanHT-12 v4 Expression BeadChio microarray technology (Illumina) was used for transcriptional profiling. Data were processed and normalized as described elsewhere (Silva et al., 2015). Genes differentially expressed were selected based on Student's t test for p value  $< 0.05$  and fold change  $|FC| \geq 1.3$ . Upstream regulators, canonical pathways and biological functions analyses were performed using IPA software. Upstream regulators were considered significantly activated when presenting an overlap p-value  $\leq 0.05$  and an IPA activation Z-score  $\geq 2.0$  and significantly inhibited when presenting an overlap p-value  $\leq 0.05$  and an IPA activation Z-score  $\leq -2.0$ . The overlap p-value measures whether there is a statistically significant overlap between the dataset genes and the genes that are regulated by a transcriptional regulator, and is calculated using Fisher's Exact Test. Activation z-score infers the activation states ("increased" or "decreased") of predicted transcriptional regulators. Given the observed differential regulation of a gene ("up" or "down") in the dataset, the activation state of an upstream regulator ("activated" or "inhibited") is determined by the regulation direction associated with the relationship from the regulator to the gene comparing with a number of findings reported in the literature. Biological Function and Pathway analysis examines genes in the dataset that are known to affect each biological function/pathway and compares their direction of change to what is expected from the literature. If the observed direction of change is mostly consistent with a particular activation state of a biological function ("increased" or "decreased"), then a prediction is made about that activation state. For KEGG Pathways analysis, DAVID Resources (<https://david.ncifcrf.gov/>) were used. R-project was used to build: i) scatter plot with the absolute values of expression for all transcripts of hiPSC-CM-2D and hiPSC-CM-3D; and ii) volcano plot using Student's t-test and fold changes of each gene in hiPSC-CM-3D compared to hiPSC-CM-2D.

## 2.7. Metabolic Analysis

### 2.7.1. Quantification of extracellular metabolite concentrations

Concentrations of glutamine (Gln), glutamate (Glu), glucose (Glc) and lactate (Lac) in cell culture supernatants were measured using YSI 7100 Multiparameter Bioanalytical System (YSI Life Sciences). The remaining amino acids were determined by HPLC using the Waters AcQ.Tag Amino Acid Analysis Method (Waters, Milford, MA) as described elsewhere (Carinhas et al., 2010). The specific metabolic rates (qMet, expressed in  $\mu\text{mol}/(10^6 \text{ cell}\cdot\text{h})$ ) were calculated using the equation:  $q\text{Met} = \Delta\text{Met}/(\Delta t \times X_v)$ , where  $\Delta\text{Met}$  (mol/L) is the variation of metabolite concentration during the time period  $\Delta t$  (h), and  $X_v$  (cell/L) the average of cell concentration during the same time period.

### 2.7.2. Isotopic tracer experiments, GC-MS analysis and nonstationary $^{13}\text{C}$ -MFA

For the isotopic labeling cultures,  $[1,2-^{13}\text{C}]$ Glucose was added to glucose depleted RPMI medium, to achieve standard glucose concentration (11 mM). Label incorporation into intracellular metabolites was assessed 24 and 48 hr after label addition. Metabolic quenching, metabolite extraction and derivatization protocols were performed as described in the literature (Carinhas et al., 2016). The EI mode (70eV) mode of a QP2010 mass spectrometer (Shimadzu, Japan) with a HP-5 MS column (Agilent Technologies) was used to detect and analyze metabolites. Acquired spectra were analyzed and integrated using GC-MS Solution software version 2.50 SU1 (Shimadzu, Japan). Mass Isotopomer Distributions (MID) were calculated after spectra integration and corrected for natural isotope abundance. Nonstationary Metabolic Flux Analysis (MFA) was performed using the software package INCA (Young, 2014), which generates and simulates material balance equations based on a user-defined metabolic network structure and experimental datasets. At least 10 restarts with random initial values for the parameters (intracellular fluxes and pools) were performed to find a global optimum (Crown and Antoniewicz, 2013). The parameter continuation method was used to determinate the 95% confidence intervals for intracellular fluxes values (Antoniewicz et al., 2006).

### 2.7.3. ATP production

ATP production was estimated by multiplying the number of ATP molecules generated in anaerobic glycolysis and glucose oxidation (Boyle, 2005) by the respective flux values determined in nonstationary  $^{13}\text{C}$ -MFA.

## 2.8. Analysis of cell functionality

hiPSC-CM-2D were dissociated to single cells, as described above (Section 2.2) and inoculated on Matrigel-coated Fluorodishes at 2,000-6,000 cells/cm<sup>2</sup>. Single contracting hiPSC-CM and hiPSC-CM clusters (<10 cells) cultured on PDMS substrates for 3-5 days were chosen for image acquisition. hiPSC-CM-3D were also plated on Matrigel-coated Fluorodishes at 10-20 aggregates/dish and allowed to slightly adhere for 3 days. For calcium imaging, culture medium was supplemented with 0.5 mM of Fluo-4<sup>AM</sup> (Life Technologies) 10 min prior to image acquiring. The Nikon Elements software package and Fiji were used for movie file conversions (Schindelin et

al., 2012). Contractile kinetics of hPSC-CMs were assessed using the method developed by (Kijlstra et al., 2015).

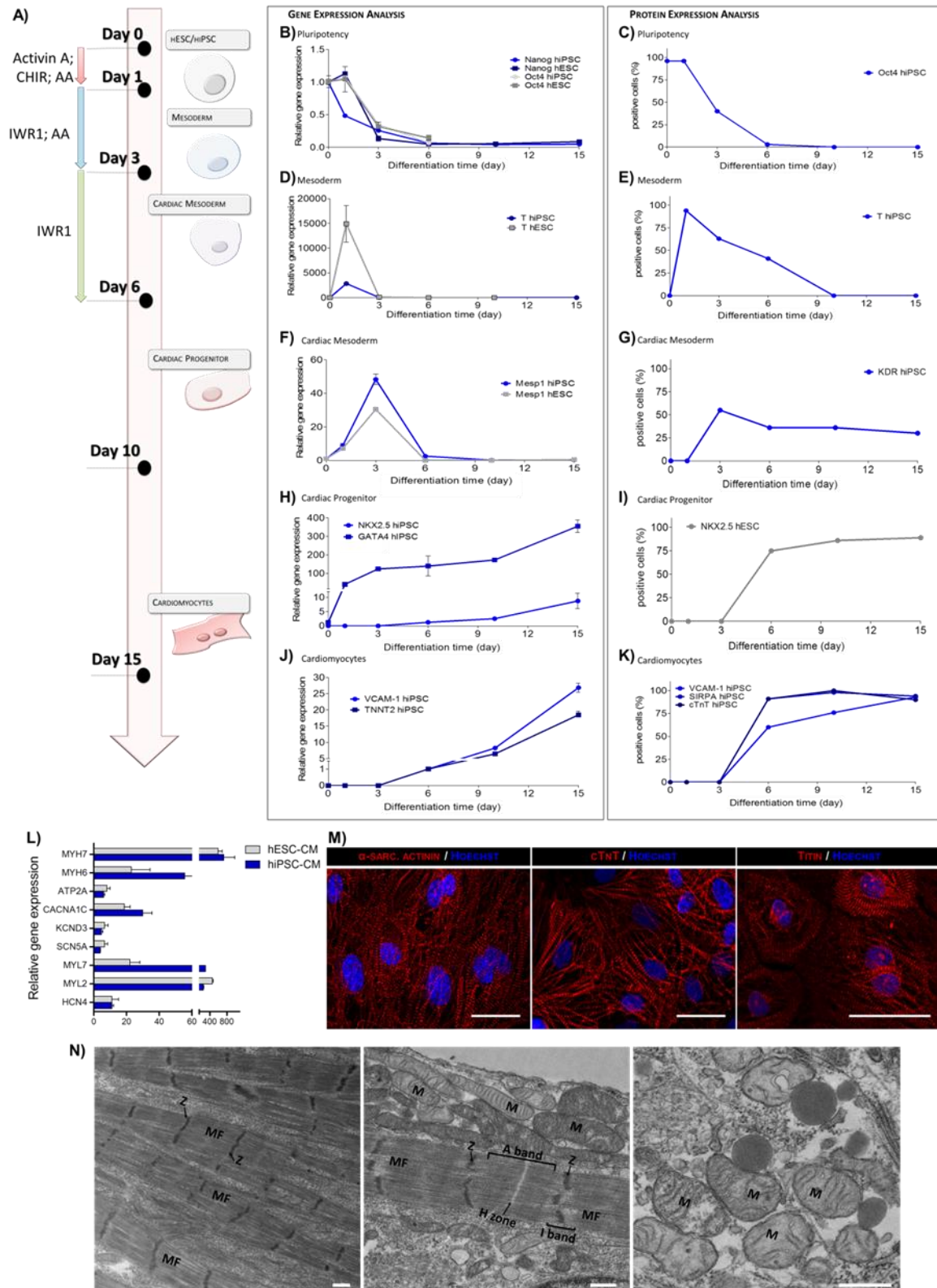
## **2.9. Statistical analysis**

Statistical analyses were performed using GraphPad Prism version 5 (GraphPad Software Inc.). Values are represented as mean±standard deviation of independent measurements or assays (at least n=3 replicates were considered). Statistical significance was evaluated using Student's t-test with values of  $p < 0.05$ .

## **3. Results**

### **3.1. Directed differentiation protocol induced the robust generation of pure 2D monolayers of CMs from multiple hPSC lines**

In this study, we used a directed cardiac differentiation protocol (Figure 3.1A) adapted from previous studies (Kattman et al., 2011; Lanier et al., 2012; Lian et al., 2013) that relies on the sequential addition of growth factors and small molecules to modulate Activin and Wnt/ $\beta$ -catenin-signalling pathways involved in mesoderm formation and cardiac lineage development (Cao et al., 2012; Kattman et al., 2011; Lian et al., 2012; Paige et al., 2010). By monitoring key markers along differentiation, we confirmed the recapitulation of the developmental steps of cardiovascular fate specification in both hESC and hiPSC lines (Figure 3.1B-3.1K). Pure CM monolayers were consistently obtained with typical gene (Figure 3.1L) and protein expression profiles (Figure 3.1K and A-3.1, Page 96), organized sarcomeric structures (Figure 3.1M-1N) and an average sarcomere length ( $1.53 \pm 0.18 \mu\text{m}$ ) similar immature hiPSC-CMs ( $1.50 \pm 0.15 \mu\text{m}$ ) (Gherghiceanu et al., 2011). Comparable CM purities were obtained with independent hiPSC and hESC lines, as assessed by the expression of CM-specific markers: VCAM-1 and SIRPA (Figure A-3.1, Page 96). Altogether these results demonstrate the efficiency and robustness of the protocol to differentiate hPSCs towards the cardiac lineage in 2D monolayer cultures.



**Figure 3.1. Direct differentiation of hPSCs towards cardiomyocytes in 2D monolayer cultures.** **A)** Schematic representation of the differentiation process. The predominant cell population at each timepoint is demarked. Timepoints in which growth factors (GFs) and/or small molecules (SM) were added are also highlighted. Characterization of the differentiation process in terms of: gene expression by qRT-PCR (**B**, **D**, **F**, **H**, **J**) and protein expression by flow cytometry analyses (**C**, **E**, **G**, **I**, **K**) in both hiPSC - DF19-9-11T.H (blue) and hESC - H3-NKX2-5(eGFP/w) (grey) lines. **L)** qRT-PCR analysis of gene expression of cardiac-related transcription factors, cardiac-specific structural genes, calcium handling and membrane ion channels, at day

15 in both hiPSC-CMs and hESC-CMs. Data are presented as mean  $\pm$  SD of at least three measurements. **M)** Immunofluorescence analysis of hPSC-CMs at the end of the differentiation process (day 15) for the CM-specific markers: sarcomeric  $\alpha$ -actinin, cardiac troponin T (cTNT) and Titin (red). Nuclei were counterstained with Hoescht (blue). Scale bars: 50  $\mu$ m. **N)** Transmission electron microscopy (TEM) images of hiPSC-CMs at day 15. Myofibrils (MF), Z-disks (Z), sarcomeric bands: A- and I-bands, intercalated disks (ID) connecting adjacent CM and mitochondria (M) are highlighted. Scale bars: 500 nm.

---

### 3.2. Metabolic characterization during hPSC differentiation towards cardiomyocytes

To characterize the metabolic modulations along CM differentiation we analyzed the changes of the main nutrients and metabolic by-products in the culture medium of hiPSCs (day 0) and of cell populations enriched in mesoderm (day 1; as verified by the rapid transient upregulation of brachyury T (Figure 3.1D and 3.1E)), cardiac mesoderm (day 3; as verified by the upregulation of the MESP1 and KDR markers (Figure 3.1F and 3.1G)), cardiac progenitors (day 6; as verified by the appearance of spontaneous contractile areas and increased expression of NKX2.5 and GATA4 markers (Figure 3.1H-I)), and cardiomyocytes (day 15; (Figure 3.1J-L)). Our results show that glucose consumption (qGlc) and lactate production (qLac) rates (Figure 3.2A-B) do not change much along the 15-day differentiation process, and the ratio qLac/qGlc (Figure 3.2C) remains high (close to 1.5), indicating that the sequential cell populations maintain the highly glycolytic metabolism of the pluripotent cells.

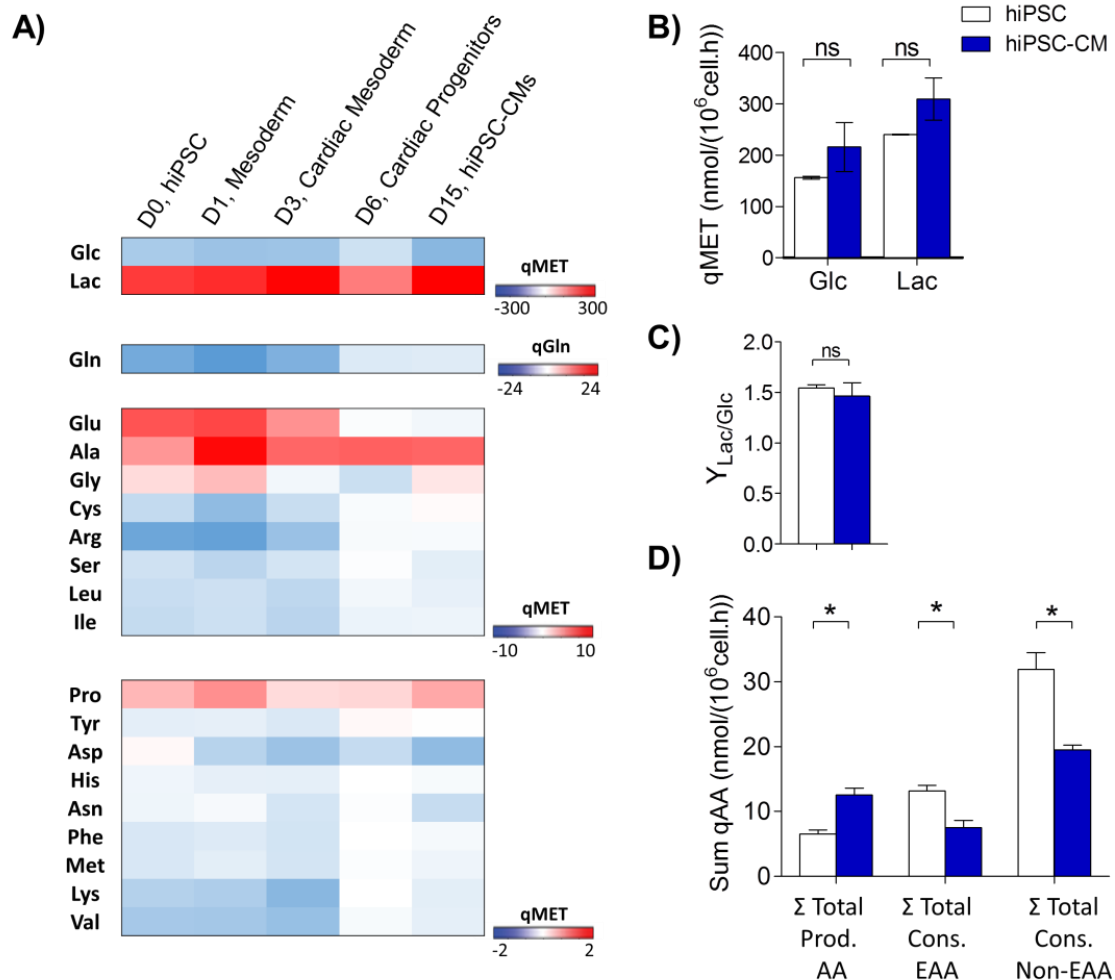
Nonetheless, significant differences were observed in amino acid metabolism (Figure 3.2A and 3.2B). Most amino acids (glutamine, cysteine, arginine, serine, leucine, isoleucine, histidine, asparagine, phenylalanine, methionine, lysine and valine) were taken up by all cell populations, however the consumptions were higher until day 3 of the differentiation. From cardiac mesoderm to cardiac committed cells there was a clear decrease in the consumption of those amino acids (Figure 3.2A). In accordance, consumption of both essential and non-essential amino acids was determined as significantly lower in hiPSC-CMs (day 15) when compared to hiPSCs (day 0) (Figure 3.2D). These results reflect the dynamic differentiation of cells within the first days until they become committed to the cardiac lineage, suggesting that hPSC-derived cardiac progenitors and hiPSC-CMs rely less on amino acid catabolism for energy production than undifferentiated or mesoderm committed cells.

Secretion of alanine and proline (at lower rates) was observed for all differentiating cell populations; alanine is a glycolytic product with a crucial role in nitrogen detoxification and proline is important in collagen synthesis (Phang et al., 2015). Both amino acids were produced at higher rates by the population enriched in mesoderm cells (day 1). Interestingly, overall amino acid production was higher in hiPSC-CMs (day 15) than in hiPSCs (day 0) (Figure 3.2D).

Glutamate was highly produced until cardiac mesoderm specification (day 3) and from this timepoint onwards became barely consumed (Figure 3.2A). Glutamate is an intermediary in the degradation of many amino acids, thus a decrease in glutamate secretion also suggests a reduction in amino acid catabolism at later differentiation stages, when the differentiating population is mainly composed by cardiac committed cells. Glycine was produced until day 1 (mesoderm phase), from day 3 to day 6 was slightly consumed, and by the end of the differentiation process, at day 15, was again produced.



Overall these results indicate that the generated hiPSC-CMs remain highly glycolytic but show significant differences in amino acid metabolism relatively to hiPSCs, including increased production of some amino acids and decreased consumption of others.



**Figure 3.2. Metabolic profiling of hiPSC during CM differentiation in 2D monolayers.** **A)** Heatmap image of specific rates of metabolite production (red) and consumption (blue) (qMET, expressed in nmol/(10<sup>6</sup>cell.h)) at specific time points of the differentiation process: day 0 (hiPSC- DF19-9-11T.H line); day 1 (mesoderm); day 3 (cardiac mesoderm); day 6 (cardiac progenitors); day 15 (hiPSC-CMs). **B)** Specific rates of glucose consumption and lactate production in hiPSC (day 0) and hiPSC-CMs (day 15). **C)** Ratio of specific rates of lactate production and glucose consumption (Y<sub>Lac/Glc</sub>). **D)** Specific consumption and production rates of amino acids in hiPSC (day 0) and hiPSC-CMs (day 15). Data are represented as mean±SD. \*p<0.05; ns, not significant.

### 3.3. Impact of 3D aggregate culture of cardiac progenitors on cardiomyocyte enrichment and commitment

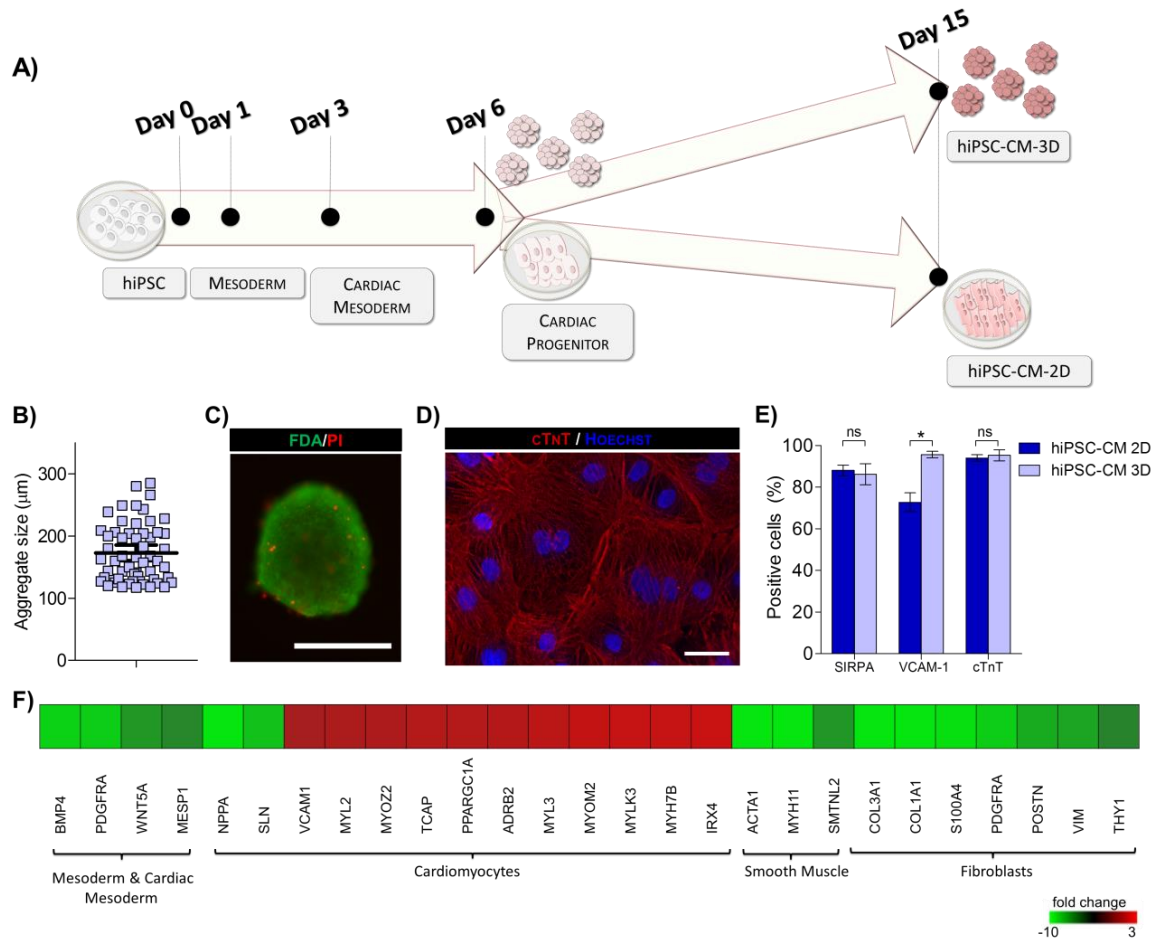
We then assessed the impact of culturing hPSC-derived cardiac progenitors as 3D aggregates on CM differentiation and enrichment using a hiPSC line (DF19-9-11T.H). Briefly, cells were harvested from 2D monolayer cultures and seeded into AggreWell™ plates at day 6 of differentiation, when cell population was enriched in cardiac progenitors, as evidenced by the high expression of NKX2.5 and GATA4 genes, Figure 3.1H). After 24 hr, aggregates were transferred to

stirred conditions to ensure an appropriate diffusion of nutrients and oxygen throughout the entire aggregate and were maintained for additional 8 days (until day 15) in these culture conditions (Figure 3.3A).

As cell aggregate size has been shown to impact cardiac induction and differentiation efficiency (Bauwens et al., 2008, 2011; Chen et al., 2015; Guo et al., 2009) we used the same cell seeding density as previously reported (Nguyen et al., 2014). The aggregates generated presented high cell viability and an average size of  $184\pm 45\ \mu\text{m}$  (Figure 3.3B-C). By day 15 the expression of CM-specific markers in cells cultured as 3D aggregates (designated hereafter as hiPSC-CM-3D) was detected by immunofluorescence analysis (Figure 3.3D) and compared by flow cytometry analysis with the expression observed in 2D monolayer cultures (designated hereafter as hiPSC-CM-2D; Figure 3.3E). Our results indicate no significant differences in the percentage of cells positive for cTnT and SIRPA, whereas the expression of VCAM-1 was significantly higher in hiPSC-CM-3D ( $95.6\pm 1.5$ ) than in hiPSC-CM-2D ( $72.8\pm 4.5$ ; Figure 3.3E).

Whole-transcriptome analysis revealed some differences at the expression level of genes related with cardiac development and specification (Figure 3.3F). In particular, several mesoderm and cardiac mesoderm genes were down-regulated in hiPSC-CM-3D comparing with hiPSC-CM-2D, suggesting that hiPSC-CM-3D are in a more advanced cardiac developmental state at day 15. Additionally, the expression of several genes associated with CM specification and maturation was higher in cells cultured as 3D aggregates, including genes related with sarcomeric structure and cardiac muscle contraction (MYL2, MYOZ2, TCAP, MYL3, MYOM2, MYLK3 and MYH7B). The expression of VCAM-1 (in accordance with flow cytometry analysis), ADRB1 ( $\beta$ -adrenergic receptor highly expressed in CMs), and PPARGC1A (coactivator of PPARs and other nuclear receptors and master regulator of mitochondrial biogenesis in heart (Ventura-Clapier et al., 2008)), were also higher in hiPSC-CM-3D than in hiPSC-CM-2D.

Interestingly, hiPSC-CM-3D showed down-regulation of atrial-like CM markers, namely NPPA encoding atrial natriuretic peptide and SLN encoding sarcolipin, and up-regulation of ventricular-like CM markers MLC2V and IRX4 in relation to hiPSC-CM-2D (Figure 3.3F). Additionally, the higher expression of marker genes of smooth muscle cells (e.g. MYH11, SMTNL2 and ACTA1) and fibroblasts (i.e. COL1A1, S100A4, PDGFRA, POSTN, VIM, THY1) in 2D monolayer cultures (Figure 3.3F) indicate that these cultures contain a higher fraction of non-CM. These results suggest that the aggregation of cardiac progenitors improves CM enrichment as well as CM differentiation and commitment into the ventricular CM subtype.



**Figure 3.3. Effect of 3D aggregate culture of cardiac progenitors on CM enrichment and commitment.** **A)** Schematic representation of the two strategies used to culture cardiac progenitors. At day 6, cells were dissociated and replated either in 2D static tissue culture plates or in AggreWell™ plates to force cell aggregation. Generated aggregates were cultured in shake flasks until day 15. **B)** Aggregate size of hiPSC-CMs at day 15. **C)** Cell viability of hiPSC-CM aggregates assessed, at day 15, by fluorescein diacetate (FDA, live cells; green) and propidium iodide (PI, dead cells; red) dye. Scale bar: 200 µm. **D)** Immunofluorescence analysis of hiPSC-CMs (from plated 3D aggregates) for Troponin T (cTnT, red). Nuclei were counterstained with Hoechst (blue). Scale bar: 30 µm. **E)** Percentage of cells positive for the cardiac specific markers: SIRPA, VCAM-1 and cTnT determined at day 15 by flow cytometry, in 2D monolayer (hiPSC-CM-2D, dark blue) and 3D aggregate (hiPSC-CM-3D, light blue) cultures. \* $p < 0.05$ ; ns, not significant. **F)** Heatmap depicting fold changes in the expression of genes associated with mesoderm, cardiac mesoderm, cardiomyocytes, smooth muscle cells and fibroblasts in hiPSC-CM-3D versus hiPSC-CM-2D at day 15. Decreased gene expression changes is represented in green while increased expression in red.

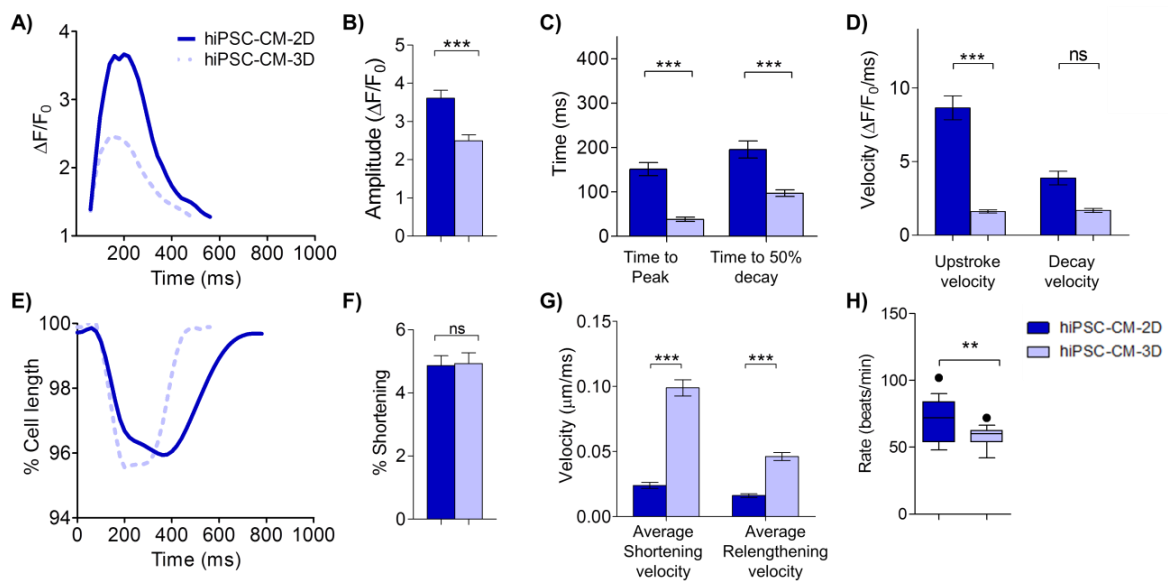
### 3.4. Impact of 3D aggregate culture approach on hiPSC-CM functionality

Functionality of both hiPSC-CM-2D and hiPSC-CM-3D was compared in terms of calcium signaling, contractility kinetics and beating rate (Figure 3.4). The results showed that hiPSC-CM-3D present calcium peaks with lower amplitude (Figure 3.4A-B), reduced time to peak and time to 50% decay (Figure 3.4C) and slower upstroke and decay velocities (Figure 3.4D) in comparison with hiPSC-CM-2D. However, the lower amplitude and velocity detected in hiPSC-CM-3D may be related with a less efficient diffusion of the dye throughout the entire plated aggregate and not necessarily with a reduced/slower calcium signaling kinetics. Nevertheless, both culture conditions

generated hiPSC-CMs with well-defined and synchronous intracellular calcium transients with a shape and duration resembling those of fetal like CMs (Louch et al., 2015).

Concerning cell contractility, no significant differences in fractional shortening were observed between conditions (Figure 3.4E-F), however hiPSC-CM-3D showed a 4-fold higher shortening velocity and a 3-fold higher relengthening velocity compared to hiPSC-CM-2D (Figure 3.4G), revealing that hiPSC-CM-3D present a faster contractility kinetics, consistent with the increased expression of genes encoding cardiac contractile proteins (Figure 3.3F).

Spontaneous contractility was observed for nearly 100% of the hiPSC-CM aggregates. The beating rate was significantly lower in hiPSC-CM-3D ( $57.9 \pm 1.8$  beats/min) than in hiPSC-CM-2D ( $69.5 \pm 3.3$  beats/min) (Figure 3.4H), values within the range previously reported for hPSC-CMs (21–84 beats/min) (Feric and Radisic, 2016). It has been reported that during heart development the spontaneous activity of CMs at early embryonic stages is replaced by a quiescent cell phenotype (Feric and Radisic, 2016). The significant decrease in beating rate may suggest that hiPSC-CM-3D are in a more advanced developmental state than hiPSC-CM-2D, as suggested above.



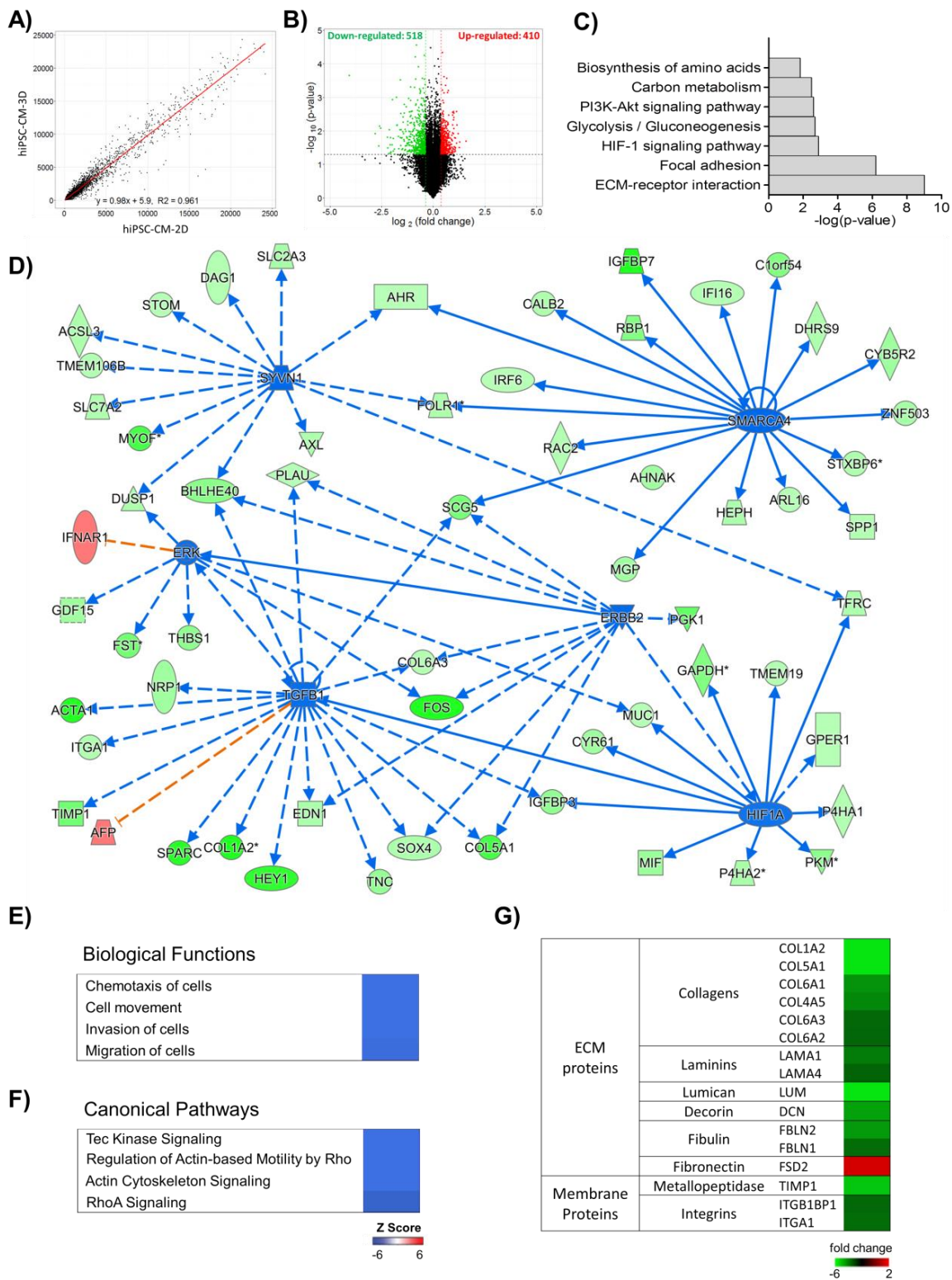
**Figure 3.4. Impact of 3D aggregate culture of cardiac progenitors on hPSC-CM functionality.** **A)** hiPSC-CM were analyzed in terms of calcium transients (**A-D**) and contractile performance (**E-H**) at the end of the differentiation process (d15) in hiPSC-CM-2D (dark blue) and hiPSC-CM-3D (light blue). Calcium transient kinetics (**A-D**) evaluated with the intracellular calcium indicator Fluo-4 AM: **A)** Representative calcium transient; **B)** Calcium transient amplitude ( $F/F_0$ ); **C)** Time to peak and time to 50% decay; **D)** Average upstroke and decay velocities.  $n=28-35$  cells/aggregates per condition. **E)** Representative contraction curves, reflecting changes in the percentage of cell length. **F)** Percentage of shortening; **G)** Maximum shortening and relengthening velocities.  $n=20-35$  cells/aggregates per condition. **H)** Boxplot depicting the beating rate of hiPSC-CMs. Whiskers: 10-90 percentile. Outliers are plotted as individual points. Data are represented as mean  $\pm$  SD. \* $p < 0.05$ ; \*\* $p < 0.01$ ; \*\*\* $p < 0.001$ ; ns, not significant.

### 3.5. Impact of 3D culture approach on transcriptome profile of hiPSC-CMs

Next, we compared global gene expression changes in hiPSC-CM-3D and hiPSC-CM-2D. Scatter plot analysis revealed that both hiPSC-CM-3D and hiPSC-CM-2D present a high degree of similarity in gene expression profiles (Figure 3.5A). A total of 928 genes were identified as differentially expressed ( $FC > |1.3|$  and  $p\text{-value} < 0.05$ ), in hiPSC-CM-3D compared to hiPSC-CM-2D, 518 of which were down-regulated and 410 were up-regulated (Figure 3.5B). KEGG pathways enrichment analysis indicated that these genes were significantly enriched in pathways related with: i) metabolism or involved in metabolism regulation (i.e. HIF-1 signaling pathway, glycolysis/gluconeogenesis, PI3K-Akt signaling, carbon metabolism and biosynthesis of amino acids) and ii) cell-ECM interactions and cell adhesion (i.e. ECM-receptor interactions and focal adhesion pathways) (Figure 3.5C).

Upstream regulator analysis of differentially expressed genes was also performed to identify possible regulators responsible for the observed changes in gene expression. This analysis identified among others, HIF1A, TGFB1, ERBB2, SYVN1, SMARCA4 and ERK as upstream transcriptional regulators in hiPSC-CM-3D (Figure 3.5D). The network showing the predicted interactions between regulators and their targets as well as the regulation direction (i.e. “activation” or “inhibition”) is illustrated in Figure 3.5D.

Pathways and functions related with focal adhesion, extracellular matrix (ECM) remodeling and actin cytoskeleton reorganization were significantly enriched in hiPSC-CM-3D compared to hiPSC-CM-2D (Figure 3.5C) probably as a consequence of cell adaptation to a 3D culture. Specifically, IPA predicted inactivation of actin cytoskeleton signaling, regulation of actin-based motility by RhoA and Tec Kinase signaling, in hiPSC-CM-3D compared with hiPSC-CM-2D, and consequently inactivation of functions related with cell movement/adhesion/migration (Figure 3.5E-F). Also, several genes encoding ECM proteins (e.g. collagen types I, IV, V, VI, XIII, laminin, lumican, decorin, fibulin), metalloproteinase (Timp1) and integrins (ITGB1BP1 and ITGA1) were down-regulated in hiPSC-CM-3D. This correlates with the reduced amount of fibroblasts in these cultures (supported by the reduced expression of fibroblast markers (Figure 3.3F), as fibroblasts and related myofibroblasts are the main producers of ECM and ECM-regulatory proteins (MMPs and TIMPs) in the heart (Fan et al., 2012; Ivey and Tallquist, 2016; Krenning et al., 2010). In accordance, both PDGF and TGF $\beta$  factors, known to induce the production of ECM proteins, MMPs and TIMPs by fibroblasts (Krenning et al., 2010; Souders et al., 2009; Takeda and Manabe, 2011), were down-regulated in hiPSC-CM-3D when compared with hiPSC-CM-2D (Figure 3.3F and 3.5D). The expression of integrins (ITGB1BP1 and ITGA1), cell surface receptors that mediate cell-ECM interaction and adhesion, was also significantly lower in hiPSC-CM-3D when compared with hiPSC-CM-2D (Figure 3.5G).



**Figure 3.5. Comparison of the transcriptional profile of hiPSC-CMs obtained in both 2D monolayer and 3D aggregate cultures.** **A)** Scatter plot depicting differences in gene expression in hiPSC-CM-2D and hiPSC-CM-3D. **B)** Volcano plot of gene expression changes. Genes up-regulated ( $FC \geq 1.3$  and  $p\text{-value} < 0.05$ ) are highlighted in red and genes down-regulated ( $FC \leq -1.3$  and  $p\text{-value} < 0.05$ ) in green. The number of regulated genes according to these criteria is shown on the top of the graphic. **C)** KEGG pathways significantly enriched in up and down regulated genes. The modified Fisher Exact p-value determined for each pathway is shown. **D)** Upstream regulator analysis of differentially expressed genes. Validated gene targets of each transcriptional regulator and their direction of change are also shown. The regulators are colored by their predicted activation state: activated (orange) or inhibited (blue). Darker colors indicate higher absolute

regulation Z-scores. The edges connecting the nodes are colored orange when leading to activation of the downstream node and blue when leading to its inhibition. **E-F**) Heatmaps highlighting the activation status of biological functions (E) and canonical pathways (F) predicted by IPA. Functions/pathways were considered significantly activated (or inhibited) with an overlap p-value  $\leq 0.05$  and an IPA activation Z-score  $\geq |2.0|$ . Blue indicates negative Z-score (inhibited function). **G**) Heat map depicting the significant differentially expressed genes (fold change  $\geq 1.3$  and p-value  $< 0.05$ ) encoding ECM proteins, metalloproteinases and integrins in hiPSC-CM-3D in relation to hiPSC-CM-2D.

---

The down-regulation of fibulin family in hiPSC-CM-3D may be related with the fact that these proteins mainly contribute to the formation of distinct ECM during early developmental stages in several tissues, including cardiac ventricular morphogenesis, and in adult tissue is mainly expressed in the heart valves (Zhang et al., 1996). Lumican and decorin, the other ECM proteins less expressed in hiPSC-CM-3D, were previously reported to be increased in various inflammatory-like conditions, presenting a role in heart failure development by modulating ECM rearrangement and collagen assembly (Engebretsen et al., 2013; Jahanyar et al., 2007). In agreement, several upstream regulators that were inhibited in hiPSC-CM-3D are involved in pro-survival and hypertrophic responses during cardiac diseases and heart failure: *Syvn1*, an important modulator of ischemic damage in heart is up-regulated by endoplasmic reticulum stress; *SMARCA4*, a chromatin-remodeling protein that in embryos, promotes CM proliferation and in adults is turned off or reactivated in hypertrophic cardiomyopathy (Hang et al., 2010); *ERBB2*, that promotes CM dedifferentiation and proliferation during heart regeneration (D'Uva et al., 2015); *ERK1*, that is activated by hypertrophic stimuli (Kehat and Molkenin, 2010); and *TGFB-1*, an important mediator of the hypertrophic growth response of the heart (Dobaczewski et al., 2011; Takeda and Manabe, 2011).

Hypoxia-inducible factor-1 alpha (*HIF-1 $\alpha$* ), a member of HIF-1 signaling pathway, was predicted as an “inhibited” up-stream regulator in hiPSC-CM-3D, consequently resulting in the inhibition of several genes, including genes related with glycolysis and glucose metabolism (e.g. *GAPDH* and *PKM*; Figure 3.5D). *HIF1 $\alpha$*  is a central transcriptional regulator, whose activation is prompted by hypoxic conditions (Prigione et al., 2014). Specifically, *HIF1 $\alpha$*  promotes cellular adaptation to reduced oxygen availability by increasing glucose uptake and glycolysis, improving angiogenesis or enhancing cell proliferation and survival (Guimarães-Camboa et al., 2015). Down-regulation of *HIF1 $\alpha$*  in hiPSC-CM-3D in relation to hiPSC-CM-2D, may suggest that agitated 3D cultures systems ensures more uniform cell exposure to oxygen tension possibly favoring an increase of oxidative metabolism.

### 3.6. Impact of 3D culture approach on hiPSC-CM metabolism

We then sought to assess whether the 3D culture approach would affect the metabolic profile of the generated hiPSC-CMs.

To compare the central carbon metabolism of hPSC-CMs obtained in both conditions we performed  $^{13}\text{C}$ -based metabolic flux analysis ( $^{13}\text{C}$ -MFA). Intracellular fluxes were determined by integrating transmembrane fluxes with  $^{13}\text{C}$  labeling profiles of intracellular metabolites from [1,2- $^{13}\text{C}$ ]Glucose tracer in a metabolic network model (Woo Suk and Antoniewicz, 2013). Reasonable

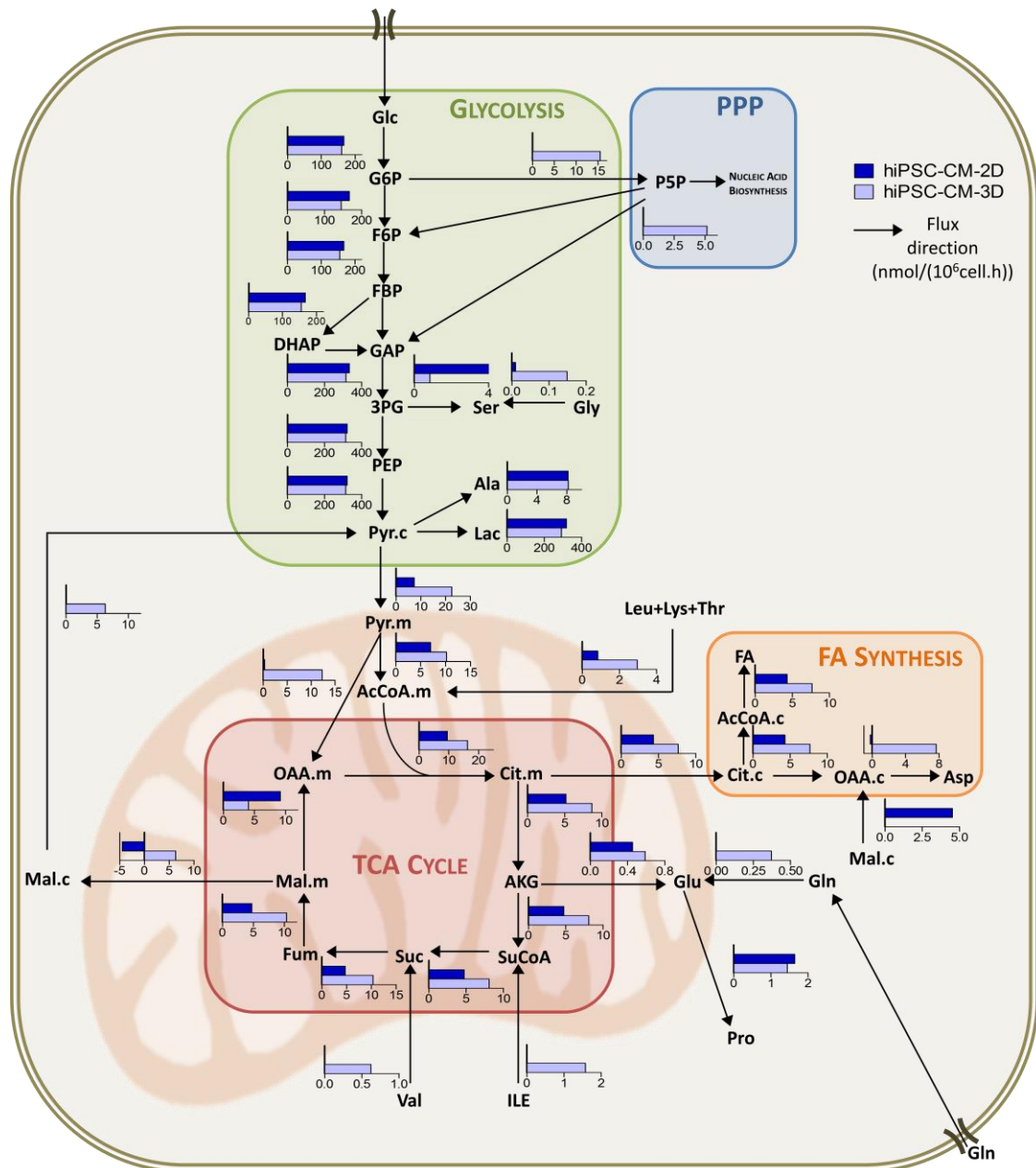
fits were obtained for both conditions (Figure A-3.2 and Figure A-3.3, Page 97); estimated fluxes and intervals are provided in Table A-3.1 (Page 98). The fluxome and metabolic transcriptome profiles of hiPSC-CM-3D and hiPSC-CM-2D were compared aiming to reveal the main differences in metabolic fluxes and to correlate them with the expression of metabolic enzymes (Figure 3.6 and 3.7A).

The flux maps clearly show that both hPSC-CM cultures exhibit high glycolytic fluxes, diverting most of the cytosolic pyruvate to lactate secretion (Figure 3.6), which is consistent with the measured extracellular rates (Figure A-3.4, Page 99). Although hiPSC-CM-3D showed relatively lower glycolytic fluxes, including a 10-15% reduction in glucose uptake and lactate production, when compared with hiPSC-CM-2D, no significant differences were determined (Figure 3.7B). The fluxes through pentose phosphate pathway (PPP) were higher in hiPSC-CM-3D, achieving values of 5.2 nmol/(10<sup>6</sup>cells.h), whereas in hiPSC-CM-2D these fluxes were negligible (Figure 3.6). Additionally, in hiPSC-CM-3D a higher amount of cytosolic pyruvate was transported to the mitochondria (22.5 vs 7.3 nmol/(10<sup>6</sup>cells.h) in hiPSC-CM-2D), and entered the TCA cycle, reflecting a slightly higher coupling of glycolysis and TCA cycle. Oxidative decarboxylation of pyruvate to acetyl-CoA increased by 45% and TCA cycle fluxes were significantly higher (approximately 54%, Figure 3.7C) in hiPSC-CM-3D comparatively to hiPSC-CM-2D, which again points towards increased glucose oxidation in hiPSC-CM-3D. In accordance, the expression of several glycolysis-annotated genes (i.e. ENO1; PGK1; GAPDH; PGAM1/4; PKM) significantly decreased while the expression of genes related with oxidative phosphorylation (e.g. ATP5, COX and NDUF family of genes) increased in hiPSC-CM-3D (Figure 3.7A).

Remarkably, in both conditions the citrate produced in TCA cycle was mainly (45-47%) transported to the cytosol, generating Acetyl-CoA precursors that are typically used for lipid biosynthesis. Additionally, in both culture conditions the consumption of glutamine was very low emphasizing the neglected role of glutamine anaplerosis. A net flux of alpha-ketoglutarate towards glutamate was estimated, contributing to an increased carbon loss from TCA cycle. To compensate the absence of glutamine anaplerosis and high withdrawal of citrate, hiPSC-CM-3D cells used other sources to fuel the TCA cycle, namely the anaplerotic pyruvate carboxylation (PC) reaction and the catabolism of alternative amino acids, such as leucine, lysine, threonine, isoleucine and valine (all significantly lower in hiPSC-CM-2D, (Figure 3.6, Figure 3.7 D,E)). The symmetric entrance of pyruvate into the TCA cycle, by the activities of pyruvate dehydrogenase (PDH) producing Acetyl-CoA (10.2 nmol/(10<sup>6</sup>cells.h) and PC producing oxaloacetate (12.3 nmol/(10<sup>6</sup>cells.h)) (Figure 3.6), and the activity through malic enzyme (ME) highlights the importance of pyruvate cycling in maintaining the balance of TCA cycle activity in hiPSC-CM-3D. Also, transcriptome profile revealed up-regulation of several genes related with amino acid metabolism (e.g. GOT1 and GPT) in hiPSC-CM-3D compared with hiPSC-CM-2D (Figure 3.7A) corroborating the idea that amino acid metabolism was more active in hiPSC-CM-3D.

In hiPSC-CM-2D, pyruvate cycling through ME and PC was rather inactive (Figure 3.6) and the most relevant anaplerotic reaction detected was a net flux of malate formation from cytosolic oxaloacetate (Figure 3.6).

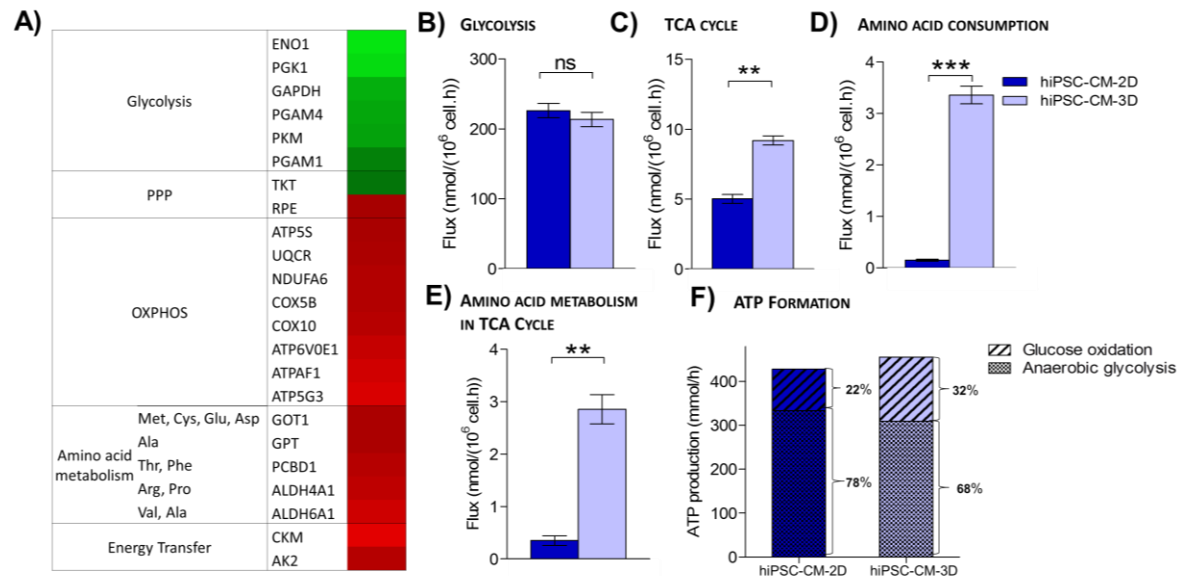




**Fig. 3.6. Metabolic flux map of the central carbon metabolism of both hiPSC-CM-2D and hiPSC-CM-3D at day 15.** Fluxes estimated by non-stationary <sup>13</sup>C-metabolic flux analysis (MFA) are shown for hiPSC-CM-2D (dark blue) and hiPSC-CM-3D (light blue) All fluxes are in nmol/(10<sup>6</sup>cell.h).

ATP production was calculated taking into account the estimated fluxes and the number of ATP molecules produced during anaerobic glycolysis and complete oxidation of glucose in the TCA cycle (Boyle, 2005). The results show that ATP production was slightly higher in hiPSC-CM-3D (456 nmol/h) than in hiPSC-CM-2D (428 nmol/h) (Figure 3.7F) but in both cultures, anaerobic glycolysis assured most of the energetic requirements contributing to 68% and 78% of total produced ATP in hiPSC-CM-3D and hiPSC-CM-2D, respectively (Figure 3.7F). Nonetheless, the amount of ATP produced through glucose oxidation was 54% higher in hiPSC-CM-3D than in hiPSC-CM-2D, originating 32% of the total ATP produced in hiPSC-CM-3D and just 22% in hiPSC-CM-2D (Figure 3.7F).

Also, hiPSC-CM-3D showed up-regulation of both creatine kinase (CK) and adenylate kinase (AK) genes comparatively to hiPSC-CM-2D (Figure 3.7A). These enzymes perform several functions in cellular energy metabolism, including maintenance of ATP homeostasis and OXPHOS regulation (Schlattner et al., 2006). Impairment or ablation of CK has shown to lead to contractile dysfunction, decreased energy reserve and ultimately cardiomyopathy and/or hypertrophy (Nahrendorf et al., 2005; Spindler et al., 2003). Thus, this result also suggests that hiPSC-CM-3D cultures present improved energetics than hiPSC-CM-2D cultures.



**Figure 3.7. Comparison of central carbon metabolism and metabolic transcriptional profile in both 2D monolayers and 3D aggregates of hiPSC-CM.** **A)** Heat map of differentially expressed genes associated with metabolic processes/pathways in hiPSC-CM-3D compared to hiPSC-CM-2D. Genes were considered enriched based on a p-value < 0.05 and a FC  $\geq$  |1.3|. Up-regulated and down-regulated genes are demarked in red and green, respectively. **B-E)** Mean fluxes and respective SD estimated for the following metabolic pathways: glycolysis (**B**); TCA cycle (**C**); amino acid consumption (**D**) and amino acid metabolism involved in TCA cycle anaplerosis (**E**). Data are represented as mean $\pm$ SD. \*\*p<0.01; \*\*\*p<0.001; ns, not significant. **F)** Total amount of ATP produced in hiPSC-CM-2D and hiPSC-CM-3D taking into account estimated fluxes and the reference amount of ATP produced per glucose molecule in anaerobic glycolysis and glucose oxidation. The contribution of both metabolic pathways for the estimated ATP production is indicated.

#### 4. Discussion

In this study we applied a directed cardiac differentiation protocol adapted from previous reports (Kattman et al., 2011; Lanier et al., 2012; Lian et al., 2013) that allows the production of pure populations of hPSC-CMs as standard 2D monolayers and as 3D aggregates when promoting the aggregation of cardiac progenitor cells, and we compared the transcriptome and fluxome of hiPSC-CMs obtained in both culture systems. Specifically, we demonstrated that the aggregation of hPSC-derived cardiac progenitors induces: i) CM enrichment and commitment; ii) significant alterations in the expression of genes related with cell-ECM interactions, cell adhesion, cell metabolism and metabolism regulation; iii) changes in central carbon metabolism, including

reduction of glucose consumption, increased oxidative decarboxylation of pyruvate, TCA cycle activity and amino acid metabolism when compared with hiPSC-CM-2D.

Even though the differentiation in standard 2D conditions robustly generated monolayers of hPSC-CMs that presented typical CM markers and functionality, promoting aggregation of hPSC-derived cardiac committed cells further improved CM differentiation, CM commitment towards ventricular-like subtype, and functionality as proved by: i) down-regulation of genes expressed in mesoderm, cardiac mesoderm, atrial-like CMs, smooth muscle and fibroblasts, ii) up-regulation of CM-specific genes, including genes encoding contractile proteins and proteins restricted to (IRX4) (Nelson et al., 2014, 2016) or strongly expressed in the ventricular myocardium (MLC2v) (O'Brien et al., 1993), and iii) faster contractility kinetics, when compared with 2D monolayer cultures. Previous studies have shown that addition of IWR-1 enhances differentiation of cardiac progenitors into ventricular-like CMs (Karakikes et al., 2014). Our results suggest that aggregation of cardiac progenitors and further differentiation as 3D aggregates may also favour CM specification into ventricular-like CM subtype. Further electrophysiological studies should be performed to validate this hypothesis.

Although several efforts have been made towards moving cardiac differentiation protocols from 2D monolayer to 3D aggregate cultures to facilitate large-scale CM production (Chen et al., 2012, 2015; Dahlmann et al., 2013; Kempf et al., 2014, 2015), adherent cultures typically yield higher differentiation efficiency (i.e. CM purity) and reproducibility (Kempf et al., 2016; Zhang et al., 2015). Most likely because several critical process parameters need to be thoroughly optimized to successfully establish an effective 3D aggregate-based differentiation protocol, including cell aggregate size, agitation rate, small molecule concentrations and induction timing (Chen et al., 2015). Also, the extensive cell death inherent to directed differentiation processes may result in aggregate disintegration or in accumulation of apoptotic/necrotic cells in the aggregate core, which may affect the development of neighbouring cells. Here, we overcome these issues by promoting cell aggregation when the differentiating population is mainly composed by cardiac committed cells.

In the last decade, cell aggregation has been used as a tool to select specific subpopulations of differentiated cells to create homotypic spheroids (Bauwens et al., 2008; Dahlmann et al., 2013; Nguyen et al., 2014; Niebruegge et al., 2008; Ungrin et al., 2008). This enrichment may be justified because aggregation of specific cell types is directly related to the cells' adhesion protein profile mediated by the collective ensemble of specific cell surface receptors. Based on this principle, cells with analogous surface proteins will adhere easier and faster (Hookway et al., 2015). Nguyen and colleagues confirmed this hypothesis by demonstrating that forced aggregation and 3D suspension culture is capable of enriching hPSC-CMs from heterogeneous differentiated cultures containing only 10%–40% hPSC-CMs (Nguyen et al., 2014). Also, this and other studies using primary CM cultures (Akins et al., 2010; Soares et al., 2012) showed that 3D aggregate cultures, due to their ability to better mimicking the *in vivo* environment, enhance structural and functional maturation of CMs compared with parallel 2D cultures. Herein, we showed the benefits of a 3D culture environment earlier in the differentiation process. We demonstrated that enriching differentiating

cultures into CM committed cells ameliorates differentiation and commitment and possibly CM maturation, contributing to reduced differentiation/maturation time. In further investigations, it will be interesting to increase culture time to more accurately evaluate the impact of 3D aggregate strategy on the induction of maturation features in hPSC-CMs.

Jha and colleagues reported that combining a 3D culture of cardiac progenitors (obtained at day 4/5 differentiation) with a 3-day culture period of simulated microgravity using a random positioning machine results in the production of highly enriched CM cultures with high viability and typical functional properties after 20 days (Jha et al., 2016). In this study, we report similar results without a period of simulated microgravity and explored much further the impact of a 3D culture on the phenotype of the produced hPSC-CMs by providing a comprehensive and quantitative molecular and metabolic comparison between these cells and those generated in parallel 2D monolayer cultures.

Integrated -omics analysis revealed that cell culture configuration induces considerable alterations in cell's transcriptome and fluxome. The most significant differences at the transcriptome level in hiPSC-CM-3D in relation to hiPSC-CM-2D are the down-regulation of canonical pathways involved in cell adhesion, biological functions related with cell movement and chemotaxis, and expression of genes encoding for ECM proteins and integrins. The decreased expression of genes that encode ECM proteins may also reflect an increased CM purity in hiPSC-CM-3D, since cardiac fibroblasts are the cell type that produce and secrete the majority of the ECM that supports the myocardium (Krenning et al., 2010). Other studies performed with cancer cell lines also support these observations showing that 3D cultures often display different gene expression profiles, especially genes that play a role in proliferation, angiogenesis, migration, invasion and chemosensitivity, when comparing with 2D cultures (reviewed in (Edmondson et al., 2014)). Recently, Fridley and colleagues showed that hydrodynamic forces that cells are exposed to in 3D cultures can alter the expression patterns of both ECM and GFs of differentiating PSC in multicellular aggregates (Fridley et al., 2014).

Additionally, we showed that cell metabolism is slightly altered in 3D aggregate cultures. Upstream regulator analysis predicted that HIF-1 $\alpha$  constitutes an inhibited transcriptional regulator in hiPSC-CM-3D, leading to down-regulation of a cascade of genes, including glycolytic genes. In later stages of cardiac development, HIF-1 $\alpha$  has been shown to act as an inhibitor in the transition from fetal to adult CM phenotype (Ahuja et al., 2007), thus the HIF-1 $\alpha$  repression observed in hiPSC-CM-3D may again indicate that this culture is in an advanced stage of development.

Several studies have reported changes in energy metabolism during hPSC differentiation (Ia et al., 2011). Specifically, cell differentiation has been associated with increased mitochondrial content and activity and with a transition from a predominant glycolysis-based metabolism in PSCs towards an increased OXPHOS-based metabolism in differentiated cells (Wanet et al., 2015). Here, we clearly show that hiPSC-CMs obtained in both 2D monolayers and 3D aggregates remain highly glycolytic, presenting a metabolic phenotype largely driven by high glucose consumption and lactate production at near stoichiometric levels. This scenario suggests that hiPSC differentiation towards CMs proceeds without a metabolic shift from glycolytic to oxidative state. This lead us to

speculate that such metabolic shift could be important in a late developmental state, probably to promote the transition from fetal to mature hPSC-CMs. Nonetheless, it should be noted that hiPSC-CM-3D showed down-regulation of several glycolytic genes, up-regulation of OXPHOS genes, increased oxidative decarboxylation of pyruvate to acetyl-CoA and TCA-cycle activity, and higher ATP production through glucose oxidation, when compared with hiPSC-CM-2D. These results indicate a slightly improved oxidative metabolism in aggregate cultures.

Importantly, we showed that amino acid metabolism significantly decreased throughout the differentiation process, suggesting that hPSC-derived cardiac progenitors and CMs rely less on amino acid catabolism for energy production than undifferentiated or mesoderm committed cells. It has been widely reported that hiPSCs are highly dependent on amino acid metabolism (Lopaschuk and Jaswal, 2010), either to feed TCA cycle or to modulate epigenetic processes that are critical to maintain pluripotency and/or induce differentiation (Harvey et al., 2016). Methionine metabolism, for example, is crucial for the production of S-adenosylmethionine that is the methyl donor for histone and DNA methylation and is required for maintenance of hPSCs self-renewal and undifferentiated state (Shiraki et al., 2014). Methionine, leucine and lysine were shown to be necessary for hPSC proliferation and their absence from the culture medium has been shown to induce G1 cell cycle arrest and eventually apoptosis (Kilberg et al., 2016).

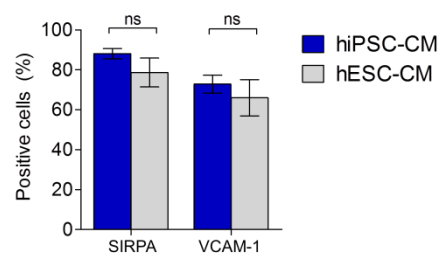
hiPSC-CM-3D showed higher amino acid metabolism that contributed to TCA cycle anaplerosis than hiPSC-CM-2D. Surprisingly, fluxome analysis revealed that in both hiPSC-CM-2D and hiPSC-CM-3D, glutamine consumption was very low and was mainly channelled to proline formation, probably to contribute for collagen synthesis (Phang et al., 2015) instead of supporting TCA cycle anaplerosis. Also, in both culture conditions a considerable outflow of citrate from TCA cycle to cytoplasm for fatty acid biosynthesis was observed. In hiPSC-CM-3D, this loss of carbon from TCA cycle was compensated by an increased catabolism of amino acids, producing Acetyl-CoA and relevant TCA cycle intermediates, and by pyruvate cycling *via* the activity of ME and PC. These anaplerotic reactions contributed to increase TCA cycle activity in hiPSC-CM-3D.

Recently, lipid deficiency in culture medium has been shown to induce the increase of PPP and fatty acid synthesis whereas lipid supplementation mitigates these metabolic pathways and increases oxidative metabolism (Zhang, 2016). In fact, the concentration of fatty acids present in the culture medium used in this study (RPMI+B27) is in the  $\mu\text{M}$  range, which might partly justify the high fluxes through PPP and fatty acid biosynthesis.

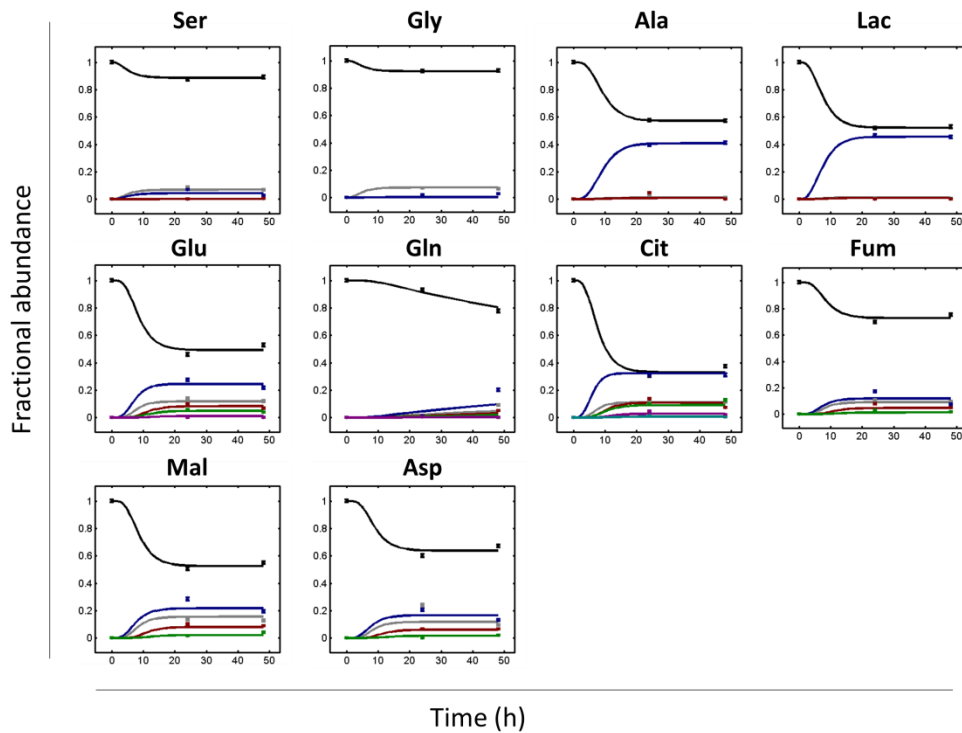
Fatty acid  $\beta$ -oxidation is the major source of energy in adult CMs *in vivo* (Lopaschuk and Jaswal, 2010) and the average concentration of free fatty acids in human plasma is within the range of 0.2–0.4 mM (Lopaschuk and Jaswal, 2010), much higher than the concentration of fatty acids in RPMI+B27 medium. Additionally, the concentration of glucose in RPMI+B27 (11 mM) exceeds the concentration of glucose in blood of healthy adults (approximately 5.5 mM) (Ceriello et al., 2008). Thus, improvements in hPSC-CM differentiation and maturation protocols in the future will probably pass by medium design strategies to optimize the concentrations of glucose, fatty acids and amino acids in culture medium to better mimic the *in vivo* carbon substrate usage in fetal and adult heart.

Overall the cardiac differentiation strategy reported herein provides novel insights for scaling up the production of hPSC-CMs. Specifically it enabled the efficient generation of pure 3D aggregates of hPSC-CMs suitable to use directly in high-throughput *in vitro* assays for drug discovery or in *in vivo* cell therapy applications, overcoming the challenges of low rates of cell retention following transplantation of single cells (Günter et al., 2016). Using an integrated experimental and computational systems biology approach, this study provides a more comprehensive picture of CM differentiation as 2D monolayers and 3D aggregates as well as a useful baseline for investigating and assessing hPSC-CM metabolism during differentiation facilitating the identification of cell populations by their metabolic signature.

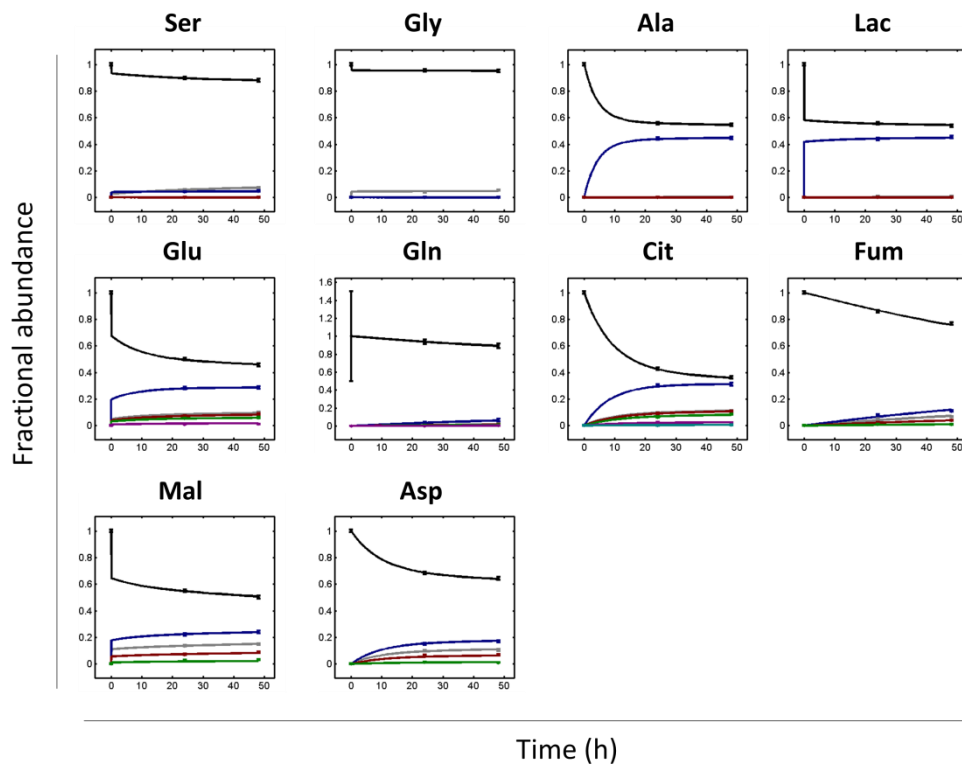
## 5. Appendix



**Figure A-3.1. Comparison of CM purity obtained after directed differentiation of 2D monolayers of hiPSC and hESCs.** Percentage of cells positive for the cardiac specific markers: SIRPA and VCAM determined by flow cytometry, at day 15, in 2D monolayer of hiPSC-CM (dark blue) and hESC-CM (grey) cultures. Data are represented as mean $\pm$ SD; ns, not significant.



**Figure A-3.2. Experimental and simulated intracellular  $^{13}\text{C}$ -labelling dynamics in hiPSC-CM-2D using  $[1,2-^{13}\text{C}]\text{GLC}$ .** Circle markers correspond to GC-MS measurements corrected for natural isotope abundance. Lines correspond to fitted MIDFs from nonstationary  $^{13}\text{C}$ -MFA flux estimation of labelling experiments.



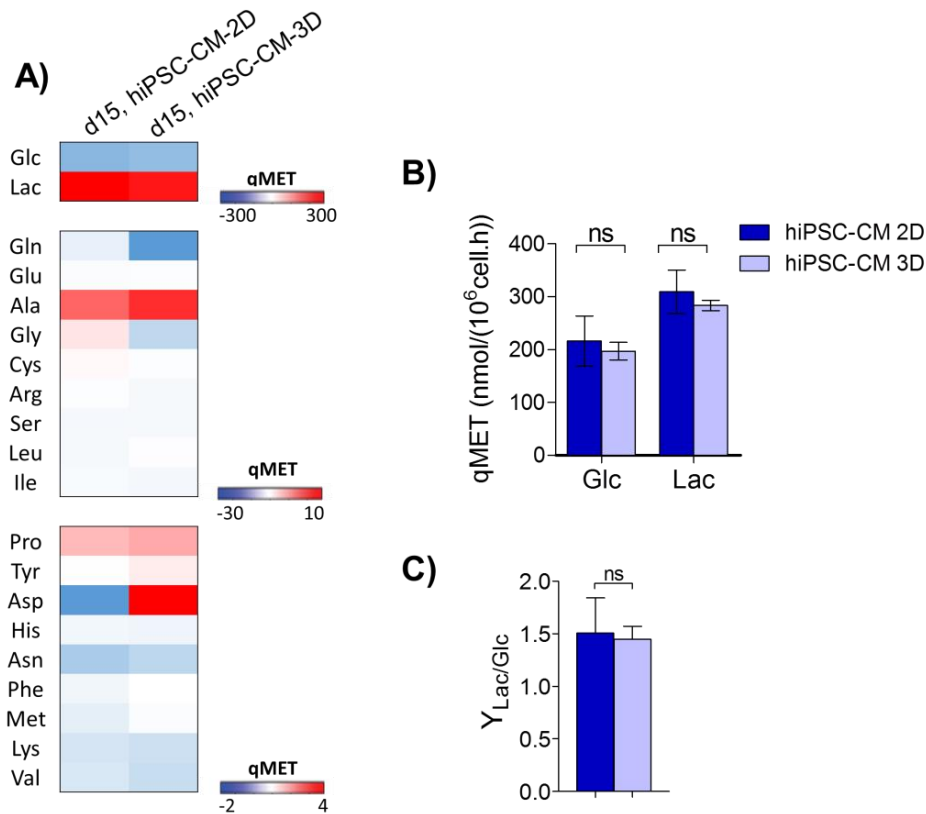
**Figure A-3.3. Experimental and simulated intracellular  $^{13}\text{C}$ -labelling dynamics in hiPSC-CM-3D using  $[1,2-^{13}\text{C}]\text{GLC}$ .** Circle markers correspond to GC-MS measurements corrected for natural isotope abundance. Lines correspond to fitted MIDFs from nonstationary  $^{13}\text{C}$ -MFA flux estimation of labelling experiments.

**Table A-3.1. Metabolic network reactions and simulated fluxes determined by nonstationary  $^{13}\text{C}$ -MFA.** Estimated flux values are shown in units of  $\text{nmol}/(10^6\text{cell}\cdot\text{h})$ . Negative flux values indicate that net direction is reverse to the direction indicated.

		hiPSC-CM-2D	hiPSC-CM-3D
v1	G6P <-> F6P	166.63	144.61
v2	F6P -> FBP	166.63	154.92
v3	FBP <-> DHAP + GAP	166.63	154.92
v4	DHAP <-> GAP	166.63	154.92
v5	GAP <-> 3PG	333.27	315.00
v6	3PG <-> PEP	321.60	314.15
v7	PEP -> Pyr.c	321.60	314.15
v8	Pyr.c <-> Pyr.m	7.30	22.51
v9	G6P -> P5P + CO2	0.00	15.47
v10	P5P + P5P <-> GAP + S7P	0.00	5.16
v11	S7P + GAP <-> E4P + F6P	0.00	5.16
v12	E4P + P5P <-> GAP + F6P	0.00	5.16
v13	Pyr.c <-> Lac	318.06	292.18
v14	Pyr.c <-> Ala	8.18	8.23
v15	Pyr.m -> AcCoA.m + CO2	7.00	10.21
v16	OAA.m + AcCoA.m -> Cit.m	9.49	16.33
v17	Cit.m <-> AKG + CO2	5.18	8.68
v18	AKG -> SucCoA + CO2	4.73	8.09
v19	SucCoA <-> Suc	4.73	8.09
v20	Suc <-> Fum.m	4.73	10.35
v21	Fum.m <-> Mal.m	4.76	10.35
v22	Mal.m <-> OAA.m	9.18	4.03
v23	Mal.c -> Pyr.c + CO2	0.10	6.32
v24	Pyr.m + CO2 -> OAA.m	0.30	12.30
v25	Gln <-> Glu	0.00	0.37
v26	AKG <-> Glu	0.45	0.59
v27	Asn <-> Asp	0.09	0.79
v28	3PG -> Ser	11.66	0.84
v29	Ser -> Pyr.c	11.84	2.45
v30	Ser <-> Gly + C1	-0.01	-0.15
v31	Glu <-> Pro	1.64	1.45
v32	Val + CO2 -> Suc + CO2 + CO2	0.00	0.62
v33	Ile + CO2 -> Suc + AcCoA.m + CO2	0.00	1.58
v34	Leu + CO2 -> AcCoA.m + AcCoA.m + AcCoA.m + CO2	0.80	0.24
v35	Thr -> AcCoA.m + Gly	0.00	2.72
v36	Phe -> Tyr	0.03	0.00
v37	Tyr -> Fum.m + AcCoA.m + AcCoA.m + CO2	0.03	0.00
v38	Met + Ser + CO2 -> Suc + Cys.snk + CO2 + C1	0.00	0.06
v39	Lys -> CO2 + CO2 + AcCoA.m + AcCoA.m	0.01	0.56
v40	His -> Glu + C1	0.01	0.09
v41	Arg -> Glu + Urea.snk	1.15	0.00
v42	Glu + CO2 -> Arg	0.03	0.00
v43	Glc.ext -> G6P	166.63	160.08
v44	Lac.ext <-> Lac	-318.06	-292.18
v45	Ala.ext <-> Ala	-8.18	-8.23
v46	Gln.ext -> Gln	0.00	0.37
v47	Glu.ext <-> Glu	0.06	0.40
v48	Ser.ext <-> Ser	0.17	1.52
v49	Gly.ext <-> Gly	0.01	-2.57
v50	Pro.ext <-> Pro	-1.64	-1.45
v51	Val.ext -> Val	0.00	0.62
v52	Ile.ext -> Ile	0.00	1.58
v53	Leu.ext -> Leu	0.80	0.24
v54	Thr.ext -> Thr	0.00	2.72
v55	Phe.ext -> Phe	0.03	0.00
v56	Tyr.ext -> Tyr	0.00	0.00
v57	Met.ext -> Met	0.00	0.06
v58	Lys.ext -> Lys	0.01	0.56
v59	His.ext -> His	0.01	0.09
v60	Arg.ext <-> Arg	1.11	0.00
v61	Asp <-> OAA.c	0.22	-7.66
v62	Cit.c -> OAA.c + AcCoA.c	4.31	7.66



v63	CO2.ext <-> CO2	-16.71	-38.19
v64	AcCoA.c -> FA.ext	4.31	7.66
v65	Cit.c -> Cit.snk	0.00	0.00
v66	Mal.m <-> Mal.c	-4.43	6.32
v67	0*Mal.c -> Mal.s	0.00	0.00
v68	0*Mal.m -> Mal.s	100.00	100.00
v69	Mal.s -> Sink	100.00	100.00
v70	0*Fum.c -> Fum.s	45.60	0.00
v71	0*Fum.m -> Fum.s	54.40	100.00
v72	Fum.s -> Sink	100.00	100.00
v73	Mal.c <-> Fum.c	0.00	0.00
v74	OAA.c <-> Mal.c	4.52	0.00
v75	Asp.ext <-> Asp	0.13	-8.44
v76	0*Cit.c -> Cit.s	0.00	100.00
v77	0*Cit.m -> Cit.s	100.00	0.00
v78	Cit.s -> Sink	100.00	100.00
v79	Cit.c <-> Cit.m	-4.31	-7.66
v80	Asn.ext -> Asn	0.09	0.79



**Figure A-3.4. Metabolic profiling of hiPSC-CMs in both 2D monolayers and 3D aggregates. A)** Heatmap image of specific rates of metabolite production (red) and consumption (blue) (qMET, expressed in nmol/(10<sup>6</sup>cell.h)) at day 15 in 2D monolayers and 3D aggregates of hiPSC-CMs, respectively designated by hiPSC-CM-2D (dark blue) and hiPSC-CM-3D (light blue). **B)** Specific rates of glucose consumption and lactate production. **C)** Ratio of specific rates of lactate production and glucose consumption (Y<sub>Lac</sub>/Glc). Data are represented as mean±SD. ns, not significant.

## 6. Acknowledgments

We thank Dr Ana Filipa Rodrigues for support in transcriptome analysis and Dr Erin Tranfield for performing TEM. This work was supported by FP7 European Union Project Cardio Repair

European Multidisciplinary Initiative (HEALTH-2009\_242038); Fundação para a Ciência e Tecnologia (FCT)-funded projects CardioRegen (HMSP-ICT/0039/2013) and CARDIOSTEM (MITPTB/ECE/0013/2013); CC was supported by FCT Grant SFRH/BD/51573/2011.

## 7. References

- Ahuja, P., Sdek, P., and Maclellan, W.R. (2007). Cardiac Myocyte Cell Cycle Control in Development, Disease, and Regeneration. *Physiol Rev* 87, 521–544.
- Akins, R.E., Rockwood, D., Robinson, K.G., Sandusky, D., Rabolt, J., and Pizarro, C. (2010). Three-dimensional culture alters primary cardiac cell phenotype. *Tissue Eng. Part A* 16, 629–641.
- Antoniewicz, M.R., Kelleher, J.K., and Stephanopoulos, G. (2006). Determination of confidence intervals of metabolic fluxes estimated from stable isotope measurements. *Metab. Eng.* 8, 324–337.
- Bauwens, C.L., Peerani, R., Niebruegge, S., Woodhouse, K. a, Kumacheva, E., Husain, M., and Zandstra, P.W. (2008). Control of human embryonic stem cell colony and aggregate size heterogeneity influences differentiation trajectories. *Stem Cells* 26, 2300–2310.
- Bauwens, C.L., Song, H., Thavandiran, N., Ungrin, M., Massé, S., Nanthakumar, K., Seguin, C., Zandstra, P.W., Ph, D., Song, H., et al. (2011). Geometric control of cardiomyogenic induction in human pluripotent stem cells. *Tissue Eng.* 17, 1901–1909.
- Bose, B., and Shenoy P, S. (2016). In Vitro Differentiation of Pluripotent Stem Cells into Functional B Islets Under 2D and 3D Culture Conditions and In Vivo Preclinical Validation of 3D Islets. *Methods Mol. Biol.* 257–284.
- Boyle, J. (2005). *Lehninger principles of biochemistry* (4th ed.): Nelson, D., and Cox, M.
- Burridge, P.W., Keller, G.M., Gold, J.D., and Wu, J.C. (2013). Production of de novo cardiomyocytes: human pluripotent stem cells differentiation and direct reprogramming. *Natl. Institutes Heal.* 10, 16–28.
- Burridge, P.W., Matsa, E., Shukla, P., Lin, Z.C., Churko, J.M., Ebert, A.D., Lan, F., Diecke, S., Huber, B., Mordwinkin, N.M., et al. (2014). Chemically defined generation of human cardiomyocytes. *Nat. Methods* 11, 855–860.
- Cao, N., Liu, Z., Chen, Z., Wang, J., Chen, T., Zhao, X., Ma, Y., Qin, L., Kang, J., Wei, B., et al. (2012). Ascorbic acid enhances the cardiac differentiation of induced pluripotent stem cells through promoting the proliferation of cardiac progenitor cells. *Cell Res.* 22, 219–236.
- Carinhas, N., Bernal, V., Monteiro, F., Carrondo, M.J.T., Oliveira, R., and Alves, P.M. (2010). Improving baculovirus production at high cell density through manipulation of energy metabolism. *Metab. Eng.* 12, 39–52.
- Carinhas, N., Pais, D.A.M., Koshkin, A., Fernandes, P., Coroadinha, A.S., Carrondo, M.J.T., Alves, P.M., and Teixeira, A.P. (2016). Metabolic flux profiling of MDCK cells during growth and canine adenovirus vector production. *Sci. Rep.* 6, 1–11.
- Ceriello, A., Barakat, M., Bahendeka, S., Colagiuri, S., Gerich, J., Hanefeld, M., Ji, L., Lalic, N., Leiter, L.A., Monnier, L., et al. (2008). Guideline for management of postmeal glucose in diabetes. *Diabetes Res. Clin. Pract.* 18, S17–S33.
- Chen, V.C., Couture, S.M., Ye, J., Lin, Z., Hua, G., Huang, H.I.P., Wu, J., Hsu, D., Carpenter, M.K., and Couture, L.A. (2012). Scalable GMP compliant suspension culture system for human ES cells. *Stem Cell Res.* 8, 388–402.
- Chen, V.C., Ye, J., Shukla, P., Hua, G., Chen, D., Lin, Z., Liu, J. chang, Chai, J., Gold, J., Wu, J., et al. (2015). Development of a scalable suspension culture for cardiac differentiation from human pluripotent stem cells. *Stem Cell Res.* 15, 365–375.
- Correia, C., Koshkin, A., Carido, M., Espinha, N., Šarić, T., Lima, P.A., Serra, M., and Alves, P.M. (2016). Effective Hypothermic Storage of Human Pluripotent Stem Cell-Derived Cardiomyocytes Compatible With Global Distribution of Cells for Clinical Applications and Toxicology Testing. *Stem*

Cells Transl. Med. 5, 658–669.

Crown, S.B., and Antoniewicz, M.R. (2013). Publishing <sup>13</sup>C metabolic flux analysis studies: A review and future perspectives. *Metab. Eng.* 20, 42–48.

D'Uva, G., Aharonov, A., Lauriola, M., Kain, D., Yahalom-Ronen, Y., Carvalho, S., Weisinger, K., Bassat, E., Rajchman, D., Yifa, O., et al. (2015). ERBB2 triggers mammalian heart regeneration by promoting cardiomyocyte dedifferentiation and proliferation. *Nat. Cell Biol.* 17, 627–638.

Dahlmann, J., Kensah, G., Kempf, H., Skvorc, D., Gawol, A., Elliott, D.A., Dräger, G., Zweigerdt, R., Martin, U., and Gruh, I. (2013). The use of agarose microwells for scalable embryoid body formation and cardiac differentiation of human and murine pluripotent stem cells. *Biomaterials* 34, 2463–2471.

van Dartel, D.A.M., Schulpen, S.H., Theunissen, P.T., Bunschoten, A., Piersma, A.H., and Keijer, J. (2014). Dynamic changes in energy metabolism upon embryonic stem cell differentiation support developmental toxicant identification. *Toxicology* 324, 76–87.

Dietmair, S., Timmins, N.E., Gray, P.P., Nielsen, L.K., and Krömer, J.O. (2010). Towards quantitative metabolomics of mammalian cells: Development of a metabolite extraction protocol. *Anal. Biochem.* 404, 155–164.

Dobaczewski, M., Chen, W., and Frangogiannis, N.G. (2011). Transforming growth factor (TGF)-B signaling in cardiac remodeling. *J. Mol. Cell. Cardiol.* 51, 600–606.

Edmondson, R., Broglie, J.J., Adcock, A.F., and Yang, L. (2014). Three-dimensional cell culture systems and their applications in drug discovery and cell-based biosensors. *Assay Drug Dev. Technol.* 12, 207–218.

Egashira, T., Yuasa, S., and Fukuda, K. (2011). Induced pluripotent stem cells in cardiovascular medicine. *Stem Cells Int.* 2011, 348960.

Elliott, D.A., Braam, S.R., Koutsis, K., Ng, E.S., Jenny, R., Lagerqvist, E.L., Biben, C., Hatzistavrou, T., Hirst, C.E., Yu, Q.C., et al. (2011). NKX2-5eGFP/w hESCs for isolation of human cardiac progenitors and cardiomyocytes. *Nat. Methods* 8, 1037–1040.

Engebretsen, K.V.T., Lunde, I.G., Strand, M.E., Waehre, A., Sjaastad, I., Marstein, H.S., Skrbic, B., Dahl, C.P., Askevold, E.T., Christensen, G., et al. (2013). Lumican is increased in experimental and clinical heart failure, and its production by cardiac fibroblasts is induced by mechanical and proinflammatory stimuli. *FEBS J.* 280, 2382–2398.

Fan, D., Takawale, A., Lee, J., and Kassiri, Z. (2012). Cardiac fibroblasts, fibrosis and extracellular matrix remodeling in heart disease. *Fibrogenesis Tissue Repair* 5, 15.

Feric, N.T., and Radisic, M. (2016). Maturing human pluripotent stem cell-derived cardiomyocytes in human engineered cardiac tissues. *Adv. Drug Deliv. Rev.* 96, 110–134.

Fridley, K.M., Nair, R., and McDevitt, T.C. (2014). Differential expression of extracellular matrix and growth factors by embryoid bodies in hydrodynamic and static cultures. *Tissue Eng. Part C. Methods* 20, 931–940.

Gherghiceanu, M., Barad, L., Novak, A., Reiter, I., Itskovitz-Eldor, J., Binah, O., and Popescu, L.M. (2011). Cardiomyocytes derived from human embryonic and induced pluripotent stem cells: Comparative ultrastructure. *J. Cell. Mol. Med.* 15, 2539–2551.

Guimarães-Camboa, N., Stowe, J., Aneas, I., Sakabe, N., Cattaneo, P., Henderson, L., Kilberg, M.S., Johnson, R.S., Chen, J., McCulloch, A.D., et al. (2015). HIF1a Represses Cell Stress Pathways to Allow Proliferation of Hypoxic Fetal Cardiomyocytes. *Dev. Cell* 33, 507–521.

Günter, J., Wolint, P., Bopp, A., Steiger, J., Cambria, E., Hoerstrup, S.P., and Emmert, M.Y. (2016). Microtissues in Cardiovascular Medicine: Regenerative Potential Based on a 3D Microenvironment. *Stem Cells Int.* 2016.

Guo, Y., Wei, Y., Zhang, X., Yan, Y., Guo, C., Li, R., Ning, B., and Zeng, Q. (2009). Effects of Mechanical Stretch on Growth and Metabolism of Cardiomyocytes In Vitro. 1–5.

Hang, C.T., Yang, J., Han, P., Cheng, H., Shang, C., Ashley, E., Zhou, B., and Chang, C.-P. (2010). Chromatin regulation by Brg1 underlies heart muscle development and disease. *Nature* 466, 62–67.

- Hartman, M.E., Dai, D.F., and Laflamme, M.A. (2016). Human pluripotent stem cells: Prospects and challenges as a source of cardiomyocytes for in vitro modeling and cell-based cardiac repair. *Adv. Drug Deliv. Rev.* 96, 3–17.
- Harvey, A.J., Rathjen, J., and Gardner, D.K. (2016). Metaboloepigenetic regulation of pluripotent stem cells. *Stem Cells Int.* 2016.
- Hattori, F., Chen, H., Yamashita, H., Tohyama, S., Satoh, Y., Yuasa, S., Li, W., Yamakawa, H., Tanaka, T., Onitsuka, T., et al. (2010). Nongenetic method for purifying stem cell-derived cardiomyocytes. *Nat. Methods* 7, 61–66.
- He, J.-Q. (2003). Human Embryonic Stem Cells Develop Into Multiple Types of Cardiac Myocytes: Action Potential Characterization. *Circ. Res.* 93, 32–39.
- Hookway, T.A., Butts, J.C., Lee, E., Tang, H., and McDevitt, T.C. (2015). Aggregate formation and suspension culture of human pluripotent stem cells and differentiated progeny. *Methods* 101, 11–20.
- Huber, I., Itzhaki, I., Caspi, O., Arbel, G., Tzukerman, M., Gepstein, A., Habib, M., Yankelson, L., Kehat, I., and Gepstein, L. (2007). Identification and selection of cardiomyocytes during human embryonic stem cell differentiation. *FASEB J.* 21, 2551–2563.
- Ivey, M.J., and Tallquist, M.D. (2016). Defining the Cardiac Fibroblast. *Circ. J.* 80.
- Jahanyar, J., Joyce, D.L., Southard, R.E., Loebe, M., Noon, G.P., Koerner, M.M., Torre-Amione, G., and Youker, K.A. (2007). Decorin-mediated Transforming Growth Factor-B Inhibition Ameliorates Adverse Cardiac Remodeling. *J. Hear. Lung Transplant.* 26, 34–40.
- Jha, R., Wu, Q., Singh, M., Preininger, M.K., Han, P., Ding, G., Cho, H.C., Jo, H., Maher, K.O., Wagner, M.B., et al. (2016). Simulated Microgravity and 3D Culture Enhance Induction, Viability, Proliferation and Differentiation of Cardiac Progenitors from Human Pluripotent Stem Cells. *Sci. Rep.* 6, 30956.
- Kadari, A., Mekala, S., Wagner, N., Malan, D., Köth, J., Doll, K., Stappert, L., Eckert, D., Peitz, M., Matthes, J., et al. (2015). Robust generation of cardiomyocytes from human iPS cells requires precise modulation of BMP and WNT signaling. *Stem Cell Rev. Reports* 11, 560–569.
- Karakikes, I., Senyei, G.D., Hansen, J., Kong, C.-W., Azeloglu, E.U., Stillitano, F., Lieu, D.K., Wang, J., Ren, L., Hulot, J.-S., et al. (2014). Small molecule-mediated directed differentiation of human embryonic stem cells toward ventricular cardiomyocytes. *Stem Cells Transl. Med.* 3, 18–31.
- Kattman, S.J., Witty, A.D., Gagliardi, M., Dubois, N.C., Niapour, M., Hotta, A., Ellis, J., and Keller, G. (2011). Stage-specific optimization of activin/nodal and BMP signaling promotes cardiac differentiation of mouse and human pluripotent stem cell lines. *Cell Stem Cell* 8, 228–240.
- Kehat, I., and Molkenkin, J.D. (2010). Extracellular signal-regulated kinase 1/2 (ERK1/2) signaling in cardiac hypertrophy. *Ann N Y Acad Sci* 1188, 96–102.
- Kehat, I., Kenyagin-Karsenti, D., Snir, M., Segev, H., Amit, M., Gepstein, A., Livne, E., Binah, O., Itskovitz-Eldor, J., and Gepstein, L. (2001). Human embryonic stem cells can differentiate into myocytes with structural and functional properties of cardiomyocytes. *J Clin Invest* 108, 407–414.
- Kempf, H., Olmer, R., Kropp, C., Rückert, M., Jara-Avaca, M., Robles-Diaz, D., Franke, A., Elliott, D.A., Wojciechowski, D., Fischer, M., et al. (2014). Controlling expansion and cardiomyogenic differentiation of human pluripotent stem cells in scalable suspension culture. *Stem Cell Reports* 3, 1132–1146.
- Kempf, H., Kropp, C., Olmer, R., Martin, U., and Zweigerdt, R. (2015). Cardiac differentiation of human pluripotent stem cells in scalable suspension culture. *Nat. Protoc.* 10, 1345–1361.
- Kempf, H., Andree, B., and Zweigerdt, R. (2016). Large-scale production of human pluripotent stem cell derived cardiomyocytes. *Adv. Drug Deliv. Rev.* 96, 18–30.
- Kijlstra, J.D., Hu, D., Mittal, N., Kausel, E., Van Der Meer, P., Garakani, A., and Domian, I.J. (2015). Integrated Analysis of Contractile Kinetics, Force Generation, and Electrical Activity in Single Human Stem Cell-Derived Cardiomyocytes. *Stem Cell Reports* 5, 1226–1238.
- Kilberg, M.S., Terada, N., and Shan, J. (2016). Influence of Amino Acid Metabolism on Embryonic Stem Cell Function and Differentiation. *Adv. Nutr.* 7, 780S–9S.

- Krenning, G., Zeisberg, E.M., and Kalluri, R. (2010). The origin of fibroblasts and mechanism of cardiac fibrosis. *J. Cell. Physiol.* 225, 631–637.
- Laflamme, M.A., Chen, K.Y., Naumova, A. V, Muskheli, V., Fugate, J.A., Dupras, S.K., Reinecke, H., Xu, C., Hassanipour, M., Police, S., et al. (2007). Cardiomyocytes derived from human embryonic stem cells in pro-survival factors enhance function of infarcted rat hearts. *Nat. Biotechnol.* 25, 1015–1024.
- Lanier, M., Schade, D., Willems, E., Tsuda, M., Spiering, S., Kalisiak, J., Mercola, M., and Cashman, J.R. (2012). Wnt inhibition correlates with human embryonic stem cell cardiomyogenesis: A structure-activity relationship study based on inhibitors for the Wnt response. *J. Med. Chem.* 55, 697–708.
- Lian, X., Hsiao, C., Wilson, G., Zhu, K., Hazeltine, L.B., Azarin, S.M., Raval, K.K., Zhang, J., Kamp, T.J., and Palecek, S.P. (2012). Robust cardiomyocyte differentiation from human pluripotent stem cells via temporal modulation of canonical Wnt signaling. *PNAS* 1–10.
- Lian, X., Zhang, J., Azarin, S.M., Zhu, K., Hazeltine, L.B., Bao, X., Hsiao, C., Kamp, T.J., and Palecek, S.P. (2013). Directed cardiomyocyte differentiation from human pluripotent stem cells by modulating Wnt/ $\beta$ -catenin signaling under fully defined conditions. *Nat. Protoc.* 8, 162–175.
- Liu, Y., Yang, M., Zhang, J., Zhi, X., Li, C., Zhang, C., Pan, F., Wang, K., Yang, Y., Martinez, J., et al. (2016). Human Induced Pluripotent Stem Cells for. 2016.
- Lopaschuk, G.D., and Jaswal, J.S. (2010). Energy metabolic phenotype of the cardiomyocyte during development, differentiation, and postnatal maturation. *J. Cardiovasc. Pharmacol.* 56, 130–140.
- Louch, W.E., Koivumäki, J.T., and Tavi, P. (2015). Calcium signalling in developing cardiomyocytes: implications for model systems and disease. *J Physiol* 5935, 1047–1063.
- Miki, K., Endo, K., Takahashi, S., Funakoshi, S., Takei, I., Katayama, S., Toyoda, T., Kotaka, M., Takaki, T., Umeda, M., et al. (2015). Efficient Detection and Purification of Cell Populations Using Synthetic MicroRNA Switches. *Cell Stem Cell* 16, 699–711.
- Nahrendorf, M., Spindler, M., Hu, K., Bauer, L., Ritter, O., Nordbeck, P., Quaschnig, T., Hiller, K.H., Wallis, J., Ertl, G., et al. (2005). Creatine kinase knockout mice show left ventricular hypertrophy and dilatation, but unaltered remodeling post-myocardial infarction. *Cardiovasc. Res.* 65, 419–427.
- Nelson, D.O., Jin, D.X., Downs, K.M., Kamp, T.J., and Lyons, G.E. (2014). *Irx4* identifies a chamber-specific cell population that contributes to ventricular myocardium development. *Dev. Dyn.* 243, 381–392.
- Nelson, D.O., Lalit, P.A., Biermann, M., Markandeya, Y.S., Capes, D.L., Adesso, L., Patel, G., Han, T., John, M.C., Powers, P.A., et al. (2016). *Irx4* Marks a Multipotent, Ventricular-Specific Progenitor Cell. *Stem Cells* 1–17.
- Nguyen, D.C., Hookway, T.A., Wu, Q., Jha, R., Preininger, M.K., Chen, X., Easley, C.A., Spearman, P., Deshpande, S.R., Maher, K., et al. (2014). Microscale generation of cardiospheres promotes robust enrichment of cardiomyocytes derived from human pluripotent stem cells. *Stem Cell Reports* 3, 260–268.
- Niebruegge, S., Nehring, A., Ba, H., Schroeder, M., Zweigerdt, R., and Lehmann, J. (2008). Cardiomyocyte Production in Mass Suspension Culture: Embryonic Stem Cells as a Source for Great Amounts of Functional Cardiomyocytes. *Tissue Eng. Part A* 14, 1591–1601.
- O'Brien, T.X., Lee, K.J., and Chien, K.R. (1993). Positional specification of ventricular myosin light chain 2 expression in the primitive murine heart tube. *Proc. Natl. Acad. Sci. U. S. A.* 90, 5157–5161.
- Paige, S.L., Osugi, T., Afanasiev, O.K., Pabon, L., Reinecke, H., and Murry, C.E. (2010). Endogenous Wnt/ $\beta$ -catenin signaling is required for cardiac differentiation in human embryonic stem cells. *PLoS One* 5, e11134.
- Phang, J.M., Liu, W., Hancock, C.N., and Fischer, J.W. (2015). Proline metabolism and cancer: emerging links to glutamine and collagen. *Curr. Opin. Clin. Nutr. Metab. Care* 18, 71–77.
- Prigione, A., Rohwer, N., Hoffmann, S., Mlody, B., Drews, K., Bukowiecki, R., Blümlein, K.,

- Wanker, E.E., Ralser, M., Cramer, T., et al. (2014). HIF1a modulates cell fate reprogramming through early glycolytic shift and upregulation of PDK1-3 and PKM2. *Stem Cells* 32, 364–376.
- Schindelin, J., Arganda-Carreras, I., Frise, E., Kaynig, V., Longair, M., Pietzsch, T., Preibisch, S., Rueden, C., Saalfeld, S., Schmid, B., et al. (2012). Fiji: an open-source platform for biological-image analysis. *Nat. Methods* 9, 676–682.
- Schlattner, U., Tokarska-Schlattner, M., and Wallimann, T. (2006). Mitochondrial creatine kinase in human health and disease. *Biochim. Biophys. Acta - Mol. Basis Dis.* 1762, 164–180.
- Shiraki, N., Shiraki, Y., Tsuyama, T., Obata, F., Miura, M., Nagae, G., Aburatani, H., Kume, K., Endo, F., and Kume, S. (2014). Methionine metabolism regulates maintenance and differentiation of human pluripotent stem cells. *Cell Metab.* 19, 780–794.
- Skelton, R.J.P., Costa, M., Anderson, D.J., Bruveris, F., Finnin, B.W., Koutsis, K., Arasaratnam, D., White, A.J., Rafii, A., Ng, E.S., et al. (2014). SIRPA, VCAM1 and CD34 identify discrete lineages during early human cardiovascular development. *Stem Cell Res.* 13, 172–179.
- Soares, C.P., Midlej, V., de Oliveira, M.E.W., Benchimol, M., Costa, M.L., and Mermelstein, C. (2012). 2D and 3D-organized cardiac cells shows differences in cellular morphology, adhesion junctions, presence of myofibrils and protein expression. *PLoS One* 7, e38147.
- Souders, C.A., Bowers, S.L.K., and Baudino, T.A. (2009). Cardiac fibroblast: The renaissance cell. *Circ. Res.* 105, 1164–1176.
- Spindler, M., Engelhardt, S., Niebler, R., Wagner, H., Hein, L., Lohse, M.J., and Neubauer, S. (2003). Alterations in the myocardial creatine kinase system precede the development of contractile dysfunction in  $\beta$ 1-adrenergic receptor transgenic mice. *J. Mol. Cell. Cardiol.* 35, 389–397.
- Takeda, N., and Manabe, I. (2011). Cellular Interplay between Cardiomyocytes and Nonmyocytes in Cardiac Remodeling. *Int. J. Inflam.* 2011, 535241.
- Tohyama, S., Hattori, F., Sano, M., Hishiki, T., Nagahata, Y., Matsuura, T., Hashimoto, H., Suzuki, T., Yamashita, H., Satoh, Y., et al. (2013). Distinct metabolic flow enables large-scale purification of mouse and human pluripotent stem cell-derived cardiomyocytes. *Cell Stem Cell* 12, 127–137.
- Ueno, S., Weidinger, G., Osugi, T., Kohn, A.D., Golob, J.L., Pabon, L., Reinecke, H., Moon, R.T., and Murry, C.E. (2007). Biphasic role for Wnt/beta-catenin signaling in cardiac specification in zebrafish and embryonic stem cells. *Proc. Natl. Acad. Sci. U. S. A.* 104, 9685–9690.
- Ungrin, M.D., Joshi, C., Nica, A., Bauwens, C., and Zandstra, P.W. (2008). Reproducible, ultra high-throughput formation of multicellular organization from single cell suspension-derived human embryonic stem cell aggregates. *PLoS One* 3, e1565.
- Ventura-Clapier, R., Garnier, A., and Veksler, V. (2008). Transcriptional control of mitochondrial biogenesis: The central role of PGC-1 $\alpha$ . *Cardiovasc. Res.* 79, 208–217.
- Wanet, A., Arnould, T., Najimi, M., and Renard, P. (2015). Connecting Mitochondria, Metabolism, and Stem Cell Fate. *Stem Cells Dev.* 24, 1957–1971.
- Wile, B.M., Ban, K., Yoon, Y.-S., and Bao, G. (2014). Molecular beacon-enabled purification of living cells by targeting cell type-specific mRNAs. *Nat. Protoc.* 9, 2411–2424.
- Woo Suk, A., and Antoniewicz, M.R. (2013). Parallel labeling experiments with [1,2-<sup>13</sup>C]glucose and [U-<sup>13</sup>C]glutamine provide new insights into CHO cell metabolism. *Metab. Eng.* 15, 34–47.
- Xu, C., Police, S., Rao, N., and Carpenter, M. (2002). Characterization and Enrichment of Cardiomyocytes Derived From Human Embryonic Stem Cells. *Circ. Res.* 91, 501–508.
- Yang, L., Soonpaa, M.H., Adler, E.D., Roepke, T.K., Kattman, S.J., Kennedy, M., Henckaerts, E., Bonham, K., Abbott, G.W., Linden, R.M., et al. (2008). Human cardiovascular progenitor cells develop from a KDR<sup>+</sup> embryonic-stem-cell-derived population. *Nature* 453, 524–528.
- Young, J.D. (2014). INCA: A computational platform for isotopically non-stationary metabolic flux analysis. *Bioinformatics* 30, 1333–1335.
- Youssef, A.A., Ross, E.G., Bolli, R., Pepine, C.J., Leeper, N.J., and Yang, P.C. (2016). The Promise and Challenge of Induced Pluripotent Stem Cells for Cardiovascular Applications. *JACC Basic to Transl. Sci.* 1, 510–523.

Zhang, H.Y., Timpl, R., Sasaki, T., Chu, M.L., and Ekblom, P. (1996). Fibulin-1 and fibulin-2 expression during organogenesis in the developing mouse embryo. *Dev. Dyn.* 205, 348–364.

Zhang, J., Wilson, G.F., Soerens, A.G., Koonce, C.H., Yu, J., Palecek, S.P., Thomson, J.A., and Kamp, T.J. (2009). Functional cardiomyocytes derived from human induced pluripotent stem cells. *Circ. Res.* 104, e30-41.

Zhang, M., Schulte, J.S., Heinick, A., Piccini, I., Rao, J., Quaranta, R., Zeuschner, D., Malan, D., Kim, K.-P., Röpke, A., et al. (2015). Universal Cardiac Induction of Human Pluripotent Stem Cells in 2D and 3D formats - Implications for In-Vitro Maturation. *Stem Cells* 33, 1456–1469.





# 4

## **Metabolic substrate availability controls the maturation of human induced pluripotent stem cells derived cardiomyocytes**

This chapter was adapted from:

Correia C., Koshkin A., Duarte P., Hu D., Teixeira A.P., Domian I.J, Serra M. and Alves, P.M. (2016). Metabolic substrate availability controls the maturation of human induced pluripotent stem cells derived cardiomyocytes. *Submitted*

**Contents**

<b>1. Introduction</b> .....	<b>110</b>
<b>2. Methods</b> .....	<b>111</b>
2.1. hiPSC maintenance and differentiation to CM.....	111
2.2. hiPSC-CM culture .....	111
2.3. Metabolic and fluxomic analysis .....	111
2.4. Transcriptomic analysis .....	112
2.5. Characterization of hiPSC-CM.....	113
2.6. Assessment of hiPSC-CM functionality .....	114
2.7. Statistical analysis .....	115
<b>3. Results</b> .....	<b>115</b>
3.1. hiPSC-CM shift their metabolism from glycolysis to OXPHOS in the absence of glucose.....	115
3.2. Culture of hiPSC-CM in fatty acid medium lacking sugar source induces lipotoxicity	117
3.3. Galactose prevents lipotoxicity in hiPSC-CM cultured in fatty acid medium and improves cellular oxidative capacity .....	118
3.4. Adaptation to LACM induces higher cell death than GFAM .....	121
3.5. hiPSC-CM cultured in GFAM or LACM&GFAM present transcriptional signatures closer to human ventricular CM .....	121
3.6. GFAM and LACM&GFAM enhance the expression of cardiac markers .....	123
3.7. GFAM improves the structure and ultrastructure of hiPSC-CM .....	124
3.8. GFAM improves calcium transients, contractility and action potential kinetics of hiPSC-CM .....	126
<b>4. Discussion</b> .....	<b>128</b>
<b>5. Appendix</b> .....	<b>132</b>
<b>6. Acknowledgments</b> .....	<b>142</b>
<b>7. References</b> .....	<b>142</b>

**Abstract**

The immature phenotype of human pluripotent stem cell derived cardiomyocytes (hPSC-CMs) constrains their potential in cell therapy and drug testing. In this study, we assessed if mimicking substrate usage during *in vivo* cardiac development induces *in vitro* hPSC-CM maturation. We report that shifting hPSC-CMs from glucose-containing to galactose- and fatty acid- containing medium promotes their fast maturation into adult-like CMs with higher oxidative metabolism, transcriptional signatures closer to those of adult ventricular tissue, and higher myofibril density and alignment. Comprehensive physiological characterization further demonstrated improved calcium handling, enhanced contractility, and more physiological action potential kinetics within 20 days in galactose- and fatty acid-containing medium. Integrated “-omics” analyses showed that addition of galactose to culture medium improves total oxidative capacity of the cells, ameliorates fatty acid oxidation avoiding the lipotoxicity that results from cell exposure to high fatty acid levels. This study provides an important link between substrate utilization and functional maturation of hPSC-CMs and facilitates the application of this promising cell type to clinical and preclinical applications.

## 1. Introduction

In the last decade remarkable progress has been made towards the establishment of protocols to direct the differentiation of human pluripotent stem cells (hPSC, including hiPSC and hESC) into cardiomyocytes (hPSC-CMs) (Denning et al., 2015). However, hPSC-CMs are often immature, showing metabolic, structural and functional characteristics that more closely resemble fetal CMs rather than adult CMs (Feric and Radisic, 2016). hPSC-CMs commonly display disarrayed sarcomeres, irregular shapes, underdeveloped mitochondria and use glucose (Glc) as major energy source, contrasting with adult CMs which present organized sarcomere structures, rod-shaped morphologies, well-developed mitochondria with mature lamellar cristae and rely on fatty acid (FA)  $\beta$ -oxidation for energy production (Feric and Radisic, 2016; Yang et al., 2014a).

Although some efforts have been made recently towards the development of methods for enhancing hPSC-CM maturity (by increasing time in culture (Lundy et al., 2013), applying mechanical and electrical stimulation (Chan et al., 2013; Mihic et al., 2014; Ruan et al., 2016), adding chemicals or small molecules (Yang et al., 2014b), adjusting substrate stiffness (Hazeltine et al., 2012) or using genetic approaches (Lieu et al., 2013; Liu et al., 2009)) the outcomes have been variable. The use of distinct sets of analyses for CM maturation profile characterization has also limited the direct comparison between different studies.

CM maturation *in vivo* has been associated with a transition from an embryonic-like glycolytic to an adult-like oxidative metabolism (Lopaschuk and Jaswal, 2010). In a normal heart, 70% of ATP generation comes from FA oxidation, whereas Glc, Lactate (Lac) and pyruvate (Pyr) provide only 30% of the energy produced (Lionetti et al., 2011). It has been shown that hPSC-CMs that are metabolically dependent on FA  $\beta$ -oxidation, *in vitro*, recapitulate cellular activities of more mature CMs, constituting a reliable model to study late onset disorders (Drawnel et al., 2014). Wen and colleagues were able to unveil the pathological phenotype associated with arrhythmogenic right ventricular dysplasia after inducing metabolic maturation in hiPSC-CMs (Wen et al., 2015). The authors used a combination of insulin, dexamethasone and 3-isobutyl-1-methyl-xanthine to increase FA synthesis and trigger the activation of PPAR $\alpha$ , which led to enhanced mitochondrial oxidative phosphorylation. Although the use of medium additives was proved to induce hiPSC-CM bioenergetics switching, the impact of key medium substrates on modulating hPSC-CM metabolism and maturation profile still need to be investigated.

In this study, we hypothesised that manipulating the composition of the hiPSC-CM culture medium to mimic the metabolic substrate usage by human adult CMs *in vivo* would promote hiPSC-CM maturation *in vitro*. We selected multiple conditions based on the fact that during cardiac development CMs start to use first Lac and then FA as major sources of energy (Lopaschuk and Jaswal, 2010). Specifically, we tested to culture hiPSC-CMs for 20 days in Glc depleted medium supplemented either with: i) FA (FAM), ii) Galactose (Gal) and FA (GFAM) or iii) Lac during the first 10 days and then with Gal and FA for the remaining period (LACM&GFAM), using standard Glc-rich hiPSC-CM maintenance medium (GLCM) as reference (Figure 4.1A). GFAM revealed to be the best feeding strategy to culture hiPSC-CMs, significantly improving

several structural and functional maturation markers. By integrating transcriptome, metabolome and fluxome profiling, we provide a comprehensive molecular basis and a quantitative dissection of hiPSC-CM phenotypes observed during culture in different media.

## 2. Methods

### 2.1. hiPSC maintenance and differentiation to CMs

In this study the hiPSC line DF19-9-11T.H from WiCell was used. hiPSCs were cultured on Matrigel® (Corning) or on fully defined Synthemax II-SC (Corning) coated plates in mTESR1 medium (STEMCELL Technologies) until reaching 80%-90% confluency. Differentiation to CM was performed as described previously (Correia et al., 2016). Briefly, we used a directed differentiation protocol that involves the use of RPMI+B27 medium and serial application of Activin A, CHIR99021, Ascorbic Acid and IWR1 in 2D monolayer culture conditions. After 15 days of differentiation, cell preparations containing >80% cardiac troponin T-positive CM (confirmed by flow cytometry) were obtained.

### 2.2. hiPSC-CM culture

After differentiation, hiPSC-CMs were cultured for 20 days in four different culture media as indicated in Figure 4.1A: GLCM: standard hiPSC-CM medium (RPMI+B27); FAM: RPMI without Glc supplemented with B27, 1mM glutamine (Gln), 100µM oleic acid (OA), 50µM palmitic acid (PA); GFAM: RPMI without Glc supplemented with B27, 1mM Gln, 10mM galactose (Gal), 100µM OA and 50µM PA; and LACM&GFAM: 10 days in RPMI without Glc supplemented with B27, 1mM Gln and 4mM sodium L-Lactate (Sigma-Aldrich) and 10 days in GFAM. At days 10 (d10) and 20 (d20), hiPSC-CMs were harvested for metabolic, transcriptomic, structural and functional analysis.

### 2.3. Metabolic and fluxomic analysis

#### 2.3.1. Metabolite analysis

Glutamine (Gln), glutamate (Glu), glucose (Glc) and lactate (Lac) concentrations from cell culture supernatants were measured using YSI 7100MBS (YSI Incorporated, USA). Ammonia was quantified with an enzymatic assay kit (NZYTech, Portugal). Amino acid concentration was determined by HPLC using the Waters AcQ.Tag Amino Acid Analysis Method (Waters, Milford, MA), as described elsewhere (Carinhas et al., 2010). The specific metabolic rates ( $q_{Met}$ , expressed in  $\text{nmol}/(10^6\text{cell}\cdot\text{h})$ ) were calculated using the equation:  $q_{Met} = \Delta\text{Met}/(\Delta t \times X_v)$ , where  $\Delta\text{Met}$  (mol/L) is the variation of metabolite concentration during the time period  $\Delta t$  (h), and  $X_v$  (cell/L) the average of cell concentration during the same time period.

#### 2.3.2. Measurement of Oxygen Consumption Rate and Extracellular Acidification Rate

OXPPOS and glycolysis in hiPSC-CMs were estimated by measuring oxygen consumption rate (OCR) and extracellular acidification rate (ECAR) in real-time using an XF-96 Extracellular Flux Analyzer (Seahorse Biosciences) according to the manufacturer's protocols.

### 2.3.3. Isotopic tracer experiments and GC-MS analysis

For the parallel isotopic labelling experiments the following isotopic tracers were used: [1,2-<sup>13</sup>C]Glucose; [U-<sup>13</sup>C]Glutamine; [3-<sup>13</sup>C]Lactate; [U-<sup>13</sup>C]Galactose (all from Cambridge Isotope Laboratories) and [18-<sup>13</sup>C]Oleic Acid; [16-<sup>13</sup>C]Palmitic Acid (from Sigma-Aldrich). Only one isotopic tracer was used at a time to allow monitoring of the incorporation of each tracer. Label incorporation was characterized 24 and 48h after label addition. Metabolic quenching, metabolite extraction and derivatization protocols were performed as described in the literature (Carinhas et al., 2016, 2017).

Metabolites were analyzed in a QP2010 mass spectrometer (Shimadzu, Japan) in the EI mode (70eV) with a HP-5 MS column (Agilent Technologies). The obtained spectra were analyzed and integrated using GC-MS Solution software version 2.50 SU1 (Shimadzu, Japan). Mass Isotopomer Distributions (MID) were calculated after spectra integration and corrected for natural isotope abundance. The percentage of incorporation of each substrate in the TCA cycle was determined as the percentage of incorporation of each labelled substrate in TCA metabolites (citrate, fumarate and malate) normalized by the total incorporation provided by the main substrates present in the media in the same metabolites.

### 2.3.4. Metabolic network and nonstationary <sup>13</sup>C-MFA

Nonstationary <sup>13</sup>C-MFA of parallel labelling experiments was performed using the software package INCA (Young, 2014), which automatically generates and simulates material balance equations from a user-defined metabolic network structure and experimental datasets. At least 10 restarts with random initial values for the parameters (intracellular fluxes and pools) were performed to find a global optimum. At convergence, the goodness-of-fit of the obtained solution was evaluated with a qui-square statistical test. The parameter continuation method was used to calculate 95% confidence intervals of the estimated fluxes (Antoniewicz et al., 2006).

### 2.3.5. ATP production

ATP production was estimated using the reference value of ATP generated in glycolysis, TCA and  $\beta$ -oxidation (Nelson and Cox, 2013), multiplied by respective flux values determined in nonstationary <sup>13</sup>C-MFA.

## 2.4. Transcriptomic analysis

### 2.4.1. RNA Extraction, Amplification, Labeling, and BeadChip Hybridization of RNA Samples

Total RNA from hiPSC-CMs was extracted using the RNeasy Mini Kit (Qiagen). RNA quality was characterized by the quotient of the 28S to 18S ribosomal RNA electropherogram peak using an Agilent 2100 bioanalyzer and the RNA Nano Chip (Agilent). Transcriptional profiling was assessed using Illumina HumanHT-12 v4 Expression BeadChip microarray technology (Illumina) and data were processed and normalized as described in (Silva et al., 2015). Genes differentially expressed/enriched were identified using Student's t test (p value <0.01) and fold change  $FC \geq |1.3|$ . 2D-Principal component analysis (2D-PCA), Pearson correlation matrixes and density plots were generated using R version 3.3.2. Kolmogorov-Smirnov test was used to calculate pvalues. Pathway analysis was performed using Ingenuity Pathway Analysis (Ingenuity Systems; Qiagen). For GO

term analysis, GO term database (<http://geneontology.org/>) was used. Human left and right ventricular RNA samples, from a commercial supplier (Biocat #R1234138-50-BC and #R1234139-50-BC, respectively), were included in the analysis as positive control.

## **2.5. Characterization of hiPSC-CMs**

### **2.5.1. Cell concentration and viability**

Cell concentration and viability were determined by cell counting in a Fuchs–Rosenthal haemocytometer (Brand, Wertheim, Germany) using the trypan blue (Sigma-Aldrich) exclusion method (0.1% (v/v) in DPBS).

### **2.5.2. Transmission electron microscopy (TEM)**

Monolayers of human hiPSC-CMs were fixed in 2% (v/v) glutaraldehyde in 0.1 M HEPES buffer (pH 7.4) for 20 min, washed in DPBS and stored in 1% (v/v) glutaraldehyde in DPBS until analyses. Samples were washed, contrasted, dehydrated, infiltrated, embedded, cured, dissected into small blocks and mounted on epon dummy blocks, as previously described (Correia et al., 2016). Ultrathin sections of cell monolayers were cut on a Leica UC6 ultramicrotome using a diamond knife. Sections were collected on formvar-coated slot grids, stained with lead citrate and uranyl acetate as described in the literature (Venable and Coggeshall, 1965), and analyzed on a FEI Morgagni 268 at 80 kV. Images were taken with an Olympus MegaView III using the iTEM software.

### **2.5.3. Sarcomere Alignment**

Sarcomere alignment was determined as previously described (Ruan et al., 2016). Briefly, alignment is defined by the inverse of the magnitude of angle dispersion (the standard deviation of angles of sarcomere edges measured in ImageJ software (National Institutes of Health)). Low angle dispersion indicates high degree of alignment. Rose plot was generated using Mathematica (Wolfram Research Inc.).

### **2.5.4. Immunofluorescence microscopy**

Cells were washed with DPBS and fixed in 4% (w/v) Paraformaldehyde (PFA) in DPBS solution for 15 min. After being permeabilized and blocked with 5% (v/v) FBS, 1% (w/v) BSA, 0.3% (v/v) Triton X-100 in DPBS for 1h, at room temperature (20-25°C), cells were incubated with primary antibodies diluted in 1% (w/v) BSA, 0.1% (w/v) TX-100 in PBS overnight at 4°C. The following primary antibodies were used:  $\alpha$ -sarcomeric actinin (1:200, Sigma-Aldrich), titin (1:100, Santa Cruz Biotechnology) and troponin I (1:100, Millipore). Afterwards, cells were washed in DPBS and incubated with secondary antibody, Alexa Fluor 594 goat anti-mouse IgG (1:500, Invitrogen), in the dark for 1h at room temperature (20-25°C). Cell nuclei were counterstained with Hoechst 33342 nucleic acid dye (1:1000, Thermo Scientific). Representative images were taken using an inverted fluorescence microscope (DMI 6000, Leica).

### **2.5.5. Cell morphology**

Cell area, circularity index and aspect ratio were determined in ImageJ software using standard analysis plugins. For each condition, at least 70 cells were analyzed.

### **2.5.6. Measurement of mitochondrial membrane potential**

Differences in membrane potential, were assessed using MitoView™ 633 (Biotium, Inc., California, USA) following manufacturer's instructions. Briefly, after incubation with the dye for 1h, fluorescence was measured in a microwell plate fluorescence reader, Infinite 200 PRO NanoQuant (TECAN).

### **2.5.7. Lipid droplets content**

Lipid droplet content was assessed using the Lipid Droplets Fluorescence Assay Kit (Cayman, USA), according to the manufacturer's instructions. Fluorescence was quantified in a microwell plate reader, Infinite 200 PRO NanoQuant (TECAN). Representative images were taken using an inverted fluorescence microscope (DMI 6000, Leica).

## **2.6. Assessment of hiPSC-CM functionality**

### **2.6.1. Dissociation and Plating**

hiPSC-CMs were dissociated into single-cell suspensions by incubation with TrypLE™ Select for 5min. Single hiPSC-CM were seeded on Matrigel-coated Fluorodishes at 2,000—6,000 cells/cm<sup>2</sup>. Single contracting hiPSC-CM and CM clusters (<10 cells) growing on PDMS substrates for 3-5 days were chosen for image acquisition.

### **2.6.2. Confocal Imaging and Drug Treatment**

hiPSC-CMs were imaged in the different culture media inside a climate control chamber at 37°C with 5% CO<sub>2</sub> (Pathology Devices) using a Nikon A1R confocal microscope with DIC microscopy using a 488- or 647-nm laser and an anti-vibration table (TMC). Movies were acquired with at least 100 fps. Movies of CMs displaying at least five contraction cycles were recorded at baseline and then 5 min after each treatment. Movies were acquired without and with field-stimulated with 10 V at 1 Hz using the RC- 37WS perfusion insert with electrodes (Warner Instruments) connected to a C-Pace EP stimulator (Ion Optix).

### **2.6.3. Calcium and Action Potential imaging**

For calcium imaging, 0.5 mM of Fluo-4 AM (Life Technologies) was added to the CM culture medium 10 min prior to image acquisition. For action potential imaging, FluoVolt membrane potential kit (Life Technologies) was used at a dilution of 1:1000 according to the manufacturer's protocol. Both fluorescence and DIC channels were recorded concurrently for multiple contraction cycles.

### **2.6.4. Data Analysis and Display**

The Nikon Elements software package and Fiji were used for movie file conversions (Schindelin et al., 2012). Movies were cropped using Fiji to isolate the contracting CM from neighboring cells and cellular debris. Contractile kinetics and force generation by the CMs were analyzed using the method developed by Kijlstra et al (Kijlstra et al., 2015). Specifically, movies were loaded into Visible™ software (Reify) to generate a similarity matrix of n rows by n columns, where n is the number of frames in the movie. Analysis of the similarity matrix was performed in Excel (Microsoft). For analysis of contraction curves, at least five contraction curves from a single video were averaged by matching the start of the contractions. Curve-fitting was applied to this



averaged curve to obtain accurate measurements of maximum shortening and relengthening velocities.

### 2.6.5. Contractile Force Determination

Contractile forces generated by shortening CMs were calculated in MATLAB based on the contractility curve generated with BASiC (Kijlstra et al., 2015), the dimensions of the CMs, and the mechanical properties of the PDMS substrate (Palchesko et al., 2012). Variable input for the MATLAB script is the width of the cell in centimeters, the length of the cell (in the direction of contraction) in centimeters, and the amount of cell shortening in centimeters. The Young's modulus of PDMS substrates was 5 kPa for all experiments.

### 2.7. Statistical analysis

Statistical analysis was performed using GraphPad Prism Software version 5. Values are represented as mean $\pm$ SD or as mean $\pm$ SEM of independent measurements or assays (at least n=3 replicates were considered). Statistical significance was evaluated using either Student's t test or one-way analysis of variance (ANOVA). Values of P<0.05 were considered statistically significant.

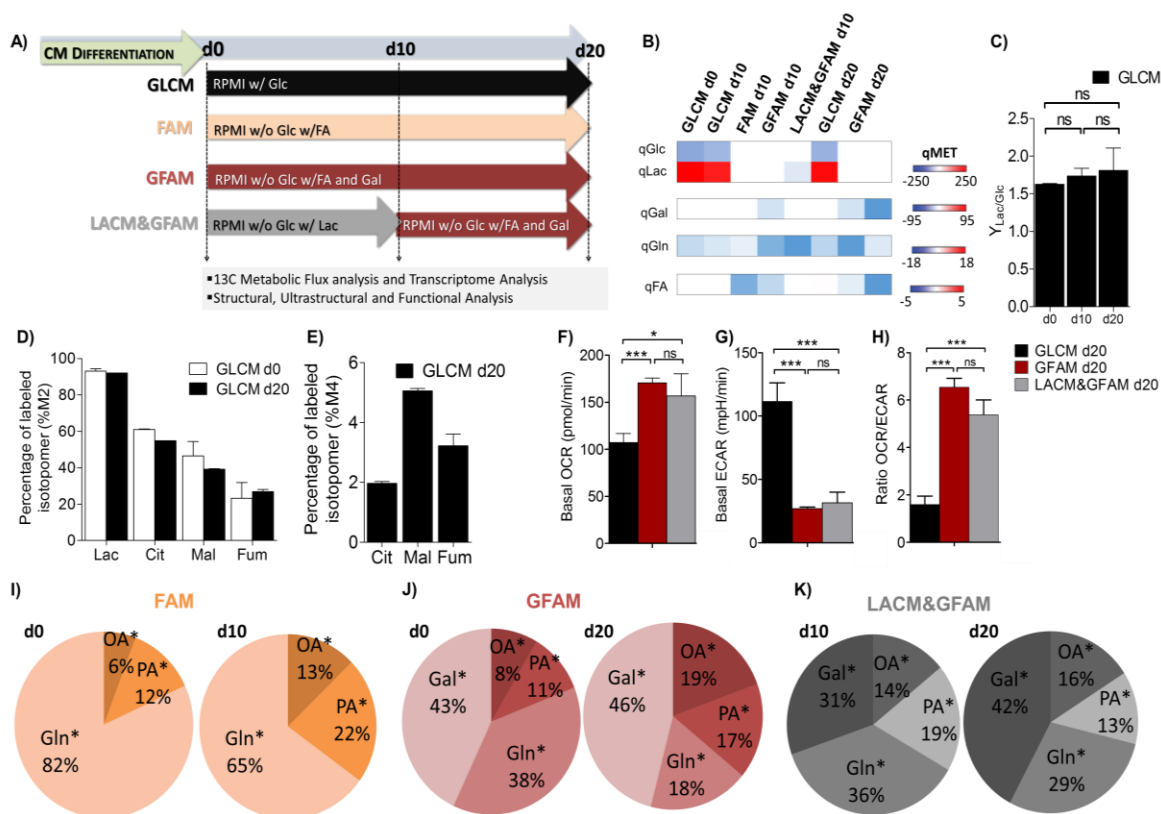
## 3. Results

### 3.1. hiPSC-CMs shift their metabolism from glycolysis to OXPHOS in the absence of glucose

Beating CMs differentiated from hiPSC exhibit a typical fetal-like glycolytic metabolism, as confirmed by a high Lac production (Figure 4.1B), high qLac/qGlc ratio (Figure 4.1C), and a high fraction of Lac (90%) derived from [1,2-<sup>13</sup>C]Glc upon 48h incubation (Figure 4.1D). These metabolic indicators as well as the fraction of intracellular TCA cycle pools derived from [1,2-<sup>13</sup>C]Glc and [U-<sup>13</sup>C]Gln, do not change significantly when keeping hiPSC-CMs in Glc rich medium (GLCM) during 20 days (Figure 4.1D-E), reflecting no improvements in the oxidative capacity of the cells when cultured in GLCM. This metabolic picture changes when removing Glc from the medium and adding FA alone (FAM) or together with galactose (GFAM), or Lac in the first 10 days followed by GFAM (LACM&GFAM) (Figure 4.1B). hiPSC-CMs were able to consume all new substrates and stop Lac secretion (Figure 4.1B) showing remarkable metabolic plasticity. In both GFAM and LACM&GFAM, hiPSC-CMs displayed a significantly higher oxygen consumption rate (OCR, Figure 4.1F), lower extracellular acidification rate (ECAR, Figure 4.1G) and consequently higher OCR/ECAR ratio (Figure 4.1H), reflecting the higher contribution of OXPHOS comparatively to glycolysis for energy generation in these conditions.

To further investigate the changes in central carbon metabolism, we cultured hiPSC-CMs in the conditions described above using uniformly <sup>13</sup>C-labelled versions of the corresponding nutrients and analysed the incorporation of <sup>13</sup>C into TCA cycle intermediates (citrate, fumarate and malate). In FAM, at day 0, 18% of the labelled fraction of these metabolites came from [U-<sup>13</sup>C]PA and [U-<sup>13</sup>C]OA and the remaining 82% from [U-<sup>13</sup>C]Gln (Figure 4.1I), suggesting that in FAM glutaminolysis is an important pathway to support TCA cycle anaplerosis when compared with

GLCM, where just a small portion of the TCA cycle pools incorporates carbon from [U-<sup>13</sup>C]Gln (Figure 4.1E). In the presence of Gal (GFAM), the incorporation of Gln decreased to 38%, whereas [U-<sup>13</sup>C]Gal accounted for approximately 40% of the label in TCA cycle (Figure 4.1J). Notably, after 10 days in FAM the contribution from FA to TCA cycle label increased to 35% (Figure 4.1I). A similar adaptation of hiPSC-CMs to FA consumption was observed in GFAM, in which FA contribution to labelled TCA cycle pools increased from 19% (day 0) to 36% (day 20) (Figure 4.1J). For hiPSC-CMs cultured in LACM&GFAM, the incorporation of FA in TCA intermediates was similar at days 10 and 20 (approximately 30%, Figure 4.1K), suggesting that initial reliance in Lac oxidation may precondition hiPSC-CMs, allowing for a better adaptation to FA metabolism upon initial exposure to this substrate. Also, like in GFAM, there is a decrease in Gln contribution concomitant with increased incorporation of Gal (Figure 4.1J-K). These results highlight the increased role of FA and Gal as fuel of TCA cycle during culture in GFAM in detriment of Gln.

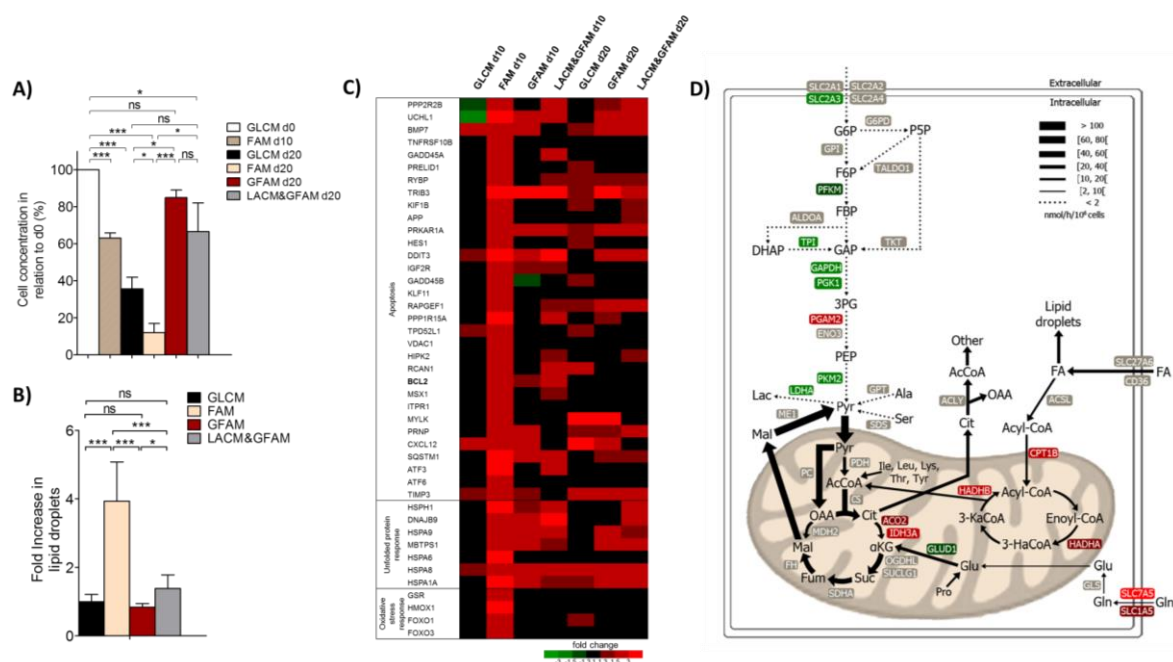


**Figure 4.1. Effect of culture medium composition on central carbon metabolism of hiPSC-CMs. A)** Representative scheme illustrating the experimental set-up. The metabolome of hiPSC-CMs was evaluated before (d0) and after 10 (d10) and 20 days (d20) of culture in different media: GLCM (black), FAM (Orange), GFAM (Red) and LACM&GFAM (Grey). **B)** Heatmap image of metabolome data illustrating specific consumption (blue) and production (red) rates of metabolites (qMET; nmol/(10<sup>6</sup>cell.h)). **C)** Ratio of Lac production to Glc consumption (Y<sub>Lac/Glc</sub>) in GLCM through culture time. **D)** Percentage of labeled M2 isotopomers from [1,2-<sup>13</sup>C]Glc in Lac and in TCA intermediates (Cit, Fum, Mal). **E)** Percentage of labeled M4 isotopomers from [U-<sup>13</sup>C]Gln in TCA intermediates. M2 and M4, reflect the first round of TCA cycling of [1,2-<sup>13</sup>C]Glc and [U-<sup>13</sup>C]Gln, respectively. **F)** Basal oxygen consumption rate (OCR). **G)** Extracellular acidification rate (ECAR). **H)** OCR/ECAR ratio reflecting the relative contribution of OXPHOS over glycolysis for energy generation. **I-K)** Pie charts indicating the contribution of the main substrates of each media, for TCA cycle pools. The percentages were determined based on the incorporation of each labelled substrate in Cit, Fum and Mal. OA: Oleic Acid and PA: Palmitic acid. Data are represented as mean±SD of 12-24 wells, n≥2 separate experiments. \*p<0.05; \*\*\*p<0.001; ns, not significant.

### 3.2. Culture of hiPSC-CMs in fatty acid medium lacking sugar source induces lipotoxicity

Our results show that when cultured in FAM, hiPSC-CMs exhibited: i) a drastic decrease in cell concentration from day 10 onwards, reaching about 10% of the initial cell concentration at day 20 (Figure 4.2A) and ii) a significant 4-fold increase in lipid droplet content when compared with hiPSC-CMs cultured in other media (Figure 4.2B). These results suggest that FA supply has surpassed the cellular oxidative capacity, leading to the intracellular accumulation of FA that has probably caused cellular damage and toxicity (Borradaile and Schaffer, 2005). Several studies have shown that cell exposure to high FA levels can affect multiple cellular processes such as reactive oxygen species (ROS) production, causing mitochondria, endoplasmic reticulum and lysosomal dysfunction and ultimately apoptosis (Drosatos and Schulze, 2013). Whole-genome transcriptome analysis revealed that FAM induced up-regulation of apoptosis-related genes and genes that encode for mediators of oxidative stress resistance and heat shock proteins (Figure 4.2C). The activation of these genes reflects an adaptive mechanism of the cells to hamper cardiac damage associated with high FA exposure. To further characterize the global changes in central carbon metabolism of hiPSC-CMs cultured in FAM when compared to other feeding strategies, uptake and production rates were integrated with the  $^{13}\text{C}$  labelling profiles of intracellular metabolites from multiple tracers in a metabolic network model using non-stationary metabolic flux analysis (MFA) (Woo Suk and Antoniewicz, 2013). Reasonable fits were obtained (Figure A-4.1-A-4.3, Pages 132-134) and the estimated fluxes and associated 95% confidence intervals are provided in Table A-4.1 (Page 140). The flux map of hiPSC-CMs cultured in FAM at day 10, confirms that most of the consumed FA (74%) is channelled to internal stores (lipid droplets) instead of entering  $\beta$ -oxidation (Figure 4.2D). Moreover, the majority of the citrate (Cit) produced in TCA is transported to the cytosol generating cytosolic Acetyl-CoA (AcCoA).

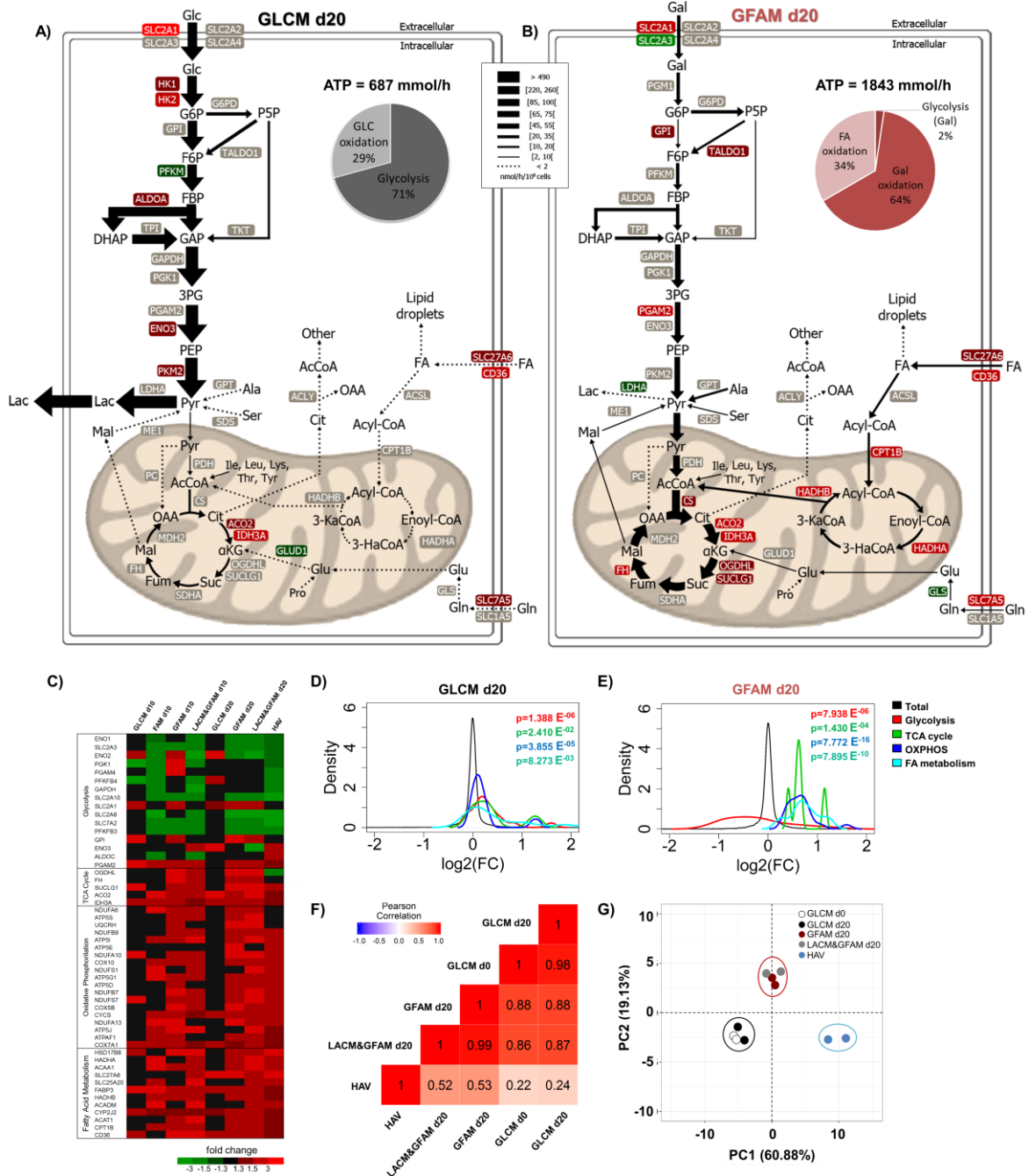
To compensate this high mitochondrial Cit withdrawal, TCA cycle activity is mainly fuelled i) by amino acid carbon sources, primarily glutamate (Glu), and ii) Pyruvate (Pyr) cycling through malic enzyme (ME) and pyruvate carboxylase (PC). Therefore, even though FA are the main substrate of the adult heart (Lopaschuk and Jaswal, 2010), culture of hiPSC-CMs in FA-rich medium lacking sugar source lead to FA accumulation and alterations in the central carbon metabolism which could justify the decrease in cell viability.



**Figure 4.2. In the absence of a sugar source, fatty acid rich medium induces lipotoxicity in hiPSC-CMs**  
**A)** Percentage of cell concentration, in all conditions tested, in relation to day 0 (d0), assessed using the Trypan Blue Exclusion Method. **B)** Analysis of lipid droplet content using a lipid droplet-specific fluorescent dye (Nile Red) of hiPSC-CMs at day 15. Fluorescence values were normalized for the values obtained in cells cultivated in GLCM. Data are represented as mean $\pm$ SD. \* $p$ <0.05; \*\*\* $p$ <0.001; ns, not significant. **C)** Heat map of differentially expressed genes closely related with apoptosis, unfolded protein and oxidative stress responses in hiPSC-CMs cultivated in different culture media. Genes were considered up- or down-regulated based on a fold change in expression  $FC \geq |1.3|$  compared to d0. **D)** Metabolic flux map of the central carbon metabolism of hiPSC-CMs cultivated for 10 days in FAM. The flux map was determined using non-stationary <sup>13</sup>C-MFA. Arrow thickness reflects flux values (see Table A-4.1 for exact flux values).

### 3.3. Galactose prevents lipotoxicity in hiPSC-CMs cultured in fatty acid medium and improves cellular oxidative capacity

When cultured in GFAM, hiPSC-CMs showed unaltered cell concentration throughout culture time (Figure 4.2A) and a significant lower intracellular FA accumulation than in FAM (Figure 4.2B), suggesting that combining FA with Gal supplementation constitutes a better approach to culture hiPSC-CM avoiding lipotoxicity. A comparison of the flux maps of hiPSC-CMs in GLCM and GFAM at day 20, reveals that hiPSC-CMs maintained in GFAM exhibited higher oxidative metabolism as indicated by a lower flux through glycolysis (around 10-fold) and higher flux through TCA cycle (over 6-fold) (Figure 4.3A-B). Most of the cytosolic Pyr was transported to the mitochondria and converted to AcCoA through pyruvate dehydrogenase (PDH) activity (72.4 in GFAM vs 5.6 nmol/(10<sup>6</sup>cells.h) in GLCM), whereas in GLCM most of the cytosolic Pyr was diverted to Lac secretion (491.4 in GLCM vs 0.0 nmol/(10<sup>6</sup>cells.h) in GFAM), consistent with the measured extracellular rates (Figure 4.1B). A pronounced effect of GFAM on hiPSC-CM central carbon metabolism was the up-regulation of the  $\beta$ -oxidation pathway, achieving fluxes of 11 nmol/(10<sup>6</sup>cells.h) whereas in GLCM these fluxes were negligible, underscoring the increased FA oxidation in GFAM (Figure 4.3A-B). Importantly, hiPSC-CMs cultured in LACM&GFAM and GFAM showed similar fluxomes (data not shown).



**Figure 4.3. Effect of culture media composition on the fluxome and metabolic transcriptome of hiPSC-CMs.** Metabolic flux maps highlighting central carbon metabolism of hiPSC-CMs cultured in GLCM (A) and GFAM (B). The contribution of each metabolic pathway for ATP production is specified in the pie chart and the total amount of ATP produced is indicated above the pie chart. Up-regulated and down-regulated genes encoding metabolic enzymes are demarked in red and green, respectively. C) Heat map of differentially expressed genes associated with metabolic processes/pathways. D–E) Density plots generated with fold change expression of genes from the four metabolic processes showed in (C), for hiPSC-CMs in GLCM (D) and GFAM (E) at day 20. X axis indicates  $\log_2$  fold change in gene expression. Black line indicates expression of all genes. Coloured lines toward the left and right side of the black line indicate down-regulation and up-regulation of pathways, respectively. Kolmogorov-Smirnov test was used to calculate p-values. F) Pairwise Pearson correlation coefficients using expression data for the metabolic processes showed in (C). The highest and the lowest coefficients are coloured in a red to blue gradient. G) 2D principal component analysis using expression data for the metabolic processes showed in (C).

The estimated changes in metabolic fluxes correlate with alterations in the metabolic transcriptome. Specifically, we observed a significant down-regulation of glycolytic genes and a significant up-regulation of most genes related to TCA cycle, OXPHOS and FA metabolism (Figure 4.3C-E, Figure A-4.4A, Page 135) in GFAM and LACM&GFAM cultures, a trend similar to that seen in human adult ventricular (HAV) tissue (Figure 4.3C, Figure A-4.4B, Page 135). Using gene expression data from these four metabolic pathways, we carried out a Pearson correlation analysis and a 2D principal component analysis (2D-PCA) comparing hiPSC-CMs at day 0 and after 20 days of culture in GLCM, GFAM, and LACM&GFAM with HAV tissue. The correlation coefficients between HAV and GFAM (0.53) and LACM&GFAM (0.52) cultures are higher than with GLCM cultures (0.24, Figure 4.3F). Additionally, 2D-PCA analysis clustered together hiPSC-CMs in GLCM at day 0 and at day 20, separating these samples from HAV in principal component 1 (PC1, 60.88% variance, Figure 4.3G), while hiPSC-CMs cultured in GFAM and LACM&GFAM at day 20 were placed in the middle of PC1 and closer to HAV tissue (Figure 4.3G). Together, these data re-enforce the idea that hiPSC-CMs cultured in GFAM and LACM&GFAM show a metabolic transcriptome more similar to HAV tissue.

We noticed a faster down-regulation of glycolysis related genes (such as ALDOC; GAPDH; PGK1) in LACM&GFAM than in GFAM (Figure 4.3C). This indicates that the first 10 days of culture in LACM contributes for a sharp inactivation of the glycolytic pathway whereas the presence of Gal in GFAM lead to a more gradual decrease in the expression of glycolytic genes. Of particular interest is the up-regulation of enzymes glucose-6-phosphate isomerase (GPI) from glycolysis and transaldolase (TALDO1) from the non-oxidative branch of pentose phosphate pathway (PPP) in GFAM (Figure 4.3B-C). Gal is converted into G6P inside the cells, and the G6P formed can enter either the glycolytic pathway or the PPP. Thus, the increased expression of GPI and TALDO1 may reflect an adaptive response of the cells to enhance Gal metabolization. Interestingly, the PPP flux was similar in GFAM and GLCM, but in GFAM represented approximately 87% of the respective glycolytic fluxes and in GLCM just 13% (Figure 4.3A-B).

The increased expression of genes related with FA metabolism, namely: CD36 that regulates the uptake of FA across the plasma membrane; CPT1B and SLC25A20 both necessary to shuttle long-chain FA from the cytosol into the intramitochondrial space; and HADHA/B involved in  $\beta$ -oxidation (Figure 4.3C) suggests that hiPSC-CMs in GFAM and in LACM&GFAM adapt also at the transcriptional level to more efficiently consume FA. Also, the higher expression of OXPHOS related genes (specifically, ATP5, COX and NDUF family of genes) (Figure 4.3C, Figure A-4.5, Page 136), re-enforces the idea that mitochondrial oxidative metabolism is enhanced in both media. In accordance, the estimated ATP production increased 2.7-fold in GFAM (1843 nmol/h) comparing with GLCM (687 nmol/h) (Figure 4.3A-B). Taking into account the estimated fluxes and the reference amount of ATP produced *per* each substrate molecule (Boyle, 2005), glycolysis accounts for 71% of the total produced ATP in GLCM, whereas in GFAM, glycolysis originates just 2% of the total ATP. In GFAM the majority of the ATP (98%) is produced through oxidation of Gal (64%) and FA (34%) (Figure 4.3A-B, pie charts).

The lower Gln consumption rates in GLCM and GFAM (1.0 and 2.6 nmol/(10<sup>6</sup> cells.h), respectively), suggests an almost negligible role of Gln in the metabolism of hiPSC-CMs cultured in these media.

Overall, <sup>13</sup>C-MFA and transcriptome analysis confirmed that in GLCM the majority of Glc is metabolized by glycolysis originating Lac, whereas in GFAM, FA and Gal are both oxidatively metabolized via TCA cycle and OXPHOS for ATP generation, providing additional evidence that hiPSC-CMs switch their metabolism from a fetal-like glycolytic metabolism to a more energetically efficient adult-like oxidative metabolism when cultured in GFAM (and LACM&GFAM).

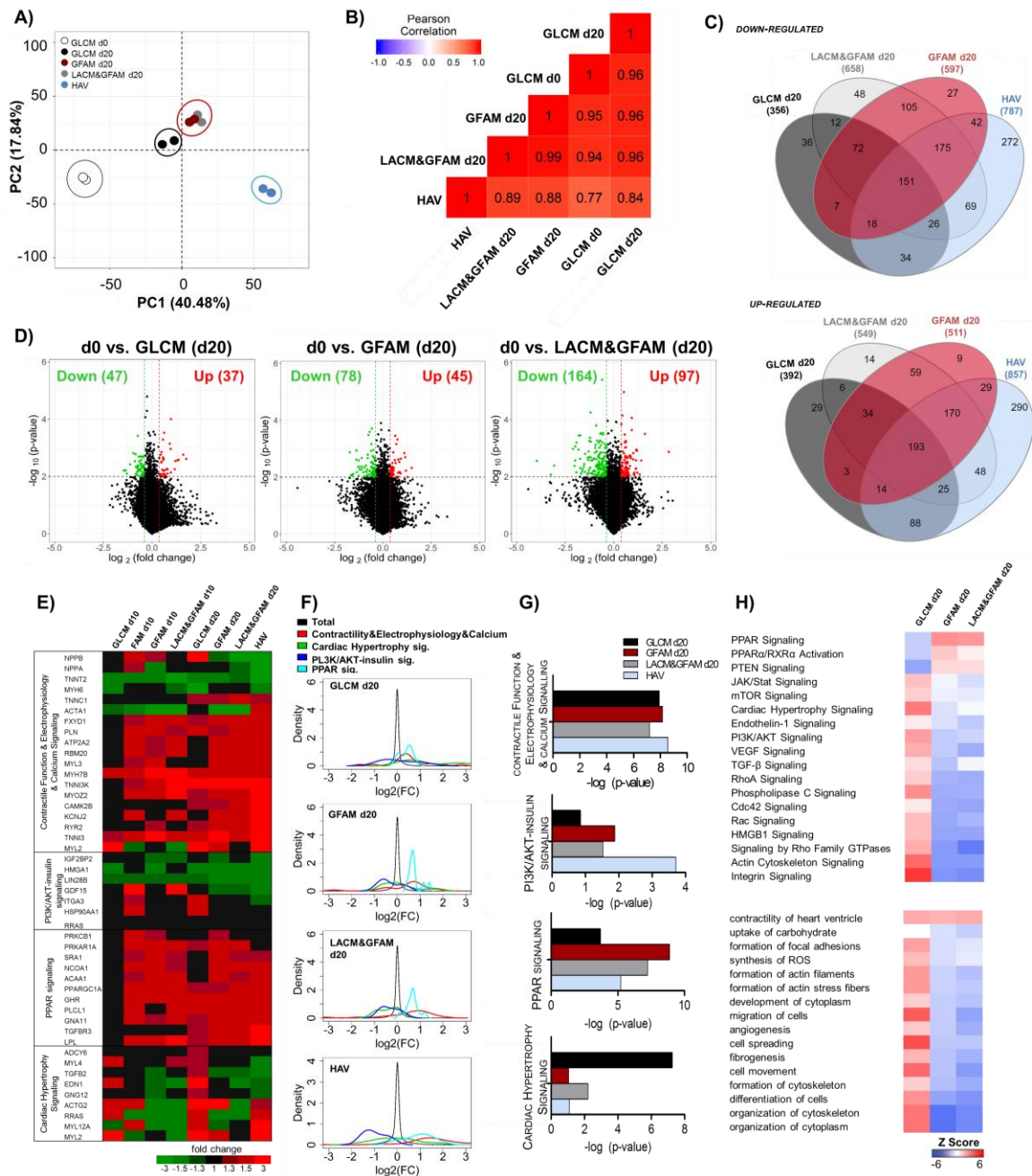
### 3.4. Adaptation to LACM induces higher cell death than GFAM

The up-regulation of some genes related with unfolded protein response in both LACM and GFAM at day 10 (Figure 4.2C), suggests that Glc depletion *per se* induced a stress for the cells resulting in the activation of survival signalling cascades. Nonetheless, the cell death (Figure 4.2A and Figure A-4.6A, Page 137) and the up-regulation of apoptotic genes (Figure 4.2C) were higher in hiPSC-CMs cultured in LACM, suggesting that the metabolic adaptation to Lac consumption is more harmful for the cells than the adaptation to Gal and FA consumption. It should be highlighted that the hiPSC-CMs used in this study were already non-proliferative, as verified by the absence of ki-67 expression at day 0 (Figure A-4.6B, Page 137). The lack of significant enrichment in cell cycle related pathways, from day 0 to day 20, in all culture media (Figure A-4.6C, Page 137), also suggest that culture in different media did not affect hiPSC-CM proliferative capacity.

### 3.5. hiPSC-CMs cultured in GFAM or LACM&GFAM present transcriptional signatures closer to human ventricular CMs

Whole transcriptome analysis showed that global gene expression patterns of hiPSC-CMs change gradually and differently along culture time in distinct media. 2D-PCA of all differently expressed genes (p-value<0.01 between the analysed sample groups) clearly separated HAV the farthest from hiPSC-CMs at day 0 in PC1, that accounted for most of the data variance (40.48%; Figure 4.4A). GLCM, GFAM and LACM&GFAM cultures were placed in the middle of the PC1 axis, but GFAM and LACM&GFAM were positioned closer to HAV and GLCM closer to day 0 in PC1 (Figure 4.4A). In accordance, gene expression of hiPSC-CMs maintained in GFAM and LACM&GFAM for 20 days showed higher correlation coefficients with HAV (0.88 and 0.89, respectively) than hiPSC-CMs in GLCM (0.84) (Figure 4.4B). In agreement, Venn diagrams showed that both GFAM and LACM&GFAM present more overlapping of significantly enriched genes with HAV tissue than GLCM (Figure 4.4C). Comparison of gene expression in all conditions at day 20 with the initial time point (day 0) using volcano plots, indicated that the total number of genes significantly up- and down-regulated (FC≥|1.3| and p-value<0.01) is higher in GFAM and LACM&GFAM than in GLCM (Figure 4.4D). This result reflects, as expected, a reduced variability in gene expression when hiPSC-CMs are maintained in GLCM for 20 days.

Overall, these results suggest that transcriptional signatures of hiPSC-CMs cultured in GFAM and LACM&GFAM were more similar to that of HAV tissue used as reference of mature CMs.



**Figure 4.4. Effect of culture medium composition on hiPSC-CM transcriptional profiling.** **A)** 2D principal component analysis of all genes significantly enriched ( $p < 0.01$ ) in hiPSC-CM cultures at day 0, after 20 days of culture in GLCM, GFAM and LACM&GFAM and HAV tissue samples. **B)** Pairwise Pearson correlation coefficients using expression data of all enriched genes ( $p < 0.01$ ). **C)** Venn diagrams of overlapping differentially-expressed genes ( $p < 0.01$  and  $FC \geq |1.3|$ ) among GLCM, GFAM, LACM&GFAM cultures at day 20 and HAV tissue. **D)** Volcano plots of gene expression changes in relation to day 0. Genes significantly up-regulated ( $FC \geq 1.3$  and  $p < 0.01$ ) are red and genes significantly down-regulated ( $FC \leq -1.3$  and  $p < 0.01$ ) are green. The number of regulated genes according to these criteria is shown on the top of the graphic. **E)** Heatmap depicting changes in the expression of genes involved in biological processes/pathways closely associated with CM development and function. **F-G)** Density plots generated with fold change expression of genes from the four cardiac-related categories shown in (E), for day 20 cultures (GLCM, GFAM and LACM&GFAM). Black line indicates expression of all genes. Colored lines toward the left and right side of the black line indicate down-regulation and up-regulation of pathways, respectively. Kolmogorov-Smirnov test was used to calculate p-values. **H)** Heatmaps highlighting the activation status of canonical pathways (upper panel) and biological functions (lower panel) predicted by IPA. Functions/pathways were considered significantly activated (or inhibited) with an overlap  $p\text{-value} \leq 0.05$  and an IPA activation Z-score  $\geq |2.0|$ . Red indicates positive Z-score (activated function) and blue indicates negative Z-score (inhibited function).



### 3.6. GFAM and LACM&GFAM enhance the expression of cardiac markers

When compared with hiPSC-CMs at day 0, hiPSC-CMs maintained in GFAM and LACM&GFAM for 20 days, exhibit enhanced expression of cardiac genes related with i) contractile function and sarcomere structure (e.g. MYL3, TNNC1, TNNI3), ii) calcium cycling (e.g. ATP2A2 and RYR2), and iii) electrophysiological properties (e.g. KCNJ2) (Figure 4.4E). Of particular interest is the 2-fold up-regulation of KCNJ2, gene that suffices to render the electrophysiological phenotype indistinguishable from the adult counterparts (Lieu et al., 2013).

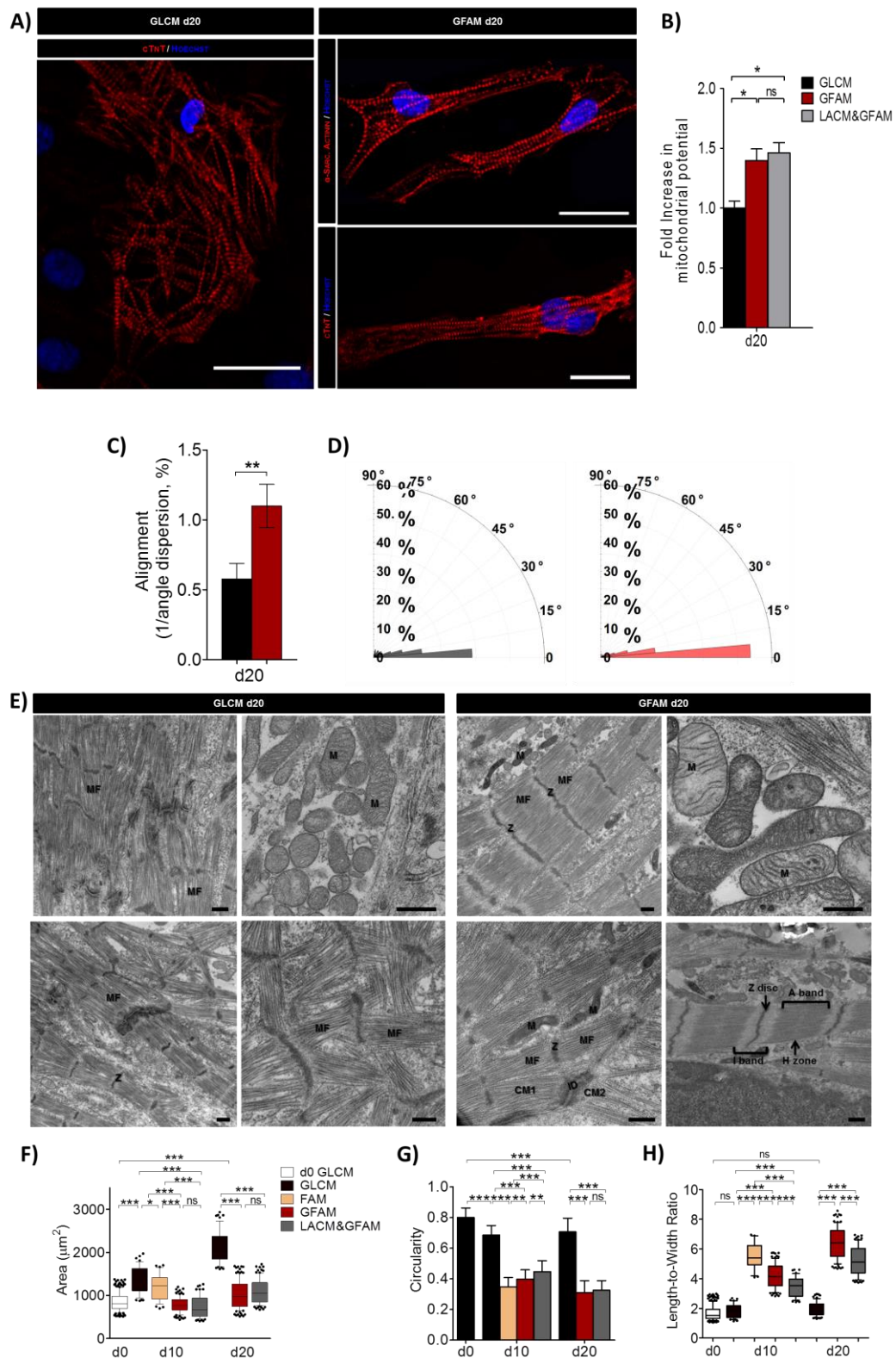
The expression of genes typically enhanced in fetal-like CMs and repressed in adult ventricular CMs (e.g. NPPB and ACTA1) (Feric and Radisic, 2016), decreased in hiPSC-CMs cultured in GFAM and LACM&GFAM. In hiPSC-CMs cultured in GLCM, the expression of NPPB and ACT1, was reactivated and kept similar to those of the immature hiPSC-CMs (day0), respectively. Although ACTA1 is part of the fetal gene program in CMs, this gene is also expressed by other cardiac cell types, including smooth muscle cells, which may justify its up-regulation in HAV tissue. Notably, expression of the TNNI3 gene that encodes for the adult cardiac troponin I (cTnI), a key hallmark of human CM maturation *in vivo* (Bedada et al., 2014), was up-regulated in all culture conditions tested, however this increase was higher in GFAM (Figure 4.4E). It should be noted that up-regulation of genes related with contractile function, calcium signaling and electrophysiology was observed already at day 10 in GFAM whereas in GLCM, only minor improvements were observed at day 20 (Figure 4.4E). Additionally, a more in-depth evaluation of the data using density plots revealed that in GFAM cultures the expression of these genes follows a distribution more similar to that observed in HAV tissue (Figure 4.4F-G).

Examination of the transcript levels of all genes in the abovementioned samples, using IPA revealed the enrichment of several canonical pathways known to be critical in *in vivo* heart development. Inhibition of PI3K/AKT/insulin signalling and activation of PPAR signalling were consistently predicted by IPA and density plots in both LACM&GFAM and GFAM, whereas the opposite trend was observed in GLCM (Figure 4.4F-G). PPAR $\alpha$  is a major transcriptional regulator abundantly expressed in heart (Lopaschuk et al., 2010). Specifically, PPAR $\alpha$  regulates the expression of genes involved in FA uptake, cytosolic FA binding and esterification, FA  $\beta$ -oxidation, and Glc oxidation (Evans, 2004; Lopaschuk et al., 2010). PPARs activation have been related with the up-regulation of FA metabolism and with down-regulation of PI3/AKT/insulin pathway, which is involved in Glc metabolism regulation (Simons et al., 2012). Of note is the up-regulation of PPARGC1A, observed in GFAM and LACM&GFAM at day 10 (Figure 4.4E), that encodes for PGC-1, a transcriptional coactivator highly expressed in cardiac tissue (Uosaki et al., 2015). Up-regulation of PGC-1 $\alpha$  results in increased mitochondrial biogenesis, FA  $\beta$ -oxidation and OXPHOS (Lehman et al., 2000; Ventura-Clapier et al., 2008), features already described as increased in GFAM and LACM&GFAM (Figure 4.1,3). The inverse relationship between FA metabolism/PPAR $\alpha$  signalling and PI3K/AKT/insulin signalling observed in GFAM and LACM&GFAM cultures is consistent with the metabolic switch detected in these cultures and is in agreement with the pattern reported for 1-year matured hESC-CM (Kuppusamy et al., 2015).

Of note is that both IPA and density plots revealed that the cardiac hypertrophy pathway is significantly up-regulated in GLCM cultures. Specifically, the main canonical pathways and biological functions, predicted by IPA, as activated in GLCM and inactivated in GFAM and LACM&GFAM were cardiac hypertrophy and related pathways, including JAK/Stat, mTOR, Endothelin-1, VEGF, TGF- $\beta$ , RhoA, Rac, Phospholipase C, Cdc42, HMGB1, actin cytoskeleton and integrin signaling (Frey et al., 2004; Heineke and Molkentin, 2006; Ruwhof and van der, 2000) (Figure 4.4H). On the other hand, PTEN pathway, identified as inactive in GLCM and active in the other media (Figure 4.4H) has been shown to attenuate CM hypertrophy (Oudit et al., 2008). At the cellular level, hypertrophy is associated with the reorganization and increase of actin filaments in the absence of cytokinesis, extracellular matrix (ECM) remodeling, increase of ROS formation, promotion of angiogenesis and fibrogenesis (Abel and Doenst, 2011; Carreño et al., 2006), biological functions also predicted as activated in GLCM (Figure 4.4H). The expression of genes related with ECM and cell surface markers dynamically changed through culture time in all media however, GLCM cultures seem to display a profile distinct from GFAM and LACM&GFAM cultures and from HAV tissue (Figure A-4.7, Page 137). For example, genes that encode for collagen (COL1A1, COL3A1, COL5A1, COL4A2, COL11A1) and vimentin (VIM) were highly up-regulated in GLCM but down-regulated or non-altered, relatively to day 0, in GFAM, LACM&GFAM and HAV (Figure A-4.7, Page 137), suggesting that in GLCM, cells suffer a high ECM remodeling, including collagen deposition, which might justify the activation of biological functions related with cell migration and spreading in GLCM (Figure 4.4H). Interestingly, we observed increased expression of some fibroblast markers from day 0 to day 20 in hiPSC-CMs cultured in GLCM together with the appearance of small niches of fibroblast-like cells (Figure A-4.8, Page 138)

### **3.7. GFAM improves the structure and ultrastructure of hiPSC-CMs**

Immunofluorescence and TEM analyses corroborated the gene expression data, confirming an improved structural maturation of hiPSC-CMs cultured in GFAM (and in LACM&GFAM) comparatively to other media. hiPSC-CMs cultured in GFAM exhibited: i) well defined cross-striated patterns of sarcomeric  $\alpha$ -actinin and cTnT; ii) high density of aligned myofibrils composed by sarcomeres with organized Z-disks, A- and I-bands and a distinctive H-zone; iii) significant higher degree of sarcomere alignment; and iv) more mitochondria with prominent cristae close to the myofibrils (Figure 4.5A-E). On the other hand, hiPSC-CMs maintained in GLCM showed disorganized and diffuse cTnT staining (Figure 4.5A) and a poorly organized contractile machinery, characterized by low myofibril density and orientation and variable Z-disc alignment (Figure 4.5C-E). In accordance, Mitoview fluorescence (inner mitochondrial membrane potential dye), was significantly higher in GFAM in relation to GLCM conditions (Figure 4.5B).



**Figure 4.5. Structural and ultrastructural analyses of hiPSC-CMs after culture in different media. A)** Representative images of hiPSC-CMs immunostained for cardiac troponin-T (cTnT) and  $\alpha$ -sarcomeric actinin. Nuclei (blue) were stained with Hoechst 33342. Scale bars=30 $\mu$ m. **B)** Fold increase in mitochondria potential assessed by the mitochondria specific dye Mitoview. Fluorescence values were normalized for the values obtained in cells cultivated in GLCM. **(C-D)** Sarcomere alignment in hiPSC-CMs cultured for 20 days in GLCM and GFAM: **C)** Inverse of the magnitude of sarcomere angle dispersion and **D)** Rose plot histogram of

sarcomere orientation.  $n > 30$  sarcomeres per condition. **E**) TEM images of hiPSC-CMs. Myofibrils (MF), Z-disks (Z), sarcomeric bands: A- and I-bands with a H-zone, intercalated disks (ID) connecting adjacent CM and Mitochondria (M) are highlighted. Scale bars=500nm. **F-H**) Cell structure characterization in terms of cell area (**F**), circularity index (**G**), length-to-width ratio (**H**).  $n > 70$  cells per condition. Data are represented as mean $\pm$ SD. \* $p < 0.05$ ; \*\* $p < 0.01$ ; \*\*\* $p < 0.001$ ; ns, not significant.

Moreover, significant changes in cell morphology were observed through time in all conditions (Figure 4.5F-H). When compared to GLCM, hiPSC-CMs cultured in GFAM or LACM&GFAM exhibited significantly lower cell area (Figure 4.5F) and circularity index (Figure 4.5G) and higher length/width ratio (Figure 4.5H). These numbers are similar to the values previously reported for adult human ventricular CMs (Feric and Radisic, 2016). For example, length/width ratios in the range of 5-9.5 have been reported for adult CMs (Denning et al., 2015) and we observed an average ratio of 6.4 in hiPSC-CMs cultured in GFAM.

The significant increase in cell surface area and spherical morphology observed in hiPSC-CMs maintained in GLCM (Figure 4.5F-H), reflects again the propensity of hiPSC-CMs to undergo hypertrophy.

### **3.8. GFAM improves calcium transients, contractility and action potential kinetics of hiPSC-CMs**

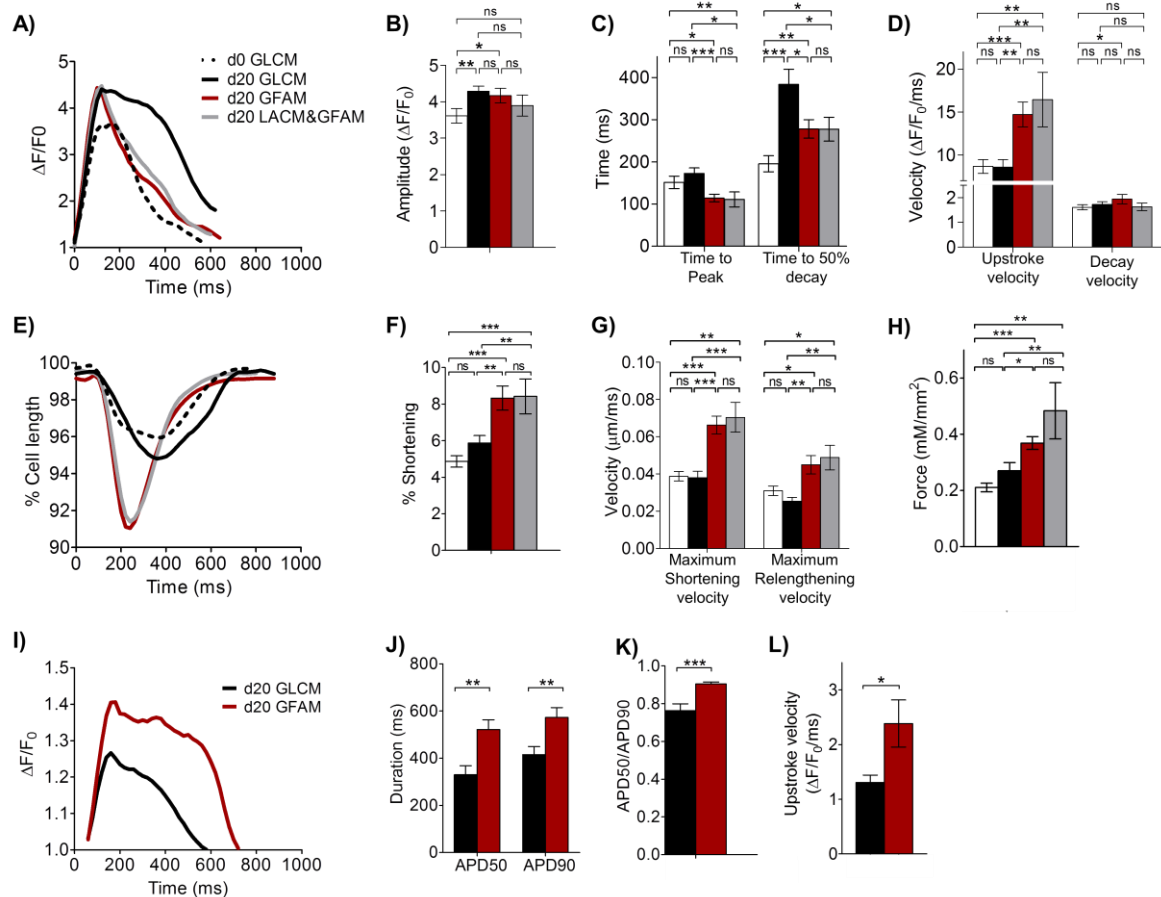
Despite showing similar transient amplitudes (Figure 4.6A-B), hiPSC-CMs cultured in GFAM and LACM&GFAM at day 20 presented significantly faster calcium-transient kinetics compared with hiPSC-CMs at days 0 and 20 in GLCM, as indicated by significantly shorter time to peak, time to 50% decay and faster  $\text{Ca}^{2+}$  transient upstroke and decay velocities (Figure 4.6C-D). The faster calcium kinetics observed in GFAM and LACM&GFAM is supported by the high expression of RYR2 and ATP2A2 that are responsible respectively for the release and uptake of  $\text{Ca}^{2+}$  in the SR (Figure 4.4E).

Additionally, compared to day 0 and to cells at day 20 in GLCM, hiPSC-CMs cultured in GFAM and LACM&GFAM exhibited improved contractility with greater fractional shortening (approximately 8.4% of resting length in both LACM&GFAM and GFAM vs. 4.9 (day 0) and 5.9 (GLCM day 20); Figure 4.6E-F), faster contractile kinetics (higher shortening and relengthening velocities; Figure 4.6G), and greater peak force ( $0.48 \pm 0.22$  (LACM&GFAM),  $0.37 \pm 0.06$  mN/mm<sup>2</sup> (GFAM) vs.  $0.21 \pm 0.04$  (GLCM day 0) and  $0.27 \pm 0.12$  (GLCM day 20); Figure 4.6H). The significantly lower contractile force generated by the cells in GLCM correlates with the lower expression of contractile and cytoskeletal genes observed in this medium (Figure 4.4E). The values of contractile force obtained at day 20 in GFAM (Figure 4.6H) were similar to the ones reported after hiPSC-CM maturation with a commercial medium containing T3 hormone ( $0.43$ - $0.51$  mN/mm<sup>2</sup>) (Ribeiro et al., 2015).

Importantly, the major functional improvements observed in hiPSC-CMs cultured in GFAM were detected as early as d10 (Figure 4.6 vs. Figure A-4.9, Page 138) with no meaningful further improvement in calcium and contractile kinetics observed between 10 and 20 days. This result provides additional evidence that GFAM stimulates a rapid functional maturation of hiPSC-CMs. In

contrast, hiPSC-CMs cultured in LACM&GFAM continued to exhibit improvements in fractional shortening, force generation, calcium uptake and shortening velocities from d10 to d20 (Table A-4.2, Page 142). These results suggest that GFAM is more efficient than LACM at promoting the rapid functional maturation of hiPSC-CMs.

Additionally, no significant differences were observed in calcium and contractile kinetics between cells cultured in GFAM and FAM at d10 (Figure A-4.9, Page 138), suggesting that Gal is not required for the enhancement of hiPSC-CM maturation.



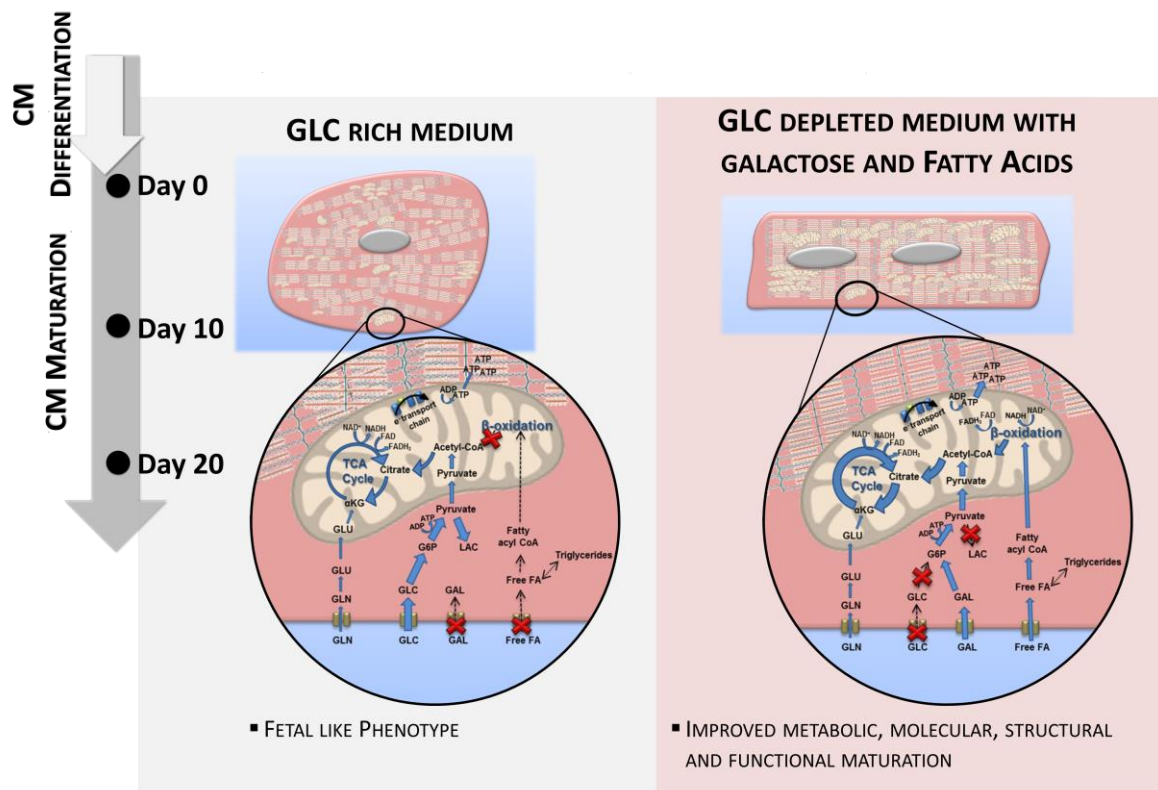
**Figure 4.6. Impact of metabolic manipulation on hiPSC-CM functionality.** hiPSC-CMs were analysed in terms of calcium transients (A-D), contractile performance (E-H) and action potential (AP) kinetics (I-L), before (d0) and after 20 days (d20) of culture in different media. Calcium transient kinetics (A-D) evaluated with the intracellular calcium indicator Fluo-4 AM: **A)** Representative calcium transient; **B)** Calcium transient amplitude ( $F/F_0$ ); **C)** Time to peak and time to 50% decay; **D)** Average upstroke and decay velocities.  $n=28-35$  cells per condition. **E)** Representative contraction curves, reflecting changes in the percentage of cell length. **F)** Percentage of shortening; **G)** Maximum shortening and relengthening velocities.  $n=20-35$  cells per condition. **H)** Maximum contractile force generated by hiPSC-CMs in each culture condition.  $n=8-17$  cells per condition. AP kinetics (I-L) were determined with a voltage-sensitive dye (FluoVolt). **I)** Changes in the fluorescence intensity of the FluoVolt AP indicator over time. **J)** AP duration at 50% (APD50) and 90% repolarization (APD90). **K)** APD50/APD90. **L)** AP upstroke velocity.  $n=24-26$  cells per condition. Data are represented as mean $\pm$ SEM. \* $p<0.05$ ; \*\* $p<0.01$ ; \*\*\* $p<0.001$ ; ns, not significant.

hiPSC-CM beating rates also varied throughout culture time in all conditions, with significantly lower rates at day 20 for all of them (Figure A-4.10A, Page 139). Although the decrease was more pronounced in GLCM (Figure A-4.10A, Page 139), all beating rates are within the range of reported values for hPSC-CMs after maturation *in vitro* (21–84 BPM) (Feric and Radisic, 2016). Interestingly, we observed that hiPSC-CMs cultured in GFAM and LACM&GFAM were more easily electrically paced at 1Hz than hiPSC-CMs at d0 and d20 in GLCM (Figure A-4.10B, Page 139). Action potential (AP) durations at 50% and 90% repolarizations (APD50 and APD90), APD50/APD90 and upstroke velocity were significantly higher in GFAM than in GLCM cultures (Figure 4.6I-L). These results are consistent with prior studies that report that adult CMs exhibit increased APD90, APD50/90 and maximum upstroke velocity than immature CMs (Kuppusamy et al., 2015; Ribeiro et al., 2015; Sartiani et al., 2007).

Altogether these data demonstrated that GFAM and LACM&GFAM cultures result not only in metabolic, molecular and morphological changes indicative of CM maturation, but also that functionally relevant parameters such as calcium signaling, contraction and action potential are appropriately regulated.

#### **4. Discussion**

In this study, we applied a systems-level approach to provide new insights on how the use of different metabolic substrates impacts metabolic, structural and functional maturation of hiPSC-CMs. Combining a set of “-omics” tools (metabolomics, fluxomics and transcriptomics) with structural, morphological and functional analyses we show that a glycolytic-to-oxidative metabolic shift is a cause, rather than a consequence, of the phenotypic alterations characteristic of the CM maturation process. We report for the first time that: i) hiPSC-CMs cultured in medium without Glc supplemented with FA and Gal (GFAM) display improved maturation markers in relation to hiPSC-CMs cultured in standard Glc medium (GLCM; Figure 4.7); ii) Gal supplementation ameliorates the oxidative capacity of the cells improving FA oxidation while avoiding lipotoxicity; and iii) hiPSC-CMs cultured in GLCM maintain a fetal-like profile and show features that resemble pathogenic hypertrophy (Figure 4.7).



**Figure 4.7. Summary of major findings in this study.** The main differences in terms of cell phenotype and metabolism after 20 days of culture in GLCM and GFAM are highlighted.

GFAM culture allows to obtain CMs with a more mature phenotype, characterized by a more energetically efficient oxidative metabolism, transcriptome signatures that more closely resemble adult ventricular CMs, elongated morphologies, organized sarcomeric structures, higher myofibril density and alignment, faster calcium-transient kinetics, higher percentage of shortening and contractile force, enhanced AP durations and higher upstroke velocities. Transcriptome analysis revealed that substrate selection induces significant alterations in the expression of key transcriptional regulators and pathways involved in cell metabolism and cardiac development. We showed that hiPSC-CMs have substrate plasticity, being able to immediately adapt to consume other substrates (FA, Gal, Lac, Gln), in the absence of Glc. Rana and colleagues also demonstrated that hiPSC-CMs are capable of utilizing anaerobic or aerobic respiration depending upon the available carbon substrate and showed that hiPSC-CMs rely on OXPHOS for ATP production when cultured in Glc-depleted medium supplemented with Pyr, Gln, Gal and FA (Rana et al., 2012). Nevertheless, to date, no studies have quantified the intracellular fluxome and simulated metabolic fluxes distribution of hiPSC-CMs cultured in distinct carbon sources neither have extensively elucidated how the utilization of major metabolic substrates modulate structural and functional maturation of hiPSC-CMs as we addressed here. Nonstationary  $^{13}\text{C}$ -MFA analysis allowed us to confirm quantitatively that hiPSC-CMs present increased metabolic fluxes through FA  $\beta$ -oxidation and TCA cycle and improved ATP production in GFAM, reflecting a highly active OXPHOS.

Even though FA are the main substrates used by adult CMs (Lopaschuk and Jaswal, 2010), Glc-depleted medium supplemented with FA (FAM) induced cell toxicity. Nonetheless, combining FA supplementation with Gal could overcome lipotoxicity by improving oxidative capacity of hiPSC-CMs. Different types of cells (cancer cells, primary fibroblasts and muscle cells) growing in medium in which Glc was replaced by Gal showed enhanced aerobic metabolism (Aguer et al., 2011; Marroquin et al., 2007; Rossignol et al., 2004), due to the induction of an energy deprivation state. Gal is metabolized at a much slower specific rate than Glc due to: i) lower affinity of the transporters (GLUT1 and GLUT4) for Gal compared to Glc and, ii) lower activity of galactokinase, the rate-limiting step in Gal metabolism, comparing to hexokinase, the rate-limiting step in Glc oxidation (Dott et al., 2014; Wagner et al., 1991); forcing cells to start to use OXPHOS to rapidly get sufficient ATP. Even though we observed increased expression of GLUT1 in hiPSC-CMs cultured in GFAM, fluxomic analysis confirmed that the uptake rate of Gal was significantly lower than Glc (30.42 vs. 254.17 nmol/(10<sup>6</sup>cell.h)) when using similar concentrations of both substrates. We confirmed that the flux from Pyr to Lac is negligible and that the majority of Gal is oxidized in TCA cycle and OXPHOS.

It has been described that accumulation of FA leads to augmented intracellular FA derivatives (e.g. fatty acyl CoA, diacylglycerol, and ceramide) that can directly modify cellular structures and activate downstream pathways leading to cellular damage and toxicity (Lopaschuk et al., 2010). Other studies have shown that saturated FA (palmitate) cause greater lipotoxicity than unsaturated FA (oleate) (Drosatos and Schulze, 2013; Nemcová-fürstová et al., 2011). Kase et al. showed that Gal increases FA oxidation and the formation of neutral lipids that avoid the generation of “lipotoxic” FA derivatives (Kase et al., 2013). Additionally, we observed that in GFAM, PPP pathway is highly active while it is negligible in FAM. Since, PPP is one of the main antioxidant cellular defence systems in the cells (Riganti et al., 2012), we can speculate that Gal also contributes to prevent the detrimental effects of free radical toxicity promoted by OXPHOS. Whether the lipotoxicity observed in FAM derives exclusively from the medium composition itself or from an inadequate adaptation of the cells to oxidative metabolism, still needs to be investigated. In the future it would be interesting to see if a pre-treatment with GFAM before adding FAM would prevent lipotoxicity.

We showed that hiPSC-CMs maintained in GLCM during 20 days display a fetal-like CM phenotype and present features of cardiac pathological hypertrophy, namely higher surface area, higher expression of fetal genes, dominant glycolytic energetics, reduced calcium dynamics and contractile force. In accordance, other studies have reported that exacerbated CM pathologies and arrhythmia frequently appear in immature iPSC-CM within 30 days of culture in non-physiological conditions (Wen et al., 2015).

In order to mimic the temporal substrate preference during CM development *in vivo*, we also evaluated the impact of culturing hiPSC-CMs in LACM for 10 days before cultivation in GFAM. Metabolome and transcriptome profiles revealed that LACM improved cells' oxidative capacity. However this strategy resulted in higher cell death and reduced structural and functional maturation comparatively to cells cultured for the same period in GFAM. Nonetheless, we showed that

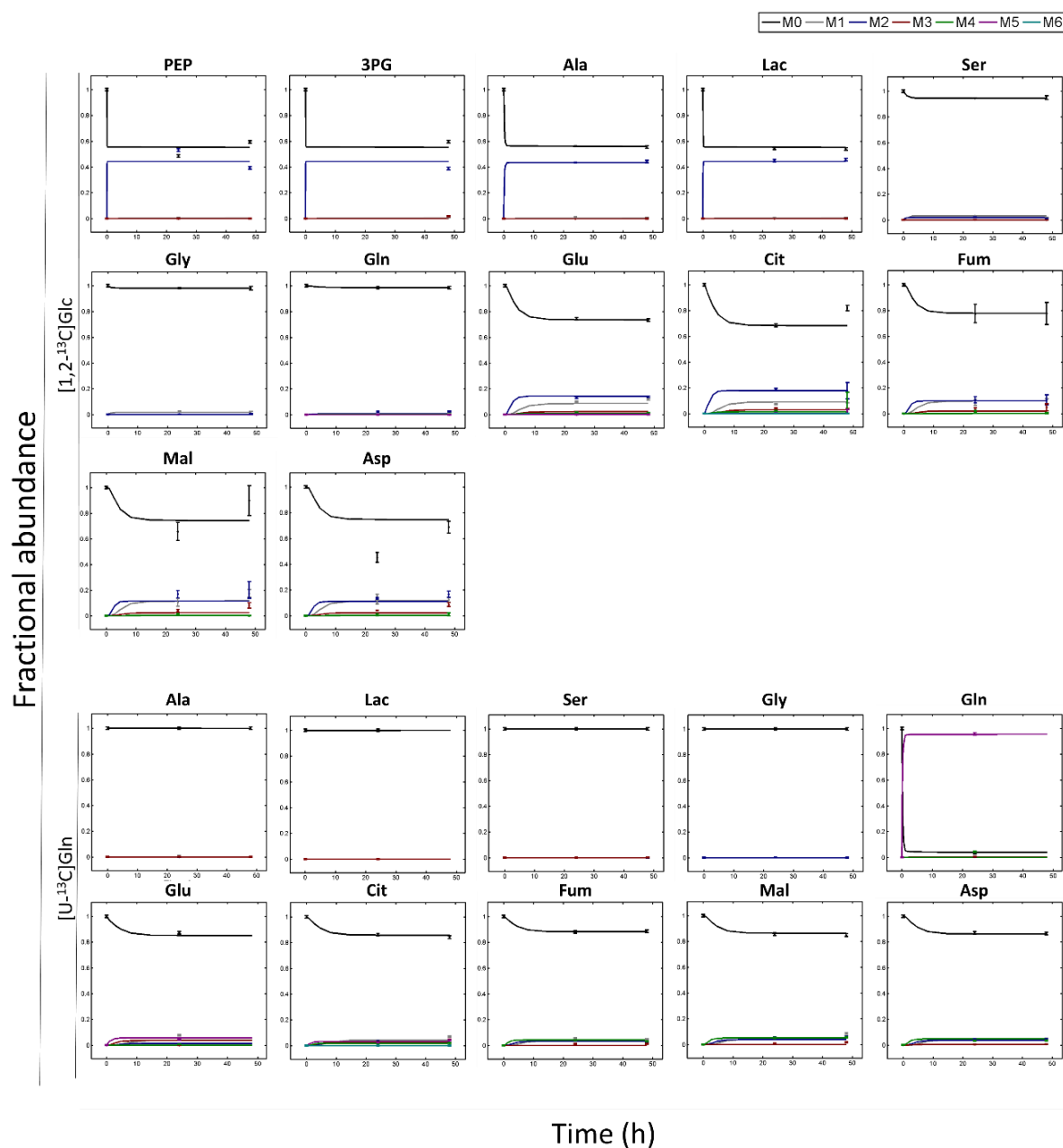


combining the additional 10 days of culture in GFAM was sufficient to improve structural and functional maturation of hiPSC-CMs, leading to a phenotype indistinguishable from hiPSC-CMs maintained in GFAM for 20 days. Therefore, we report two valuable strategies to induce metabolism switching and to improve hiPSC-CM maturation, with similar outcomes. The choice of the strategy to use may be dependent on the initial purity state of hiPSC-CM cultures (Tohyama et al., 2013).

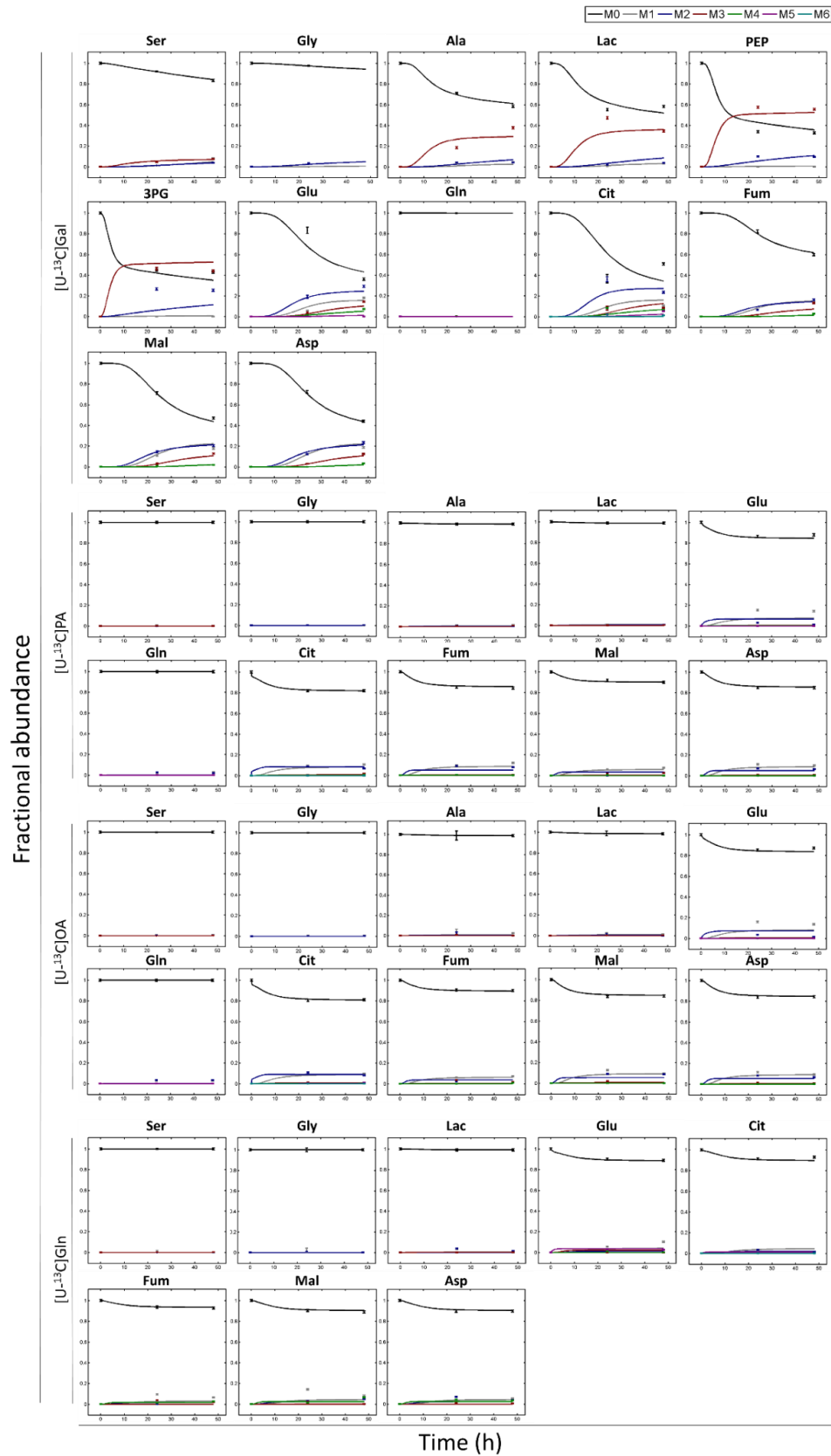
During development *in vivo*, CM maturation is regulated by several cues including cell-cell interactions, ECM, soluble factors, mechanical signals and substrate stiffness (Denning et al., 2015; Feric and Radisic, 2016). To further improve hiPSC-CM maturation *in vitro*, our strategy can be combined with other approaches described in literature, such as electrical/mechanical stimulation (Chan et al., 2013), co-culture with supporting cells (Kim et al., 2010), and medium supplementation (e.g. T3 hormone (Yang et al., 2014b)). Also, it can be adopted for 3D cell culturing approaches (Zhang et al., 2015), which in combination with the use of environmentally controlled bioreactors (Correia et al., 2014) constitute a promising strategy towards scalable production of mature hiPSC-CMs.

Overall, by bringing a holistic and quantitative metabolic analysis into the stem cell field, this work not only provides novel insight into the interaction of metabolism and maturation but also establishes a robust method to improve hiPSC-CM maturation. This method holds technical and economic advantages over the existing protocols due to its simplicity (a simple medium-exchange procedure) and ease of application (does not require specific equipment or addition of expensive factors/chemicals). It is noteworthy that 10 days of culture in GFAM was sufficient to promote hiPSC-CM phenotypic and functional maturation comparable to what has been described in the literature after 80-100 days of culture (Lundy et al., 2013). Therefore GFAM treatment constitutes a great advance for the maturation of hiPSC-CMs in a timely efficient manner. This will strengthen the utility of hiPSC-CMs in cell therapy, drug discovery, toxicity testing and cardiac disease modeling.

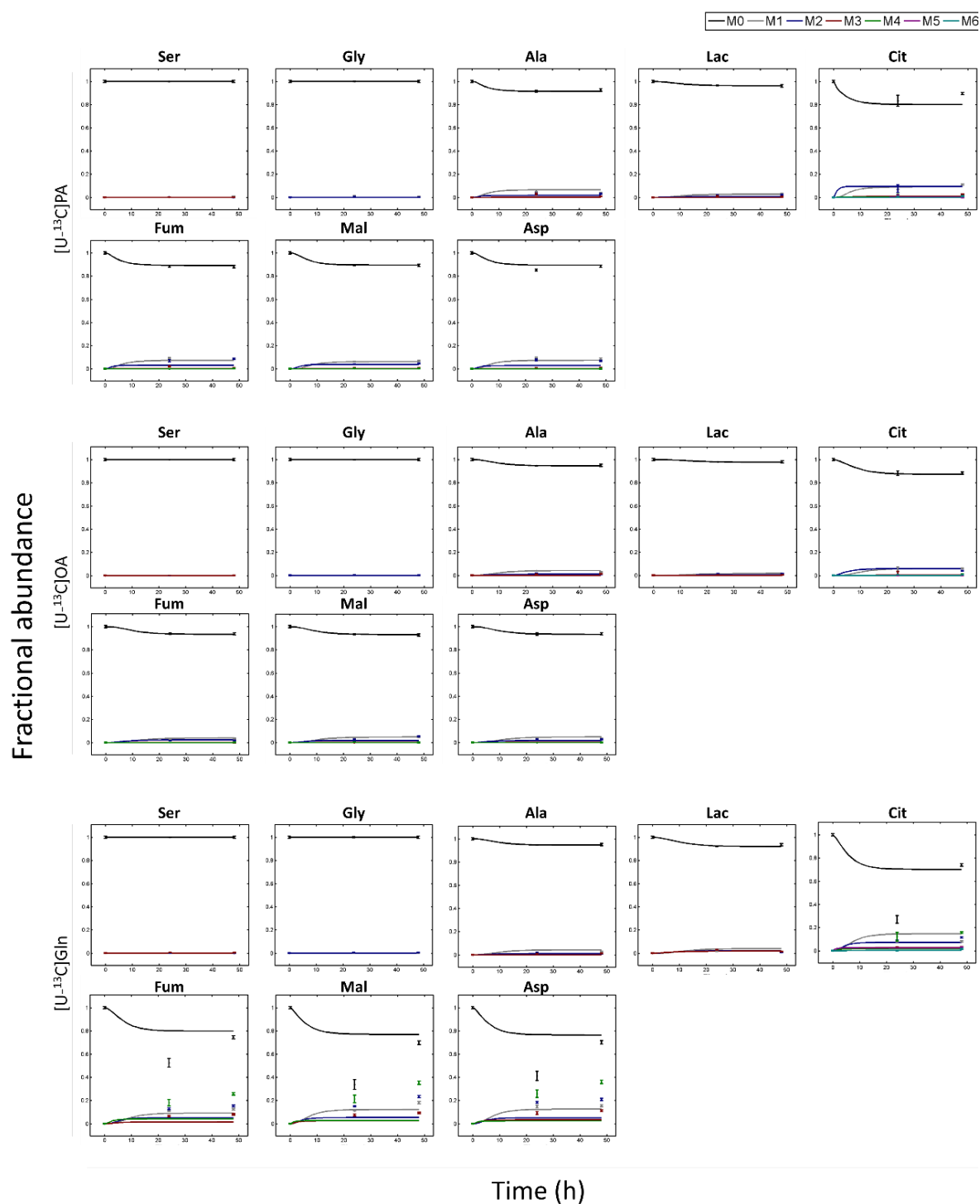
## 5. Appendix



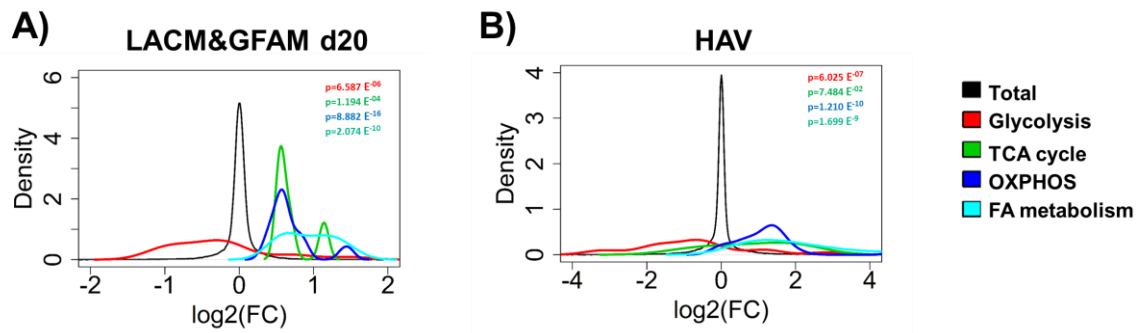
**Figure A-4.1. Experimental and simulated intracellular  $^{13}\text{C}$ -labelling dynamics in GLCM condition using  $[1,2-^{13}\text{C}]\text{GLC}$  and  $[\text{U}-^{13}\text{C}]\text{GLN}$ .** Circle markers correspond to GC-MS measurements corrected for natural isotope abundance. Lines correspond to fitted MIDFs from nonstationary  $^{13}\text{C}$ -MFA flux estimation of parallel labelling experiments.



**Figure A-4.2. Experimental and simulated intracellular  $^{13}\text{C}$ -labelling dynamics in GFAM condition using  $[\text{U-}^{13}\text{C}]\text{GAL}$ ,  $[\text{U-}^{13}\text{C}]\text{PA}$ ,  $[\text{U-}^{13}\text{C}]\text{JOA}$  and  $[\text{U-}^{13}\text{C}]\text{Gln}$ .** Circle markers correspond to GC-MS measurements corrected for natural isotope abundance. Lines correspond to fitted MIDs from nonstationary  $^{13}\text{C}$ -MFA flux estimation of parallel labelling experiments.

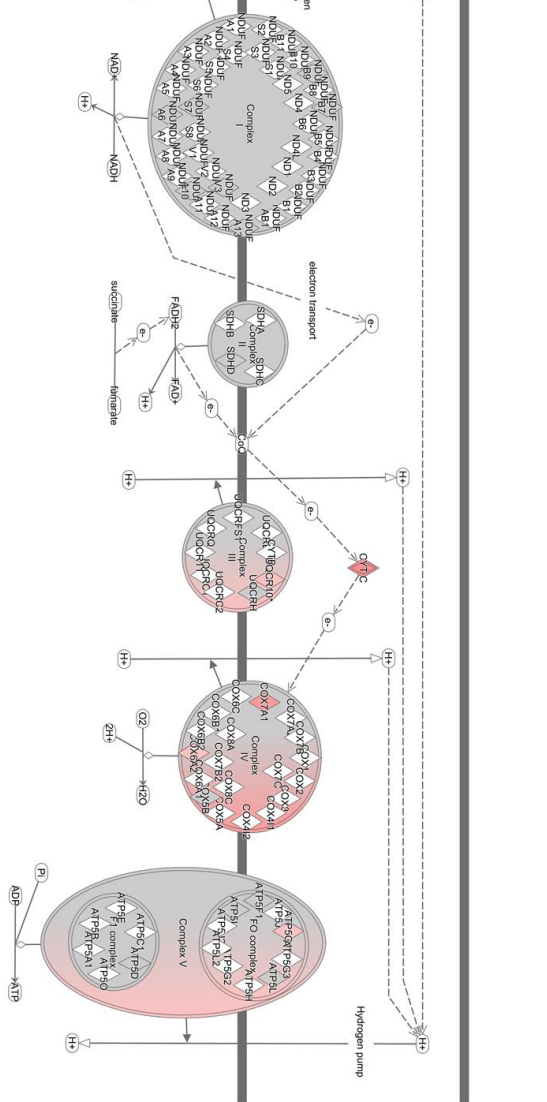


**Figure A-4.3. Experimental and simulated intracellular  $^{13}\text{C}$ -labelling dynamics in FAM condition using  $[\text{U}-^{13}\text{C}]\text{PA}$ ,  $[\text{U}-^{13}\text{C}]\text{OA}$  and  $[\text{U}-^{13}\text{C}]\text{Gln}$ .** Circle markers correspond to GC-MS measurements corrected for natural isotope abundance. Lines correspond to fitted MIDs from nonstationary  $^{13}\text{C}$ -MFA flux estimation of parallel labelling experiments.



**Figure A-4.4. Density Plots generated with fold change in expression of genes from representative metabolic categories. A) LACM&GFAM d20 and B) HAV.** X axis indicates log<sub>2</sub> fold change in gene expression. Black line indicates expression of all genes. Coloured lines toward the left and right side of the black line indicate down-regulation and up-regulation of pathways, respectively.

# GLCM d20



# GFAM d20

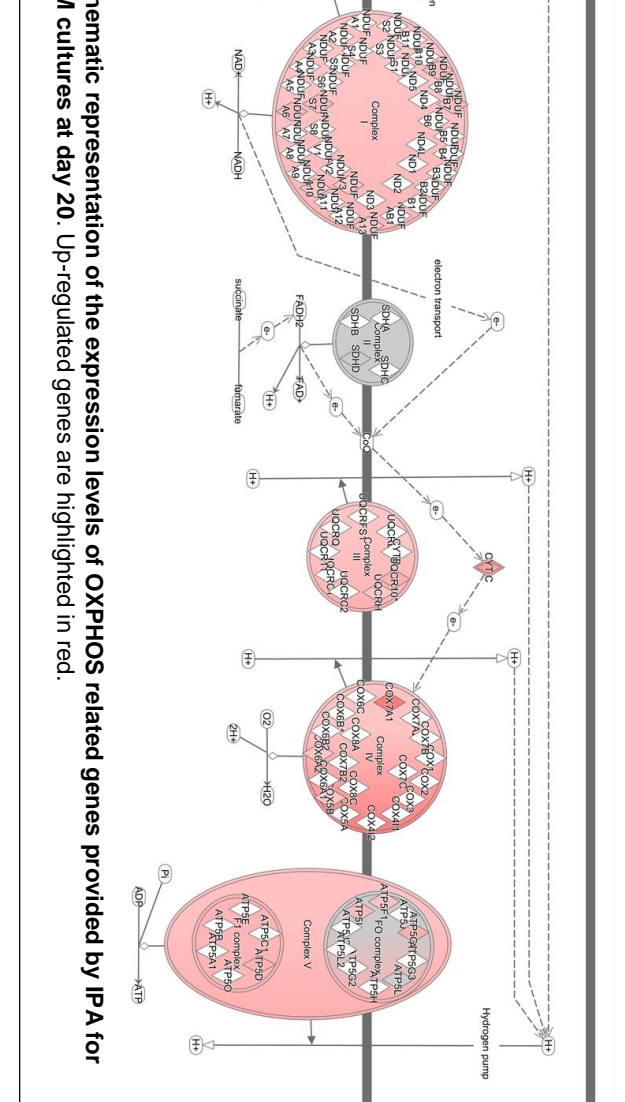
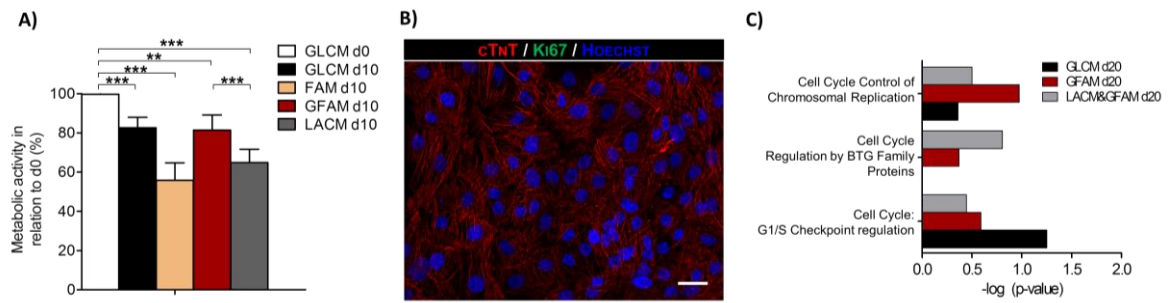


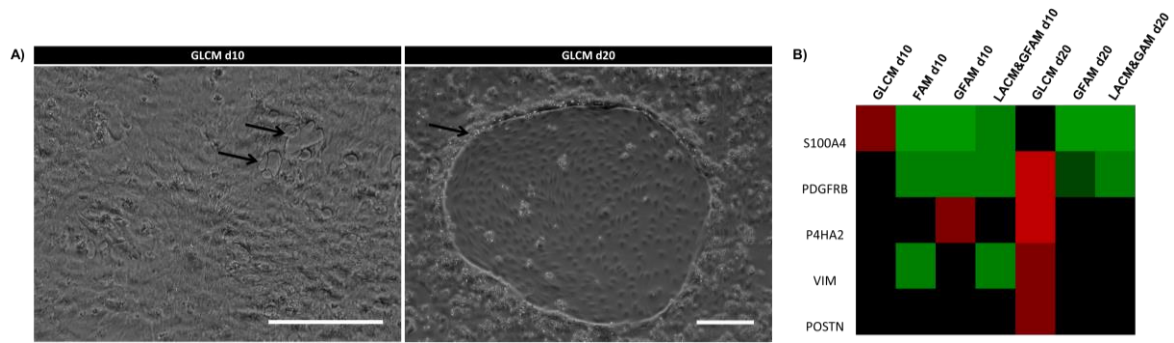
Figure A-4.5. Schematic representation of the expression levels of OXPHOS related genes provided by IPA for GLCM and GFAM cultures at day 20. Up-regulated genes are highlighted in red.



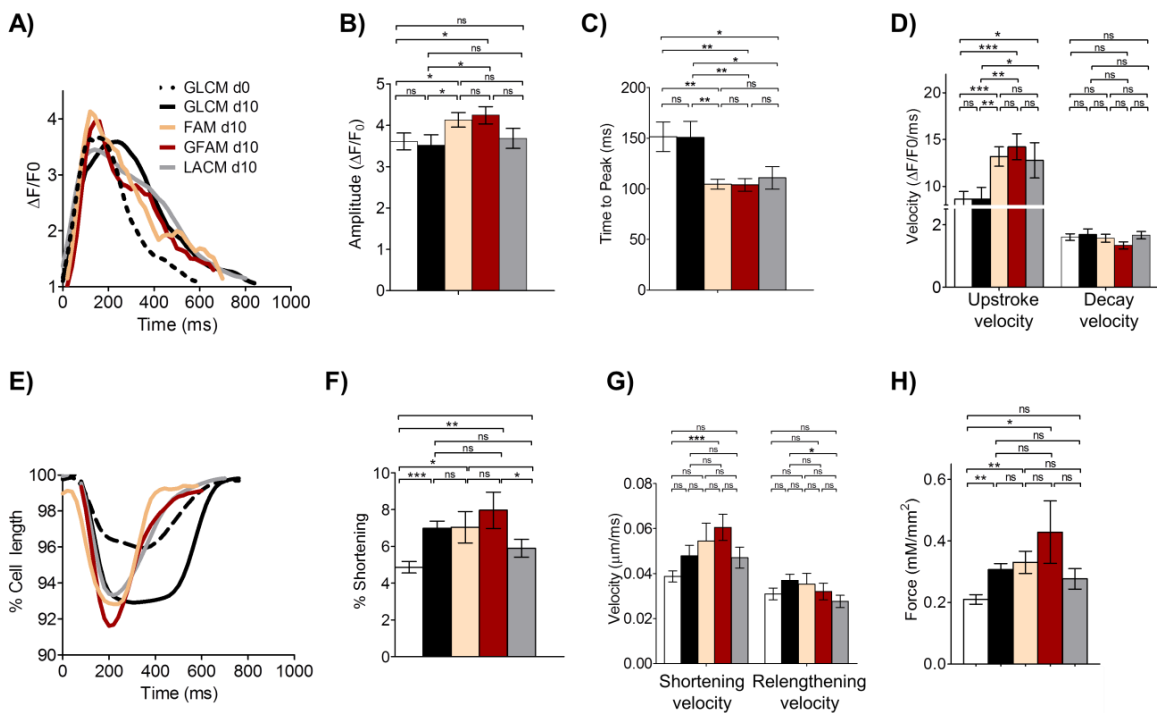
**Figure A-4.6. Impact of culture media composition on metabolic activity and proliferative capacity. A)** Metabolic activity at day 0 and day 10 in all conditions was assessed with PrestoBlue. **B)** Representative image of immature hiPSC-CMs (at day 0) immunostained for cardiac troponin-T (cTnT) revealing the absence of Ki67+ cells (green). Nuclei (blue) were stained with Hoechst 33342. Scale bars=30 μm. **C)** Adjusted P-value determined by IPA reflecting non-statistically significant enrichment of cell-cycle related pathways in all culture condition.



**Figure A-4.7. Impact of culture media composition and culture time on the expression of genes related with extracellular matrix composition in hiPSC-CMs cultivated in different culture media.** Heat map of differentially expressed genes. Colour gradient indicates gene expression fold-change values of all culture conditions tested compared with d0. Green and red represent down- and up- regulation, respectively.

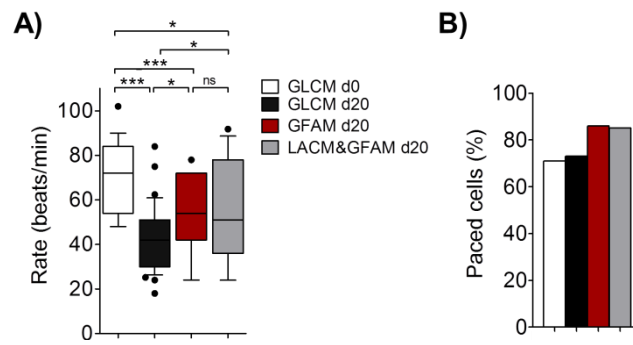


**Figure A-4.8. hiPSC-CM culture in GLCM showed up-regulation of fibroblastic markers.** **A)** Phase contrast microscope photos. The arrows highlight the appearance of zones with fibroblast-like cells at day 10 (left panel) and day 20 (right panel). Scale bars=100 $\mu$ m. **B)** Heatmap reflecting the up-regulation of fibroblast markers (at day 20) in GLCM cultures.



**Figure A-4.9. Impact of metabolic manipulation in hiPSC-CM functionality.** hiPSC-CMs were analysed in terms of calcium signalling profiles (**A-D**) and contractile performance (**E-H**), before (white) and after 10 days of culture in different culture medium (GLCM-black, LACM -grey, GFAM-red and FAM). Calcium transient kinetic was evaluated by loading the hiPSC-CMs with the intracellular calcium indicator Fluo-4 AM: **A)** Representative calcium transients.  $F/F_0$ : change of fluorescence signal over background fluorescence; **B)** Calcium transient amplitude ( $F/F_0$ ); **C)** Time to peak. **D)** Average upstroke and decay velocities.  $n = 24-35$  cells per condition. Contractile kinetics for each culture condition is described in: **E)** Representative contraction curves for each culture condition, reflecting changes in the percentage of cell length. **F)** Percentage of shortening; **G)** Average shortening and relengthening velocities.  $n = 15-22$  cells per condition. **H)** Maximum contractile force generated.  $n = 8-17$  cells per condition. Data are represented as mean $\pm$ SEM. \* $p < 0.05$ ; \*\* $p < 0.01$ ; \*\*\* $p < 0.001$ ; ns, not significant.





**Figure A-4.10. Impact of metabolic manipulation in beating rate and paced capacity. A)** Boxplot depicting the beating rate of hiPSC-CMs before (white) and after 20 days in culture in GLCM (black), LACM&GFAM (grey) and GFAM (red). Whiskers: 10-90 percentile. Outliers are plotted as individual points. **B)** Percentage of cells at each culture condition that was able to be paced after electrical stimulation at 1Hz.

**Table A-4.1. Metabolic network reactions and simulated fluxes determined by nonstationary <sup>13</sup>C-MFA.** Flux values are shown in units of nmol/(106cell.h). Negative flux values indicate that net direction is reverse to the direction indicated. LB – lower bound; UB – upper bound.

Equation	GLCM d20			FAM d10			GFAM d20		
	Value	LB	UB	Value	LB	UB	Value	LB	UB
v1 G6P <-> F6P	220.5	[ 150 ; 347.1 ]		0	[ 0 ; 0 ]		3.9	[ 1.8 ; 5.4 ]	
v2 F6P -> FBP	242.9	[ 165 ; 326.2 ]		0	[ 0 ; 0 ]		21.6	[ 15.9 ; 22.3 ]	
v3 FBP <-> DHAP + GAP	242.9	[ 165 ; 326.2 ]		0	[ 0 ; 0 ]		21.6	[ 15.9 ; 22.3 ]	
v4 DHAP <-> GAP	242.9	[ 165 ; 326.2 ]		0	[ 0 ; 0 ]		21.6	[ 15.9 ; 22.3 ]	
v5 GAP <-> 3PG	497.1	[ 338.4 ; 660.4 ]		0	[ 0 ; 0 ]		52	[ 38.1 ; 54 ]	
v6 3PG <-> PEP	496.9	[ 334.3 ; 658.4 ]		0	[ 0 ; 0 ]		49.7	[ 36.8 ; 53.2 ]	
v7 PEP -> Pyr.c	496.9	[ 334.3 ; 658.4 ]		0	[ 0 ; 0 ]		49.7	[ 36.8 ; 53.2 ]	
v8 Pyr.c <-> Pyr.m	5.6	[ 1.4 ; 8.6 ]		109.2	[ 106.3 ; 109.3 ]		72.4	[ 56.3 ; 75.6 ]	
v9 G6P -> P5P + CO2	33.7	[ 0 ; 50.2 ]		0	[ 0 ; 0 ]		26.5	[ 18.8 ; 29.2 ]	
v10 P5P + P5P <-> GAP + S7P	11.2	[ 0 ; 16.7 ]		0	[ 0 ; 0 ]		8.8	[ 6.3 ; 9.7 ]	
v11 S7P + GAP <-> E4P + F6P	11.2	[ 0 ; 16.7 ]		0	[ 0 ; 0 ]		8.8	[ 6.3 ; 9.7 ]	
v12 E4P + P5P <-> GAP + F6P	11.2	[ 0 ; 16.7 ]		0	[ 0 ; 0 ]		8.8	[ 6.3 ; 9.7 ]	
v13 Pyr.c <-> Lac	491.4	[ 336.4 ; 651.4 ]		0	[ 0 ; 0 ]		0	[ 0 ; 0 ]	
v14 Pyr.c <-> Ala	0	[ -7.8 ; 14 ]		0	[ 0 ; 0 ]		-11	[ -12.3 ; -9.1 ]	
v15 Pyr.m -> AcCoA.m + CO2	5.6	[ 2.6 ; 8.6 ]		30.3	[ 30.2 ; 30.3 ]		72.4	[ 54.8 ; 75.3 ]	
v16 OAA.m + AcCoA.m -> Cit.m	14.1	[ 6.3 ; 21.6 ]		55.4	[ 55.3 ; 55.4 ]		88.5	[ 66.5 ; 92.2 ]	
v17 Cit.m <-> AKG + CO2	14.1	[ 6.4 ; 20.3 ]		22.1	[ 22.1 ; 22.2 ]		88.5	[ 66.7 ; 92.1 ]	
v18 AKG -> SucCoA + CO2	14.7	[ 6.9 ; 27.2 ]		43.3	[ 43.2 ; 43.4 ]		95.7	[ 71.1 ; 100.1 ]	
v19 SucCoA <-> Suc	14.7	[ 6.9 ; 27.2 ]		43.3	[ 43.2 ; 43.4 ]		95.7	[ 71.1 ; 100.1 ]	
v20 Suc <-> Fum.m	14.7	[ 6.8 ; 26.7 ]		45.7	[ 45.6 ; 45.9 ]		95.7	[ 72 ; 99.4 ]	
v21 Fum.m <-> Mal.m	14.7	[ 4 ; 22.8 ]		52.1	[ 52.0 ; 52.2 ]		95.7	[ 72.2 ; 99.3 ]	
v22 Mal.m <-> OAA.m	14.1	[ 6.3 ; 21.4 ]		-23.5	[ -23.7 ; -23.4 ]		88.5	[ 66.4 ; 91.5 ]	
v23 Mal.c -> Pyr.c + CO2	0	[ 0 ; 4.2 ]		108.9	[ 108.7 ; 109.5 ]		7.2	[ 4.7 ; 8.3 ]	
v24 Pyr.m + CO2 -> OAA.m	0	[ 0 ; 0 ]		78.9	[ 78.4 ; 79.4 ]		0	[ 0 ; 0.5 ]	
v25 Gln <-> Glu	1	[ 0.4 ; 1.7 ]		3.8	[ 3.6 ; 3.9 ]		2.6	[ 1.9 ; 2.7 ]	
v26 AKG <-> Glu	-0.6	[ -6.4 ; -0.3 ]		-21.2	[ -22.8 ; -20.2 ]		-7.2	[ -8.4 ; -4.8 ]	
v27 Asn <-> Asp	0	[ 0 ; 0 ]		0	[ 0 ; 0 ]		0	[ 0 ; 0 ]	
v28 3PG -> Ser	0.2	[ 0 ; 13.2 ]		0	[ 0 ; 0 ]		2.3	[ 0.7 ; 3.8 ]	
v29 Ser -> Pyr.c	0	[ 0 ; 8.3 ]		0.3	[ 0.2 ; 0.3 ]		4.5	[ 1.1 ; 7 ]	
v30 Ser <-> Gly + C1	-1.8	[ -4.1 ; 0 ]		-2.4	[ -2.4 ; -2.4 ]		-0.3	[ -2 ; 0 ]	
v31 Glu <-> Pro	0	[ -4.4 ; 3.5 ]		-10.5	[ -10.5 ; -10.5 ]		-1.4	[ -4.1 ; 1.4 ]	
v32 Val + CO2 -> Suc + CO2 + CO2	0	[ 0 ; 0.1 ]		0	[ 0 ; 0 ]		0	[ 0 ; 0.5 ]	
v33 Ile + CO2 -> Suc + AcCoA.m + CO2	0	[ 0 ; 0.1 ]		0	[ 0 ; 0 ]		0	[ 0 ; 0.5 ]	
v34 Leu + CO2 -> AcCoA.m + AcCoA.m + AcCoA.m + CO2	2.2	[ 1.2 ; 3.3 ]		0	[ 0 ; 0 ]		1.6	[ 0.1 ; 2.6 ]	
v35 Thr -> AcCoA.m + Gly	0	[ 0 ; 1.6 ]		3.9	[ 3.9 ; 4.0 ]		0.3	[ 0.1 ; 0.6 ]	
v36 Phe -> Tyr	0	[ 0 ; 0.1 ]		0	[ 0 ; 0 ]		0	[ 0 ; 0.4 ]	
v37 Tyr -> Fum.m + AcCoA.m + AcCoA.m + CO2	0	[ 0 ; 0.1 ]		6.4	[ 6.3 ; 6.4 ]		0	[ 0 ; 0.4 ]	
v38 Met + Ser + CO2 -> Suc + Cys.snk + CO2 + C1	0	[ 0 ; 0 ]		2.4	[ 2.4 ; 2.5 ]		0	[ 0 ; 0.4 ]	
v39 Lys -> CO2 + CO2 + AcCoA.m + AcCoA.m	0.9	[ 0 ; 1.8 ]		0	[ 0 ; 0 ]		0	[ 0 ; 1.5 ]	
v40 His -> Glu + C1	1.8	[ 0 ; 4.2 ]		0	[ 0 ; 0 ]		0.3	[ 0 ; 2 ]	
v41 Arg -> Glu + Urea.snk	59.8	[ 0 ; Inf ]		0	[ 0 ; 0 ]		3.6	[ 0 ; 4.1 ]	
v42 Glu + CO2 -> Arg	64	[ 0.7 ; Inf ]		0	[ 0 ; 0 ]		2.7	[ 0 ; 2.9 ]	
v43 Glc.ext -> G6P	254.2	[ 178 ; 326.1 ]		0	[ 0 ; 0 ]		0	[ 0 ; 0.2 ]	

Metabolic substrate availability controls the maturation of hiPSC-CM

<b>v44</b> Lac.ext <-> Lac	-491.4 [ -651.4 ; -336.4 ]	0 [ 0 ; 0 ]	0 [ 0 ; 0 ]
<b>v45</b> Ala.ext <-> Ala	0 [ -14 ; 7.8 ]	0 [ 0 ; 0 ]	11 [ 9.1 ; 12.3 ]
<b>v46</b> Gln.ext -> Gln	1 [ 0.4 ; 1.7 ]	3.8 [ 3.8 ; 3.8 ]	2.6 [ 1.9 ; 2.7 ]
<b>v47</b> Glu.ext <-> Glu	2 [ -1.2 ; 5.8 ]	6.9 [ 6.9 ; 6.9 ]	2.1 [ -0.2 ; 4.4 ]
<b>v48</b> Ser.ext <-> Ser	-1.9 [ -9.7 ; 0.8 ]	0.3 [ 0.2 ; 0.4 ]	1.9 [ 0.7 ; 3.0 ]
<b>v49</b> Gly.ext <-> Gly	1.8 [ -1.6 ; 4.1 ]	-1.5 [ -1.6 ; -1.4 ]	-0.1 [ -0.6 ; 1.6 ]
<b>v50</b> Pro.ext <-> Pro	0 [ -3.5 ; 4.4 ]	10.5 [ 10.5 ; 10.5 ]	1.4 [ -1.4 ; 4.1 ]
<b>v51</b> Val.ext -> Val	0 [ 0 ; 0.1 ]	0 [ 0 ; 0 ]	0 [ 0 ; 0.5 ]
<b>v52</b> Ile.ext -> Ile	0 [ 0 ; 0.1 ]	0 [ 0 ; 0 ]	0 [ 0 ; 0.5 ]
<b>v53</b> Leu.ext -> Leu	2.2 [ 1.2 ; 3.3 ]	0 [ 0 ; 0 ]	1.6 [ 0.1 ; 2.6 ]
<b>v54</b> Thr.ext -> Thr	0 [ 0 ; 1.6 ]	3.9 [ 3.9 ; 4 ]	0.3 [ 0.1 ; 0.6 ]
<b>v55</b> Phe.ext -> Phe	0 [ 0 ; 0.1 ]	0 [ 0 ; 0 ]	0 [ 0 ; 0.4 ]
<b>v56</b> Tyr.ext -> Tyr	0 [ 0 ; 0.1 ]	6.4 [ 6.3 ; 6.4 ]	0 [ 0 ; 0.3 ]
<b>v57</b> Met.ext -> Met	0 [ 0 ; 0 ]	2.4 [ 2.4 ; 2.5 ]	0 [ 0 ; 0.4 ]
<b>v58</b> Lys.ext -> Lys	0.9 [ 0 ; 1.8 ]	0 [ 0 ; 0 ]	0 [ 0 ; 1.5 ]
<b>v59</b> His.ext -> His	1.8 [ 0 ; 4.2 ]	0 [ 0 ; 0 ]	0.3 [ 0 ; 2 ]
<b>v60</b> Arg.ext <-> Arg	-4.2 [ -7 ; -1.3 ]	0 [ 0 ; 0 ]	0.9 [ -2.4 ; 3.8 ]
<b>v61</b> Asp <-> OAA.c	-0.6 [ -1.8 ; -0.3 ]	0 [ 0 ; 0 ]	0 [ -1 ; 0 ]
<b>v62</b> Cit.c -> OAA.c + AcCoA.c	0 [ 0 ; 0.1 ]	33.3 [ 33.2 ; 33.3 ]	0 [ 0 ; 1.8 ]
<b>v63</b> CO2.ext <-> CO2	-5.9 [ -90 ; Inf ]	-132.1 [ -132.2 ; -132.1 ]	-287.8 [ -303.4 ; -213.4 ]
<b>v64</b> AcCoA.c -> FA.ext	0 [ 0 ; 0.1 ]	33.3 [ 33.2 ; 33.3 ]	0 [ 0 ; 1.8 ]
<b>v65</b> AP.ext -> AP.c	0 [ 0 ; 0 ]	1.9 [ 1.9 ; 1.9 ]	0.7 [ 0.5 ; 0.7 ]
<b>v66</b> AP.m -> 8 x AcCoA.m	0 [ 0 ; 0 ]	8x0.6 [ 8x0.6 ; 8x0.7 ]	8x0.7 [ 8x0.5 ; 8x0.7 ]
<b>v67</b> AO.ext -> AO.c	0 [ 0 ; 0 ]	1.7 [ 1.7 ; 2.3 ]	0.6 [ 0.5 ; 0.7 ]
<b>v68</b> AO.m -> 9 x AcCoA.m	0 [ 0 ; 0 ]	9x0.4 [ 9x0.4 ; 9x1.5 ]	9x0.6 [ 9x0.5 ; 9x0.6 ]
<b>v69</b> Gal.ext -> G6P	0 [ 0 ; 0 ]	0 [ 0 ; 0 ]	30.4 [ 22 ; 32.1 ]
<b>v70</b> Cit.c -> Cit.snk	0 [ 0 ; 1.9 ]	0 [ 0 ; 0 ]	0 [ 0 ; 1.5 ]
<b>v71</b> Mal.m <-> Mal.c	0.6 [ 0.2 ; 4.4 ]	75.6 [ 75.3 ; 75.7 ]	7.2 [ 4.5 ; 8.3 ]
<b>v72</b> 0*Mal.c -> Mal.s	3.9 [ 0 ; 100 ]	0 [ 0 ; 6.4 ]	0.5 [ 0 ; 100 ]
<b>v73</b> 0*Mal.m -> Mal.s	96.1 [ 0 ; 100 ]	100 [ 93.6 ; 100 ]	99.5 [ 0 ; 100 ]
<b>v74</b> Mal.s -> Sink	100 [ 100 ; 100 ]	100 [ 100 ; 100 ]	100 [ 100 ; 100 ]
<b>v75</b> 0*Fum.c -> Fum.s	14 [ 6.2 ; 21.6 ]	0 [ 0 ; 0.2 ]	32.2 [ 28.9 ; 36.3 ]
<b>v76</b> 0*Fum.m -> Fum.s	86 [ 78.4 ; 93.8 ]	100 [ 99.8 ; 100 ]	67.8 [ 63.7 ; 71.1 ]
<b>v77</b> Fum.s -> Sink	100 [ 100 ; 100 ]	100 [ 100 ; 100 ]	100 [ 100 ; 100 ]
<b>v78</b> Mal.c <-> Fum.c	0 [ 0 ; 0 ]	0 [ 0 ; 0 ]	0 [ 0 ; 0 ]
<b>v79</b> OAA.c <-> Mal.c	-0.6 [ -1.9 ; -0.2 ]	33.3 [ 33.3 ; 33.3 ]	0 [ -1 ; 0 ]
<b>v80</b> Asp.ext <-> Asp	-0.6 [ -1.8 ; -0.3 ]	0 [ 0 ; 0 ]	0 [ -1 ; 0 ]
<b>v81</b> 0*Cit.c -> Cit.s	0 [ 0 ; 100 ]	0 [ 0 ; 100 ]	83.5 [ 0 ; 100 ]
<b>v82</b> 0*Cit.m -> Cit.s	100 [ 0 ; 100 ]	100 [ 0 ; 100 ]	16.5 [ 0 ; 100 ]
<b>v83</b> Cit.s -> Sink	100 [ 100 ; 100 ]	100 [ 100 ; 100 ]	100 [ 100 ; 100 ]
<b>v84</b> Cit.c <-> Cit.m	0 [ -2 ; 0 ]	-33.3 [ -33.3 ; -33.2 ]	0 [ -1.6 ; 0 ]
<b>v85</b> AP.c -> AP.m	0 [ 0 ; 0 ]	0.6 [ 0.6 ; 0.7 ]	0.7 [ 0.5 ; 0.7 ]
<b>v86</b> AP.c -> AP.snk	0 [ 0 ; 0 ]	0.4 [ 0.4 ; 1.5 ]	0.6 [ 0.5 ; 0.6 ]
<b>v87</b> AO.c -> AO.m	0 [ 0 ; 0 ]	1.3 [ 1.2 ; 1.3 ]	0 [ 0 ; 0.1 ]
<b>v88</b> AO.c -> AO.snk	0 [ 0 ; 0 ]	1.3 [ 1.3 ; 3.5 ]	0 [ 0 ; 0.1 ]

Abbreviations: G6P. glucose-6-phosphate; F6P. fructose-6-phosphate; FBP. fructose-1,6-bisphosphate; DHAP. Dihydroxyacetone phosphate; GAP. glyceraldehyde 3-phosphate; 3PG. 3-Phosphoglyceric acid; PEP. phosphoenolpyruvate; Pyr. pyruvate; P5P. pentose-5-phosphate; CO2. carbon dioxide; S7P. sedoheptulose-7-phosphate; E4P. erythrose 4-phosphate; Lac. lactate; Ala. alanine; AcCoA. acetyl-CoA; OAA. oxaloacetate;

Cit. citrate;  $\alpha$ KG.  $\alpha$ -ketoglutarate; Suc. succinate; Fum. fumarate; Mal. malate; Glu. glutamate; Pro. proline; Val. valine; Ile. isoleucine; Leu. leucine; Thr. threonine; Phe. phenylalanine; Tyr. tyrosine. Met. methionine; Ser. serine; Cys. cyteine; lys. lysine; His. histidine; Arg. arginine; Gln. glutamine; Asp. aspartate; FA. fatty acid; PA. palmitic acid; AO. oleic acid; c. cytosolic; m. mitochondrial; s. sink.

Fumarate and succinate were considered as symmetric molecules during flux estimation. Compartmentalization of Pyr, Fum, Mal, Cit, AcCoA, OAA, AO and AP pools were taken in account in the model. Sink pools were considered for metabolites that could not be balanced.

Balanced metabolite pools: G6P, F6P, FBP, DHAP, GAP, 3PG, PEP, Pyr.c, Pyr.m, P5P, CO 2, S7P, E4P, Lac, Ala, AO.c, AO.m, AP.c, AP.m, AcCoA.c, AcCoA.m, OAA.c, OAA.m, Pyr.c, Pyr.m, Cit.c, Cit.m, AKG, SucCoA, Suc, Fum.c, Fum.m, Mal.c, Mal.m, Gln, Glu, Asn, Asp, Ser, Gly, C1, Pro, Val, Ile, Leu, Thr, Phe, Tyr, Met, Lys, His, Arg.

Unbalanced metabolite pools: AO.ext, AP.ext, Ao.snk, Ap.snk, Cit.snk, FA.ext, CO 2.ext, Glc.ext, Gal.ext, Lac.ext, Ala.ext, Gln.ext, Glu.ext, Asp.ext, Asn.ext, Ser.ext, Gly.ext, Pro.ext, Val.ext, Ile.ext, Leu.ext, Thr. ext, Phe.ext, Tyr.ext, Met.ext, Lys.ext, His.ext, Arg.ext, Cys.snk, Urea.snk.

**Table A-4.2. Comparison of contractility kinetics and contractile force generated by cells cultivated in LACM&GFAM at d10 and d20.** Data are represented as mean $\pm$ SD. \* $p$ <0.05; \*\* $p$ <0.01.

	LACM&GFAM d10	LACM&GFAM d20	Statistical Analysis
<b>Force (mM/mm<sup>2</sup>)</b>	0.28 $\pm$ 0.10	0.48 $\pm$ 0.22	*
<b>% Shortening</b>	5.90 $\pm$ 2.17	8.42 $\pm$ 3.30	*
<b>Maximum shortening velocity (<math>\mu</math>m/ms)</b>	0.05 $\pm$ 0.02	0.07 $\pm$ 0.03	*
<b>Maximum relengthening velocity (<math>\mu</math>m/ms)</b>	0.03 $\pm$ 0.01	0.05 $\pm$ 0.02	**

## 6. Acknowledgments

We thank Dr Ana Filipa Rodrigues and Dr Inês Isidro for support in transcriptome analysis and Dr Madalena Carido and Dr Erin Tranfield for performing TEM. This work was supported by FP7 European Union Project Cardio Repair European Multidisciplinary Initiative (HEALTH-2009\_242038); Fundação para a Ciência e Tecnologia (FCT)-funded projects CardioRegen (HMSP-ICT/0039/2013) and CARDIOSTEM (MITPTB/ECE/0013/2013); CC was supported by FCT Grant SFRH/BD/51573/2011.

## 7. References

- Abel, E.D., and Doenst, T. (2011). Mitochondrial adaptations to physiological vs. pathological cardiac hypertrophy. *Cardiovasc. Res.* 90, 234–242.
- Aguer, C., Gambarotta, D., Mailloux, R.J., Moffat, C., Dent, R., McPherson, R., and Harper, M.E. (2011). Galactose enhances oxidative metabolism and reveals mitochondrial dysfunction in human primary muscle cells. *PLoS One* 6.
- Antoniewicz, M.R., Kelleher, J.K., and Stephanopoulos, G. (2006). Determination of confidence intervals of metabolic fluxes estimated from stable isotope measurements. *Metab. Eng.* 8, 324–337.
- Bedada, F.B., Chan, S.S.K., Metzger, S.K., Zhang, L., Zhang, J., Garry, D.J., Kamp, T.J., Kyba, M., and Metzger, J.M. (2014). Acquisition of a quantitative, stoichiometrically conserved ratiometric marker of maturation status in stem cell-derived cardiac myocytes. *Stem Cell Reports* 3, 594–605.
- Borradaile, N.M., and Schaffer, J.E. (2005). Lipotoxicity in the heart. *Curr. Hypertens. Rep.* 7, 412–417.

- Boyle, J. (2005). *Lehninger principles of biochemistry* (4th ed.): Nelson, D., and Cox, M.
- Carinhas, N., Bernal, V., Monteiro, F., Carrondo, M.J.T., Oliveira, R., and Alves, P.M. (2010). Improving baculovirus production at high cell density through manipulation of energy metabolism. *Metab. Eng.* 12, 39–52.
- Carinhas, N., Pais, D.A.M., Koshkin, A., Fernandes, P., Coroadinha, A.S., Carrondo, M.J.T., Alves, P.M., and Teixeira, A.P. (2016). Metabolic flux profiling of MDCK cells during growth and canine adenovirus vector production. *Sci. Rep.* 6, 1–11.
- Carinhas, N., Koshkin, A., Pais, D.A.M., Alves, P.M., and Teixeira, A.P. (2017). (13) C-metabolic flux analysis of human adenovirus infection: Implications for viral vector production. *Biotechnol. Bioeng.* 114, 195–207.
- Carreño, J.E., Apablaza, F., Ocaranza, M.P., and Jalil, J.E. (2006). Cardiac hypertrophy: molecular and cellular events. *Rev. Esp. Cardiol.* 59, 473–486.
- Chan, Y.-C., Ting, S., Lee, Y.-K., Ng, K.-M., Zhang, J., Chen, Z., Siu, C.-W., Oh, S.K.W., and Tse, H.-F. (2013). Electrical stimulation promotes maturation of cardiomyocytes derived from human embryonic stem cells. *J. Cardiovasc. Transl. Res.* 6, 989–999.
- Correia, C., Serra, M., Espinha, N., Sousa, M., Brito, C., Burkert, K., Zheng, Y., Hescheler, J., Carrondo, M.J.T., Sarić, T., et al. (2014). Combining Hypoxia and Bioreactor Hydrodynamics Boosts Induced Pluripotent Stem Cell Differentiation Towards Cardiomyocytes. *Stem Cell Rev.* 10, 786–801.
- Correia, C., Koshkin, A., Carido, M., Espinha, N., Šarić, T., Lima, P.A., Serra, M., and Alves, P.M. (2016). Effective Hypothermic Storage of Human Pluripotent Stem Cell-Derived Cardiomyocytes Compatible With Global Distribution of Cells for Clinical Applications and Toxicology Testing. *Stem Cells Transl. Med.* 5, 658–669.
- Denning, C., Borgdorff, V., Crutchley, J., Firth, K.S.A., George, V., Kalra, S., Kondrashov, A., Hoang, M.D., Mosqueira, D., Patel, A., et al. (2015). Cardiomyocytes from human pluripotent stem cells: From laboratory curiosity to industrial biomedical platform. *Biochim. Biophys. Acta - Mol. Cell Res.* 1863, 1728–1748.
- Dott, W., Mistry, P., Wright, J., Cain, K., and Herbert, K.E. (2014). Modulation of mitochondrial bioenergetics in a skeletal muscle cell line model of mitochondrial toxicity. *Redox Biol.* 2, 224–233.
- Drawnel, F.M., Boccardo, S., Prummer, M., Delobel, F., Graff, A., Weber, M., Gérard, R., Badi, L., Kam-Thong, T., Bu, L., et al. (2014). Disease modeling and phenotypic drug screening for diabetic cardiomyopathy using human induced pluripotent stem cells. *Cell Rep.* 9, 810–820.
- Drosatos, K., and Schulze, P.C. (2013). Cardiac lipotoxicity: Molecular pathways and therapeutic implications. *Curr. Heart Fail. Rep.* 10, 109–121.
- Evans, R.M. (2004). PPARs and the complex journey to obesity. *Keio J. Med.* 53, 53–58.
- Feric, N.T., and Radisic, M. (2016). Maturing human pluripotent stem cell-derived cardiomyocytes in human engineered cardiac tissues. *Adv. Drug Deliv. Rev.* 96, 110–134.
- Frey, N., Katus, H.A., Olson, E.N., and Hill, J.A. (2004). Hypertrophy of the Heart: A New Therapeutic Target? *Circulation* 109, 1580–1589.
- Hazeltine, L.B., Simmons, C.S., Salick, M.R., Lian, X., Badur, M.G., Han, W., Delgado, S.M., Wakatsuki, T., Crone, W.C., Pruitt, B.L., et al. (2012). Effects of substrate mechanics on contractility of cardiomyocytes generated from human pluripotent stem cells. *Int. J. Cell Biol.*
- Heineke, J., and Molkentin, J.D. (2006). Regulation of cardiac hypertrophy by intracellular signalling pathways. *Nat. Rev. Mol. Cell Biol.* 7, 589–600.
- Kase, E.T., Nikolić, N., Bakke, S.S., Bogen, K.K., Aas, V., Thoresen, G.H., and Rustan, A.C. (2013). Remodeling of Oxidative Energy Metabolism by Galactose Improves Glucose Handling and Metabolic Switching in Human Skeletal Muscle Cells. *PLoS One* 8.
- Kijlstra, J.D., Hu, D., Mittal, N., Kausel, E., Van Der Meer, P., Garakani, A., and Domian, I.J. (2015). Integrated Analysis of Contractile Kinetics, Force Generation, and Electrical Activity in Single Human Stem Cell-Derived Cardiomyocytes. *Stem Cell Reports* 5, 1226–1238.
- Kim, C., Majdi, M., Xia, P., Wei, K.A., Talantova, M., Spiering, S., Nelson, B., Mercola, M., Chen,

- H.V., and Al, K.I.M.E.T. (2010). Non-cardiomyocytes influence the electrophysiological maturation of human embryonic stem cell-derived cardiomyocytes during differentiation. *Stem Cells Dev.* 19, 783–795.
- Kuppusamy, K.T., Jones, D.C., Sperber, H., Madan, A., Fischer, K. a., Rodriguez, M.L., Pabon, L., Zhu, W.-Z., Tulloch, N.L., Yang, X., et al. (2015). Let-7 family of microRNA is required for maturation and adult-like metabolism in stem cell-derived cardiomyocytes. *Proc. Natl. Acad. Sci.* 201424042.
- Lehman, J.J., Barger, P.M., Kovacs, A., Saffitz, J.E., Medeiros, D.M., and Kelly, D.P. (2000). Peroxisome proliferator – activated receptor  $\gamma$  coactivator-1 promotes cardiac mitochondrial biogenesis. *J. Clin. Invest.* 106, 847–856.
- Lieu, D.K., Fu, J.-D., Chiamvimonvat, N., Tung, K.C., McNerney, G.P., Huser, T., Keller, G., Kong, C.-W., and Li, R. a. (2013). Mechanism-Based Facilitated Maturation of Human Pluripotent Stem Cell-Derived Cardiomyocytes. *Circ. Arrhythmia Electrophysiol.* 6, 191–201.
- Lionetti, V., Stanley, W.C., and Recchia, F. a. (2011). Modulating fatty acid oxidation in heart failure. *Cardiovasc. Res.* 90, 202–209.
- Liu, J., Lieu, D.K., Siu, C.W., Fu, J., Tse, H., and Li, R.A. (2009). Facilitated maturation of  $Ca^{2+}$  handling properties of human embryonic stem cell-derived cardiomyocytes by calsequestrin expression. *Am. J. Physiol. Cell Physiol.* 297, C152-9.
- Lopaschuk, G.D., and Jaswal, J.S. (2010). Energy metabolic phenotype of the cardiomyocyte during development, differentiation, and postnatal maturation. *J. Cardiovasc. Pharmacol.* 56, 130–140.
- Lopaschuk, G.D., Ussher, J.R., Folmes, C.D.L., Jaswal, J.S., and STANLEY, W.C. (2010). Myocardial Fatty Acid Metabolism in Health and Disease. *Physiol. Rev.* 90, 207–258.
- Lundy, S.D., Zhu, W.-Z., Regnier, M., and Laflamme, M. (2013). Structural and Functional Maturation of Cardiomyocytes Derived From Human Pluripotent Stem Cells. *Stem Cells Dev.* 22, 1991–2002.
- Marroquin, L.D., Hynes, J., Dykens, J.A., Jamieson, J.D., and Will, Y. (2007). Circumventing the crabtree effect: Replacing media glucose with galactose increases susceptibility of hepG2 cells to mitochondrial toxicants. *Toxicol. Sci.* 97, 539–547.
- Mihic, A., Li, J., Miyagi, Y., Gagliardi, M., Li, S.-H., Zu, J., Weisel, R.D., Keller, G., and Li, R.-K. (2014). The effect of cyclic stretch on maturation and 3D tissue formation of human embryonic stem cell-derived cardiomyocytes. *Biomaterials* 35, 2798–2808.
- Nelson, D.L., and Cox, M.M. (2013). *Lehninger Principles of Biochemistry* 6th ed.
- Nemcová-fürstová, V., James, R.F.L., and Kovár, J. (2011). Inhibitory Effect of Unsaturated Fatty Acids on Saturated Fatty Acid-Induced Apoptosis in Human Pancreatic E -Cells: Activation of Caspases and ER Stress Induction. *Cell Physiol Biochem* 525–538.
- Oudit, G.Y., Kassiri, Z., Zhou, J., Liu, Q.C., Liu, P.P., Backx, P.H., Dawood, F., Crackower, M. a., Scholey, J.W., and Penninger, J.M. (2008). Loss of PTEN attenuates the development of pathological hypertrophy and heart failure in response to biomechanical stress. *Cardiovasc. Res.* 78, 505–514.
- Palchesko, R.N., Zhang, L., Sun, Y., and Feinberg, A.W. (2012). Development of Polydimethylsiloxane Substrates with Tunable Elastic Modulus to Study Cell Mechanobiology in Muscle and Nerve. *PLoS One* 7.
- Rana, P., Anson, B., Engle, S., and Will, Y. (2012). Characterization of human-induced pluripotent stem cell-derived cardiomyocytes: Bioenergetics and utilization in safety screening. *Toxicol. Sci.* 130, 117–131.
- Ribeiro, M.C., Tertoolen, L.G., Guadix, J. a, Bellin, M., Kosmidis, G., D’Aniello, C., Monshouwer-Kloots, J., Goumans, M.-J., Wang, Y.-L., Feinberg, A.W., et al. (2015). Functional maturation of human pluripotent stem cell derived cardiomyocytes in vitro--correlation between contraction force and electrophysiology. *Biomaterials* 51, 138–150.
- Riganti, C., Gazzano, E., Polimeni, M., Aldieri, E., and Ghigo, D. (2012). The pentose phosphate pathway: An antioxidant defense and a crossroad in tumor cell fate. *Free Radic. Biol. Med.* 53,

421–436.

Rosignol, R., Gilkerson, R., Aggeler, R., Yamagata, K., Remington, S.J., and Capaldi, R.A. (2004). Energy substrate modulates mitochondrial structures and oxidative capacity in cancer cells. *Cancer Res.* *64*, 985–993.

Ruan, J., Tulloch, N.L., Razumova, M. V, Saiget, M., Muskheli, V., Pabon, L., and Reinecke, H. (2016). Mechanical Stress Conditioning and Electrical Stimulation Promote Contractility and Force Maturation of Induced Pluripotent Stem Cell-Derived Human Cardiac Tissue. *Circulation* *134*, 1557–1567.

Ruwhof, C., and van der, L.A. (2000). Mechanical stress-induced cardiac hypertrophy: mechanisms and signal transduction pathways. *Cardiovasc Res* *47*, 23–37.

Sartiani, L., Bettiol, E., Stillitano, F., Mugelli, A., Cerbai, E., and Jaconi, M.E. (2007). Developmental changes in cardiomyocytes differentiated from human embryonic stem cells: a molecular and electrophysiological approach. *Stem Cells* *25*, 1136–1144.

Schindelin, J., Arganda-Carreras, I., Frise, E., Kaynig, V., Longair, M., Pietzsch, T., Preibisch, S., Rueden, C., Saalfeld, S., Schmid, B., et al. (2012). Fiji: an open-source platform for biological-image analysis. *Nat. Methods* *9*, 676–682.

Silva, M.M., Rodrigues, A.F., Correia, C., Sousa, M.F.Q., Brito, C., Coroadinha, A.S., Serra, M., and Alves, P.M. (2015). Robust Expansion of Human Pluripotent Stem Cells: Integration of Bioprocess Design With Transcriptomic and Metabolomic Characterization. *Stem Cells Transl. Med.* *4*, 731–742.

Simons, A.L., Orcutt, K.P., Madsen, J.M., Scarbrough, P.M., and Spitz, D.R. (2012). The Role of Akt Pathway Signaling in Glucose Metabolism and Metabolic Oxidative Stress. In *Oxidative Stress in Cancer Biology and Therapy*, pp. 21–46.

Tohyama, S., Hattori, F., Sano, M., Hishiki, T., Nagahata, Y., Matsuura, T., Hashimoto, H., Suzuki, T., Yamashita, H., Satoh, Y., et al. (2013). Distinct metabolic flow enables large-scale purification of mouse and human pluripotent stem cell-derived cardiomyocytes. *Cell Stem Cell* *12*, 127–137.

Uosaki, H., Cahan, P., Lee, D.I., Wang, S., Miyamoto, M., Fernandez, L., Kass, D. a., and Kwon, C. (2015). Transcriptional Landscape of Cardiomyocyte Maturation. *Cell Rep.* *13*, 1705–1716.

Venable, J.H., and Coggeshall, R. (1965). A Simplified Lead Citrate Stain for use in Electron Microscopy. *J. Cell Biol.* *25*, 407–408.

Ventura-Clapier, R., Garnier, A., and Veksler, V. (2008). Transcriptional control of mitochondrial biogenesis: The central role of PGC-1 $\alpha$ . *Cardiovasc. Res.* *79*, 208–217.

Wagner, a, Marc, a, Engasser, J.M., and Einsele, a (1991). Growth and Metabolism of Human Tumor Kidney-Cells on Galactose and Glucose. *Cytotechnology* *7*, 7–13.

Wen, J.-Y., Wei, C.-Y., Shah, K., Wong, J., Wang, C., and Chen, H.-S.V. (2015). Maturation-Based Model of Arrhythmogenic Right Ventricular Dysplasia Using Patient-Specific Induced Pluripotent Stem Cells. *Circ. J.* *79*, 1402–1408.

Woo Suk, A., and Antoniewicz, M.R. (2013). Parallel labeling experiments with [1,2-<sup>13</sup>C]glucose and [U-<sup>13</sup>C]glutamine provide new insights into CHO cell metabolism. *Metab. Eng.* *15*, 34–47.

Yang, X., Pabon, L., and Murry, C.E. (2014a). Engineering adolescence: Maturation of human pluripotent stem cell-derived cardiomyocytes. *Circ. Res.* *114*, 511–523.

Yang, X., Rodriguez, M., Pabon, L., Fischer, K. a., Reinecke, H., Regnier, M., Sniadecki, N.J., Ruohola-Baker, H., and Murry, C.E. (2014b). Tri-iodo-L-thyronine promotes the maturation of human cardiomyocytes-derived from induced pluripotent stem cells. *J. Mol. Cell. Cardiol.* *72*, 296–304.

Young, J.D. (2014). INCA: A computational platform for isotopically non-stationary metabolic flux analysis. *Bioinformatics* *30*, 1333–1335.

Zhang, M., Schulte, J.S., Heinick, A., Piccini, I., Rao, J., Quaranta, R., Zeuschner, D., Malan, D., Kim, K.-P., Röpke, A., et al. (2015). Universal Cardiac Induction of Human Pluripotent Stem Cells in 2D and 3D formats - Implications for In-Vitro Maturation. *Stem Cells* *33*, 1456–1469.





# 5

## **Effective hypothermic storage of human pluripotent stem cell derived cardiomyocytes compatible with global distribution of cells for clinical applications and toxicology testing**

This chapter was adapted from:

Correia, C., Koshkin, A., Carido, M., Espinha, N., Šarić, T., Lima, P.A., Serra, M., and Alves, P.M. (2016). Effective Hypothermic Storage of Human Pluripotent Stem Cell-Derived Cardiomyocytes Compatible With Global Distribution of Cells for Clinical Applications and Toxicology Testing. *Stem Cells Transl. Med.* 5, 658–669.

**Contents**

<b>1. Introduction</b> .....	<b>150</b>
<b>2. Methods</b> .....	<b>151</b>
2.1. CM layers Differentiation of mPSCs .....	151
2.2. CM layers Differentiation of hPSCs .....	152
2.3. Hypothermic storage of PSC-CM .....	152
2.4. Assessment of PSC-CM viability and metabolic activity after storage .....	153
2.5. Metabolite analysis .....	154
2.6. Assessment of PSC-CM structure and ultrastructure after hypothermic storage.....	154
2.7. Evaluation of aggregate size .....	155
2.8. Characterization of PSC-CMs after hypothermic storage.....	155
2.9. Assessment of PSC-CM function after hypothermic storage .....	156
2.10. Statistical analysis.....	158
<b>3. Results</b> .....	<b>158</b>
3.1. Impact of hypothermic storage on PSC-CM viability and metabolic activity.....	158
3.2. Effect of hypothermic storage on PSC-CM phenotype.....	163
3.3. Characterization of hiPSC-CM function after hypothermic storage .....	167
<b>4. Discussion</b> .....	<b>169</b>
<b>5. Appendix</b> .....	<b>172</b>
<b>6. Acknowledgments</b> .....	<b>174</b>
<b>7. References</b> .....	<b>174</b>

## **Abstract**

To fully explore the potential of human pluripotent stem cell-derived cardiomyocytes (hPSC-CMs) efficient methods for storage and shipment of these cells are required. Here, we evaluated the feasibility to cold store monolayers and aggregates of functional CMs obtained from different PSC lines using a fully-defined clinical compatible preservation formulation, and investigated the time frame that hPSC-CMs could be subjected to hypothermic storage.

We showed that 2D monolayers of hPSC-CMs can be efficiently stored at 4°C for 3 days without compromising cell viability. However, cell viability decreased when the cold storage interval was extended to 7 days. We demonstrated that hPSC-CMs are more resistant to prolonged hypothermic storage–induced cell injury in 3D aggregates than in 2D monolayers, showing high cell recoveries (>70%) after 7 days of storage. Importantly, hPSC-CMs maintained their typical (ultra)structure, gene and protein expression profile, electrophysiological profiles and drug responsiveness.

## 1. Introduction

The emerging potential of human pluripotent stem cell derived cardiomyocytes (hPSC-CM) in cell-based cardiac repair, patient-specific disease modelling and drug toxicity (Lundy et al., 2014; Sinnecker et al., 2014) is strongly pushing these cell-based products towards a global marketplace. Up to date, many efforts have been made in improving PSC expansion (Chen et al., 2014; Serra et al., 2010, 2012; Wang et al., 2014), CM-lineage differentiation and enrichment processes (Correia et al., 2014; Lundy et al., 2014; Mummery et al., 2012), however little attention has been given to methodologies and protocols to preserve and transport these cell products from the manufacturing site to the clinical setting, for immediate administration in patients, to research institutes or to biotechnology companies. The complexity is associated with the laborious and time-consuming differentiation protocols, as well as the inability of maintaining the differentiated non-replicative cells in culture for long periods of time, highlight the need for developing efficient strategies for preservation of PSC-CMs. The cryopreservation protocols are still highly inefficient, usually resulting in a substantial loss of cell viability and function (Abbasalizadeh and Baharvand, 2013; Healy et al., 2011). Additionally, the majority of these protocols use animal-derived components (*e.g.*, proteins, serum...) and/or toxic cryoprotective agents (CPAs, *e.g.*, DMSO) (Li and Ma, 2012) rendering them unsuitable for clinical applications. It has been demonstrated that serum residues in the therapeutic product can trigger adverse reactions in patients (Thirumala et al., 2009). Washing protocols are therefore required to remove CPAs, serum and cellular debris from therapeutic cells prior to patient administration (Li and Ma, 2012; Thirumala et al., 2009).

Hypothermic preservation can be an alternative to cryopreservation in short-term storage situations (*e.g.* to perform a inter- or trans-continental transport of the cells). During hypothermic storage, cells are maintained at temperatures that range between 4 and 10°C. These lower temperatures affect cell physiology namely by reducing their metabolism, energy storage degradation and oxygen demand (Rubinsky, 2003). Effective hypothermic preservation requires the use of preservation solutions that: i) provide optimal concentrations of ions and impermeable molecules to maintain ionic and osmotic balance, ii) prevent the formation of free radicals, iii) maintain an oncotic balance, and iv) supply energy substitutes (Baust, 2005; Mathew et al., 2004). A variety of preservation solutions such as ViaSpan® (University of Wisconsin solution), Celsior®, HTK-Custodiol and, more recently, HypoThermosol® (HTS), were developed taking these factors into consideration (Mathew et al., 2004) and are commercially available today. These solutions showed to be effective for hypothermic storage of a large diversity of cells, tissues and organs (including neonatal rat ventricular cardiomyocytes (Snyder et al., 2005), renal cells (Mathew et al., 2002), hepatocytes (Duret et al., 2015; Gramignoli et al., 2014), liver tissue (Bessems et al., 2004), synthetic human epidermis tissue (Cook et al., 1995), kidney (Hrabalová et al., 2003), pancreas (Squifflet et al., 2011), liver (Bessems et al., 2004) and heart (Minasian et al., 2014; Wakayama et al., 2012)). Importantly, some of these formulations can be directly administered into patients, avoiding additional post-storage culture manipulations/costs and washing steps. HTS for example has been used as a vehicle solution for different therapeutic cells in several clinical trials, such as

in the treatment of autoimmune disorders including rheumatoid arthritis with allogeneic adipose-derived stem cells (NCT01743222), advanced heart failure with myogenic cells (NCT00526253), and restrictive scars using allogeneic dermal fibroblasts (NCT01564407).

The time interval that a cardiac graft can be efficiently cold-stored remains limited to 6h (Minasian et al., 2014). This finite time frame further limits donor heart supply, access and utility. The ability to efficiently cold preserve functional CMs for extended periods will provide an appealing off-the-shelf solution for the treatment of cardiac diseases. Several studies have evaluated the ability to preserve adult/neonatal rat/mouse CMs at hypothermic conditions (Abi-Gerges et al., 2013; Lu et al., 2006; Orita et al., 1995; Snyder et al., 2005; Uchida et al., 2011). For example, Snyder and colleagues reported the successful hypothermic storage of neonatal rat ventricular CM monolayers for up to 72h in HTS. After this storage period, CMs retained their viability, metabolic activity (82% by day 1 post-storage) and spontaneous contractile activity (Snyder et al., 2005); nevertheless, the impact of hypothermic storage on CM structure, ultrastructure, action potential and drug responsiveness was not evaluated.

To date, there are no studies reporting the efficient hypothermic storage of PSC-CMs. Therefore, in this study we aimed to develop efficient strategies for hypothermic storage of murine and human PSC-CMs. The CM differentiation protocols are conventionally performed in 2D monolayers, or more recently in 3D cell configurations, such as cell aggregates (Mummery et al., 2012; Zhang et al., 2015). It is well known that cell-cell and cell-matrix interactions play a critical role in cell survival/recovery after thawing (Serra et al., 2011). Disruption of these interactions may result in dissociation-induced apoptosis (Wong et al., 2006). Consequently, we evaluated the feasibility to cold store CMs obtained from different PSC lines as 2D monolayers and 3D aggregates and assessed the impact of the hypothermic storage time on cell viability and metabolic activity recovery. Cell phenotype, including structure, ultrastructure, gene and protein expression, and functionality were assessed post-storage by quantitative RT-PCR, flow cytometry, fluorescent microscopy, scanning electron microscopy, transmission electron microscopy, and electrophysiology analyses.

## 2. Methods

### 2.1. CM layers Differentiation of mPSCs

A murine transgenic  $\alpha$ PIG induced pluripotent stem cell (miPSC) line was used in this study. This cell line was genetically modified to integrate and stably express a transgene containing puromycin-N-acetyl transferase and eGFP (enhanced green fluorescent protein) genes, both under control of the cardiac-restricted promoter  $\alpha$ -myosin heavy chain ( $\alpha$ -MHC) (Halbach et al., 2013). miPSC were expanded and differentiated as aggregates in fully controlled bioreactors as previously described by our group (Correia et al., 2014). Briefly, iPSCs were inoculated in the Wave Cellbag™ (GE Healthcare) as single cells, at a concentration of  $7 \times 10^4$  cell/mL, and were cultivated under defined conditions (temperature: 37°C; pO<sub>2</sub>: 4% O<sub>2</sub>; CO<sub>2</sub>: 5%; surface aeration rate: 0.1 vvm;

rocking angle: 4°; agitation rate: 10-26 rpm; working volume: 1 L) in differentiation medium (Iscove's modified Dulbecco's medium (IMDM) with GlutaMAX, supplemented with 20 % (v/v) fetal bovine serum (FBS), 1 % (v/v) non-essential amino acids (NEAA), 1 % (v/v) Pen/Strep, 50  $\mu$ M  $\beta$ -mercaptoethanol (all from Invitrogen)). At day 9, cell lineage selection was induced by addition of puromycin (8  $\mu$ g/mL). At day 11, cell aggregates composed of more than 97% of iPSC-CMs were harvested from Wave bioreactor. These cell aggregates were either preserved (as described in section 2.3.) or dissociated into single cells using 0.25% (w/v) Trypsin/EDTA, and plated, at  $5 \times 10^5$  cell/cm<sup>2</sup>, in 24-well plates coated with CELLstart CTS (Invitrogen)). Cells were cultivated at 37°C, in a humidified atmosphere of 5% CO<sub>2</sub>, until hypothermic storage studies were performed.

## **2.2. CM layers Differentiation of hPSCs**

Two hPSC lines were used: hiPSC (DF19-9-11T.H from WiCell) and human embryonic stem cell (hESC) line (NKX2-5(eGFP/w) (Elliott et al., 2011), kindly provided by Dr. David Elliott from Murdoch Childrens Research Institute). HPSC were cultured on Synthemax® II – SC Substrate (Corning) coated plates in mTESR1 (STEMCELL Technologies) medium until reaching 80% confluence. Cardiac differentiation was induced as described by Lian et al (Lian et al., 2013). Using this protocol, 2D monolayer cultures composed by 50-70% of hPSC-CMs were obtained. To enrich the cell population into CMs, cells were cultured in CM enrichment medium (RPMI 1640 without glucose (Invitrogen) supplemented with B27 without insulin (Invitrogen) and 4 mM sodium L-lactate (Sigma-Aldrich)) for 10 days as described elsewhere [32]. After CM enrichment (more than 80% VCAM positive cells), monolayer cultures were dissociated into single cells by incubation with TrypLE™Select (Invitrogen) for 5 min. These cells were: i) re-plated at  $5 \times 10^5$  cell/cm<sup>2</sup> in Synthemax® II – SC Substrate (Corning) coated 24-well plates, and maintained for one week at 37°C in a humidified atmosphere of 5% CO<sub>2</sub>, until hypothermic storage studies; and ii) aggregated as described in literature (Skelton et al., 2014). Briefly,  $5 \times 10^5$  cells were inoculated per well of low-adherent U bottom 96 well plates (Nunc), centrifuged at 500 g for 5 min, and cultured in differentiation media (RPMI 1640 (Invitrogen) supplemented with B27 without insulin) for one week until preservation tests.

## **2.3. Hypothermic storage of PSC-CM**

2D Monolayer cultures and 3D aggregates of murine and human PSC-CMs were stored at 4°C in HypoThermosol®-FRS solution (HTS, BioLife Solutions) for 3, 5 and 7 days (designated as S3, S5 and S7, respectively). Immediately before hypothermic storage, culture medium was replaced by the following volumes of HTS solution: 2D monolayers - 300  $\mu$ L/well in 24 well plate; 3D aggregates - 150  $\mu$ L/well in 96 well plate (1 aggregate/ well) or 1 mL/cryovial (300 Aggregates/cryovial). After the hypothermic storage interval, HTS solution was removed, murine and human PSC-CMs were washed once with the respective differentiation media (described in sections 2.1. and 2.2.) and cultivated in the same medium for 7 days. In the first 24 hours post-storage, medium was supplemented with 10  $\mu$ M of Rho-associated kinase inhibitor (ROCKi, Biogen Scientifica SL). Medium was totally exchanged at days 0, 1, 3 and 7 of culture.

## **2.4. Assessment of PSC-CM viability and metabolic activity after storage**

Cell viability, metabolic activity, and metabolism were evaluated at days 0, 1, 3 and 7 of culture post-storage, using the methods described below.

### **2.4.1. Fluorescein diacetate-propidium iodide staining.**

The qualitative assessment of the cell plasma membrane integrity was performed using the enzyme substrate fluorescein diacetate (FDA, Sigma-Aldrich), and the DNA-binding dye propidium iodide (PI, Sigma-Aldrich), as described in the literature (Jones and Senft, 1985). Briefly, cells were incubated with 20 µg/mL FDA and 10 µg/mL PI in Dulbecco's Phosphate Buffered Saline (DPBS, Invitrogen) for 2-3 min and visualized by fluorescence microscopy (DMI 6000, Leica Microsystems GmbH).

### **2.4.2. Lactate Dehydrogenase (LDH) activity in the supernatant.**

The release of intracellular LDH to the supernatant can be correlated with the extent of cell lysis as described by Decker et al (Decker and Lohmann-Matthes, 1988). LDH activity from the supernatant of centrifuged (300 g, 5 min) samples was determined spectrophotometrically following (at 340 nm) the rate of oxidation of NADH to NAD<sup>+</sup> coupled with the reduction of pyruvate to lactate as described elsewhere (Serra et al., 2011).

### **2.4.3. Trypan Blue exclusion method.**

Cells cultured as monolayers were dissociated as described in section 2.2. Cell concentration was estimated by counting cells using a Fuchs–Rosenthal haemocytometer (Brand). Viable cells were determined by using the trypan blue dye (0.1% (v/v) in DPBS) exclusion method. The percentage of cell recovery was estimated taking into account the number of viable cells before cold storage.

### **2.4.4. PrestoBlue™ assay.**

Metabolic activity was determined using the metabolic indicator PrestoBlue (Invitrogen) reagent following manufacturer's recommendation. Briefly, cells were incubated for 1-2 h with culture medium containing 10% (v/v) PrestoBlue reagent. Fluorescence was measured (excitation wavelength: 570 nm, emission wavelength: 585 nm) using a microwell plate fluorescence reader Infinite 200 PRO NanoQuant (TECAN). The active ingredient of PrestoBlue (resazurin) is a nontoxic, non-fluorescence indicator dye that is reduced to red-fluorescent resorufin by metabolically active cells. Fluorescence intensity is proportional to the number of live and metabolic active cells. Thus, PrestoBlue assay provides a quantitative measure of cell viability and metabolic activity. Fluorescence values were normalized to the values obtained with the same cells before cold storage, and are indicated as a percentage of metabolic activity recovery.

### **2.4.5. NucView™ 488 and MitoView™ 633 Apoptosis Assay.**

A qualitative assessment of apoptosis was performed using the Apoptosis Assay Kit NucView™ 488 and MitoView™ 633 (Biotium, Inc., California, USA) following manufacturer's instructions. This kit contains the green fluorescent NucView 488 caspase-3 substrate and the far-red fluorescent MitoView 633 mitochondrial dye for profiling caspase-3 activity and changes in mitochondrial membrane potential, respectively, in intact cells. After incubation with both reagents

for 1 h, cells were observed using fluorescence microscopy (DMI 6000, Leica) and representative images were taken.

#### **2.4.6. Quantification of caspase activity.**

A quantitative assessment of apoptosis was performed using the Caspase Family Fluorometric Substrate Kit II Plus (Abcam) following manufacturer's instructions. Briefly, the activity of caspases -3/7, -6, -8, -9 and -10 was determined by incubation with the respective AFC conjugated substrates. AFC-based substrates yield fluorescence upon protease cleavage (Ex/Em=400 nm/505 nm). The fold increase in caspase activity was determined by the ratio of the values of fluorescence obtained for the cells subject to cold storage to the values obtained by the cells immediately before storage.

### **2.5. Metabolite analysis**

Glucose (GLC), glutamine (GLN) and lactate (LAC) concentrations in the culture medium were analyzed using an YSI 7100MBS (YSI Incorporated). Specific metabolic rates ( $q_{Met.}$ , mol.h<sup>-1</sup>.cell<sup>-1</sup>) were calculated using the equation:  $q_{Met.} = \Delta Met / (\Delta t \Delta X_v)$ , where  $\Delta Met$  (mol/L) is the variation of metabolite concentration during the time period  $\Delta t$  (h), and  $\Delta X_v$  (cell/L) the average of cell concentration during the same time period.

### **2.6. Assessment of PSC-CM structure and ultrastructure after hypothermic storage**

#### **2.6.1. Scanning electron microscopy (SEM) and Transmission electron microscopy (TEM)**

Monolayers and aggregates of human PSC-CMs were fixed in 2% (v/v) glutaraldehyde in 0.1 M HEPES buffer (pH 7.4) for 20 min, washed in DPBS and stored in 1% (v/v) glutaraldehyde in DPBS until analyses. For TEM analyses, cell aggregates were immersion fixed in a mixture of 2% glutaraldehyde and 2% paraformaldehyde in 50 mM HEPES. Subsequently, the samples were washed once in 100 mM HEPES, twice in DPBS, and twice in double-distilled water before postfixation with osmium tetroxide (1% (v/v) in water, 2 h on ice). After several washes in water, the samples were contrasted *en-bloc* with aqueous uranyl acetate (1% (w/v), 2 h on ice), washed several times in distilled water, dehydrated in a graded series of ethanol, infiltrated in epon 812 (epon/ethanol mixtures: 1:3, 1:1, 3:1, 1 h each, pure epon overnight, pure epon 6 h), and embedded in flat embedding molds. Finally, the samples were cured at 65°C in the oven. 2D-Monolayers were fixed with 2% (v/v) glutaraldehyde in 100 mM HEPES for 1 h, and washed in 100 mM HEPES and distilled water. Postfixation, *en-bloc* contrasting, dehydration, epon infiltration and curing were performed as described above. After curing, the samples were dissected into small blocks and mounted on epon dummy blocks. Ultrathin sections of aggregates and monolayers were cut on a Leica UC6 ultramicrotome using a diamond knife. Sections were collected on formvar-coated slot grids, stained with lead citrate and uranyl acetate as described in the literature (Venable and Coggeshall, 1965), and analysed on a FEI Morgagni 268 at 80 kV. Images were taken with an Olympus MegaView III using the iTEM software.

For SEM analyses cell aggregates were immersion fixed in 2% (v/v) glutaraldehyde with 2% (w/v) paraformaldehyde (PFA) in 50 mM HEPES, and washed once in 100 mM HEPES, twice in



DPBS, and twice in double-distilled water before post-fixation with osmium tetroxide (1% in water, 2 h on ice). After several washes in distilled water, the samples were dehydrated in a graded series of ethanol, critical-point dried using the Leica CPD 300, mounted to carbon tabs which were glued to 12 mm aluminum stubs, and sputter coated with gold using the Baltec SCD 050 sputter coater. Samples were imaged in a Jeol 7500F cold field emission SEM at 5kV acceleration voltage and 8 mm working distance using the lower secondary electron detector.

## **2.7. Measurement of aggregate size**

The aggregate size was determined using an inverted-microscope (DMI 6000, Leica) by measuring two perpendicular diameters of each aggregate. These measures were used to calculate the average diameter of each aggregate.

## **2.8. Characterization of PSC-CMs after hypothermic storage**

### **2.8.1. Flow cytometry.**

After a 5 min dissociation with TypLE™ Select, human PSC-CMs were washed twice with DPBS and a total of  $5 \times 10^5$  cells were incubated with each of the antibodies VCAM-1 (CD106-PE, BD Biosciences), SIRP $\alpha/\beta$  (CD172a/b-PE, BioLegend) and isotype controls IgG1, $\kappa$ -PE (BD Biosciences) for 1 h at 4°C. Cells were washed twice with DPBS, and analysed in a CyFlow® space (Partec GmbH) instrument, registering 10,000 events/sample.

### **2.8.2. Immunofluorescence microscopy.**

Cells were washed with DPBS and fixed in 4% (w/v) PFA and 4% (w/v) sucrose in DPBS solution for 15 min. Afterwards, cells were permeabilized for 10 min in 0.5 M Ammonium chloride (Sigma-Aldrich), 0.25% (v/v) Triton X-100 in DPBS and blocked with 5% (v/v) FBS in DPBS for 1 h, at room temperature. Cells were subsequently incubated overnight at 4°C with primary antibodies diluted in 0.2% (w/v) Fish Skin Gelatin (FSG), 0.1% (w/v) TX-100 in DPBS. The following primary antibodies were used:  $\alpha$ -sarcomeric actinin (1:200, Sigma-Aldrich), titin (1:100, Santa Cruz Biotechnology), troponin I (TnI, 1:100, Millipore), troponin T (Tnt, 1:100, Millipore), MYL2 (1:140, ABCAM), MYL7 (H-60, 1:50, Santa Cruz Biotechnology). Non reporter cell lines were also incubated with F-actin Alexa Fluors 488 dye (Life technologies). Cells were washed in DPBS and secondary antibodies were incubated for 60 min at room temperature in the dark. Secondary antibodies used were: AlexaFluor 594 goat anti-mouse IgG and AlexaFluor 594 goat anti-rabbit IgG (1:500 dilution in 0.2% (w/v) FSG, 0.1% (w/v) TX-100 in DPBS). Cell nuclei were counterstained with Hoechst 33342 nucleic acid dye. Cells were visualized using an inverted fluorescence microscope (DMI 6000, Leica).

### **2.8.3. Quantitative RT-PCR.**

Total RNA was extracted using the High Pure RNA Isolation Kit (Roche), and reverse transcription was performed with High Fidelity cDNA Synthesis Kit (Roche), following manufacturer's instructions. Relative quantification of gene expression was performed using LightCycler 480 Probes Master (Roche) in 20  $\mu$ L reactions with 50 ng cDNA template and 20x concentrated TaqMan probes. The reactions were performed in 96-well plates using a LightCycler

480 Real-Time PCR System (Roche). Cycle threshold (Ct's) were determined by LightCycler 480 Software. All data was analyzed using the  $2^{-\Delta\Delta Ct}$  method for relative gene expression analysis. Changes in gene expression were normalized to the average of RFLP0 and GAPDH gene expression as internal control. The TaqMan probes used for human ISL1, KDR, GATA4, NKX2.5, TNNT2, VCAM1, MYH7, MYL2, MYL7, HCN4, CACNA1C, ACTC1, MYH6, MYH7, SCN5A, RFLP0 and GAPDH genes were HS00158126\_m1, HS00911699\_m1, Hs00171403\_m1, Hs00231763\_m1, Hs00165960\_m1, Hs01003372\_m1, Hs01110632\_m1, Hs00166405\_m1, Hs00221909\_m1, Hs00175760\_m1, Hs00167681\_m1, Hs00606316\_m1, Hs01101425\_m1, Hs01110632\_m1, Hs00165693\_m1, Hs99999902\_m1 and Hs99999905\_m1, respectively.

## **2.9. Assessment of PSC-CM function after hypothermic storage**

### **2.9.1. Electrophysiological analyses of mPSC-CMs.**

Single mPSC-CMs were plated on glass cover slips coated with 0.1% gelatin. The patch clamp experiments were performed as described previously (Kuzmenkin et al., 2009). Briefly, cover slips were placed into a recording chamber (37°C) and cells were continuously perfused with extracellular solution. Cell membrane capacitance was determined online using Pulse software (Heka Elektronik). Action potential (AP) recordings of spontaneously beating murine PSC-CMs were performed utilizing the whole-cell current-clamp technique with an EPC-9 amplifier (HEKA Elektronik), and operated through the Pulse acquisition software. Response to hormonal regulation was analyzed by administering 1  $\mu$ M isoproterenol (Iso, Sigma-Aldrich).

### **2.9.2. Electrophysiological analyses of hPSC-CMs.**

Single hPSC-CMs were plated on 35 mm plastic petri dishes previously coated with Synthemax. These dishes were used as recording chambers mounted on the stage of an inverted microscope. A gravity based superfusion system was used for the exchange of extracellular solution (2–3 mL/min), which had the following composition: 135 mM NaCl, 5 mM KCl, 1.5 mM MgSO<sub>4</sub>, 0.33 mM NaH<sub>2</sub>PO<sub>4</sub>, 10 mM HEPES, 1 mM CaCl<sub>2</sub>, 15 mM D-glucose, adjusted to pH 7.35 with 1 mM NaOH. Cells were voltage-clamped using the whole cell patch-clamp configuration, as described previously (Vicente et al., 2010). Briefly, the patch pipettes (2–5 M $\Omega$ ) were pulled from borosilicate glass capillaries (Science Products GmbH, GB150T-8P) and filled with an internal solution containing: 135 mM potassium gluconate, 5 mM KCl, 5 mM NaCl, 10 mM Na<sub>1</sub>/2HEPES, 1 mM MgCl<sub>2</sub>, 0.1 mM EGTA, 2 mM Na<sub>2</sub>ATP, 0.4 mM NaGTP (pH 7.3 adjusted with 1 mM KOH; 305 $\pm$ 5 mOsm). The estimated junction potential for the filling and bathing solution combinations mentioned above is -8.9 mV (calculated with JPCalc 2.00, School of Physiology and Pharmacology University of New South Wales). Data were not corrected for the junction potential. Currents were recorded with an Axopatch 200B electrometer (Axon Instruments Inc., USA) and stored on a PC computer using pClamp 6.0.3 software (Axon Instruments Inc., USA) and an analogue digital interface (Digidata 1200; Axon Instruments, USA). Signals were acquired at a sampling rate of 5 kHz and filtered at 2 kHz (-3 dB, four pole Bessel). Electrode and cell membrane capacitances were compensated whenever possible. Cells with significant leak currents were rejected.

The holding potential (VH) was kept at -70mV. Current-voltage relationships were investigated using a set of 10 mV (260 ms) command pulses from -130 to 0 mV. More depolarizing potentials, greater than 0 mV, were not used as in this protocol because patch seals tend to brake. Thus, to avoid depolarization-induced cells damage, we excluded the depolarizing steps above 0 mV from the current-voltage relationships, focusing more on the evaluation of the inward currents. The K<sup>+</sup> outward currents were observable only at potentials greater than  $\pm 40$ mV (Figure 6.A).

The Ca<sup>2+</sup> dependence of the outward K<sup>+</sup> currents was assessed using a two-pulse protocol, which consists of a triple set of double depolarizing pulses (Figure 6.B). A prepulse lasting 50 ms to -40, -10 or +20 mV was delivered to trigger Ca<sup>2+</sup> influx through voltage-activated channels. The prepulse was immediately followed by a second depolarizing pulse to +40 mV for 750 ms to elicit the outward K<sup>+</sup> current.

### 2.9.3. Pharmacological responses of hPSC-CMs.

Single hPSC-CMs were plated on 35 mm plastic petri dishes previously coated with Synthemax. These dishes were used as recording chambers mounted on the stage of an inverted microscope. A gravity based superfusion system was used for the exchange of extracellular solution (2–3 mL/min), which had the following composition: 135 mM NaCl, 5 mM KCl, 1.5 mM MgSO<sub>4</sub>, 0.33 mM NaH<sub>2</sub>PO<sub>4</sub>, 10 mM HEPES, 1 mM CaCl<sub>2</sub>, 15 mM D-glucose, adjusted to pH 7.35 with 1 mM NaOH. Cells were voltage-clamped using the whole cell patch-clamp configuration, as described previously (Vicente et al., 2010). Briefly, the patch pipettes (2–5 M $\Omega$ ) were pulled from borosilicate glass capillaries (Science Products GmbH, GB150T-8P) and filled with an internal solution containing: 135 mM potassium gluconate, 5 mM KCl, 5 mM NaCl, 10 mM Na<sub>1/2</sub>HEPES, 1 mM MgCl<sub>2</sub>, 0.1 mM EGTA, 2 mM Na<sub>2</sub>ATP, 0.4 mM NaGTP (pH 7.3 adjusted with 1 mM KOH; 305 $\pm$ 5 mOsm). The estimated junction potential for the filling and bathing solution combinations mentioned above is -8.9 mV (calculated with JPCalc 2.00, School of Physiology and Pharmacology University of New South Wales). Data were not corrected for the junction potential. Currents were recorded with an Axopatch 200B electrometer (Axon Instruments Inc., USA) and stored on a PC computer using pClamp 6.0.3 software (Axon Instruments Inc., USA) and an analogue digital interface (Digidata 1200; Axon Instruments, USA). Signals were acquired at a sampling rate of 5 kHz and filtered at 2 kHz (-3 dB, four pole Bessel). Electrode and cell membrane capacitances were compensated whenever possible. Cells with significant leak currents were rejected.

The holding potential (VH) was kept at -70mV. Current-voltage relationships were investigated using a set of 10 mV (260 ms) command pulses from -130 to 0 mV. More depolarizing potentials, greater than 0 mV, were not used as in this protocol because patch seals tend to brake. Thus, to avoid depolarization-induced cells damage, we excluded the depolarizing steps above 0 mV from the current-voltage relationships, focusing more on the evaluation of the inward currents. The K<sup>+</sup> outward currents were observable only at potentials greater than  $\pm 40$ mV (Figure 5.6.A).

The Ca<sup>2+</sup> dependence of the outward K<sup>+</sup> currents was assessed using a two-pulse protocol, which consists of a triple set of double depolarizing pulses (Figure 5.6.B). A prepulse lasting 50 ms to -40, -10 or +20 mV was delivered to trigger Ca<sup>2+</sup> influx through voltage-activated channels. The

prepulse was immediately followed by a second depolarizing pulse to +40 mV for 750 ms to elicit the outward K<sup>+</sup> current.

### **2.9.2. Pharmacological responses of hPSC-CMs.**

The effect of pharmacological treatment on the contractile activity of hPSC-CMs was analyzed by administering in the superfusion fluid: 300 pM Nimodipina; 30 mM KCL; 1 μM Verapamil; 0.5 mM Adrenaline. hPSC-CMs were visualized using a Nikon Eclipse Ti-U inverted microscope at room temperature ( $\pm$  25°C). Bright field video/images were recorded with a FASTCAM MC2 camera (Photron Europe, Limited) controlled with PFV (Photron FASTCAM Viewer) software. A region of interest was drawn around the contracting structures filmed at 10 fps. Pixel density, used as indirect measurement of contraction, was digitized using ImageJ software (National Institutes of Health [NIH]).

### **2.9.4. Detection of Ca<sup>2+</sup> Transients.**

Ca<sup>2+</sup> imaging was performed according to the standard protocol provided in Rhod-3- Calcium Imaging kit (Invitrogen). Aggregates of human PSC-CMs were plated onto eight-well culture plates coated with Synthemax and cultured for 1 week, to promote cell adherence and migration to the plate. Briefly, cells were labelled with Rhod-3 for 1 h at 37°C, washed twice in DPBS, incubated for 1 h with a water-soluble reagent to reduce baseline signal and washed again in DPBS. Cells were imaged live using a spinning disk confocal microscope (Nikon Eclipse Ti-E; System: Andor Revolution XD; Confocal Scanner: Yokogawa CSU-x1) and calcium transients were determined using Micro-Manager 1.4 and ImageJ software.

### **2.10. Statistical analysis**

All statistical analyses were performed using GraphPad Prism version 5 (GraphPad Software Inc.). Values are represented as mean $\pm$ standard deviation of independent measurements or assays (at least n=3 replicates were considered). Statistical significance was evaluated using either Student's t test with Welch's correction or one-way analysis of variance (ANOVA). Values of P<0.05 were considered statistically significant.

## **3. Results**

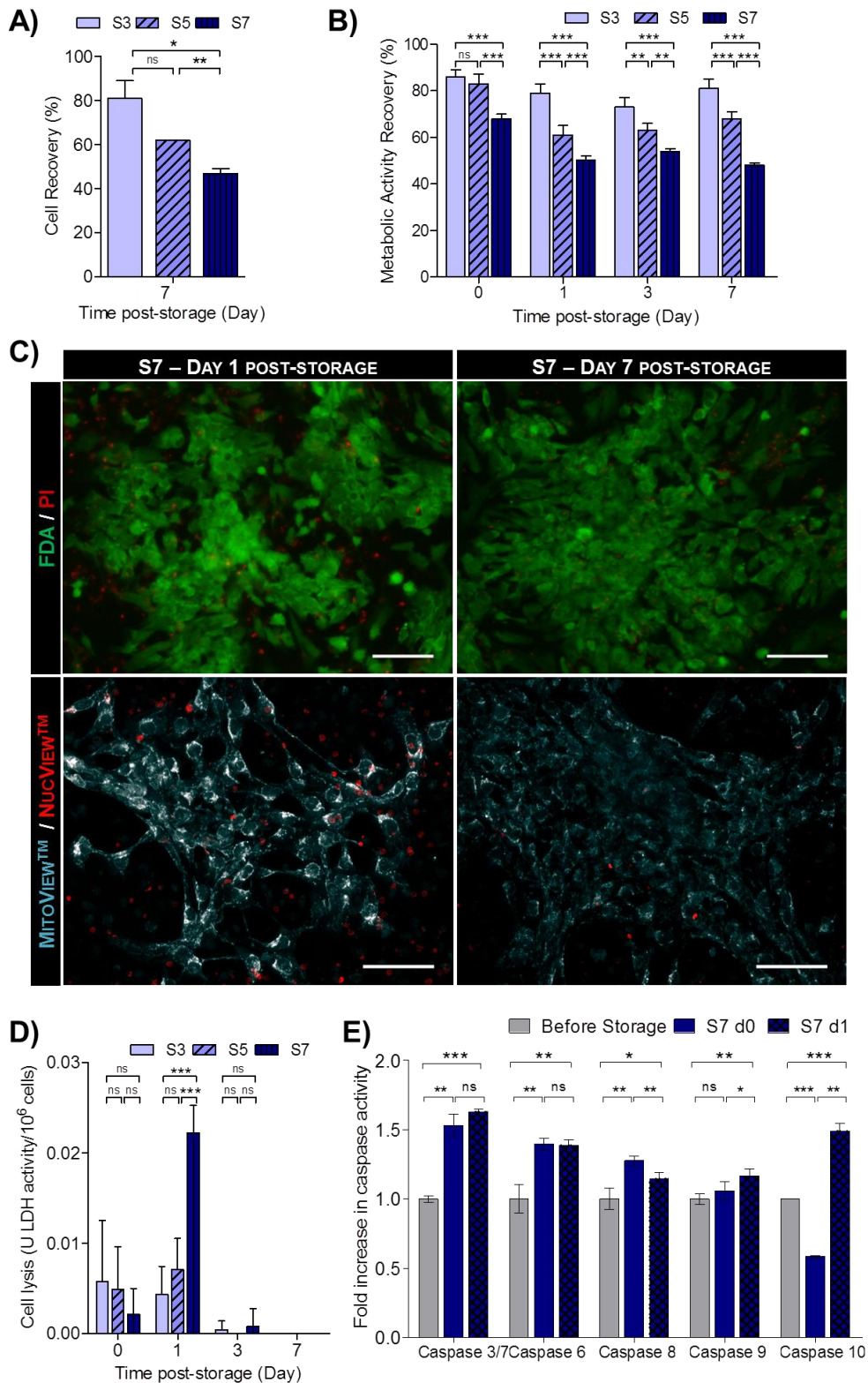
### **3.1. Impact of hypothermic storage on PSC-CM viability and metabolic activity**

In this study we aimed at developing a protocol for hypothermic storage of PSC-CMs, cultured either as 2D monolayers or 3D aggregates, to ensure efficient short-term preservation and/or shipping of PSC-CM suitable for clinical applications and toxicology testing. Murine and human PSC-CMs were preserved at hypothermic conditions (4°C) for 3, 5 and 7 days (designated hereafter as S3, S5 and S7, respectively), in HypoThermosol®-FRS (HTS) preservation solution. HTS was used since it is a xeno-free, cGMP and clinical compatible solution that has been

successfully utilized for hypothermic preservation of multiple cell types including neonatal rat CMs (Snyder et al., 2005).

Our results show that miPSC-CMs can be efficiently stored for 7 days in hypothermic conditions in HTS solution, without compromising cell viability or metabolic activity (Figure A-5.1, Page 172). Both 2D monolayers and 3D aggregates of iPSC-CMs remained highly viable after cold storage (Figure A-5.1A, Page 172) and maintained  $\alpha$ -MHC driven eGFP expression (Figure A-5.1A, Page 172). By day 7 of culture post-storage, both 2D monolayers and 3D aggregates of mPSC-CMs have nearly recovered their metabolic activity (>90%, as determined by the PrestoBlue assay - Figure A-5.1B, Page 172).

hPSC-CMs were more sensitive to hypothermia induced stress than mPSC-CMs. Our results showed that high cell viabilities (80%) can be obtained when 2D monolayers of hPSC-CMs were preserved at hypothermic conditions for 3 days (S3 condition, Figure 5.1A-B). However, cell viability post-storage decreased with increased cold storage intervals (Figure 5.1, Table 5.1). Specifically, cell viabilities, determined by the Trypan Blue exclusion method (Figure 5.1A) and metabolic activity recoveries, evaluated using the PrestoBlue assay (Figure 5.1B, Table 5.1), of approximately 60% and 50% were estimated for S5 and S7 conditions, respectively. The marked PI and NucView™ Caspase-3 substrate staining (Figure 5.1C) and the significantly higher cell lysis measured by the LDH activity in the supernatant (Figure 5.1D) at day 1 post-storage, confirmed that cell death was more pronounced in S7 condition. In agreement, we verified that the caspase activity of stored hiPSC-CMs (immediately and 24 hours after cold storage) in S7 condition increased in relation to the hiPSC-CMs before hypothermic storage (Figure 5.1E). More specifically, we observed a significant increase in the activity of apoptotic initiator caspases (-8, -9 and -10) and apoptotic effector caspases (-3/7 and -6). The highest increase in caspase activity (~1.7 fold increase) was registered in caspase 3/7, 24 hours after cells were removed from hypothermic storage corroborating the pronounced NucView™ Caspase-3 substrate staining observed in Figure 5.1C. All together these results allowed us also to perceive that cell death occurred mainly from day 0 to day 1 of culture post-storage by both necrosis and apoptosis. Nonetheless, after 7 days in culture post-storage, cells that recovered from hypothermia remained viable, adherent to culture dishes without meaningful PI/NucView™ staining (Figure 5.1C). MitoView™ staining also highlighted the presence of abundant and functional mitochondria, a typical CM feature (Figure 5.1C - lower panel). It is worth noting that after all cold storage intervals (S3, S5 and S7), cells restored their metabolism, as shown by similar values of specific glucose and glutamine consumption rates and lactate production rate when compared with the control, hiPSC-CMs not subjected to hypothermic storage i.e., maintained in culture during the storage period (Table 5.1).



**Figure 5.1. Hypothermic storage of hiPSC-CM as 2D monolayers.** hiPSC-CMs were stored for 3 (S3), 5 (S5) and 7 (S7) days at 4°C, in HTS solution. Cell recovery was evaluated for 7 days post-storage. **A)** Evaluation of cell recovery after the storage interval and 7 days of culture post-storage using the Trypan Blue exclusion method. **B)** Assessment of metabolic activity recovery using the PrestoBlue test. The cell concentration (A) and the Fluorescence values of PrestoBlue (B) are presented as a % in relation to the values obtained in the cells immediately before cold storage. **C - upper panel)** Viability analysis of hiPSC-CMs from S7 condition, assessed at days 1 and 7 post-storage, using the FDA (live cells, green) and PI (dead cells, red). **C - lower panel)** Detection of caspase-3 activity using NucView™ Caspase-3 Substrate (red) and the MitoView™ mitochondrial dye (cyan), at day 1 and day 7 post-storage in S7 cultures. Scale bars: 100µm.

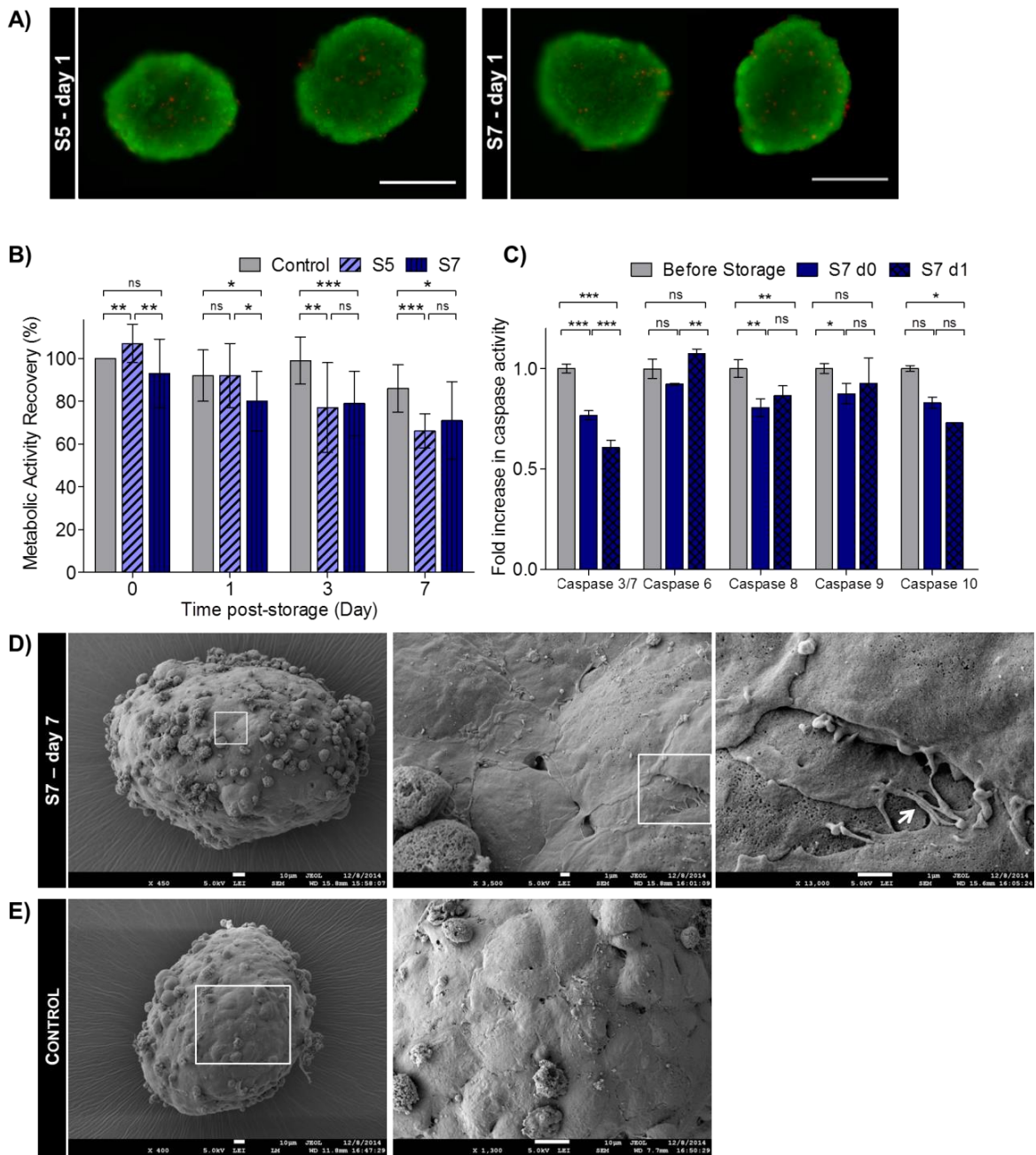
**D)** Cell lysis measured by the LDH activity in the culture supernatant. Values are normalized by the number of cells. **E)** Fold increase in the activity of caspases -3/7, -6, -8, -9 and -10 immediately and 24h after hypothermic storage in S7 condition in relation to the cells before storage. Data are presented as mean  $\pm$  SD of three (**A**), four (**E**) and five (**B**, **D**) measurements.  $P < 0.05$  (\*),  $P < 0.01$  (\*\*),  $P < 0.001$  (\*\*\*), Not-significant (ns), determined by one-way analysis of variance and unpaired t test.

Similar profiles of cell recovery were obtained when CMs derived from a hESC line were preserved as 2D monolayers (Figure A-5.2, Page 173). Specifically, cell recoveries of 80% were obtained after 5 days of hypothermic storage (Figure A-5.2A, Page 173 - condition S5) but increased storage intervals (condition S7) led to a significant decrease in cell viability and metabolic activity recovery (42%, as determined by the PrestoBlue assay, Figure A-5.2A, Page 173). After both storage intervals, cells that survived to hypothermic storage recovered their metabolism (Figure A-5.2B, Page 173).

Hypothermic preservation of hiPSC-CMs cultured as 3D aggregates led to higher cell recoveries than when cultured as 2D monolayers. From 3 days in culture post-storage onwards, no significant differences in metabolic activity recovery were detected between S5 and S7 conditions (Figure 5.2B). By day 7 of culture post-storage, metabolic activity recoveries of 66% and 71% were determined by the PrestoBlue assay, in S5 and S7 conditions, respectively (Figure 5.2B, Table 5.1). No necrotic centers were observed in aggregates from S5 and S7 and just a few PI-positive cells randomly distributed through the aggregate were detected at day 1 post-storage (Figure 5.2A). Importantly, contrary to what was observed in 2D monolayer cultures (Figure 5.1E), after hypothermic storage of hiPSC-CM aggregates the activity of initiator and effector caspases did not change significantly, and was even lower for some stored samples in relation to hiPSC-CMs before hypothermic storage (Figure 5.2C). These data indicate that when hiPSC-CM are stored in this configuration cell death by apoptosis is not meaningful. In scanning electron microscopy (SEM) images it was possible to identify a higher amount of dead cells/cellular debris on the surface of the aggregates subjected to hypothermic storage comparatively to control aggregates (hiPSC-CM aggregates not subjected to cold storage; Figure 5.2D vs. 5.2E).

**Table 5.1. Evaluation of hiPSC-CM recovery after 3 (S3), 5 (S5) and 7 (S7) days of storage at 4°C in HTS preservation solution.** Error bars denote the mean $\pm$ SD of five (2D Monolayers) and fifteen (3D Aggregates) measurements. Significant differences in relation to the Control (cells not subjected to hypothermic storage cells, maintained under conventional culture conditions for 14 days (i.e. equivalent to 7 days of storage plus 7 days of post-storage recovery)) were determined by unpaired t test with Welch's correction and are indicated by:  $P < 0.01$  (\*\*),  $P < 0.001$  (\*\*\*). NS: Non-significant differences to the Control. Specific consumption rates of glutamine (qGLN), glucose (qGLC) and specific production rate of lactate (qLAC).

	2D monolayers				3D aggregates		
	S3	S5	S7	Control	S5	S7	Control
Metabolic activity recovery (%)							
Day 1 poststorage	79 $\pm$ 5	61 $\pm$ 5	50 $\pm$ 3	—	92 $\pm$ 15	80 $\pm$ 14	92 $\pm$ 12
Day 7 poststorage	81 $\pm$ 4	68 $\pm$ 3	48 $\pm$ 2	—	63 $\pm$ 17	70 $\pm$ 18	86 $\pm$ 11
qMet (mmol $\cdot$ 10 <sup>-9</sup> cells $\cdot$ hour <sup>-1</sup> )							
qGLN	0.03 $\pm$ 0.01 <sup>a</sup>	0.02 $\pm$ 0.00 <sup>b</sup>	0.02 $\pm$ 0.00 <sup>b</sup>	0.01 $\pm$ 0.00	0.03 $\pm$ 0.00, NS	0.02 $\pm$ 0.01, NS	0.02 $\pm$ 0.00
qGLC	0.08 $\pm$ 0.01, NS	0.09 $\pm$ 0.01, NS	0.07 $\pm$ 0.01, NS	0.08 $\pm$ 0.01	0.10 $\pm$ 0.02, NS	0.11 $\pm$ 0.04, NS	0.09 $\pm$ 0.03
qLAC	0.13 $\pm$ 0.01, NS	0.11 $\pm$ 0.02, NS	0.09 $\pm$ 0.01, NS	0.13 $\pm$ 0.01	0.15 $\pm$ 0.02, NS	0.14 $\pm$ 0.02, NS	0.17 $\pm$ 0.03



**Figure 5.2. Hypothermic storage of hiPSC-CM as 3D aggregates.** Aggregates were stored for 5 (S5) and 7 days (S7) at 4°C in HTS solution. Cell recovery was evaluated for 7 days post-storage. **A)** Evaluation of metabolic activity recovery post-storage by PrestoBlue assay. The Fluorescence values are presented as a % in relation to the values obtained in the cells immediately before cold storage. **B)** Cell viability at day 1 post-storage assessed using FDA (live cells, green) and PI (dead cells, red) dyes. **C)** Fold increase in the activity of caspases -3/7, -6, -8, -9 and -10 immediately and 24h after hypothermic storage in S7 condition in relation to the cells before storage. **D-E)** Scanning electron microscopy of hiPSC-CM aggregates from S7 condition after 7 days in culture post-storage (**D**) and the control (hiPSC-CM aggregates not subjected to cold storage i.e., maintained in culture during the storage period, **E**). The boxed regions were magnified to show cell boundaries and cell-cell contacts (arrow). Scale bars: 200 μm (**B**), 10 μm (**C-left** and **D**), 1 μm (**C-middle** and **C-right**). Data are presented as mean ± SD of four (**C**) and fifteen (**B**) measurements.  $P < 0.05$  (\*),  $P < 0.01$  (\*\*),  $P < 0.001$  (\*\*\*), Not-significant (ns) determined by unpaired t test.

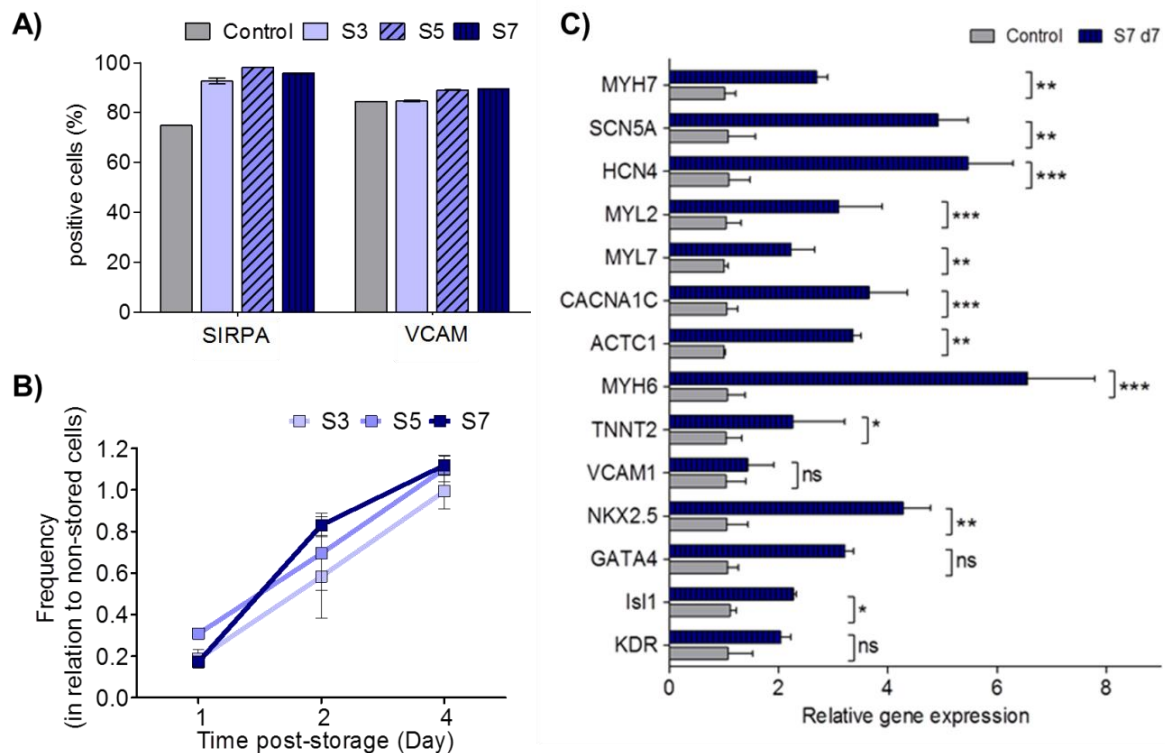


These results were also confirmed by PrestoBlue assay as lower cell viabilities and metabolic activities post-storage were attained in S5 and S7 conditions comparatively to the control (Figure 5.2B). Noteworthy, after 7 days of culture post-storage, aggregates from S7 condition maintained their structure, being almost indistinguishable from control aggregates (Figure 5.2D vs. 5.2E). In accordance, no significant differences ( $p>0.05$ ) in aggregate size were detected between aggregates from S7 condition ( $269\pm 17\ \mu\text{m}$ , Figure 5.2D) and control aggregates ( $256\pm 13\ \mu\text{m}$ , Figure 5.2E). The metabolic profile, namely specific glucose and glutamine consumption rates and lactate production rate, was also not significantly different from control aggregates (Table 5.1).

### 3.2. Effect of hypothermic storage on PSC-CM phenotype

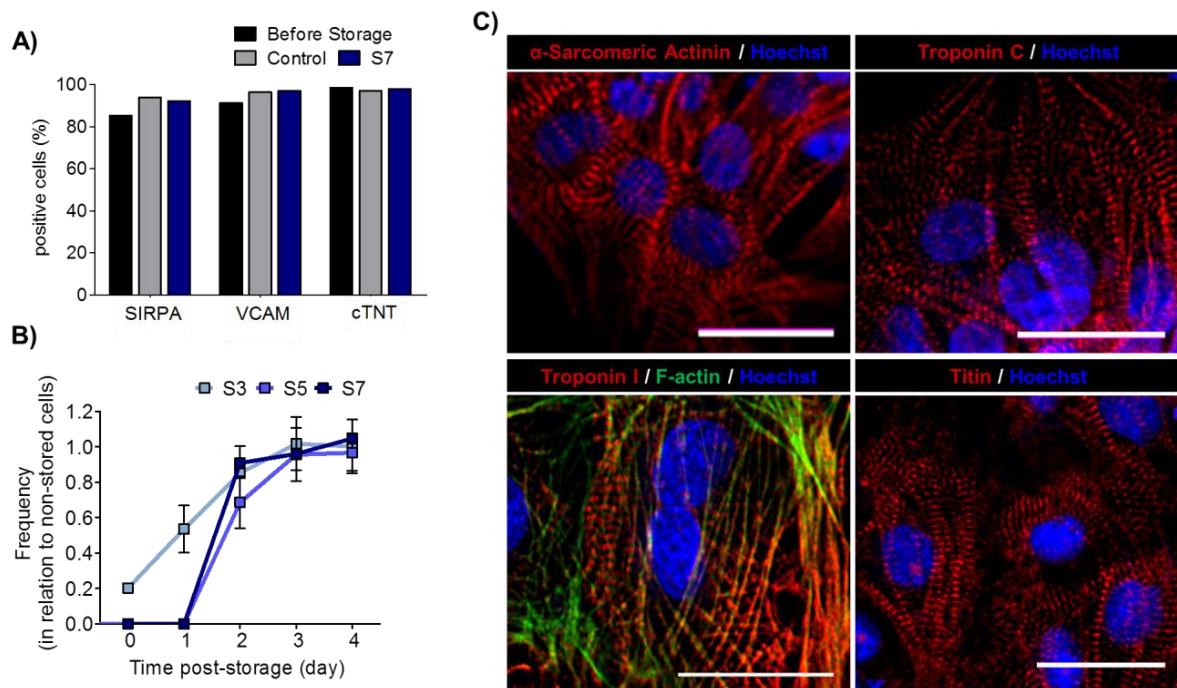
Hypothermic storage may affect not only cell viability and metabolic activity but also cell phenotype and function (Taylor, 2006). Although we showed that hPSC-CMs are more resistant to prolonged hypothermic storage-induced cell injury in 3D aggregates than in 2D monolayers, we intended to confirm also that viable cells recovered after hypothermic storage in 2D-monolayers, maintain their phenotype. Thus, we assessed the effect of hypothermic storage on the structure and functional features of hPSC-CMs storage as 2D monolayers and 3D aggregates. Our results showed that PSC-CMs, stored either as 2D monolayers or 3D aggregates, recovered from all hypothermic storage intervals (S3, S5 and S7), restored their metabolism (Table 5.1), retained the expression of cardiac markers (determined by flow cytometry, Figure 5.3A and 5.4A) and the contractile function (Figure 5.3B and 5.4B). Therefore, cells subjected to a longer period of hypothermic storage (S7 condition) were selected and further characterized in terms of gene expression, cell structure, ultrastructure and function.

Quantitative RT-PCR analyses was performed for hiPSC-CMs stored as 2D monolayers. The results revealed that, after seven days in culture post-storage, all CM specific genes, with the exception of VCAM1, and the cardiac progenitor related genes, KDR and GATA4, were highly expressed in hPSC-CMs subjected to cold storage than in the control (i.e. non-stored cells that were maintained in culture for 14 days, which corresponds to the 7 days of hypothermic storage plus 7 days in culture post-storage) (Figure 5.3B). These data suggests a hypothetical role of hypothermia in CM enrichment (cardiac progenitor cells present in culture prior to hypothermia might be more sensitive to cold storage induced-stresses than CMs with a more mature phenotype).



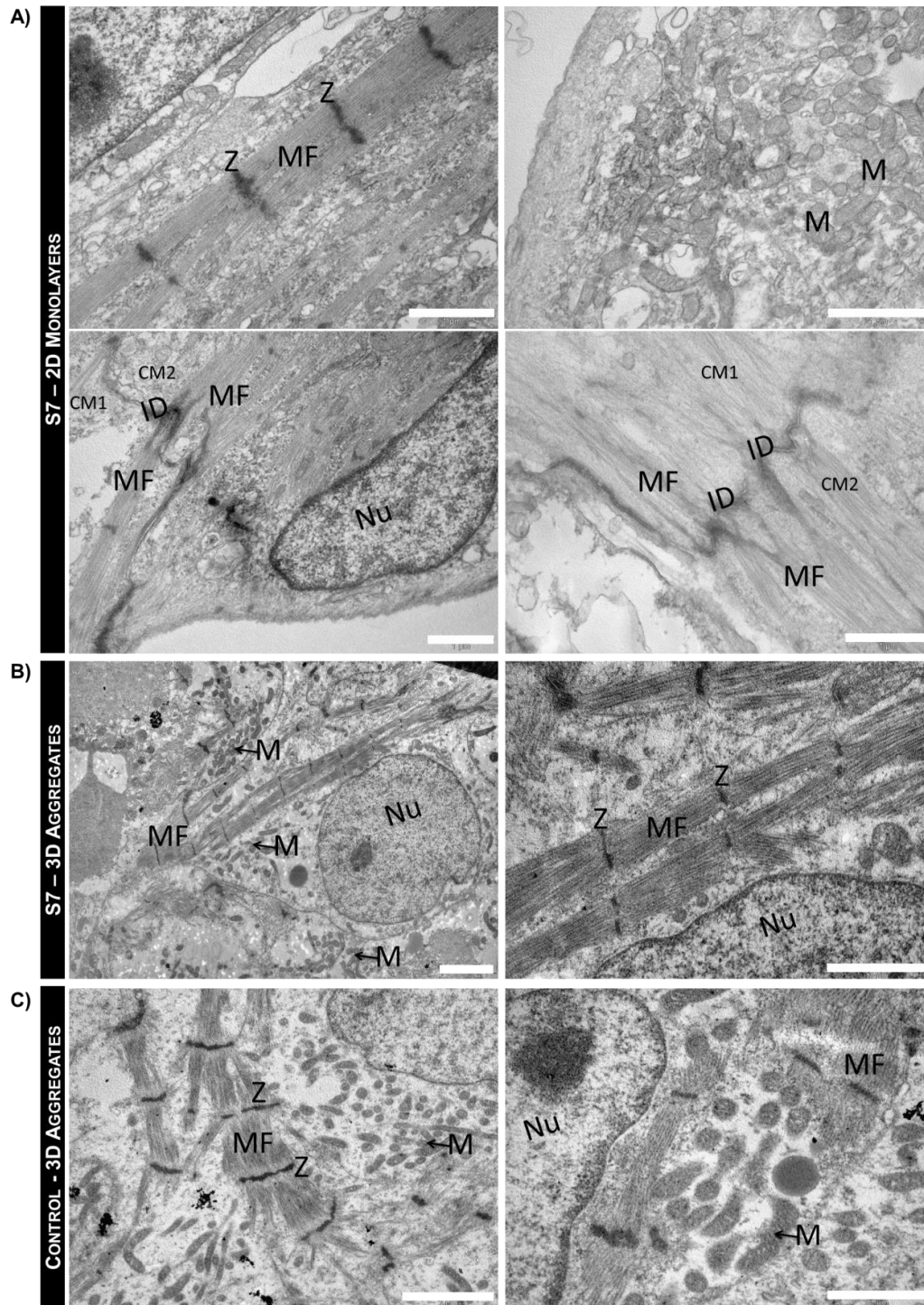
**Figure 5.3. Characterization of hiPSC-CMs stored as 2D monolayers in hypothermic conditions for up to 7 days.** **A)** Percentage of SIRPA and VCAM-positive cells determined by flow cytometry. **B)** The beating frequency (beats per minute) after all storage intervals (S3, S5, and S7) was monitored until day 4 of culture post-storage in hiPSC-CM cultured as 2D monolayers. The results were normalized to the beating frequency measured in the control cells not subjected to cold storage. **C)** Quantitative RT-PCR analysis showing the relative expression of cardiac-related transcription factors, cardiac-specific structural genes, calcium handling and membrane ion channels in S7 condition, after 7 days in culture post-storage (d7). Values were normalized to the control, cells not subjected to cold storage and maintained in culture for the same time period. Data are presented as mean  $\pm$  SD of at least three measurements.  $P < 0.05$  (\*),  $P < 0.01$  (\*\*),  $P < 0.001$  (\*\*\*), Not-significant (ns) determined by unpaired t test.

To access morphology and structure of hiPSC-CM stored as 3D aggregates, immunofluorescence microscopy analysis was carried out. Our results showed that hiPSC-CM, exhibited a typical cardiac morphology with highly organized sarcomeric  $\alpha$ -actinin, titin, troponin I and troponin T after 7 days of hypothermic storage (Figure 5.4C). Similar results were attained for miPSC-CM that also expressed Myl2, Myl7 and  $\alpha$ -MHC (Figure A-5.3, Page 173), as well as for cells stored as 2D monolayers (not shown).



**Figure 5.4. Characterization of hiPSC-CMs stored as 3D aggregates in hypothermic conditions for up to 7 days.** After hypothermic storage and one week in culture post-storage, cells were characterized by flow cytometry (**A**) and immunofluorescence staining (**C**) for cardiac specific markers. The regained of contractile activity was also assessed by phase contrast microscopy (**B**). **A**) Percentage of SIRPA, VCAM and cTNT-positive cells determined by flow cytometry. **B**) The beating frequency (beats per minute) after all storage intervals (S3, S5, and S7) was monitored until day 4 of culture post-storage. The results were normalized to the beating frequency measured in the control cells not subjected to cold storage. **C**) Immunofluorescence analysis of hiPSC-CMs (from plated 3D aggregates), after hypothermic storage, for the CM-specific markers: sarcomeric  $\alpha$ -actinin, Troponin C, Troponin I, Titin (red) antibodies. F-actin is stained with phalloidin (green). Nuclei were counterstained with Hoechst (blue). Scale bars: 30  $\mu$ m.

Transmission electron microscopy (TEM) analysis revealed that after the storage interval and 7 days in culture post-storage, hiPSC-CMs cultured either as 2D monolayers (Figure 5.5A) or 3D aggregates (Figure 5.5B) did not display signals of microstructural damage (such as damaged cell membranes and organelles) and showed ultrastructural features indistinguishable from the hiPSC-CMs not subjected to hypothermic storage (control; Figure 5.5C). Myofilaments organized in myofibrils with a sarcomeric pattern were observed as well as abundant long and slender mitochondria. Z bands delimiting the sarcomeres and highly specialized cell-cell junctions (intercalated disks) were also identified in both culture configurations (Figure 5.5A and 5.5B). No other bands were visible in the sarcomere construct, in the cold stored hiPSC-CMs and control (Figure 5.5A-C). The aligned sarcomeres in stored hiPSC-CMs presented a mean length of  $1.40 \pm 0.06 \mu\text{m}$ , similar to the control ( $1.49 \pm 0.09 \mu\text{m}$ ), and to sarcomere length reported in literature for early and immature hiPSC-CMs ( $1.50 \pm 0.15 \mu\text{m}$ ) (Gherghiceanu et al., 2011).



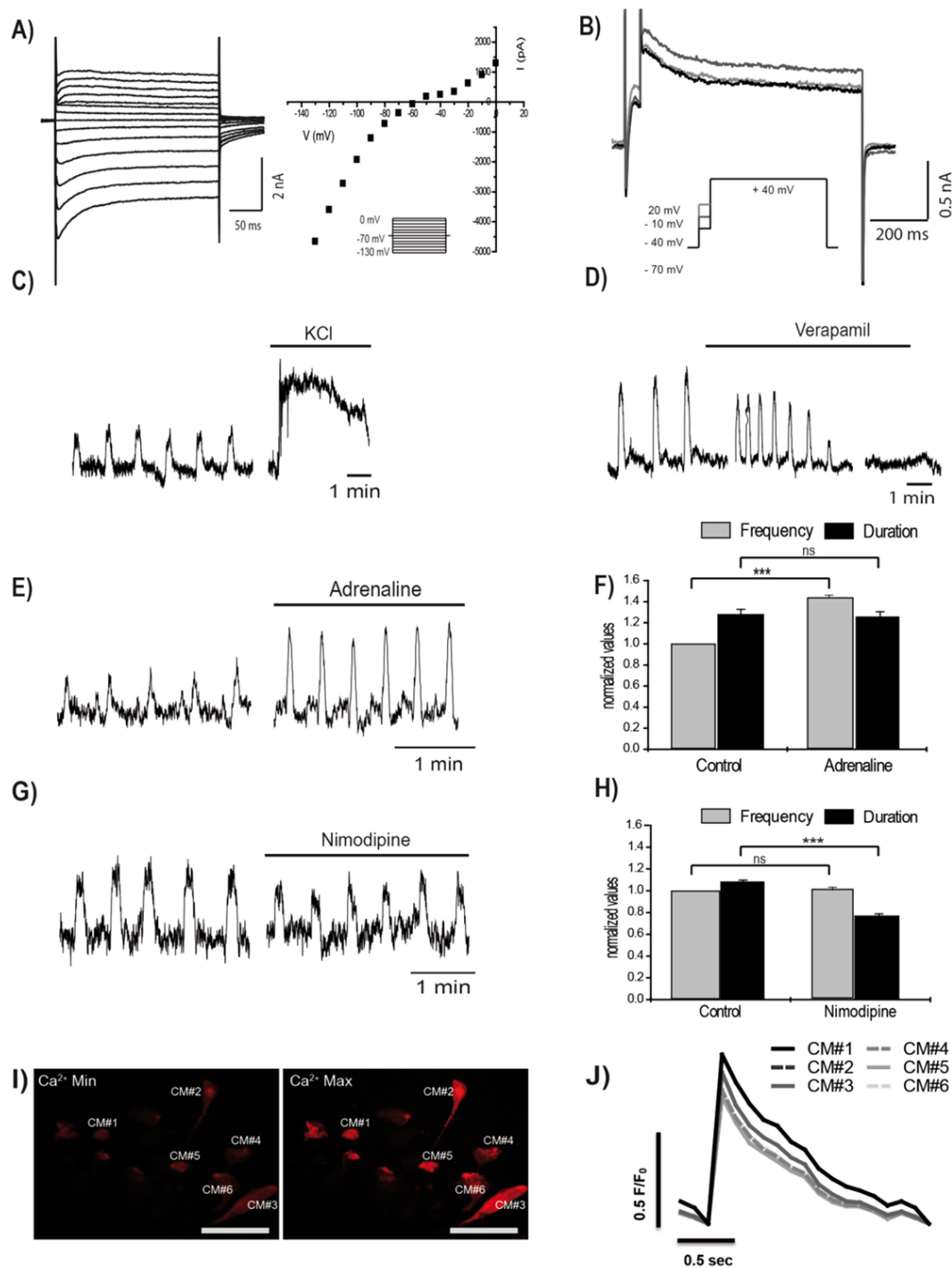
**Figure 5.5. Ultrastructural characterization of hiPSC-CMs after hypothermic preservation.** Transmission electron microscopy (TEM) images of hiPSC-CMs, stored at hypothermic conditions for 7 days (S7), as 2D monolayers (**A**) and as 3D aggregates (**B**). **C**) TEM images of the control 3D aggregates - hiPSC-CMs not subjected to hypothermic storage i.e., maintained in culture during the storage period (control). HiPSC-CMs presented a large nucleus (Nu)-to-cytoplasm ratio and contained many myofibrils (MF) aligned and organized in a sarcomeric pattern. Z-bands (Z) and neighbouring CMs (CM1, CM2) connected by intercalated disks (ID) were also observed. Scale bars: 1  $\mu$ m (**A**, **B-right**, **C-right**); 2  $\mu$ m (**B-left**, **C-left**).

### 3.3. Characterization of hiPSC-CM function after hypothermic storage

We verified that after all storage intervals murine (not shown) and human iPSC-CMs stored as 2D monolayers and 3D aggregates regained their normal beating frequency after 3-4 days in culture (Figure 5.3B, Figure A-5.4B, Page 174). The action potential (AP) characteristics of miPSC-CMs cold stored as 2D monolayers were very similar to control miPSC-CMs, showing comparable maximum diastolic potential (MDP), beating frequency, velocity of diastolic depolarization (V<sub>dd</sub>), AP upstroke velocity (V<sub>max</sub>), and AP duration (APD) (Figure A-5.4A, Page 174). Moreover, the response of cold stored and control miPSC-CMs to cardiostimulatory drugs was not significantly different. When the adrenergic agonist isoproterenol was administered, a similar increase of AP frequency was observed (Figure A-5.4B, Page 174). Positive chronotropic effects of isoproterenol were reversible upon washout (Figure A-5.4B, Page 174).

Characterization of hiPSC-CM function after 7 days of hypothermic storage as 2D monolayers plus 7 days in culture was accessed by recording inward and outward whole-cell K<sup>+</sup> conductances in voltage-clamp experiments using the whole-cell patch-clamp configuration. After obtaining 'whole-cell mode', brief measurements of membrane potential (V<sub>m</sub>, under Current-clamp) were conducted before shifting to voltage clamp. These recordings revealed that cell membranes were adequately polarized after 7 days of cold storage (V<sub>m</sub> = -69.2 ± 0.6 mV; n=8). To evaluate voltage dependence of transmembrane currents, a wide range of potentials were used to record currents following 10 mV steps (of 260 ms) from -130 to +0 mV, while keeping the holding potential at -70 mV (Figure 5.6A left panel). The corresponding curves revealed three main components: i) a clear inward component from -130 to -60 mV (component that may correspond to the typical cardiac inward K rectifier – I<sub>Kr</sub>); ii) a inward 'hump' from -50 to -20 mV; and iii) a typical delayed outward K<sup>+</sup> current above -10 mV (Figure 5.6A right panel). To investigate the outward K<sup>+</sup> current, a less abrasive single voltage step (to +40 mV) was performed (Figure 5.6B). This protocol consisted in a brief depolarization (50 ms) to -10 mV aiming at Ca<sup>2+</sup> influx through voltage-activated channels, which was immediately followed by a longer depolarizing step (750 ms) to +40 mV.

The inward current 'hump' detected in the current-voltage relationship between -50 and 0 mV (Figure 5.6A) suggests the activation of voltage-gated calcium channels allowing Ca<sup>2+</sup> influx mainly through Ca<sub>v</sub>1 (L-type) channels (Grant, 2009). Even though we did not perform experiments to directly evaluate calcium dynamics, it is likely that activation of voltage-activated calcium channels may account for the inward current 'hump' observed here. Thus, Ca<sup>2+</sup> recruitment through voltage-gated channels, most probably via Ca<sub>v</sub>1 (L-type) channels, ensures that coupling to small-conductance Ca<sup>2+</sup>-activated K<sup>+</sup> outward currents occur as described for CMs (Lu et al., 2007). Consistent with this, we showed that the outward K<sup>+</sup> current (Figure 5.6B) was clearly voltage-dependent with the maximal amplitude obtained when cells were depolarized with a prepulse reaching -10 mV, *i.e.* close to the maximum activation of Ca<sub>v</sub>1 (L-type) currents. Indirect measurements of contractions obtained from video data analysis revealed that hiPSC-CMs subjected to 7 days of cold storage as 2D monolayers respond appropriately to different chronotropic agents (Figure 5.6C-H).



**Figure 5.6. Functional characterization of hiPSC-CMs subjected to hypothermic storage for 7 days.** After hypothermic storage for 7 days and one week in culture post-storage, cell functionality was evaluated by the detection of CM-specific action potentials (AP, **A-B**), typical CM response to drugs (**C-H**) and calcium transients (**I-J**). **A**) Whole-cell voltage-clamp recordings from hiPSC-CMs subjected to 7 days of hypothermic storage as 2D monolayers. **A - left panel)** Representative currents following a set of voltage pulses (260 ms), covering a wide range of potentials, with incremental depolarization steps (10 mV) from -130 to 0 mV (holding voltage -70 mV) (see inset). **A - right panel)** Corresponding current-voltage relationship showing 3 different components in terms of voltage dependence: a strong inward rectifier, an inward 'hump', and a delayed outward current. **B)** Representative current traces from a triple set of double depolarizing pulses: one first step to -40, -10 and +20 mV, lasting 50 ms, followed by a second pulse to +40 mV, lasting 750 ms (see inset). One can notice a larger outward current at +40 mV when preceded by a prepulse to -10mV, which suggest a  $Ca^{2+}$ -dependent current component. **C-H)** Effect of chronotropic drugs: 30 mM KCL **C)**, 1  $\mu$ M Verapamil **D)**, 0.5 mM

Adrenaline (**E-F**), and 300 pM Nimodipina (**G-H**), on contractile activity of hiPSC-CMs (cultured as 2D monolayers) subjected to 7 days of hypothermic storage, analysed by video recording in an inverted microscopy. **I**) Pseudo-color images showing minimal ( $\text{Ca}^{2+}$  min, left image) and maximal ( $\text{Ca}^{2+}$  max, right image) intensity of the calcium indicator dye Rhod-3. The six hiPSC-CMs analysed (from plated 3D aggregates) are highlighted. **J**) Graphical representation of calcium level cycling, during hiPSC-CMs contraction, determined by confocal imaging of the Rhod-3 dye, for the six different hiPSC-CMs. Data are presented as mean  $\pm$  SD of twenty four (**F, H**) measurements.  $P < 0.001$  (\*\*\*), Not-significant (ns) determined by unpaired t test.

An increase in  $\text{K}^+$  concentration from 5 to 30 mM shifted the potential equilibrium of  $\text{K}^+$  resulting in membrane potential depolarization and consequently in a strong and sustained contraction (Figure 5.6C).

The addition of verapamil (1  $\mu\text{M}$ ), which specifically blocks L-type  $\text{Ca}^{2+}$  channels, reduced the beating frequency and ultimately arrested beating (Figure 5.6D). On the other hand the administration of 0.5  $\mu\text{M}$  of Adrenaline, a  $\beta$ -receptor agonist, increased significantly the beating frequency of hiPSC-CMs but not the duration of the contraction events (Figure 5.6E-F). The treatment with nimodipine (300 pM), a L-type  $\text{Ca}^{2+}$  channel blocker, evoked subtle but meaningful effects on beating behaviour. Beating frequency remained constant whereas the duration of the contractions significantly decreased (Figure 5.6G-H). These data strongly suggested the existence of L-type voltage activated  $\text{Ca}^{2+}$  currents in hiPSC-CMs after hypothermic storage.

Real-time intracellular calcium imaging, using the calcium indicator dye Rhod-3, revealed that 2D monolayers (not shown) and 3D aggregates of hiPSC-CMs present synchronized oscillatory patterns of intracellular calcium concentrations (Figure 5.6I-J).

Overall, these results clearly show that murine and human iPSC-CMs exhibit intact molecular, ultrastructural and functional properties after one week of hypothermic storage.

#### 4. Discussion

Several studies have focused on the development of methods to preserve primary cultures of neonatal and adult CMs from rat and mouse origin (Ku et al., 1997; Orita et al., 1994; See et al., 1992; Snyder et al., 2005; Vettel et al., 2014; Wheeler and Chien, 2012), but little has been done to optimize the short- and long- term storage of hPSC-CMs that more accurately reflect the physiology of human CMs. In this study we developed efficient strategies for the hypothermic storage of 2D monolayers and 3D aggregates of hPSC-CMs. We showed that both 2D cell monolayers and 3D cell aggregates of mPSC-CMs can be maintained for up to one week in hypothermic conditions without meaningful effects on cell viability (>90% of cell recovery), structure and functionality (including action potential and drug responsiveness). However, we verified that hPSC-CMs are more sensitive to hypothermia/rewarming-induced stress than mPSC-CMs. A 30% decrease in cell viability was observed in hPSC-CMs preserved as monolayers, when the storage interval was extended from 3 to 7 days. In fact, it is not surprising that murine and human PSC-CMs present such a different tolerance to hypothermic storage as several studies have described significant differences in the transcriptional networks, global molecular signatures and signaling pathways in mouse and human PSC (Ernst et al., 2015; Schnerch et al., 2010). These differences likely justify the distinct developmental potentials, culture requirements and epigenetic landscapes

observed in these cells (Schnerch et al., 2010). Mu and coworkers showed significant differences in the induction of differentiation of murine and human ESCs into CMs as well as in specific features of each CM derivative, including average beating frequency and response to 24h of hypoxia stimulation (Mu et al., 2014).

In this work, we showed that hPSC-CM aggregates subjected to 5 and 7 days of hypothermic preservation present similar cell recoveries post-storage. After 7 days of hypothermic storage, cell recoveries were higher in PSC-CM aggregates (70%) than in PSC-CM monolayers (50%). These results suggest that a 3D architecture confers an additional protection to extended hypothermia-induced stress, possibly due to the formation of vast and stable cell-to-cell and cell-to-extracellular matrix (ECM) interactions. It has been reported that a tridimensional organization favors the establishment and maintenance of cellular junctions between cardiac cells (Soares et al., 2012). In the same study, the authors demonstrated that aggregates of cardiac cells exhibit a larger number of intercellular junctions and a higher amount of ECM connecting the cells comparatively to 2D-cultures (Soares et al., 2012). Interestingly, it has been shown that in 3D conformations, cell extensions become entangled with ECM fibrils, resulting in integrin-independent mechanical interactions that strengthen cell anchorage (Jiang and Grinnell, 2005). All these findings support our supposition that spatial organization of PSC-CMs may affect their biological response to hypothermic storage.

It has been reported that hypothermic storage may induce adverse effects on cells, including hypoxic stress, ischemia and reperfusion injury, disruptions in membrane potential (redox balance), cellular ionic imbalances (disturbance of  $\text{Na}^+$ ,  $\text{Ca}^{2+}$  and  $\text{Fe}^{2+}$  homeostasis), generation of reactive oxygen species (ROS), collapse of cytoskeleton and ultrastructural damage (Bishopric et al., 2001; Boutilier, 2001; Rauen and De Groot, 1998; Stefanovich et al., 1995; Taylor, 2006; Taylor et al., 2005). These effects are more pronounced with increasing hypothermic storage interval, resulting in the activation of necrotic or apoptotic cell death pathways (Taylor, 2006; Taylor et al., 2005). Activation of the apoptotic cascade takes hours to days to be fully manifested after cells or tissues were removed from storage. Thus, to assess the efficiency of the preservation strategy, cell recovery should be assessed for an extended time period in culture post-storage and preferably using complementary characterization techniques. In this study we evaluated CM recovery during 7 days of culture post-storage, through the analysis of cellular membrane integrity (FDA/PI staining, trypan blue exclusion test); metabolic activity (PrestoBlue assay) and detection of apoptosis activation and mitochondrial activity (Quantification of caspase activity and MitoView/NucView™ staining). As expected, extended hypothermic preservation intervals induced both necrosis and apoptosis of hPSC-CMs, particularly in 2D monolayer cultures. Nonetheless, hPSC-CMs that recovered from hypothermic storage, either in 3D aggregate or in 2D monolayer cultures, maintained their phenotype as reflected by a typical CM structure/ultrastructure and cardiac protein expression profile. The expression of typical CM genes (including transcription factors, specific structural genes and ionic channels) revealed to be significantly higher in stored hiPSC-CMs than in the control, suggesting that hypothermia state may enhance CM enrichment/maturation processes. A recent study reported that apoptotic *stimuli*, more specifically a sublethal caspase-



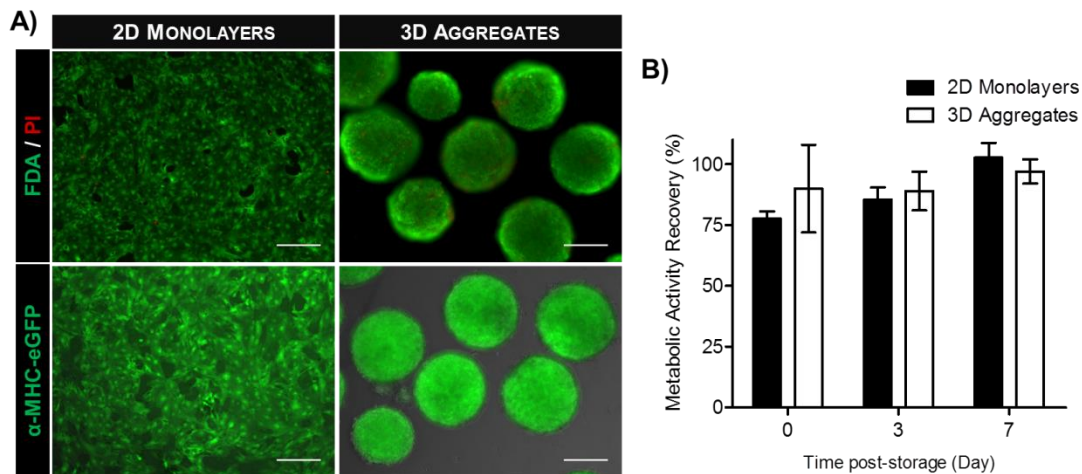
activation, up-regulates cardiac progenitor and CM differentiation, increasing the final yield of CMs (Bulatovic et al., 2015). As shown in our study and in others (Mahler et al., 2003; Snyder et al., 2005; Taylor, 2006) the hypothermic state promotes caspase activation, consequently we could also speculate about an interference of cold preservation in cardiogenic pathways. Importantly, hiPSC-CMs subjected to 7 days of hypothermic storage maintained their functionality, exhibiting features typical from healthy CMs including: i) several ionic conductances (IKr, outward delayed rectifiers, and Ca<sup>2+</sup> activated K<sup>+</sup> currents) (Ma et al., 2011), ii) indirect 'fingerprints' of voltage activated L-type Ca<sup>2+</sup> currents (Ma et al., 2011), and iii) appropriate contractile activity response to chronotropic agents (Dick et al., 2010).

Commercially available hypothermic solutions, such as HTS, were carefully formulated to maintain the ionic and osmotic balances, inhibit acidosis and prevent cell swelling at low temperatures (Mathew et al., 2004; Taylor, 2006). These features facilitate preservation of cell homeostasis, not achievable when using just culture medium as a preservation formulation. For example, normal human epidermal keratinocytes can be maintained for periods exceeding one week at 4°C in HTS and only 24 hours in normal growth media at 4°C (Van Buskirk et al., 1996). Currently, the incorporation of protective agents, including antioxidants, ion chelators and membrane stabilizers in preservation media has been reported to markedly improve preservation efficacy. For example, fructose-1,6-bisphosphate (Wheeler and Chien, 2012; Wheeler et al., 2005), 2,3-butanedione (Fagbemi and Northover, 1996; Wheeler and Chien, 2012), Myosin II ATPase inhibiting-agents (Abi-Gerges et al., 2013), dopamine and lipophilic derivatives (Vettel et al., 2014), and human neuregulin-1 peptide (Jabbour et al., 2011) proved to be efficient in improving the post-storage viability in mouse/rat hearts and/or CMs. A recent study with preserved bioartificial livers showed that an improved protective effect can be obtained if distinct agents are added to the storage solution during the appropriate preservation stage (pre-incubation, hypothermia and rewarming) (Dai and Meng, 2011). Specific protective agents could also be combined with our cold storage preservation protocol to further enhance preservation efficacy after extended storage intervals.

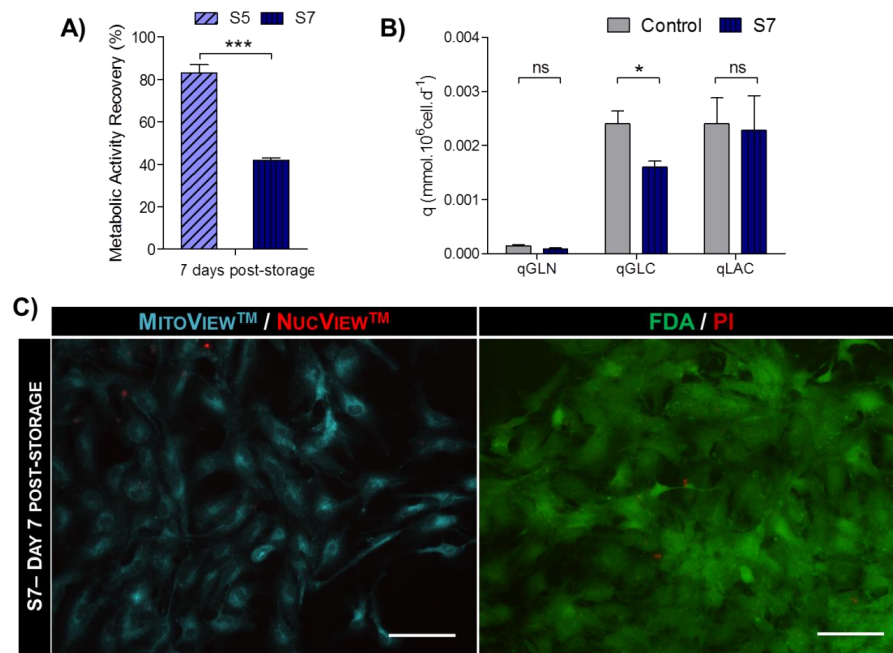
In summary, we established effective and clinical compatible strategies for cold storage of 2D monolayers and 3D aggregates of murine and human PSC-CMs and provided some evidences about the appropriate time interval to store PSC-CMs at hypothermic conditions without compromising their viability, phenotype and function. These preservation strategies can be integrated with the differentiation process, avoiding additional and possible harmful manipulation of cells, such as monolayer/aggregate dissociation. Moreover, these strategies enable cell products to be manufactured off-site in certified companies. Importantly, our approach for hypothermic storage of 2D monolayers of PSC-CM will facilitate the delivery of certified, validated, ready-to-use cell plates suitable for high-throughput cardiac drug testing and toxicity screening, whereas the one-week storage strategy for PSC-CM aggregates will allow the distribution of not only off-the-shelf tissue like *in vitro* models for cardiac toxicity drug testing but also therapeutic cells that could be directly used in cardiac regenerative therapies. In fact, it has been demonstrated that the delivery of cardiac progenitor cells in the form of 3D cell aggregates improved *in vivo* survival of implanted

cells in a murine model of cardiac injury (Bauer et al., 2012). The strategies for cold preservation of PSC-CM described herein contribute to overcome the hurdles and needs of the regenerative medicine market and scientific community, constituting a step forward towards improved worldwide commercial distribution of hPSC-CMs for use in the clinic and biopharmaceutical industry.

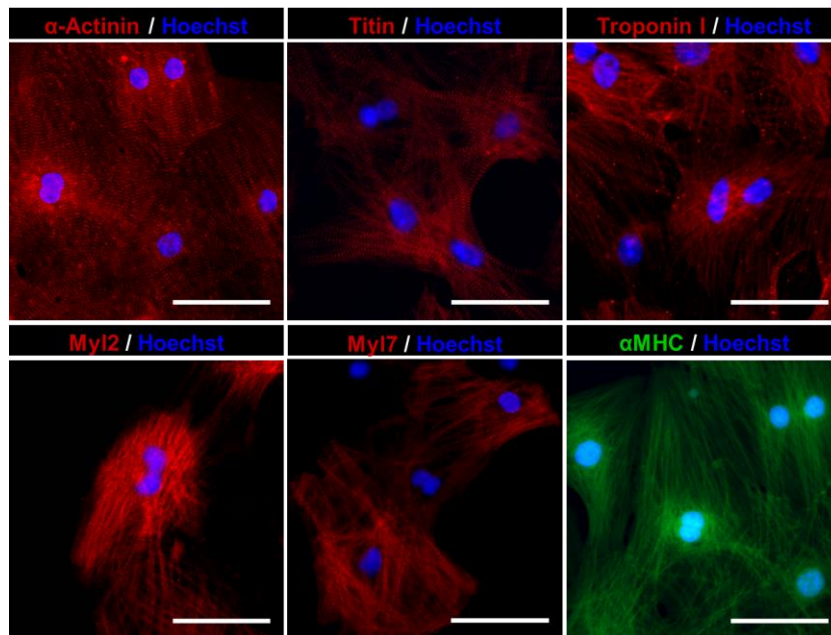
## 5. Appendix



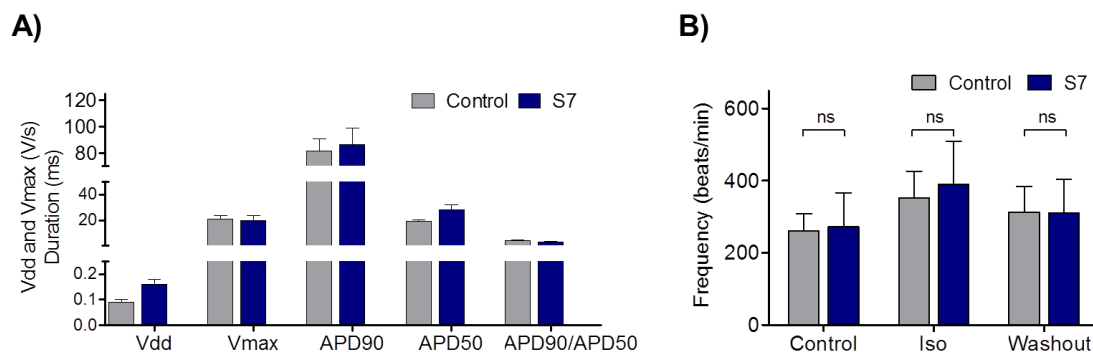
**Figure A-5.1. Hypothermic storage of murine iPSC-CMs.** 2D monolayers and 3D aggregates of miPSC-CMs were stored for 7 days at 4°C in HTS solution. Cell recovery post-storage was evaluated for 7 days. Cell viability was assessed by cell staining with FDA (live cells, green) and PI (dead cells, red) - **A upper panel** - and by evaluation of  $\alpha$ -MHC-eGFP expression (green) - **A lower level**. Photos were taken at day 1 post-storage. Scale bars: 200  $\mu$ m. **B)** Evaluation of metabolic activity recovery during 7 days post-storage using the PrestoBlue assay. The fluorescence values of PrestoBlue are presented as a % in relation to the values obtained with the same cells immediately before cold storage.



**Figure A-5.2. Hypothermic preservation of hESC-CM as 2D monolayers.** Cells were stored for 5 (S5) and 7 (S7) days at 4°C in HTS solution. Cell recovery was evaluated for 7 days post-storage. **A-B)** Metabolic performance of hESC-CMs post-storage. **A)** Evaluation of metabolic activity recovery using the PrestoBlue assay. **B)** Mean specific rates of glutamine (qGLN) and glucose (qGLC) consumption and lactate production (qLAC) during one week in culture post-storage. Control refers to cells not subjected to hypothermic storage. Data are presented as mean  $\pm$  SD of five measurements.  $P < 0.05$  (\*),  $P < 0.001$  (\*\*\*), Not-significant (ns), determined by unpaired t test. **C)** Viability analysis of hESC-CMs stored for 5 days at 4°C, assessed at day 7 post-storage, using the MitoView™ (functional mitochondria, cyan) and NucView™ (apoptotic cells, red) – **right panel** and FDA (live cells, green) and PI (dead cells, red) – **left panel**. Scale bars: 100µm.



**Figure A-5.3. Immunofluorescence labelling of miPSC-CMs after hypothermic storage as 2D monolayers.** Cells were stained using the CM-specific, sarcomeric  $\alpha$ -actinin, titin, troponin I, Myl2 and Myl7, antibodies (red). Expression of eGFP driven by the cardiac promoter  $\alpha$ -MHC (green) was also detected. Nuclei were labelled with Hoeschst 33432 (blue). Scale bars: 50 µm.



**Figure A-5.4. Functional characterization of miPSC-CMs subjected to hypothermic storage for 7 days.** Cell functionality was evaluated in cells stored for 7 days (S7, blue bars) and non-stored miPSC-CMs (control, grey bars) cultured as 3D aggregates by the detection of CM-specific action potentials (AP, **A**) and typical CM response to drugs (**B**). **A**) Action potential properties of miPSC-CMs: Vdd, velocity of diastolic depolarization; Vmax, the maximum rate of rise of the action potential upstroke; APD90, action potential duration at 90% of repolarization; APD50, action potential duration at 50% of repolarization. **B**) Effect of 1  $\mu$ M Isoproterenol (Iso) on beating frequency of miPSC-CMs. Data are presented as mean  $\pm$  SD of six (**A-B**) measurements. Not-significant (ns) determined by unpaired t test.

## 6. Acknowledgments

The authors acknowledge: Dr. David Elliott for providing the PSC lines used in this study and support on the cardiomyocyte differentiation protocol; Dr. Thomas Kurth for performing TEM/SEM analyses and helping with result interpretation. Pedro Sampaio and Susana Lopes (CEDOC) for the use and assistance of Image acquisition and analyses system. This work was supported by FP7 EU project CARE-MI (HEALTH-2009\_242038) and the Fundação para a Ciência e Tecnologia (FCT) funded projects CARDIOSTEM (MITP-TB/ECE/0013/2013), CardioRegen (HMSP-ICT/0039/2013) and CardioRecept (PTDC/BBB-BIO/1414) for financial support. iNOVA4Health - UID/Multi/04462/2013, a program financially supported by FCT / Ministério da Educação e Ciência, through national funds and co-funded by FEDER under the PT2020 Partnership Agreement is also acknowledged. CC acknowledges the FCT for her PhD grant (SFRH/BD/51573/2011).

## 7. References

- Abbasalizadeh, S., and Baharvand, H. (2013). Technological progress and challenges towards cGMP manufacturing of human pluripotent stem cells based therapeutic products for allogeneic and autologous cell therapies. *Biotechnol. Adv.* 31, 1600–1623.
- Abi-Gerges, N., Pointon, A., Pullen, G.F., Morton, M.J., Oldman, K.L., Armstrong, D., Valentin, J.P., and Pollard, C.E. (2013). Preservation of cardiomyocytes from the adult heart. *J. Mol. Cell. Cardiol.* 64, 108–119.
- Bauer, M., Kang, L., Qiu, Y., Wu, J., Peng, M., Chen, H.H., Camci-Unal, G., Bayomy, A.F., Sosnovik, D.E., Khademosseini, A., et al. (2012). Adult cardiac progenitor cell aggregates exhibit survival benefit both in vitro and in vivo. *PLoS One* 7, e50491.
- Baust, J.M. (2005). Advances in Media for Cryopreservation and Hypothermic Storage. *Bioprocess Biosyst Eng* 46–56.
- Bessems, M., Doorschodt, B.M., van Vliet, A.K., and van Gulik, T.M. (2004). Preservation of rat livers by cold storage: a comparison between the University of Wisconsin solution and Hypothermosol. *Ann. Transplant.* 9, 35–37.

- Bishopric, N.H., Andreka, P., Slepak, T., and Webster, K.A. (2001). Molecular mechanisms of apoptosis in the cardiac myocyte. *Curr. Opin. Pharmacol.* *1*, 141–150.
- Boutillier, R.G. (2001). Mechanisms of cell survival in hypoxia and hypothermia. *J. Exp. Biol.* *204*, 3171–3181.
- Bulatovic, I., Ibarra, C., Österholm, C., Wang, H., Beltrán-Rodríguez, A., Varas-Godoy, M., Månsson-Broberg, A., Uhlén, P., Simon, A., and Grinnemo, K.-H. (2015). Sublethal Caspase Activation Promotes Generation of Cardiomyocytes from Embryonic Stem Cells. *PLoS One* *10*, e0120176.
- Van Buskirk, R.G., Rauch, J., Robert, S., Taylor, M.J., and Baust, J.G. (1996). Assessment of hypothermic storage of normal human epidermal keratinocytes (NHEK) using Alamar Blue. *Vitr. Tox.* *9*, 297–303.
- Chen, K.G., Mallon, B.S., McKay, R.D.G., and Robey, P.G. (2014). Human pluripotent stem cell culture: considerations for maintenance, expansion, and therapeutics. *Cell Stem Cell* *14*, 13–26.
- Cook, J.R., Eichelberger, H., Robert, S., Rauch, J., Baust, J.G., Taylor, M.J., and Buskirk, R.G. (1995). Cold-Storage of Synthetic Human Epidermis in HypoThermosol. *Tissue Eng.* *1*, 361–377.
- Correia, C., Serra, M., Espinha, N., Sousa, M., Brito, C., Burkert, K., Zheng, Y., Hescheler, J., Carrondo, M.J.T., Sarić, T., et al. (2014). Combining Hypoxia and Bioreactor Hydrodynamics Boosts Induced Pluripotent Stem Cell Differentiation Towards Cardiomyocytes. *Stem Cell Rev.* *10*, 786–801.
- Dai, J., and Meng, Q. (2011). Differential function of protective agents at each stage of the hypothermic preservation of hepatocytes. *J. Biochem.* *149*, 739–745.
- Decker, T., and Lohmann-Matthes, M.L. (1988). A quick and simple method for the quantitation of lactate dehydrogenase release in measurements of cellular cytotoxicity and tumor necrosis factor (TNF) activity. *J. Immunol. Methods* *115*, 61–69.
- Dick, E., Rajamohan, D., Ronksley, J., and Denning, C. (2010). Evaluating the utility of cardiomyocytes from human pluripotent stem cells for drug screening. *Biochem. Soc. Trans.* *38*, 1037–1045.
- Duret, C., Moreno, D., Anangi, B., and Roux, S. (2015). Cold-preservation of human adult hepatocytes for liver cell therapy.
- Elliott, D.A., Braam, S.R., Koutsis, K., Ng, E.S., Jenny, R., Lagerqvist, E.L., Biben, C., Hatzistavrou, T., Hirst, C.E., Yu, Q.C., et al. (2011). NKX2-5eGFP/w hESCs for isolation of human cardiac progenitors and cardiomyocytes. *Nat. Methods* *8*, 1037–1040.
- Ernst, M., Dawud, R.A., Kurtz, A., Schotta, G., Taher, L., and Fuellen, G. (2015). Comparative computational analysis of pluripotency in human and mouse stem cells. *Sci. Rep.* *5*, 7927.
- Fagbemi, O.S., and Northover, B.J. (1996). Effect of protein kinase C inhibitors and 2,3-butanedione monoxime on the long-term hypothermic preservation of isolated rat hearts. *Clin. Sci. (Lond.)* *91*, 745–754.
- Gherghiceanu, M., Barad, L., Novak, A., Reiter, I., Itskovitz-Eldor, J., Binah, O., and Popescu, L.M. (2011). Cardiomyocytes derived from human embryonic and induced pluripotent stem cells: Comparative ultrastructure. *J. Cell. Mol. Med.* *15*, 2539–2551.
- Gramignoli, R., Dorko, K., Tahan, V., Skvorak, K.J., Ellis, E., Jorns, C., Ericzon, B.G., Fox, I.J., and Strom, S.C. (2014). Hypothermic storage of human hepatocytes for transplantation. *Cell Transplant.* *23*, 1143–1151.
- Grant, A.O. (2009). Cardiac ion channels. *Circ. Arrhythmia Electrophysiol.* *2*, 185–194.
- Halbach, M., Peinkofer, G., Baumgartner, S., Maass, M., Wiedey, M., Neef, K., Krausgrill, B., Ladage, D., Fatima, A., Saric, T., et al. (2013). Electrophysiological integration and action potential properties of transplanted cardiomyocytes derived from induced pluripotent stem cells. *Cardiovasc. Res.* *100*, 432–440.
- Healy, L., Young, L., and Stacey, G.N. (2011). Stem cell banks: Preserving cell lines, maintaining genetic integrity, and advancing research. *Methods Mol. Biol.* *767*, 15–27.
- Hrabalová, M., Bachleda, P., Lubuská, L., Kojecký, Z., Zadrazil, J., Krejčí, K., and Al Jabry, S.

- (2003). Effect of various protective solutions on function after kidney transplantation. *Biomed. Pap. Med. Fac. Univ. Palacký, Olomouc, Czechoslov.* 147, 197–202.
- Jabbour, A., Gao, L., Kwan, J., Watson, A., Sun, L., Qiu, M.R., Liu, X., Zhou, M.D., Graham, R.M., Hicks, M., et al. (2011). A recombinant human neuregulin-1 peptide improves preservation of the rodent heart after prolonged hypothermic storage. *Transplantation* 91, 961–967.
- Jiang, H., and Grinnell, F. (2005). Cell-matrix entanglement and mechanical anchorage of fibroblasts in three-dimensional collagen matrices. *Mol. Biol. Cell* 16, 5070–5076.
- Jones, K.H., and Senft, J.A. (1985). An improved method to determine cell viability by simultaneous staining with fluorescein diacetate-propidium iodide. *J. Histochem. Cytochem.* 33, 77–79.
- Ku, K., Oku, H., Alam, M.S., Saitoh, Y., Nosaka, S., and Nakayama, K. (1997). Prolonged hypothermic cardiac storage with histidine-tryptophan-ketoglutarate solution: comparison with glucose-insulin-potassium and University of Wisconsin solutions. *Transplantation* 64, 971–975.
- Kuzmenkin, A., Liang, H., Xu, G., Pfannkuche, K., Eichhorn, H., Fatima, A., Luo, H., Saric, T., Wernig, M., Jaenisch, R., et al. (2009). Functional characterization of cardiomyocytes derived from murine induced pluripotent stem cells in vitro. *FASEB J.* 23, 4168–4180.
- Li, Y., and Ma, T. (2012). Bioprocessing of cryopreservation for large-scale banking of human pluripotent stem cells. *Biores. Open Access* 1, 205–214.
- Lian, X., Zhang, J., Azarin, S.M., Zhu, K., Hazeltine, L.B., Bao, X., Hsiao, C., Kamp, T.J., and Palecek, S.P. (2013). Directed cardiomyocyte differentiation from human pluripotent stem cells by modulating Wnt/ $\beta$ -catenin signaling under fully defined conditions. *Nat. Protoc.* 8, 162–175.
- Lu, J., Hou, R., Booth, C.J., Yang, S.-H., and Snyder, M. (2006). Defined culture conditions of human embryonic stem cells. *Proc. Natl. Acad. Sci. U. S. A.* 103, 5688–5693.
- Lu, L., Zhang, Q., Timofeyev, V., Zhang, Z., Young, J.N., Shin, H.-S., Knowlton, A.A., and Chiamvimonvat, N. (2007). Molecular coupling of a Ca<sup>2+</sup>-activated K<sup>+</sup> channel to L-type Ca<sup>2+</sup> channels via  $\alpha$ -actinin2. *Circ. Res.* 100, 112–120.
- Lundy, S.D., Gantz, J.A., Pagan, C.M., Filice, D., and Laflamme, M.A. (2014). Pluripotent stem cell derived cardiomyocytes for cardiac repair. *Curr. Treat. Options Cardiovasc. Med.* 16, 319.
- Ma, J., Guo, L., Fiene, S.J., Anson, B.D., Thomson, J. a, Kamp, T.J., Kolaja, K.L., Swanson, B.J., and January, C.T. (2011). High purity human-induced pluripotent stem cell-derived cardiomyocytes: electrophysiological properties of action potentials and ionic currents. *Am. J. Physiol. Heart Circ. Physiol.* 301, H2006-17.
- Mahler, S., Desille, M., Frémond, B., Chesné, C., Guillouzo, A., Campion, J.P., and Clément, B. (2003). Hypothermic storage and cryopreservation of hepatocytes: The protective effect of alginate gel against cell damages. *Cell Transplant.* 12, 579–592.
- Mathew, A.J., Van Buskirk, R.G., and Baust, J.G. (2002). Improved Hypothermic Preservation of Human Renal Cells Through Suppression of Both Apoptosis and Necrosis. *Cell Preserv. Technol.* 1, 239–253.
- Mathew, A.J., Baust, J.M., Van Buskirk, R.G., and Baust, J.G. (2004). Cell preservation in reparative and regenerative medicine: evolution of individualized solution composition. *Tissue Eng.* 10, 1662–1671.
- Minasian, S.M., Galagudza, M.M., Dmitriev, Y. V., Karpov, a. a., and Vlasov, T.D. (2014). Preservation of the donor heart: from basic science to clinical studies. *Interact. Cardiovasc. Thorac. Surg.* 1–10.
- Mu, J., Li, X., Yuan, S., Zhang, J., and Bo, P. (2014). Comparative study of directional differentiation of human and mouse embryonic stem cells into cardiomyocytes. *Cell Biol. Int.* 38, 1098–1105.
- Mummery, C.L., Zhang, J., Ng, E.S., Elliott, D. a, Elefanty, A.G., and Kamp, T.J. (2012). Differentiation of human embryonic stem cells and induced pluripotent stem cells to cardiomyocytes: a methods overview. *Circ. Res.* 111, 344–358.
- Orita, H., Fukasawa, M., Hirooka, S., Uchino, H., Fukui, K., Kohi, M., and Washio, M. (1994). Cardiac myocyte functional and biochemical changes after hypothermic preservation in vitro.

- Protective effects of storage solutions. *J. Thorac. Cardiovasc. Surg.* 107, 226–232.
- Orita, H., Fukasawa, M., Uchino, H., Uchida, T., Shiono, S., and Washio, M. (1995). Long-term hypothermic preservation of cardiac myocytes isolated from the neonatal rat ventricle: A comparison of various crystalloid solutions. *Surg. Today* 25, 251–256.
- Rauen, U., and De Groot, H. (1998). Cold-induced release of reactive oxygen species as a decisive mediator of hypothermia injury to cultured liver cells. *Free Radic. Biol. Med.* 24, 1316–1323.
- Rubinsky, B. (2003). Principles of low temperature cell preservation. *Heart Fail. Rev.* 8, 277–284.
- Schnerch, A., Cerdan, C., and Bhatia, M. (2010). Distinguishing between mouse and human pluripotent stem cell regulation: the best laid plans of mice and men. *Stem Cells* 28, 419–430.
- See, Y.P., Weisel, R.D., Mickle, D.A., Teoh, K.H., Wilson, G.J., Tumati, L.C., Mohabeer, M.K., Madonik, M.M., Axford-Gatley, R.A., and Salter, D.R. (1992). Prolonged hypothermic cardiac storage for transplantation. The effects on myocardial metabolism and mitochondrial function. *J. Thorac. Cardiovasc. Surg.* 104, 817–824.
- Serra, M., Brito, C., Sousa, M.F.Q., Jensen, J., Tostões, R., Clemente, J., Strehl, R., Hyllner, J., Carrondo, M.J.T., and Alves, P.M. (2010). Improving expansion of pluripotent human embryonic stem cells in perfused bioreactors through oxygen control. *J. Biotechnol.* 148, 208–215.
- Serra, M., Correia, C., Malpique, R., Brito, C., Jensen, J., Bjorquist, P., Carrondo, M.J.T., and Alves, P.M. (2011). Microencapsulation Technology: A Powerful Tool for Integrating Expansion and Cryopreservation of Human Embryonic Stem Cells. *PLoS One* 6, 1–13.
- Serra, M., Brito, C., Correia, C., and Alves, P.M. (2012). Process engineering of human pluripotent stem cells for clinical application. *Trends Biotechnol.* 30, 1–10.
- Sinnecker, D., Laugwitz, K.-L., and Moretti, A. (2014). Induced pluripotent stem cell-derived cardiomyocytes for drug development and toxicity testing. *Pharmacol. Ther.* 143, 246–252.
- Skelton, R.J.P., Costa, M., Anderson, D.J., Bruveris, F., Finnin, B.W., Koutsis, K., Arasaratnam, D., White, A.J., Rafii, A., Ng, E.S., et al. (2014). SIRPA, VCAM1 and CD34 identify discrete lineages during early human cardiovascular development. *Stem Cell Res.* 13, 172–179.
- Snyder, K.K., Baust, J.M., Van Buskirk, R.G., and Baust, J.G. (2005). Enhanced Hypothermic Storage of Neonatal Cardiomyocytes. *Cell Preserv. Technol.* 3, 61–74.
- Soares, C.P., Midlej, V., de Oliveira, M.E.W., Benchimol, M., Costa, M.L., and Mermelstein, C. (2012). 2D and 3D-organized cardiac cells shows differences in cellular morphology, adhesion junctions, presence of myofibrils and protein expression. *PLoS One* 7, e38147.
- Squifflet, J.P., Ledinh, H., De Roover, A., and Meuris, M. (2011). Pancreas preservation for pancreas and islet transplantation: A minireview. In *Transplantation Proceedings*, pp. 3398–3401.
- Stefanovich, P., Ezzell, R.M., Sheehan, S.J., Tompkins, R.G., Yarmush, M.L., and Toner, M. (1995). Effects of hypothermia on the function, membrane integrity, and cytoskeletal structure of hepatocytes. *Cryobiology* 32, 389–403.
- Taylor, M.J. (2006). Biology of Cell Survival in the Cold: The Basis for Biopreservation of Tissues and Organs. In *Advances in Biopreservation*, J. Baust, and J. Baust, eds. (Boca Raton, Fla: CRC/Taylor & Francis), pp. 15–62.
- Taylor, M.J., Rhee, P., Chen, Z., and Alam, H.B. (2005). Design of preservation solutions for universal tissue preservation in vivo: Demonstration of efficacy in preclinical models of profound hypothermic cardiac arrest. In *Transplantation Proceedings*, pp. 303–307.
- Thirumala, S., Goebel, W.S., and Woods, E.J. (2009). Clinical grade adult stem cell banking. *Organogenesis* 5, 143–154.
- Uchida, T., Nagayama, M., Taira, T., Shimizu, K., Sakai, M., and Gohara, K. (2011). Optimal temperature range for low-temperature preservation of dissociated neonatal rat cardiomyocytes. *Cryobiology* 63, 279–284.
- Venable, J.H., and Coggeshall, R. (1965). A Simplified Lead Citrate Stain for use in Electron Microscopy. *J. Cell Biol.* 25, 407–408.
- Vettel, C., Hottenrott, M.C., Spindler, R., Benck, U., Schnuelle, P., Tsagogiorgas, C., Krämer, B.K.,

Hoeger, S., El-Armouche, A., Wieland, T., et al. (2014). Dopamine and lipophilic derivatives protect cardiomyocytes against cold preservation injury. *J. Pharmacol. Exp. Ther.* 348, 77–85.

Vicente, M.I., Costa, P.F., and Lima, P.A. (2010). Galantamine inhibits slowly inactivating K<sup>+</sup> currents with a dual dose-response relationship in differentiated N1E-115 cells and in CA1 neurones. *Eur. J. Pharmacol.* 634, 16–25.

Wakayama, K., Fukai, M., Yamashita, K., Kimura, T., Hirokata, G., Shibasaki, S., Fukumori, D., Haga, S., Sugawara, M., Suzuki, T., et al. (2012). Successful transplantation of rat hearts subjected to extended cold preservation with a novel preservation solution. *Transpl. Int.* 25, 696–706.

Wang, Y., Cheng, L., and Gerecht, S. (2014). Efficient and scalable expansion of human pluripotent stem cells under clinically compliant settings: A view in 2013. *Ann. Biomed. Eng.* 42, 1357–1372.

Wheeler, T.J., and Chien, S. (2012). Protection of rat cardiac myocytes by fructose-1,6-bisphosphate and 2,3-butanedione. *PLoS One* 7, e35023.

Wheeler, T.J., Wiegand, C.B., and Chien, S. (2005). Fructose-1,6-bisphosphate enhances hypothermic preservation of cardiac myocytes. *J. Hear. Lung Transplant.* 24, 1378–1384.

Wong, R.C.B., Dottori, M., Koh, K.L.L., Nguyen, L.T. V, Pera, M.F., and Pébay, A. (2006). Gap junctions modulate apoptosis and colony growth of human embryonic stem cells maintained in a serum-free system. *Biochem. Biophys. Res. Commun.* 344, 181–188.

Zhang, M., Schulte, J.S., Heinick, A., Piccini, I., Rao, J., Quaranta, R., Zeuschner, D., Malan, D., Kim, K.-P., Röpke, A., et al. (2015). Universal Cardiac Induction of Human Pluripotent Stem Cells in 2D and 3D formats - Implications for In-Vitro Maturation. *Stem Cells* 33, 1456–1469.





## **Discussion**

**Contents**

<b>1. Discussion .....</b>	<b>181</b>
1.1. Modulating dissolved oxygen and bioreactor hydrodynamic to improve CM differentiation .....	183
1.2. Using soluble molecules to guide the differentiation of hPSC towards CMs.....	185
1.3. Three dimensional cultures improve CM differentiation and confer resistance to prolonged hypothermic storage .....	186
1.4. Unveiling the role of metabolic substrate availability on CM differentiation and maturation .....	187
1.5. Assessment of hPSC-CM quality.....	189
1.6. hPSC-CM maturation: achievements and biological relevance. ....	190
1.7. Facilitating the widespread distribution of hPSC-CMs: Improvements in short-term storage and shipping of hPSC-CMs .....	192
<b>2. Future perspectives .....</b>	<b>193</b>
<b>3. Conclusion .....</b>	<b>194</b>
<b>4. References .....</b>	<b>194</b>

## 1. Discussion

Human pluripotent stem cells (hPSCs) have emerged as the most promising solution to overcome human cardiomyocyte (CM) scarcity. Due to their high proliferation capacity and differentiation potential, hPSCs can provide unlimited quantities of functional CMs for disease modeling, drug discovery, toxicity screening, mechanistic research and cell-based regenerative therapies (Denning et al., 2015). However, the high complexity of network signaling pathways, environmental factors and paracrine signaling involved in cardiac development *in vivo*, makes its *in vitro* recapitulation a tremendous challenge. Despite all the advances observed in this field, current protocols for hPSC differentiation towards CMs still generate limited numbers of metabolically, structurally and functionally immature CMs. Therefore, the production of hPSC derived CMs (hPSC-CMs) with improved maturation status, in sufficient quantity and with consistent quality (i.e. with the safety and standardization required in clinical-grade manufacturing processes or in pharmaceutical development) still remains as an unmet need. Moreover, the development of efficient, simple and safe methods for storage and worldwide shipment of these cells is another major requirement for the widespread use of hPSC-CMs.

The work developed in this thesis focused at addressing these needs with the ultimate goal of developing robust, scalable and integrated platforms for the production, maturation and storage of hPSC-CMs. The main bottlenecks and the strategies used to address them as well as the major achievements obtained in each chapter of this thesis are summarized in Figure 6.1.

The impact of several environmental and/or biological factors on CM differentiation, maturation and storage processes was studied (Figure 6.2). Briefly, in **Chapter 2** the impact of dissolved oxygen and bioreactor hydrodynamics on CM differentiation was studied using a murine reporter iPSC line, as a model system for bioprocess development, and a simple spontaneous embryoid body differentiation protocol to clearly identify the impact of each culture condition tested. In **Chapter 3** the effect of combining a directed differentiation protocol induced by a cocktail of soluble molecules (i.e. small molecules and growth factors) with forced aggregation of hPSC-derived cardiac committed cells on CM differentiation and enrichment was addressed. **Chapter 4** explored the impact of carbon substrate source availability on hPSC-CM maturation. In **Chapter 5** the feasibility to store 2D monolayers and 3D aggregates of hPSC-CMs at hypothermic conditions was evaluated and compared.

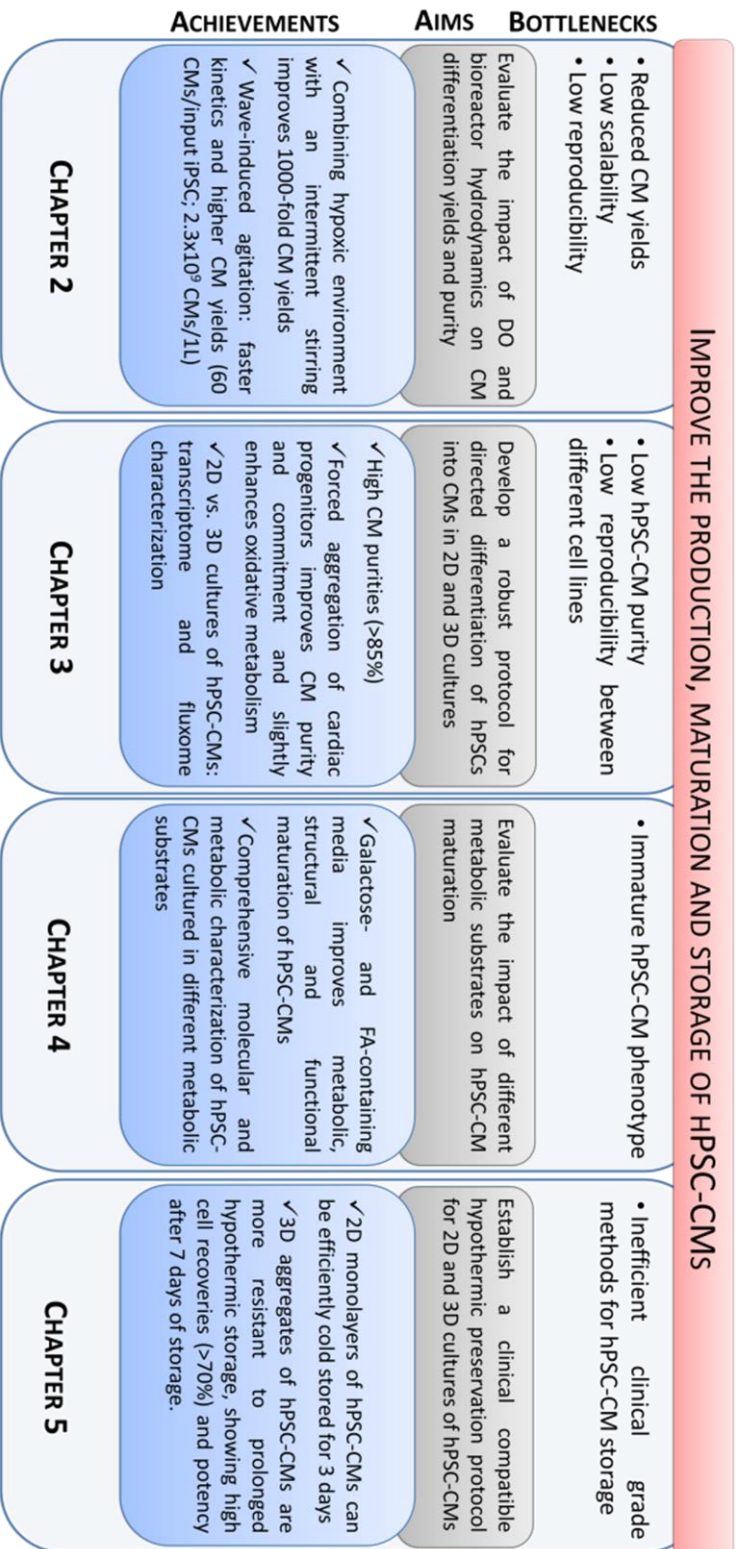
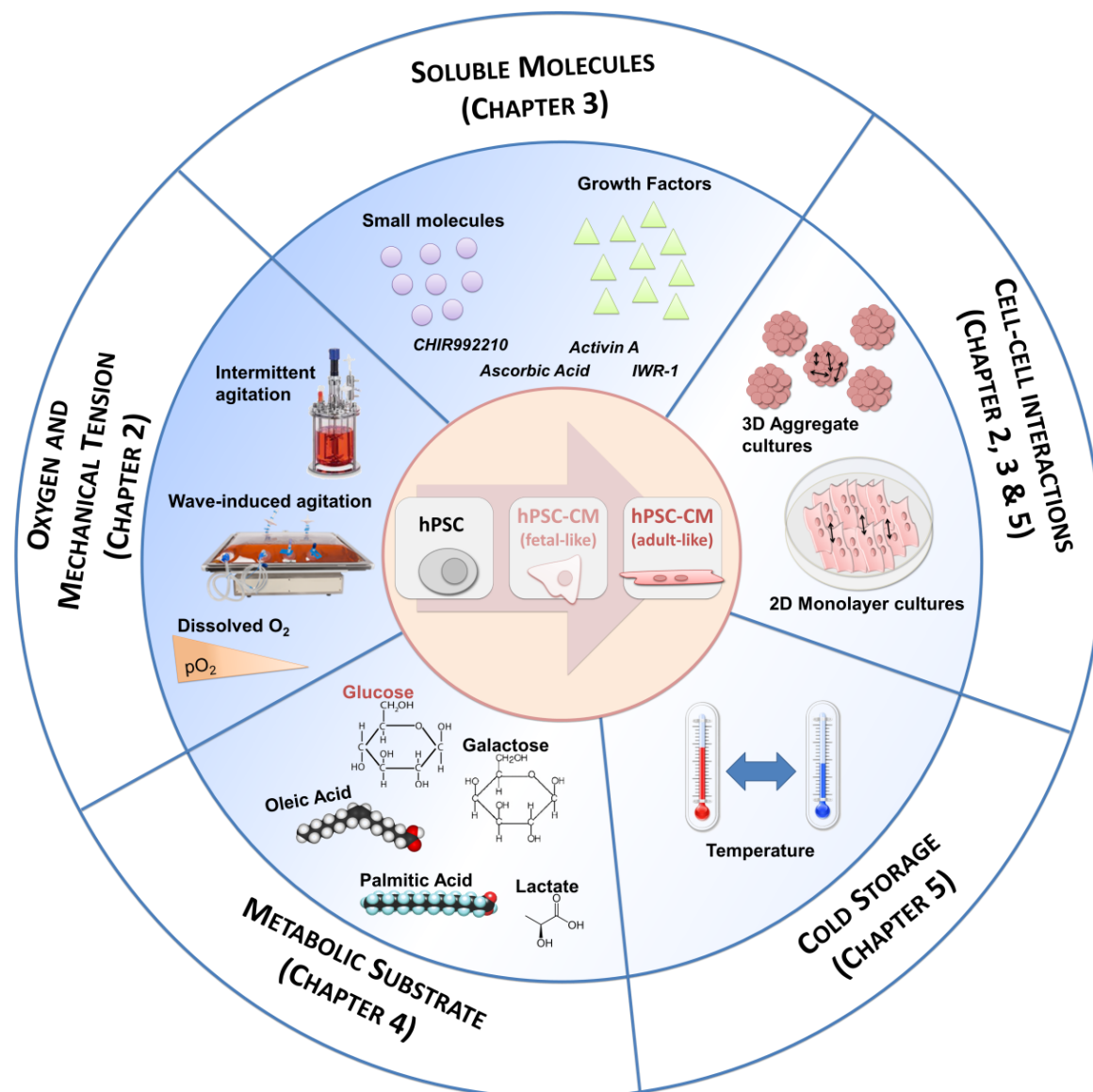


Figure 6.1 - Major bottlenecks, aims and achievements of each chapter of this thesis.



**Figure 6.2 - Microenvironmental features studied in this thesis.** The manipulation of these features improved differentiation, maturation and hypothermic storage of CMs.

### 1.1. Modulating dissolved oxygen and bioreactor hydrodynamics to improve CM differentiation

In **Chapter 2** we evaluated the effect of dissolved oxygen and compared the impact of different bioreactor hydrodynamics (in stirred tank and WAVE) on iPSC differentiation towards CMs. The results showed that combining an atmospheric hypoxia culture (4% O<sub>2</sub> tension) with an intermittent agitation profile in stirred tank bioreactors improves 1000-fold the CM yields when compared to atmospheric normoxia (20% O<sub>2</sub> tension) and continuously agitated cultures. Additionally, we show for the first time that wave-induced agitation further favours CM differentiation as demonstrated by faster kinetics, higher CM yields (60 CMs/input iPSC) and improved numbers of functional CMs ( $2.3 \times 10^9$  CMs generated in 1 L bioreactor).

In particular, this study showed that: i) controlled dissolved oxygen (DO) of 4% O<sub>2</sub> maximizes cell proliferation, and ii) intermittent stirring and wave induced agitation significantly improved CM differentiation efficiency (CM purity and yields).

The beneficial impact of lowering the dissolved oxygen tension from normoxic atmospheric (20% O<sub>2</sub>) to an atmospheric hypoxia level of 4% O<sub>2</sub>, that is within the range of physiological oxygen levels (2–5% O<sub>2</sub>), can be justified by the importance of this environmental condition during embryonic development. In fact, it is known that the low-oxygen levels (7–20 mm Hg, 1–3% O<sub>2</sub>) (Patterson and Zhang, 2010) that the cells are exposed to, in the early developing embryo, induces the expression of genes, such as hypoxia inducible factor 1 (HIF-1) and vascular endothelial growth factor (VEGF), that modulate cell metabolism, proliferation, angiogenesis, vasculogenesis and foetal heart remodelling (Patterson and Zhang, 2010; Simon and Keith, 2008). Also, oxygen availability has been shown to affect directly the viability, proliferation and differentiation propensity of stem cells *in vitro* (Simon and Keith, 2008). In particular, several studies showed improved hPSC expansion at atmospheric hypoxia (Forsyth et al., 2006; Gibbons et al., 2006; Serra et al., 2010). Nonetheless, the conclusions regarding the direct impact of low-oxygen levels on CM differentiation are still misleading. Some studies have reported improved CM differentiation yields (Bauwens et al., 2005; Horton and Auguste, 2012; Niebruegge et al., 2009), others have shown best results when applying hypoxia only in specific intervals of the differentiation process (Burrige et al., 2011; Medley et al., 2013) and others have shown reduction in spontaneous differentiation in hypoxic (1–5% O<sub>2</sub>) conditions compared to normoxic (20% O<sub>2</sub>) conditions (Ezashi et al., 2005) and that EBs formed in 20% O<sub>2</sub> generated CMs earlier and with the highest efficiency than EBs exposed 5% O<sub>2</sub> for four days (Kurosawa et al., 2006). Kempf and colleagues recently published a novel efficient bioreactor protocol for hPSC differentiation towards CMs without controlling DO (Kempf et al., 2014, 2015). The different results reported in these studies may be related with differences in: culture approach (2D monolayer vs 3D aggregate or static vs agitated), dynamics of agitation (type and rate) and aggregate size since all these parameters affect the O<sub>2</sub> levels experience at the cellular level. This highlights the importance of exploring the O<sub>2</sub> profile that cells experience in different culture systems and bioreactor hydrodynamics as well as within the aggregates, to allow better comparison and interpretation of the results. Recently, Wu and colleagues developed a mathematical model to simulate the oxygen distribution within mouse and human ESC aggregates based on the O<sub>2</sub> consumption rate and number of cells (Wu et al., 2014). This study may contribute to improve the understanding of the effects of O<sub>2</sub> on the physiology of stem cells organized in 3D aggregates.

Additionally, it should be noted that the oxygen levels slightly increase during embryonic development, reaching in the adult heart, 18 to 35 mmHg (2–5% O<sub>2</sub>) (Sanada et al., 2014). In fact, mature CMs are more sensitive to low oxygen levels than adult CMs since they rely essentially on oxidative metabolism for energy production. Therefore, atmospheric hypoxia may be beneficial in earlier phases of CM differentiation *in vitro*, contributing to improve proliferation of hPSCs and cardiac progenitors (and ultimately cell numbers at the end of the process) but in later stages of development, oxygen limitations might be an issue. Hence, we can speculate that CM

differentiation efficiencies and yields may be improved if an increased gradient of oxygen tension, that better mimics the slight increase in oxygen tension from the foetus to the adult heart, is provided to the cells throughout the differentiation process.

The improved CM differentiation efficiency and yields observed in WAVE bioreactor cultures compared to stirred tank bioreactors can be justified by the distinct hydrodynamic environment imposed by each of these two bioreactor designs. Whereas stirred tank bioreactor uses an impeller, the WAVE system relies on the use of plastic bag placed on a horizontally shaken plate to generate a wave, to mix and homogenize the cell culture. Thus, these conceptually distinct systems provide different i) mixing, ii) mass and heat transfer dynamics and iii) hydrodynamic stress to the cells (Fridley et al., 2012; Placzek et al., 2009; Serra et al., 2012, 2014; Sieblist et al., 2011) and all these parameters can hugely impact the culture outcome. In particular, it has been demonstrated that fluid shear stress may play a significant role in cardiomyogenesis (Stoppel et al., 2016). Previous studies have shown that the shear-stress induced by laminar flow (Illi et al., 2005) and medium perfusion (Shachar et al., 2012) have potential to improve the efficiency of hPSCs differentiation into CMs. For example, perfusion can be applied cyclically, using a peristaltic pump, to promote a pulsatile flow frequency that mimics heart rate of humans (1 Hz = 60 beats per min (bpm)) or rodents (2 Hz or 3 Hz, 120 or 180 bpm).

Although, we have not performed a comparative study of the hydrodynamic environment in both culture systems, we speculate that the improvements observed, in the temporal gene expression pattern and cardiac differentiation efficiency, in the WAVE compared to stirred tank bioreactor cultures, may be related to the frequency of mechanical loading applied in both systems. In stirred tank bioreactors, using an intermittent stirring, mechanical forces at frequencies close to 0.033 Hz were generated, whereas with a wave-induced agitation higher frequencies were reached (0.82-0.86 Hz). Nonetheless, more detailed information about the impact of these mechanical forces (and the bioreactor hydrodynamics as whole), on physiological and molecular mechanisms is needed. For this a more physical-mathematical driven approach should be pursued to provide a comprehensive characterization of the hydrodynamic environment and quantification of the type and magnitude of the stresses generated in each culture strategy using for example computational fluid dynamics and/or laser doppler anemometry (Wang et al., 2013). This knowledge will contribute to explain the biological outcomes and to further optimize the bioreactor-based protocol by defining the culture conditions that promote more efficient mechanical stimulation to the cells.

## **1.2. Using soluble molecules to guide the differentiation of hPSC towards CMs**

Cardiomyogenesis *in vivo* is orchestrated by spatiotemporal changes in soluble cues (including growth factors, small molecules, etc) that act as agonists and/or antagonists of signaling pathways that drive myocardial differentiation, specification and maturation. Nowadays the majority of the CM differentiation protocols rely on the temporal modulation of Wnt signaling, that induces mesoderm differentiation and cardiac lineage specification (Lian et al., 2012, 2013; Ueno et al., 2007). However, the complexity of the human cardiomyogenesis process allied to the line-to-line variability still compromise the effectiveness of the existing differentiation protocols to reproducibly

generate high-quality hPSC-CM with consistent efficiency from multiple hPSC lines or differentiation batches. In **Chapter 3** we applied a directed cardiac differentiation protocol adapted from others previously described in the literature (Kattman et al., 2011; Lanier et al., 2012; Lian et al., 2013) that relies on the sequential addition of a cocktail of growth factors and small molecules, including: Activin A, CHIR99021, and IWR1, known to modulate Activin and Wnt/ $\beta$ -catenin-signalling pathways, which are involved in cardiac lineage development (Kattman et al., 2011; Kim et al., 2015; Lian et al., 2012); and Ascorbic Acid that promotes the proliferation of both mesoderm and cardiac mesoderm cells (Cao et al., 2012). We showed that this protocol could be applied to four different hPSC lines (including hESCs and hiPSC) and generate 2D monolayers of hPSC-CMs that present typical CM gene and protein expression profiles, structure, ultrastructure, calcium signalling and contractility kinetics, within 15 days of culture.

### **1.3. Three dimensional cultures improve CM differentiation and confer resistance to prolonged hypothermic storage**

The impact of 3D aggregate culture on CM differentiation and hypothermic storage of hPSC-CMs was assessed in **Chapters 2** and **5**, respectively.

Since the transition of CM differentiation protocols from 2D to 3D cultures typically results in lower CM purities and reduced reproducibility when compared to 2D cultures, in **Chapter 3** we devised a protocol for CM differentiation and enrichment that relies on two steps. First, cardiac differentiation is induced in 2D monolayers and when the majority of the cell population is cardiac committed (day 6), forced aggregation is promoted. We demonstrated that aggregation of cardiac progenitors improves CM enrichment and commitment, induces significant alterations in the extracellular matrix and metabolic transcriptomes, and a slight increase of TCA-cycle activity, amino acid metabolism and ATP production through glucose oxidation when compared with parallel 2D monolayer cultures. Also, we observed a slight improvement of contractile kinetics in 3D aggregate cultures when compared to 2D monolayer cultures. Although forced aggregation may have contributed to enrich differentiating cultures into CMs, as demonstrated elsewhere (Nguyen et al., 2014), the 3D culture environment may have also contributed to enhance CM differentiation, commitment and functionality. Several studies have demonstrated that 3D culture strategies improve maturation of primary CMs (Akins et al., 2010; Soares et al., 2012) and hPSC-CM (Chan et al., 2013; Mihic et al., 2014; Nunes et al., 2013; Ruan et al., 2016; Zhang et al., 2013). Nonetheless, the majority of these studies did not provide a direct comparison with 2D cultures, as we performed in **Chapter 3**, and often combine other strategies that also affect CM maturation, such as mechanical stretch or electrical stimulation, making the results ambiguous. In **Chapter 3**, we observed slight improvements in hPSC-CM functionality with just 9 days of culture as 3D aggregates, thus we may speculate that prolonging the culture time would further improve CM functionality and ultimately CM maturation.

In **Chapter 5** we showed that 3D conformation confers an additional protection to extended hypothermia-induced stress. We demonstrated that cell viability and recovery in 2D monolayers of hPSC-CMs significantly decreased when the cold storage interval was extended from 3 to 7 days,



whereas 3D aggregates of hPSC-CMs show high cell viabilities after 7 days of cold storage and maintained their metabolic activity, (ultra)structure, phenotype and function. This work highlights that 3D aggregate cultures are more resistant to prolonged hypothermic storage intervals, probably by promoting the formation of more abundant and strong cell-cell interactions.

#### **1.4. Unveiling the role of metabolic substrate availability on CM differentiation and maturation**

CMs undergo several metabolic changes, during development to meet the increased energetic demands imposed by the continuous heart beating. While in early cardiac development, glycolysis is the major source of energy, as CMs mature and become terminally differentiated, mitochondrial oxidative capacity increases, and fatty acid oxidation becomes the major fuel source of energy (Lopaschuk and Jaswal, 2010). This correlation between the changes in cellular metabolic status and *in vivo* development encouraged our interest in exploring cell metabolism during hPSC differentiation towards CMs, *in vitro*. A systematic metabolic characterization during differentiation and maturation processes was performed in **Chapters 3** and **4**, respectively. In **Chapter 3** it was demonstrated that cells remain highly glycolytic throughout all the differentiation process, and that the hPSC-CMs generated in both 2D and 3D cultures present a metabolic phenotype largely driven by high glucose consumption and lactate production at near stoichiometric levels. In addition, in **Chapter 4** it was demonstrated that when hPSC-CMs were cultured in the standard glucose rich medium formulation for additional 20 days, cells maintain their glycolytic metabolism and a fetal-like phenotype. These results motivated us to speculate that inducing a metabolic shift from glycolytic to an oxidative state, by replacing glucose in culture medium with other carbon sources preferably used by CMs (Lopaschuk and Jaswal, 2010), could improve the maturation status of hPSC-CMs *in vitro*, in a faster way than just prolonging the culture time, as previously demonstrated (Lundy et al., 2013).

Even though we demonstrated that culturing hPSC-CMs in glucose depleted medium supplemented with fatty acids, the major substrate used by adult CMs (Lopaschuk and Jaswal, 2010) improved CM structure and functionality, we also showed that this culture condition lead to a drastic cell death after 10 days of culture. Probably hPSC-CMs still present a poor oxidative capacity after the differentiation process (day 15 after induction of differentiation) that limits an efficient fatty acid metabolization. We showed that fatty acid uptake superseded fatty acid metabolization through  $\beta$ -oxidation and TCA cycle, leading to the intracellular accumulation of fatty acid. Excess accumulation of lipids and overactivation of lipid signalling pathways typically trigger cellular dysfunction and ultimately apoptotic cell death or lipoapoptosis (D'Souza et al., 2016).

Nonetheless, we demonstrated that supplementation of fatty acid medium with galactose, commonly used to improve the oxidative capacity in different cell types including cancer cells, primary fibroblasts and muscle cells (Aguer et al., 2011; Kase et al., 2013), circumvented the lipotoxicity issue, contributing to improve fatty acid oxidation. We found out that after 20 days of culture in galactose- and fatty acid-containing media (GFAM), hPSC-CMs show a highly oxidative

metabolism and improved molecular, structural and functional maturation when compared with hPSC-CMs cultured in glucose rich medium (GLCM).

In order to mimic the temporal substrate preference during *in vivo* CM development, we also evaluated the impact of culturing hiPSC-CMs in glucose depleted medium supplemented with lactate for 10 days before cultivation in GFAM. Although the culture in lactate rich medium has contributed to improve cellular oxidative capacity, this approach resulted in lower structural and functional maturation comparatively to GFAM cultures. Of note is that, we showed that combining 10 days in GFAM after 10 days of culture in lactate rich medium is sufficient to improve structural and functional maturation of hPSC-CMs, leading to a phenotype indistinguishable from hPSC-CMs maintained in GFAM for the entire 20 days. This combined approach is better suited to cultures with reduced hPSC-CM purity, since it enables a fast and efficient purification of CMs. In glucose depleted- and lactate-abundant conditions hPSCs and other proliferating cells that depend mainly on glycolysis do not survive in contrast to hPSC-CMs that can use lactate as an alternative energy source (Tohyama et al., 2013).

In pathological conditions such as heart failure, cardiac energy metabolism, specifically fatty acid and glucose metabolism, is altered and has been implicated as a contributing factor to impaired heart efficiency and function (Fillmore et al., 2014; Sankaralingam and Lopaschuk, 2015). Studies using rodent models of cardiac diseases have provided emerging evidences that correcting these changes in energy metabolism by modulating mitochondrial oxidative metabolism may help in the treatment of heart failure (Fillmore and Lopaschuk, 2013). Nonetheless, due to substantial species differences in cardiac physiology, animal models cannot accurately recapitulate many aspects of human cardiac syndromes/pathologies. In this regard, the use of hPSC-CMs to study cardiac metabolism or to recapitulate key pathophysiological phenotypes is more appealing however it is still hampered by the poor hPSC-CM metabolic maturation observed *in vitro*. In few studies, hPSC-CMs were cultured with complex adipogenic cocktails (Kim et al., 2013; Wen et al., 2015) to enhance metabolic maturation and specifically fatty acid  $\beta$ -oxidation. Herein, we used GFAM to improve the metabolic maturation of hPSC-CMs. This simple and cost-effective approach may contribute to streamline the manufacturing of more mature hPSC-CMs. Additionally, this thesis contributed to improve the knowledge in cardiac metabolism field, providing new evidences that a glycolytic-to-oxidative metabolic shift can be a cause, rather than a consequence of CM maturation. The comprehensive metabolic characterization performed throughout this thesis also provided novel insights for the identification/characterization of the differentiated population based on its metabolic signature. Importantly, it was demonstrated that manipulation of culture medium composition induces metabolic, molecular and phenotypic alterations that resemble physiological but also pathophysiological conditions such as cardiac hypertrophy and lipotoxicity. The metabolic models described in this thesis can be used to study scenarios of cardiac lipotoxicity and hypertrophy. These metabolic disorders can be triggered by several etiologies including obesity, diabetes mellitus, myocardial ischemia reperfusion/infarction and aging (D'Souza et al., 2016), thus these models might be relevant for a broad scientific area.

This thesis as well as other previous studies showed that metabolic manipulation can dictate cell fate decisions *in vitro* (Shyh-Chang et al., 2013). However, it remains to be determined whether modulating metabolic processes directly *in vivo* could serve as instructive regulatory signals for resident cells to enhance tissue repair. This may open the way for the development of novel pharmacological therapies for tissue regeneration based on the manipulation of cell metabolism *in vivo*. For example, drugs that target specific metabolic enzymes involved in the balance between glycolysis, mitochondrial oxidative phosphorylation and oxidative stress could be applied locally to potentiate cell proliferation/differentiation/maturation. Advanced metabolomics technologies that allow tracking real-time changes in cellular metabolism *in vivo*, with high sensitivity, will be useful in the future to evaluate the feasibility and efficiency of these therapies.

### 1.5. Assessment of hPSC-CM quality

One major requirement for the manufacturing of stem cell derivatives is to ensure that the final product fulfils the desired quality requisites for biomedical applications. Throughout this thesis an extensive characterization of the generated PSC-CMs was performed, including phenotypic, metabolic and functional interrogation. Using several analytical methods ranging from quantitative reverse-transcription polymerase chain reaction (RT-PCR), flow cytometry, fluorescent microscopy, scanning and transmission electron microscopy, to patch clamp analysis we were able to confirm that the produced hPSC-CMs present typical cardiac gene and protein expression profiles, (ultra)structure, electrophysiology, drug responsiveness and rhythmic intracellular calcium transients. “Omics” tools, specifically, transcriptomics, metabolomics and fluxomics were also explored in this thesis. Integration of all the layers of information provided by these powerful tools pushed this study to new levels of understanding: **Chapter 3** provides valuable molecular insights on the influence of culture system configuration on CM differentiation and **Chapter 4** provides a comprehensive quantitative dissection of hiPSC-CM phenotypes cultured in different metabolic substrates.

In particular, <sup>13</sup>Carbon-Metabolic Flux Analysis (<sup>13</sup>C-MFA) constituted a valuable resource in this thesis, enabling the quantitative description of central carbon metabolism (glycolysis, TCA cycle, FA oxidation and amino acid metabolism) and the estimation of energetic output (ATP synthesis) in hPSC-CM cultured in distinct carbon sources. As introduced in **Chapter 1**, in <sup>13</sup>C-MFA, isotopic labelling data are fitted to a predefined metabolic network model to estimate intracellular metabolic fluxes. In our work, we used a simplified metabolic network of central carbon metabolism, adapted from the literature (Woo Suk and Antoniewicz, 2013). To facilitate the accurate estimation of the fluxes, the complexity and redundancy of the metabolic network is typically simplified (Calheiros Gomes and Simoes, 2012; Zamboni, 2011). Therefore, improving model network complexity, for example to include data from more comprehensive lipidomics analysis, will be very useful in the future to better describe CM metabolism but also to uncover how the increase in myocardial FA uptake and the accumulation of lipid metabolites are interconnected and how these processes trigger lipotoxic cardiomyopathy.

## 1.6. hPSC-CM maturation: achievements and biological relevance.

### How close are we from reproducing adult CMs *in vitro*?

It has been shown that hPSC-CMs remain immature in culture and resemble heart cells of mid-gestation human foetuses (Veerman et al., 2015). In **Chapter 4** we established a novel method for hPSC-CM maturation based on metabolic substrate manipulation (GFAM culture). We showed that shifting hPSC-CMs from glucose-containing to galactose- and FA-containing media promotes their faster maturation, resulting in hPSC-CMs with energetically efficient oxidative metabolism, transcriptome signatures closer to that of adult ventricular CMs, higher myofibril density and alignment, improved calcium, contractility and action potential kinetics when compared with hPSC-CMs cultured in glucose rich medium. This method holds technical and economic advantages over the existing protocols due to its scalability (it can be applied to a large number of cells, for example cells cultured in a bioreactor), simplicity (a simple medium-exchange procedure) and ease of application (does not require specific equipment or addition of expensive factors/chemicals). Table 6.1 compares GFAM strategy with other approaches reported in the literature for hPSC-CM maturation that have used the same markers to assess maturation status, namely: structure (aspect ratio; circularity index; surface area); functionality (contractile force) and metabolism (metabolic substrate; oxygen consumption rate). The total time of culture is also indicated since it can also affect the culture outcome. It is possible to note that not all approaches use the same parameters to evaluate hPSC-CM maturation, making it difficult to compare the efficiency of different protocols. Cell metabolism, for instance, has been rarely measured and taken into consideration in maturation studies. Also, the methodologies used to assess maturation status, for example, the contractile force, typically varies which also hampers a reliable comparison of the results. Nonetheless, we can conclude that GFAM culture is a competitive and advantageous strategy, capable to induce metabolic, phenotypic and functional maturation of hPSC-CMs in a timely efficient manner, when compared to what has been described in the literature.

Although, after GFAM treatment hPSC-CMs present certain features more similar to human adult CMs than hPSC-CMs obtained with strategies previously reported (Table 6.1), hPSC-CMs are still far from becoming structurally and functionally identical to adult CMs. There are certain features of the adult CM phenotype which have not yet been ubiquitously observed in culture, including the presence of: i) M-bands, a hallmark of sarcomeric structural maturation (Feric and Radisic, 2016), and ii) T-tubules, key structures of the excitation-contraction coupling mechanism in mature CMs that are important for normal  $\text{Ca}^{2+}$  handling (Yang et al., 2014). Even though it is speculated that probably a phenotype completely resembling adult CMs might never be attainable in *in vitro* cell culture systems, the scientific community is still pursuing strategies that more efficiently allow reaching this state.

**Table 6.1. Comparison of structural, functional and metabolic features of hPSC-CMs cultured in GFAM and other approaches reported in the literature with human adult CMs.** Abbreviations: OCR – Oxygen Consumption Rate; T3 – triiodothyronine; (-) – Non determined or reported in the literature; (~) – Approximately.

	Metabolic substrate manipulation (GFAM)	Pluricyte Medium (with T3 hormone) (Ribeiro et al., 2015)	T3 hormone treatment (Yang et al., 2014)	Mechanical and electrical stimulation 3D scaffold (Ruan et al., 2016)	Electrical stimulation 3D culture (Chan et al., 2013)	Overexpression of let-7 (Kuppusamy et al., 2015)	Prolonged culture time (Lundy et al., 2013)	Human Adult CMs (Denning et al., 2015; Feric and Radisic, 2016)
Structure	Aspect ratio	-	-	3.7±0.2	-	-	-	5-9.5:1
	Circularity index	0.5±0.0	-	-	-	-	0.3±0.0	~0.43
Functionality	Surface area ( $\mu\text{m}^2$ )	991±58	2169±110	-	795±46	let-7i: 1110±101 let-7g: 980±95	1716±150	10212-14418
	Contractile Force	12.3±0.7 (nN/cell)	0.5±0.0 (mN/mm <sup>2</sup> )	-	1.3±0.2 (mN/mm <sup>2</sup> )	Let-7i: 11.3±0.9 Let-7g: 9.3±0.7 (nN/cell)	-	>10 (mN/mm <sup>2</sup> )
Metabolism	Metabolic substrate	Glucose	Glucose	Glucose	Glucose	Glucose	Glucose	Fatty Acids
	Metabolism	-	-	-	-	-	-	Oxidative
Time in culture	OCR (pmoles/min)	~169-216	-	-	-	~150-200	-	-
	(day)	7 (27 total)	20 (33 total)	4 (23 total)	14 (40 total)	Transduced at day 12 (30 total)	80-120 total	-

The more immediate interest in using mature hPSC-CMs is for drug screening or cardiotoxicity assessment since toxic side effects on the heart often limit implementation of valuable drug therapies (Denning et al., 2015). Specifically, hiPSC-CMs have been differentiated from hiPSC lines generated from patients affected by cardiac diseases to study patient- and disease-specific mutations or polymorphisms and facilitate insights into disease mechanisms and therapeutic approaches (Bayzigitov et al., 2016; Sala et al., 2016; Sallam et al., 2015). The use of hPSC-CMs for cardiac tissue replacement, although actively investigated, is still far from being a routine clinical practice (Fox et al., 2014; Veerman et al., 2015). The key question that remains unclear is whether more mature cells are preferable for cell transplantation experiments. First, it was speculated that hPSC-CMs whose electrical and mechanical properties more closely resemble those of native myocardium would pose less arrhythmic risk and have enhanced contractile performance (Yang et al., 2014). Nonetheless, immature hPSC-CMs have been shown to be better suited for cell therapy applications, as they are more hypoxic-resistant and tolerant to the ischemic environment after transplantation (Boheler et al., 2011). Also, it has been demonstrated that immature CMs exhibit a markedly higher engraftment rate than more mature CMs when transplanted into the injured heart (Reinecke et al., 1999), and can mature *in vivo* after integration into the recipient myocardium (Chong et al., 2014; van Laake et al., 2007). It should be highlighted that a recently published case report has shown that transplantation of hESC-derived cardiac progenitors (Isl-1<sup>+</sup> and SSEA-1<sup>+</sup>) in infarcted myocardium improved functional and clinical outcome in a patient with severe ischaemic heart failure without the induction of arrhythmias, tumour formation or immunosuppression-related adverse events (Menasché et al., 2015). This trial (ESCORT) is actually in Phase I (ClinicalTrials.gov: NCT02057900). In addition, the use of less differentiated but mesoderm-committed hPSC-derived cells may constitute another solution for clinical applications, since these cells might restore myocardial tissue and also contribute to revascularization (Hulot et al., 2014). Further investigations are still needed to determine the ideal level of differentiation and/or maturation status for *in vivo* transplantation, however it is imperative to find a balance between safety and efficacy to obtain better engrafting and functional improvements.

### **1.7. Facilitating the widespread distribution of hPSC-CMs: Improvements in short-term storage and shipping of hPSC-CMs**

The enhanced applicability of hPSC-CMs has increased the demand for effective methods for their storage and shipping. In **Chapter 5**, effective clinically compatible strategies for cold storage of hPSC-CMs cultured as 2D monolayers and 3D aggregates were established. It was shown for the first time that 2D monolayers and 3D aggregates of hPSC-CMs can be efficiently stored at 4°C, using a fully defined clinical-compatible preservation formulation, HypoThermosol® (HTS), for 3 and 7 days, respectively, without compromising cell viability, (ultra)structure, gene and protein expression profile, electrophysiological profiles, and drug responsiveness. To evaluate the efficiency and robustness of the hypothermic storage process, we assessed cell viability and biological activity/potency for one week post-storage period. The storage protocol was considered efficient when cell viability/recovery was ≥70%, since this is the minimum cell viability specification

generally acceptable for somatic cellular therapies (Food and Drug Administration, 2008). It should be noted that the hypothermic storage studies were performed with non-proliferative hPSC-CMs, therefore the high cell recovery/viability observed after storage clearly reflects the efficiency of the process. Importantly, this study constitutes a promising avenue for the delivery of certified, validated, ready-to-use monolayers and aggregates of hPSC-CMs, manufactured in specialized companies to customers/physicians worldwide, facilitating the use of these cells in high-throughput cardiac drug testing, toxicity screening or regenerative therapies.

It is important to highlight that the hypothermic storage protocol described in **Chapter 5** was used and validated in **Chapter 2, 3** and **4**. Murine and human PSC-CMs, at different culture timepoints (from days 13 to 35 post-differentiation induction), were shipped in these conditions, to our collaborators at University of Cologne (Germany) and at Harvard Medical School (Boston, EUA), to carry out electrophysiology and contractility studies (**Chapter 2, 3** and **4**). The shipping was performed at controlled temperature of 4°C and lasted from 2 to 5 days and no impact on cell viability and functionality studies was observed.

As introduced in **Chapter 1**, hypothermic storage consists in the use of refrigerated temperatures (typically within the range of 4–10 °C) to store biologics (Baust et al., 2016). The principle behind this technique is that at cold temperatures metabolic activity of the cells is reduced in a reversible manner. In addition, preservation of cell homeostasis is facilitated by the use of commercially available hypothermic solutions, such as HTS, that were carefully formulated to maintain the ionic and osmotic balances, control of pH, supply energy substitutes, prevent cell swelling and the formation of free radicals at low temperatures (Brockbank and Taylor, 2006). For short-time storage periods and/or shipment of the cells, hypothermic preservation is preferable to cryopreservation, since it is simpler, safer, more versatile and with low operational/technical demand. Hypothermic preserved hPSC-CMs can be easily manipulated by researchers/physicians with minimal knowledge of hPSC culture. When using a clinical compatible solution, such as HTS, cells can be directly injected in patients after the shipment/storage. For other applications, hypothermic solution just needs to be replaced by culture medium. In contrast, the methods described in the literature for cryopreservation of hPSC-CMs, besides poorly efficient and reproducible, are time- and technically demanding, requiring: pre-treatment (heat-shock and incubation with specific factors), cell culture dissociation into single-cell suspension before freezing and several washes to remove FBS and toxic cryoprotective agents such as DMSO, after thawing (Preininger and Singh, 2016; Shiba et al., 2012; Xu et al., 2011). Nonetheless, the development of more efficient strategies to cryopreserve hPSC-CMs, also as 2D monolayers and 3D aggregates, will be a very important achievement, enabling to generate large and validated cell banks of hPSC-CMs for later use in biomedical applications.

## 2. Future perspectives

This thesis contributed to progress beyond the state of the art on the stem cell field. However, as a fast moving scientific field, there is still room for improvement towards the development of

more effective strategies for CM differentiation and maturation. Future studies mimicking even further the complexity of *in vivo* microenvironment, by combining approaches that simultaneously provide regulatory cues at different levels are needed. Therefore, the maturation strategy described in **Chapter 4** should be translated to 3D aggregate cell culture strategy and combined with a directed differentiation process in a bioreactor protocol that could assure an increased gradient of oxygen throughout culture time and a cyclic mechanical rich environment, accordingly to the insights described in **Chapter 2**. Integration of all environmental stimuli investigated in this thesis will increase physiological relevance and hopefully provide a scalable, robust and straightforward bioprocess for mass production of pure and more mature hPSC-CMs in the near future.

Looking forward, synergistic, multidisciplinary approaches bridging biology, engineering, physics, material sciences and mathematics should be pursued to collectively define the best path forward to improve efficiency, standardization and cost-effectiveness of the bioprocesses and to predict their outcome. Additionally, the combination of distinct high-throughput omic technologies will fill gaps in the understanding of the mechanisms governing cardiomyogenesis and cardiovascular diseases at the molecular, cellular, and organ level. This knowledge will facilitate the design of subtype-specific cardiac differentiation and ultimately improve prediction, prevention and the design of novel therapeutic treatments of cardiovascular diseases.

### 3. Conclusion

In summary, this thesis contributes to the advance of scalable hPSC differentiation towards CMs, hPSC-CM maturation and hypothermic storage of hPSC-CMs and simultaneously provides a detailed quantitative characterization of hPSC-CM phenotype, in terms of transcriptome, metabolome and fluxome, at different developmental states. The knowledge generated will, hopefully, contribute to potentiate the worldwide commercial distribution and utilization of hPSC-CMs in applications ranging from tissue replacement in heart failure after myocardial infarction to basic science on heart development, cardiac disease modelling, drug discovery, and cardiac safety pharmacology.

### 4. References

- Aguer, C., Gambarotta, D., Mailloux, R.J., Moffat, C., Dent, R., McPherson, R., and Harper, M.E. (2011). Galactose enhances oxidative metabolism and reveals mitochondrial dysfunction in human primary muscle cells. *PLoS One* 6.
- Akins, R.E., Rockwood, D., Robinson, K.G., Sandusky, D., Rabolt, J., and Pizarro, C. (2010). Three-dimensional culture alters primary cardiac cell phenotype. *Tissue Eng. Part A* 16, 629–641.
- Baust, J.M., Corwin, W., Snyder, K.K., Buskirk, R. Van, and Baust, J.G. (2016). Cryopreservation: Evolution of Molecular Based Strategies. In *Biobanking and Cryopreservation of Stem Cells*, pp. 13–29.
- Bauwens, C., Yin, T., Dang, S., Peerani, R., and Zandstra, P.W. (2005). Development of a perfusion fed bioreactor for embryonic stem cell-derived cardiomyocyte generation: oxygen-mediated enhancement of cardiomyocyte output. *Biotechnol. Bioeng.* 90, 452–461.
- Bayzigitov, D.R., Medvedev, S.P., Demytyeva, E. V, Bayramova, S.A., Pokushalov, E.A., Karaskov, A.M., and Zakian, S.M. (2016). Human induced pluripotent stem cell-derived



- cardiomyocytes afford new opportunities in inherited cardiovascular disease modeling. *2016*, 1–32.
- Boheler, K.R., Joodi, R.N., Qiao, H., Juhasz, O., Urick, A.L., Chuppa, S.L., Gundry, R.L., Wersto, R.P., and Zhou, R. (2011). Embryonic stem cell-derived cardiomyocyte heterogeneity and the isolation of immature and committed cells for cardiac remodeling and regeneration. *Stem Cells Int.* *2011*, 214203.
- Brockbank, K.G.M., and Taylor, M.J. (2006). Tissue Preservation. In *Advances in Biopreservation*, pp. 157–196.
- Burridge, P.W., Thompson, S., Millrod, M.A., Weinberg, S., Yuan, X., Peters, A., Mahairaki, V., Koliatsos, V.E., Tung, L., and Zambidis, E.T. (2011). A Universal System for Highly Efficient Cardiac Differentiation of Human Induced Pluripotent Stem Cells That Eliminates Interline Variability. *PLoS One* *6*, 16.
- Calheiros Gomes, L., and Simoes, M. (2012). <sup>13</sup>C Metabolic Flux Analysis: From the Principle to Recent Applications. *Curr. Bioinform.* *7*, 77–86.
- Cao, N., Liu, Z., Chen, Z., Wang, J., Chen, T., Zhao, X., Ma, Y., Qin, L., Kang, J., Wei, B., et al. (2012). Ascorbic acid enhances the cardiac differentiation of induced pluripotent stem cells through promoting the proliferation of cardiac progenitor cells. *Cell Res.* *22*, 219–236.
- Chan, Y.-C., Ting, S., Lee, Y.-K., Ng, K.-M., Zhang, J., Chen, Z., Siu, C.-W., Oh, S.K.W., and Tse, H.-F. (2013). Electrical stimulation promotes maturation of cardiomyocytes derived from human embryonic stem cells. *J. Cardiovasc. Transl. Res.* *6*, 989–999.
- Chong, J.J.H., Yang, X., Don, C.W., Minami, E., Liu, Y.-W., Weyers, J.J., Mahoney, W.M., Van Biber, B., Cook, S.M., Palpant, N.J., et al. (2014). Human embryonic-stem-cell-derived cardiomyocytes regenerate non-human primate hearts. *Nature* *510*, 273–277.
- D'Souza, K., Nzirorera, C., and Kienesberger, P.C. (2016). Lipid metabolism and signaling in cardiac lipotoxicity. *Biochim. Biophys. Acta - Mol. Cell Biol. Lipids* *1861*, 1513–1524.
- Denning, C., Borgdorff, V., Crutchley, J., Firth, K.S.A., George, V., Kalra, S., Kondrashov, A., Hoang, M.D., Mosqueira, D., Patel, A., et al. (2015). Cardiomyocytes from human pluripotent stem cells: From laboratory curiosity to industrial biomedical platform. *Biochim. Biophys. Acta - Mol. Cell Res.* *1863*, 1728–1748.
- Ezashi, T., Das, P., and Roberts, R.M. (2005). Low O<sub>2</sub> tensions and the prevention of differentiation of hES cells. *Proc. Natl. Acad. Sci. U. S. A.* *102*, 4783–4788.
- Feric, N.T., and Radisic, M. (2016). Maturing human pluripotent stem cell-derived cardiomyocytes in human engineered cardiac tissues. *Adv. Drug Deliv. Rev.* *96*, 110–134.
- Fillmore, N., and Lopaschuk, G.D. (2013). Targeting mitochondrial oxidative metabolism as an approach to treat heart failure. *Biochim. Biophys. Acta - Mol. Cell Res.* *1833*, 857–865.
- Fillmore, N., Mori, J., and Lopaschuk, G.D. (2014). Mitochondrial fatty acid oxidation alterations in heart failure, ischaemic heart disease and diabetic cardiomyopathy. *Br. J. Pharmacol.* *171*, 2080–2090.
- Food and Drug Administration (2008). Content and Review of Chemistry, Manufacturing, and Control (CMC) Information for Human Somatic Cell Therapy Investigational New Drug Applications (INDs). In *Guidance for FDA Reviewers and Sponsors*, p.
- Forsyth, N.R., Musio, A., Vezzoni, P., Simpson, a H.R.W., Noble, B.S., and McWhir, J. (2006). Physiologic oxygen enhances human embryonic stem cell clonal recovery and reduces chromosomal abnormalities. *Cloning Stem Cells* *8*, 16–23.
- Fox, I.J., Daley, G.Q., Goldman, S.A., Huard, J., Kamp, T.J., and Trucco, M. (2014). Stem cell therapy. Use of differentiated pluripotent stem cells as replacement therapy for treating disease. *Science* (80-. ). *345*, 1247391.
- Fridley, K.M., Kinney, M. a, and McDevitt, T.C. (2012). Hydrodynamic modulation of pluripotent stem cells. *Stem Cell Res. Ther.* *3*, 45.
- Gibbons, J., Hewitt, E., and Gardner, D.K. (2006). Effects of oxygen tension on the establishment and lactate dehydrogenase activity of murine embryonic stem cells. *Cloning Stem Cells* *8*, 117–122.

- Horton, R.E., and Auguste, D.T. (2012). Synergistic effects of hypoxia and extracellular matrix cues in cardiomyogenesis. *Biomaterials* 33, 6313–6319.
- Hulot, J.-S., Stillitano, F., Salem, J.E., Kovacic, J.C., Fuster, V., and Hajjar, R.J. (2014). Considerations for pre-clinical models and clinical trials of pluripotent stem cell-derived cardiomyocytes. *Stem Cell Res. Ther.* 5, 1.
- Illi, B., Scopece, A., Nanni, S., Farsetti, A., Morgante, L., Biglioli, P., Capogrossi, M.C., and Gaetano, C. (2005). Epigenetic histone modification and cardiovascular lineage programming in mouse embryonic stem cells exposed to laminar shear stress. *Circ. Res.* 96, 501–508.
- Kase, E.T., Nikolić, N., Bakke, S.S., Bogen, K.K., Aas, V., Thoresen, G.H., and Rustan, A.C. (2013). Remodeling of Oxidative Energy Metabolism by Galactose Improves Glucose Handling and Metabolic Switching in Human Skeletal Muscle Cells. *PLoS One* 8.
- Kattman, S.J., Witty, A.D., Gagliardi, M., Dubois, N.C., Niapour, M., Hotta, A., Ellis, J., and Keller, G. (2011). Stage-specific optimization of activin/nodal and BMP signaling promotes cardiac differentiation of mouse and human pluripotent stem cell lines. *Cell Stem Cell* 8, 228–240.
- Kempf, H., Olmer, R., Kropp, C., Rückert, M., Jara-Avaca, M., Robles-Diaz, D., Franke, A., Elliott, D.A., Wojciechowski, D., Fischer, M., et al. (2014). Controlling expansion and cardiomyogenic differentiation of human pluripotent stem cells in scalable suspension culture. *Stem Cell Reports* 3, 1132–1146.
- Kempf, H., Kropp, C., Olmer, R., Martin, U., and Zweigerdt, R. (2015). Cardiac differentiation of human pluripotent stem cells in scalable suspension culture. *Nat. Protoc.* 10, 1345–1361.
- Kim, C., Wong, J., Wen, J., Wang, S., Wang, C., Spiering, S., Kan, N.G., Forcales, S., Puri, P.L., Leone, T.C., et al. (2013). Studying arrhythmogenic right ventricular dysplasia with patient-specific iPSCs. *Nature* 494, 105–110.
- Kim, M.S., Horst, A., Blinka, S., Stamm, K., Mahnke, D., Schuman, J., Gundry, R., Tomita-Mitchell, A., and Lough, J. (2015). Activin-A and Bmp4 levels modulate cell type specification during CHIR-induced cardiomyogenesis. *PLoS One* 10, 1–16.
- Kuppusamy, K.T., Jones, D.C., Sperber, H., Madan, A., Fischer, K. a., Rodriguez, M.L., Pabon, L., Zhu, W.-Z., Tulloch, N.L., Yang, X., et al. (2015). Let-7 family of microRNA is required for maturation and adult-like metabolism in stem cell-derived cardiomyocytes. *Proc. Natl. Acad. Sci.* 201424042.
- Kurosawa, H., Kimura, M., Noda, T., and Amano, Y. (2006). Effect of Oxygen on In Vitro Differentiation of Mouse Embryonic Stem Cells. *J. Biosci. Bioeng.* 101, 26–30.
- van Laake, L.W., Passier, R., Monshouwer-Kloots, J., Verkleij, A.J., Lips, D.J., Freund, C., den Ouden, K., Ward-van Oostwaard, D., Korving, J., Tertoolen, L.G., et al. (2007). Human embryonic stem cell-derived cardiomyocytes survive and mature in the mouse heart and transiently improve function after myocardial infarction. *Stem Cell Res.* 1, 9–24.
- Lanier, M., Schade, D., Willems, E., Tsuda, M., Spiering, S., Kalisiak, J., Mercola, M., and Cashman, J.R. (2012). Wnt inhibition correlates with human embryonic stem cell cardiomyogenesis: A structure-activity relationship study based on inhibitors for the Wnt response. *J. Med. Chem.* 55, 697–708.
- Lian, X., Hsiao, C., Wilson, G., Zhu, K., Hazeltine, L.B., Azarin, S.M., Raval, K.K., Zhang, J., Kamp, T.J., and Palecek, S.P. (2012). Robust cardiomyocyte differentiation from human pluripotent stem cells via temporal modulation of canonical Wnt signaling. *PNAS* 1–10.
- Lian, X., Zhang, J., Azarin, S.M., Zhu, K., Hazeltine, L.B., Bao, X., Hsiao, C., Kamp, T.J., and Palecek, S.P. (2013). Directed cardiomyocyte differentiation from human pluripotent stem cells by modulating Wnt/ $\beta$ -catenin signaling under fully defined conditions. *Nat. Protoc.* 8, 162–175.
- Lopaschuk, G.D., and Jaswal, J.S. (2010). Energy metabolic phenotype of the cardiomyocyte during development, differentiation, and postnatal maturation. *J. Cardiovasc. Pharmacol.* 56, 130–140.
- Lundy, S.D., Zhu, W.-Z., Regnier, M., and Laflamme, M. (2013). Structural and Functional Maturation of Cardiomyocytes Derived From Human Pluripotent Stem Cells. *Stem Cells Dev.* 22, 1991–2002.

- Medley, T.L., Furtado, M., Lam, N.T., Idrizi, R., Williams, D., Verma, P.J., Costa, M., and Kaye, D.M. (2013). Effect of oxygen on cardiac differentiation in mouse iPS cells: Role of hypoxia inducible factor-1 and Wnt/beta-catenin signaling. *PLoS One* 8, 1–8.
- Menasché, P., Vanneaux, V., Hagège, A., Bel, A., Cholley, B., Cacciapuoti, I., Parouchev, A., Benhamouda, N., Tachdjian, G., Tosca, L., et al. (2015). Human embryonic stem cell-derived cardiac progenitors for severe heart failure treatment: First clinical case report. *Eur. Heart J.* 36, 2011–2017.
- Mihic, A., Li, J., Miyagi, Y., Gagliardi, M., Li, S.-H., Zu, J., Weisel, R.D., Keller, G., and Li, R.-K. (2014). The effect of cyclic stretch on maturation and 3D tissue formation of human embryonic stem cell-derived cardiomyocytes. *Biomaterials* 35, 2798–2808.
- Nguyen, D.C., Hookway, T.A., Wu, Q., Jha, R., Preininger, M.K., Chen, X., Easley, C.A., Spearman, P., Deshpande, S.R., Maher, K., et al. (2014). Microscale generation of cardiospheres promotes robust enrichment of cardiomyocytes derived from human pluripotent stem cells. *Stem Cell Reports* 3, 260–268.
- Niebruegge, S., Bauwens, C.L., Peerani, R., Thavandiran, N., Masse, S., Sevaptisidis, E., Nanthakumar, K., Woodhouse, K., Husain, M., Kumacheva, E., et al. (2009). Generation of human embryonic stem cell-derived mesoderm and cardiac cells using size-specified aggregates in an oxygen-controlled bioreactor. *Biotechnol. Bioeng.* 102, 493–507.
- Nunes, S.S., Miklas, J.W., Liu, J., Aschar-Sobbi, R., Xiao, Y., Zhang, B., Jiang, J., Massé, S., Gagliardi, M., Hsieh, A., et al. (2013). Biowire: a platform for maturation of human pluripotent stem cell-derived cardiomyocytes. *Nat. Methods* 10, 781–787.
- Patterson, A.J., and Zhang, L. (2010). Hypoxia and fetal heart development. *Curr. Mol. Med.* 10, 653–666.
- Placzek, M.R., Chung, I.-M., Macedo, H.M., Ismail, S., Mortera Blanco, T., Lim, M., Cha, J.M., Fauzi, I., Kang, Y., Yeo, D.C.L., et al. (2009). Stem cell bioprocessing: fundamentals and principles. *J. R. Soc. Interface* 6, 209–232.
- Preininger, M.K., and Singh, M. (2016). Cryopreservation of Human Pluripotent Stem Cell-Derived Cardiomyocytes: Strategies, Challenges, and Future Directions. In *Biobanking and Cryopreservation of Stem Cells*, pp. 123–135.
- Reinecke, H., Zhang, M., Bartosek, T., and Murry, C.E. (1999). Survival, Integration, and Differentiation of Cardiomyocyte Grafts. A Study in Normal and Injured Rat Hearts. *Circulation* 100, 202.
- Ribeiro, M.C., Tertoolen, L.G., Guadix, J. a, Bellin, M., Kosmidis, G., D’Aniello, C., Monshouwer-Kloots, J., Goumans, M.-J., Wang, Y.-L., Feinberg, A.W., et al. (2015). Functional maturation of human pluripotent stem cell derived cardiomyocytes in vitro--correlation between contraction force and electrophysiology. *Biomaterials* 51, 138–150.
- Ruan, J., Tulloch, N.L., Razumova, M. V, Saiget, M., Muskheli, V., Pabon, L., and Reinecke, H. (2016). Mechanical Stress Conditioning and Electrical Stimulation Promote Contractility and Force Maturation of Induced Pluripotent Stem Cell-Derived Human Cardiac Tissue. *Circulation* 134, 1557–1567.
- Sala, L., Bellin, M., and Mummery, C.L. (2016). Integrating cardiomyocytes from human pluripotent stem cells in safety pharmacology: has the time come? *Br. J. Pharmacol.* 1–17.
- Sallam, K., Li, Y., Sager, P.T., Houser, S.R., and Wu, J.C. (2015). Finding the Rhythm of Sudden Cardiac Death: New Opportunities Using Induced Pluripotent Stem Cell-Derived Cardiomyocytes. *Circ. Res.* 116, 1989–2004.
- Sanada, F., Kim, J., Czarna, A., Chan, N.Y.K., Signore, S., Ogórek, B., Isobe, K., Wybieralska, E., Borghetti, G., Pesapane, A., et al. (2014). C-kit-positive cardiac stem cells nested in hypoxic niches are activated by stem cell factor reversing the aging myopathy. *Circ. Res.* 114, 41–55.
- Sankaralingam, S., and Lopaschuk, G.D. (2015). Cardiac energy metabolic alterations in pressure overload – induced left and right heart failure ( 2013 Grover Conference Series ). *Pulm. Circ.* 5, 15–28.
- Serra, M., Brito, C., Sousa, M.F.Q., Jensen, J., Tostões, R., Clemente, J., Strehl, R., Hyllner, J.,

- Carrondo, M.J.T., and Alves, P.M. (2010). Improving expansion of pluripotent human embryonic stem cells in perfused bioreactors through oxygen control. *J. Biotechnol.* *148*, 208–215.
- Serra, M., Brito, C., Correia, C., and Alves, P.M. (2012). Process engineering of human pluripotent stem cells for clinical application. *Trends Biotechnol.* *30*, 1–10.
- Serra, M., Correia, C., Brito, C., and Alves, P.M. (2014). Bioprocessing of Human Pluripotent Stem Cells for Cell Therapy Applications. In *Stem Cells and Cell Therapy.*, pp. 71–95.
- Shachar, M., Benishti, N., and Cohen, S. (2012). Effects of mechanical stimulation induced by compression and medium perfusion on cardiac tissue engineering. *Biotechnol. Prog.* *28*, 1551–1559.
- Shiba, Y., Fernandes, S., Zhu, W.-Z., Filice, D., Muskheli, V., Kim, J., Palpant, N.J., Gantz, J., Moyes, K.W., Reinecke, H., et al. (2012). Human ES-cell-derived cardiomyocytes electrically couple and suppress arrhythmias in injured hearts. *Nature* *489*, 322–325.
- Shyh-Chang, N., Daley, G.Q., and Cantley, L.C. (2013). Stem cell metabolism in tissue development and aging. *Development* *140*, 2535–2547.
- Sieblist, C., Jenzsch, M., Pohlscheidt, M., and Lübbert, A. (2011). Insights into large-scale cell-culture reactors: I. Liquid mixing and oxygen supply. *Biotechnol. J.* *6*, 1532–1546.
- Simon, M.C., and Keith, B. (2008). The role of oxygen availability in embryonic development and stem cell function. *Nat. Rev. Mol. Cell Biol.* *9*, 285–296.
- Soares, C.P., Midlej, V., de Oliveira, M.E.W., Benchimol, M., Costa, M.L., and Mermelstein, C. (2012). 2D and 3D-organized cardiac cells shows differences in cellular morphology, adhesion junctions, presence of myofibrils and protein expression. *PLoS One* *7*, e38147.
- Stoppel, W.L., Kaplan, D.L., and Black, L.D. (2016). Electrical and mechanical stimulation of cardiac cells and tissue constructs. *Adv. Drug Deliv. Rev.* *96*, 135–155.
- Tohyama, S., Hattori, F., Sano, M., Hishiki, T., Nagahata, Y., Matsuura, T., Hashimoto, H., Suzuki, T., Yamashita, H., Satoh, Y., et al. (2013). Distinct metabolic flow enables large-scale purification of mouse and human pluripotent stem cell-derived cardiomyocytes. *Cell Stem Cell* *12*, 127–137.
- Veerman, C.C., Kosmidis, G., Mummery, C.L., Casini, S., Verkerk, A.O., and Bellin, M. (2015). Immaturity of human stem-cell-derived cardiomyocytes in culture: fatal flaw or soluble problem? *Stem Cells Dev.* *24*, 1035–1052.
- Wang, Y., Chou, B.K., Dowe, S., He, C., Gerecht, S., and Cheng, L. (2013). Scalable expansion of human induced pluripotent stem cells in the defined xeno-free E8 medium under adherent and suspension culture conditions. *Stem Cell Res.* *11*, 1103–1116.
- Wen, J.-Y., Wei, C.-Y., Shah, K., Wong, J., Wang, C., and Chen, H.-S.V. (2015). Maturation-Based Model of Arrhythmogenic Right Ventricular Dysplasia Using Patient-Specific Induced Pluripotent Stem Cells. *Circ. J.* *79*, 1402–1408.
- Woo Suk, A., and Antoniewicz, M.R. (2013). Parallel labeling experiments with [1,2-<sup>13</sup>C]glucose and [U-<sup>13</sup>C]glutamine provide new insights into CHO cell metabolism. *Metab. Eng.* *15*, 34–47.
- Wu, J., Rostami, M.R., Cadavid Olaya, D.P., and Tzanakakis, E.S. (2014). Oxygen transport and stem cell aggregation in stirred-suspension bioreactor cultures. *PLoS One* *9*, 1–12.
- Xu, C., Police, S., Hassanipour, M., Li, Y., Chen, Y., Priest, C., O'Sullivan, C., Laflamme, M. a, Zhu, W.-Z., Van Biber, B., et al. (2011). Efficient generation and cryopreservation of cardiomyocytes derived from human embryonic stem cells. *Regen. Med.* *6*, 53–66.
- Yang, X., Pabon, L., and Murry, C.E. (2014). Engineering adolescence: Maturation of human pluripotent stem cell-derived cardiomyocytes. *Circ. Res.* *114*, 511–523.
- Zamboni, N. (2011). <sup>13</sup>C metabolic flux analysis in complex systems. *Curr. Opin. Biotechnol.* *22*, 103–108.
- Zhang, D., Shadrin, I.Y., Lam, J., Xian, H.Q., Snodgrass, H.R., and Bursac, N. (2013). Tissue-engineered cardiac patch for advanced functional maturation of human ESC-derived cardiomyocytes. *Biomaterials* *34*, 5813–5820.